THE SPATIAL AND TEMPORAL CHARACTERISATION OF FUNCTIONAL INTERACTIONS BETWEEN THE KEY MEMBRANE STRESS PROTEINS AT THE SINGLE MOLECULE LEVEL IN LIVE *ESCHERICHIA COLI* CELLS

PARUL MEHTA

Imperial College London

Department Of Life Sciences

Submitted for the degree of Doctor of Philosophy

ABSTRACT

All the cell types must maintain the integrity of their membranes which is important for cell viability. The membrane structure and function is maintained by many different response mechanisms. One such unique bacterial membrane stress response is the Phage shock protein response (Psp). It is composed of a transcriptional activator, negative regulator, signal sensors and transducers and stress effectors.

Using milli second time-scale single-molecule fluorescence microscopy in live *E. coli* cells, the localisations, two dimensional diffusion dynamics and stoichiometry of functional Psp proteins were determined under non-stress and membrane stress conditions. The two major proteins studied in this research are a bacterial enhancer binding protein phage shock protein F (PspF) and the negative regulator and major effector phage shock protein A (PspA). For the imaging studies stable and functional chromosomal fusions of PspF and PspA to Venus fluorescent protein were used replacing the native proteins. It was established that a stable repressive PspF-PspA complex is located in the nucleoid and PspF displays DNA associated diffusion dynamics similar to other DNA-binding transcription factors such as LacI. PspF as a hexamer activated a single *psp* promoter at a time. The effector V-PspA assembled as higher order oligomers localised at the lateral membrane and showed very slow dynamics. In addition *in vivo* and *in vitro* structural studies of PspA showed that N-terminal amphipathic helix governed the balance between the dual functions of PspA.

In a proposed model of the cellular landscape of the Psp response, the PspF-PspA inhibitory complex localised at the nucleoid transiently communicated with the polar regions of cells occupied by PspBC under non-stress conditions. With the stress conditions PspA retained at the polar membrane along with PspBC, while PspF associated with the active transcription complex to initiate the expression of *psp* genes. With the increase in the amounts of PspA, it organised itself into higher order effector moving along the MreB directed helical path contacting with the membrane via RodZ and in this way facilitated the organisation of membrane repair pathways at the damaged sites.

DECLARATION OF ORIGINALITY

I certify that this thesis entitled “The spatial and temporal characterisation of functional interactions between the key membrane stress proteins at the single molecule level in live *E. coli* cells” is written entirely by myself and that the research to which it refers to is my own. The information and conclusions derived from published or unpublished works by others have been correctly cited in the text and listed in the references.

Parul Mehta

COPYRIGHT DECLARATION

The copyright of this thesis rests with the author and is made available under a Creative Commons Attribution Non-Commercial No Derivatives licence. Researchers are free to copy, distribute or transmit the thesis on the condition that they attribute it, that they do not use it for commercial purposes and that they do not alter, transform or build upon it. For any reuse or redistribution, researchers must make clear to others the licence terms of this work.

ACKNOWLEDGMENTS

I would like to thank my PhD supervisor Prof. Martin Buck for unmatched guidance, support and encouragement. It has been a very rewarding experience starting from not so visible PspF to playing with complicated image analyses for these “shiny bright spots”. I was always given the best of opportunities to attend prestigious conferences and space to develop my own ideas and methods. I would like to thank Dr. Liming Ying for helping me, providing the ever so important microscope and his imaging expertise. I also want to thank Dr. Goran Jovanovic for being so patient with me during my PhD, for being a great mentor and in pushing me to produce good work. Thanks a lot to Martin Buck, Goran Jovanovic and Liming Ying for their prompt comments during the editing process of this thesis too.

I would like to give a special mention to Andreas Bruckbauer for his continuous help with daunting Matlab based image analysis and the Matlab diffusion analysis scripts. I acknowledge Anne Vaahtokari along with Dr. Andreas Bruckbauer for support at the Super-Resolution Microscopy Core Facility (London Research Institute, Cancer Research UK). Thanks to Dr. Tchern Yeung Lenn, Povilas Užˇdavinys, Anthony Davidson and Nathan Sweeney for helping me with lab work and in progressing the research further. Thanks to Thomas Branch for technical help with Matlab.

I would like to thank Lucy Rayner for sharing and empathising with me the ordeals of thesis writing and for proof reading my thesis. Thanks to Anu for all those relaxing lunches and for scientific chit-chats. Thanks Ed for all the miscellaneous discussions, Chris W and Chris M for all the fun lab activities. And thanks to all other lab members for continuous positive feedback during the PhD

I would like to give my gratitude to mom and dad for their unconditional support and their belief in me; they inspire me to always excel in life and a special thanks to my baby brother Bhavya for motivating me to be a good student.

Big thanks to my husband Pranay for always being there through the thick and thin of the PhD. For giving me company late at night when I was writing and in shaping the thesis to its completion. A special mention to my in-laws for being there with their constant cheers and stimulus. Thanks to family and friends for reminding me that there is more to life than just work.

ABBREVIATIONS

AAA^+	ATPases associated with various cellular activities
A22	S-(3, 4-Dichlorobenzyl) isothiourea
aa	amino acid – Standard 1 and 3 amino acid codes are used throughout
ADP	Adenosine diphosphate
Ah	Amphipathic helix
ATP	Adenosine triphosphate
B. subtilis	*Bacillus subtilis*
bEBP	Bacterial enhancer binding protein
bps	Base pairs
CCCP	Carbonyl cyanide *m*-chlorophenyl hydrazone
CHAPS	3-[(3-Cholamidopropyl) dimethylammonio]-1-propanesulfonate
CL	Cardiolipin
CRP	Cyclic-AMP Receptor Protein
E. coli	*Escherichia coli*
EMCCD	Electron Multiplier Charged-couple Device
EDTA	Ethylenediaminetetraacetic acid
eGFP	Enhanced green fluorescent protein
GFP	Green fluorescent protein
EM	Electron Microscopy
EPEC	Enteropathogenic *Escherichia coli*
FRT	Flippase Recognition Targets
D	Diffusion Coefficient

Da	Apparent diffusion coefficient
Da	Dalton
DctD	C4 -dicarboxylic transport protein D
DMF	Dimethyl formamide
DMSO	Dimethyl sulphoxode
DNA	Deoxyribonucleic Acid
DNApol	DNA polymerase
DTT	Dithiothreitol
FP	Fluorescent protein
FPLC	Fast Protein Liquid Chromatography
FtsZ	Filamenting temperature-sensitive mutant Z
Fw	Forward primers
HD	Helix Domain
HRP	Horseradish peroxidase
HrpR	Pathogenicity locus probable regulatory protein R
HrpS	Pathogenicity locus probable regulatory protein S
HrpH	Hypersensitivity response secretion protein
HTH	Helix-Turn-Helix
IHF	Integration Host Factor
IM	Inner membrane
IPTG	Isopropyl β-D-1-thiogalactopyranoside
K	Kilo / 1000
MW	Molecular weight

µl	Microlitre
ml	Millilitre
mM	Millimolar
mRNA	Messenger RNA
ms	Milliseconds
MSD	Mean Square Displacement
mW	Milliwatts
NA	Numerical Aperture
nm	Nanometer
ng	Nanogram
NifA	Nitrogen fixation protein A
NorR	Anaerobic Nitric oxide reductase transcription regulator
NtrC	Nitrogen regulatory protein C
OD_{600}	Optical Density measured at 600 nm
OM	Outer Membrane
OMP	Outer-Membrane protein
ONPG	Ortho-Nitro phenyl-β-galactoside
OutD	Pectic enzymes secretion protein
Pi	Inorganic phosphate
PE	Phosphotidylethanolamine
PG	Phosphatidylglycerol
PGL	Phenolic glycolipids
PMF	Proton motive force

ppGpp	Guanosine tetraphosphate
Psp	Phage shock protein Response
PspA	Phage shock protein A
PspB	Phage shock protein B
PspC	Phage shock protein C
PspD	Phage shock protein D
PspE	Phage shock protein E
PspF	Phage shock protein F
PspG	Phage shock protein G
P*pspA*	*pspA* promoter
PpspG	*pspG* promoter
PulD	Pullulanase secretion envelope
Rcf	Relative Centrifugal Force
RNAP or E	RNA polymerase
RPc	Closed complex
RPi	Intermediate complex
RPo	Open complex
R-finger	Arginine finger
RR	Response regulator
Rv	Reverse primer
s	Seconds
SDS-PAGE	Sodium Dodecyl Sulphate Polyacrylamide Gel Electrophoresis
σ^{54}	Sigma 54 transcription factor

σ^{70}	Sigma 70 transcription factor
SMI	Single Molecule Imaging
smFRET	Single molecule Fluorescence Resonance Energy Transfer
SRH	Second Region of Homology
sRNA	small RNA
TFs	Transcription factors
TIRF	Total Internal Reflection Fluorescence
TRIS	Tris (hydroxyl-methyl) amino methane
UAS	Upstream activating sequences
V-PspF	Venus-PspF
V-PspA	Venus-PspA
V4R	Vinyl-4-reductase
WF	Wide field mode of illumination
WT	Wild type
YFP	Yellow fluorescent protein
Ypet	Yellow fluorescent protein optimised for Fluorescence resonance energy transfer
YscC	Yop proteins translocation protein
ZraR	Zinc resistance associated regulator

TABLE OF CONTENTS

LIST OF FIGURES, TABLES AND EQUATIONS

Figures in the thesis

Tables in the thesis

Equations in the thesis

CHAPTER 1

1 Introduction

The bacterial cell within its simple single-celled structural disguise entails a complex cellular matrix of DNA, RNA and proteins. These biomolecules interact and cross talk in the living cell in order to maintain homeostasis. In recent years the advances in fluorescence microscopy have made it possible to report on this complexity and heterogeneity within the bacterial cytoplasm in detail. Microorganisms like bacteria are characterised by their prokaryotic cell structure. The definition of prokaryote has three major criteria: 1) the absence of membrane-bound organelles performing specific cellular functions, 2) nuclear fission instead of mitosis, and 3) the presence of the peptidoglycan in the cell wall (Pelczar *et al*., 2003). A typical definition of bacterial cell has evolved considerably since its discovery – from being a "concentrated soup" and primitive amorphous vessel, to being highly organised with intricate sub-cellular organisations and architecture (Golding and Cox, 2006 and Whitman, 2009). With the help of numerous microscopic structural studies, morphological changes and typical structures were observed in bacteria such as pili, stalk, flagella, and division septa (Thompson *et al*., 2006; Whitman, 2009 and Lord *et al*., 2010). However, it was not until the 1990s that they were characterised as containing highly coordinated multi-protein assemblies such as the ring-like localisation of the cytokinetic protein (Filamenting temperature-sensitive mutant Z– FtsZ) at the mid-cell position (Bi and Lutkenhaus, 1991 and Chiu and Leake, 2012); clusters of the chemotaxis proteins at the poles of the cells (Alley *et al*., 1992); and the helical conformations of the actin-like bacterial cytoskeleton protein at the cell surface (Nilsen *et al*., 2005; Kim *et al*., 2006 and Chiu and Leake, 2012). All these remarkable investigations were done using powerful methods such as immunoelectron and immunofluorescence microscopy on fixed bacterial cells.

This thesis focuses on how single molecule imaging (SMI) methodology will permit quantitative analysis of functional multi-protein or transient complexes of a specific membrane stress response in *Escherichia coli (E. coli).* In bacteria a number of membrane associated stress response systems operate. The widely distributed Phage shock protein (Psp) system mounts an adaptation to inner membrane (IM) stress, by repairing the membrane damage and so conserving the proton motive force and energy production (Joly *et al*., 2010). Induction of Psp response is unique in the sense that it is dependent on the alternative σ factor – σ^{54} and requires a specific activator, bacterial enhancer binding protein (bEBP) (Joly *et al*., 2010). In this way Psp response is highly specific response and tightly regulated by specific Psp proteins for example, PspF, which is the bEBP that activates the transcription of various *psp* genes under stress inducing conditions. PspA regulates PspF activity during non-stress conditions and then functions as an effector during the stress conditions (Joly *et al*., 2010). A detailed knowledge of PspF and PspA localisations and their self-associations is a key to establishing how the response is controlled

and functions. With the help of SMI in live *E. coli* cells under non-stress as well as stress conditions, fluorescent protein fused to PspF and PspA, their localisations, 2D dynamics and stoichiometry will be characterised. *E. coli* will be used as a laboratory test tube for SMI experiments to elucidate the mechanism of control and activation of the Psp response in intact native cell environment (Chiu and Leake, 2011).

1.1 Escherichia coli

E. coli has a rod-shaped bacterial cell about 2 μm long and about 1 μm wide. It is a Gram-negative bacterium belonging to the enterobacteriaceae class of bacteria, and inhabiting the human intestinal tract (Pelczar et al., 2003). As a prokaryotic cell, *E. coli* lacks an internal organelle system and instead the supramolecular complexes carry out important functions from within the cell cytoplasm such as supporting the transport of proteins across the membrane, cellular mobility, signal transduction, replication and the regulation of gene expression. It has a plasma membrane that is essential to maintain cell viability and communication with external milieu, but it lacks any extensive internal membrane systems. The bacterial cell consists of a unique cell wall composed of peptidoglycan forming part of the periplasm, which is fairly complex chemically and morphologically. The bacterial cell envelope with the bacterial cytoplasm plays a very important role in the survival and regulation of bacterial cell growth in different stress inducing conditions. Gram-negative bacteria like *E. coli* have an additional protective outer membrane enclosing the inner membrane. The *E. coli* K12 wild type strain has been widely used in understanding the basic biochemistry of living cells driven by molecular machines.

1.1.1 The E. coli Bacterial Cell Envelope

As shown in Figure 1.1, the bacterial cell wall and cell membrane form what is called the bacterial cell envelope surrounding the cytoplasm. The Outer Membrane (OM), periplasm and an Inner Membrane (IM) form the bacterial cell envelope in Gram-negative bacteria. The inner membrane or cytoplasmic membrane includes approximately 75% phosphotidylethanolamine (PE), 20% phosphotidylglycerol (PG) and 5% cardiolipin (CL) (Cronan, 2003 and Romantsov *et al.,* 2007). Thus, anionic lipids dominate the composition of IM.

<u>The Outer Membrane (OM)</u>

The outer-membrane is made up of phospholipids, proteins (β-barrel proteins and lipoproteins) and polysaccharides; therefore in part it is also termed the Lipopolysaccharide (LPS), (Mulhradt and Golecki, 1975) Figure 1.1.The LPS forms the outer layer of the outer membrane interacting with the extracellular medium. LPS is sub-divided into three structural domains (Pelczar *et al*, 2003):

- O-specific oligosaccharide or O antigens which extend into the external medium like whiskers
- Core-polysaccharide are located at the membrane surface
- Lipid A: consists of fatty acids linked to N-acetylglucosamine and these are firmly embedded into the membrane

The LPS is important for several reasons. The core polysaccharide usually contains charged sugars and phosphate ions, which contribute to the negative charge on the bacterial surface. The core polysaccharide and O-specific polysaccharide are variable and species-specific. Lipid A is often toxic and as a result the LPS can act as an endotoxin. The OM is anchored to the underlying peptidoglycan layer using Braun's lipoprotein. The OM also contains lipoproteins and outer membrane proteins. The OM can allow smaller molecules to pass through such as oligosaccharides, peptides by means of channels made of outer membrane proteins spanning the membrane called porins.

The Periplasm

The periplasm contains several different classes of proteins involved in varied cellular processes such as substrate transport, degradation of nutrients like hydrolytic enzymes, and chemoreceptors involved in the chemotaxis response. The polysaccharide peptidoglycan constitutes an important component of the periplasm, formed by layers of alternating N-acetylglucosamine and N-acetylmuramic acid. The individual layers are inter-connected by peptides containing the amino acids D-alanine, L-alanine, D-glutamic acid and di-aminopimelic acid. The main function of peptidoglycan is to confer rigidity to the bacterial cell.

The Inner Membrane (IM)

The inner membrane (also called plasma membrane) forms a barrier between the cytoplasm and the periplasm. The exchange of proteins from the cytoplasm across the membrane to the external environment is mediated by various specific and non-transport mechanisms localised in the inner membrane. The exchange is highly selective and often requires active energy-dependent transport of substrates. The mislocalisation of outer membrane and effector proteins to the inner membrane causes damage to the inner membrane. The consequence of the inner membrane damage is the activation of specific membrane stress responses.

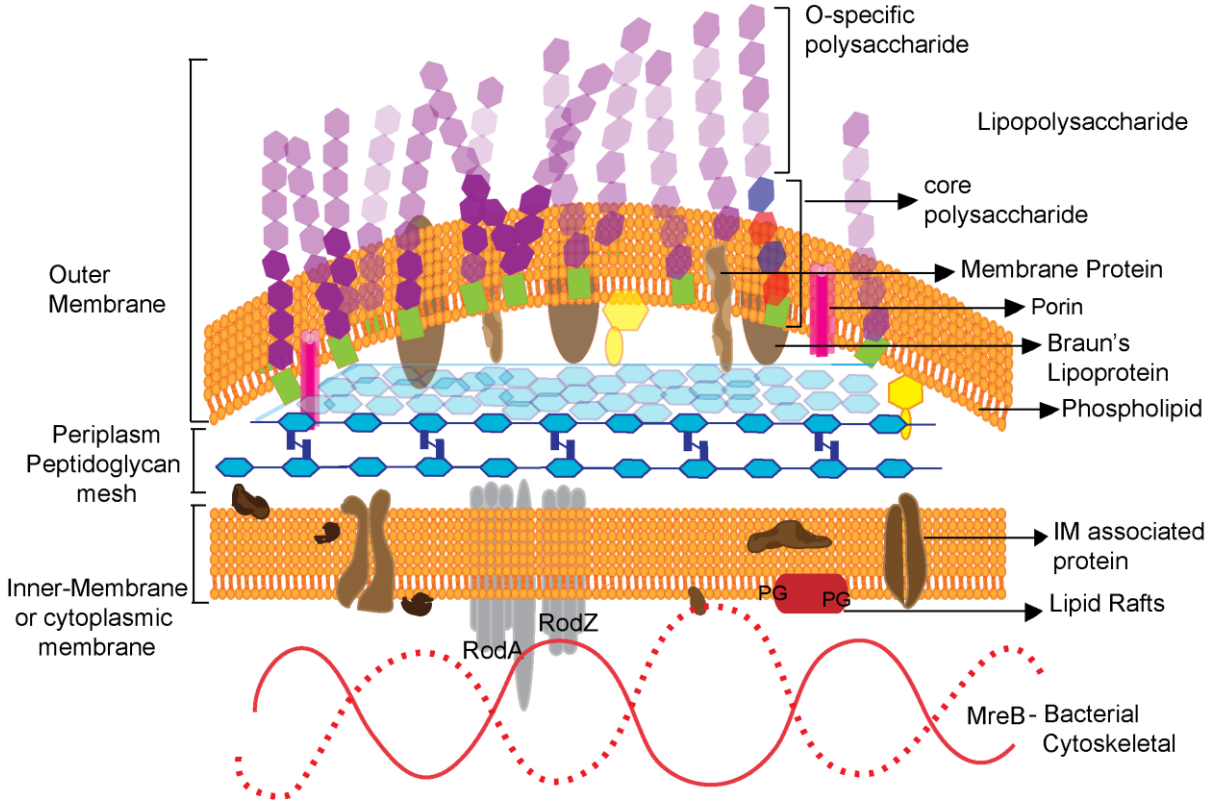

Figure 1.1 **Cell Envelope of Gram-Negative Bacteria.** The cell envelope of bacteria consists of the OM periplasm and the IM. The OM is in direct contact with the extracellular milieu and contains proteins embedded, phospholipids and the LPS. The periplasm underneath contains proteins and layers of peptidoglycan that confer rigidity to the cell. The IM separates the cytoplasm from the periplasm. It consists of a bilayer of phospholipids as well as proteins either embedded or associated with the bilayer. It also consists of peptidoglycan synthesis proteins, morphogenetic proteins such as RodZ, bacterial cytoskeletal proteins MreB and potential lipid rafts with anionic lipids such as phosphotidylglycerol.

The cell envelope, along with being an energy generator, also mobilizes secretory and protein translocation pathways. Therefore, any physical or chemical damage to the cell envelope directly induces highly specific stress responses in the cell to counteract the damaged cell envelope.

1.1.2 Bacterial Cytoskeletal Network

The bacterial cell wall, made up of peptidoglycan, had been known to confer rigidity to the cell and dictate cell shape. In a classic experiment, Henning *et al* (1972) showed that the action of lysozyme on the *E. coli* cell wall resulted in the spherical morphology of the cells. For many years, it was understood that peptidoglycan was the major determinant of cell morphology and it was assumed that an intracellular cytoskeleton was absent in bacteria. However, studies in *E. coli* and *B.subtilis* have shown the presence of an actin-like filament protein called MreB (Ausmees *et al*., 2003; Salje *et al*., 2011 and van den Ent *et al*., 2010), that forms an integral part of the bacterial cytoskeleton and plays a crucial role in maintaining cell shape and integrity. The bacterial cytoskeleton has been described to be dynamic and

multi-faceted, controlling cell shape, growth and signalling in the bacterial cells. The main component of the cytoskeletal system in *E. coli* is MreB protein and it maintains the cell shape by positioning the trans-membrane and periplasmic cell wall synthesising proteins (Löwe *et al*., 2004; van den Ent *et al.,* 2010 and Salje *et al*., 2011). MreB forms spiral shaped bands underneath the inner membrane (Gitai *et al*., 2005 and Salje *et al*., 2011) as shown in the Figure 1.1. The MreB protein has also been shown to have a role in protein movement and trafficking within *E. coli* cells. The MreB spirals are associated with the larger network of peptidoglycan synthesis proteins such as MraY, MurB, MurC, MurE and MurG; all exhibit a specific subcellular localisation governing the cytoskeletal interactions (White *et al.,* 2010). In the same way it has been shown that morphogenic proteins including RodA, RodZ and MreD determine the MreB localisation and its point of contact with the IM (White *et al.,* 2010). The bacterial cytoskeleton along with the bacterial cell envelope is implicated in many cellular activities such as energy conservation and chemotaxis. The various proteins interact and cooperate to establish the intracellular cytoskeletal network in order to keep the cell and cell envelope viable.

1.1.3 Protein Translocation in bacteria

Many of the cellular proteins (at least 30%) are destined to have functions in the cell envelope or external milieu (Driessen and Nouwen, 2008). The transport occurs through the hydrophilic channel that not only translocates secretory proteins but also integrates membrane proteins into the IM or OM (Matlack *et al*., 1998). There are two fundamental translocation pathways in bacteria – the Sec pathway and Twin-arginine translocation pathway shown in Figure 1.2. There are some common key features that distinguish between the Sec and Tat pathway for membrane protein export (DeLisa *et al*., 2004).

- The Sec pathway is comprised of a heterotrimeric, highly conserved membrane channel - SecYEG and peripherally bound motor protein SecA which is either ribosome or ATP-dependent. This channel translocates proteins recognised as a ribosome-bound nascent chain by the signal recognition particle (SRP) or by the secretion-dedicated chaperon SecB (Figure 1.2). On the other hand, the Tat pathway translocates the leader peptide with a signature arginine-arginine (RR) dipeptide. The Tat pathway consists of Tat (A/E) BC proteins, which share no homology with the SecYEG complex.
- The Tat pathway is able to transport modified proteins with tertiary or quaternary structures across the membrane (Figure 1.2).
- The Sec pathway is highly energy dependent requiring ATP hydrolysis while the Tat pathway is solely dependent on the proton motive force ($\Delta\mu\ H^+$).

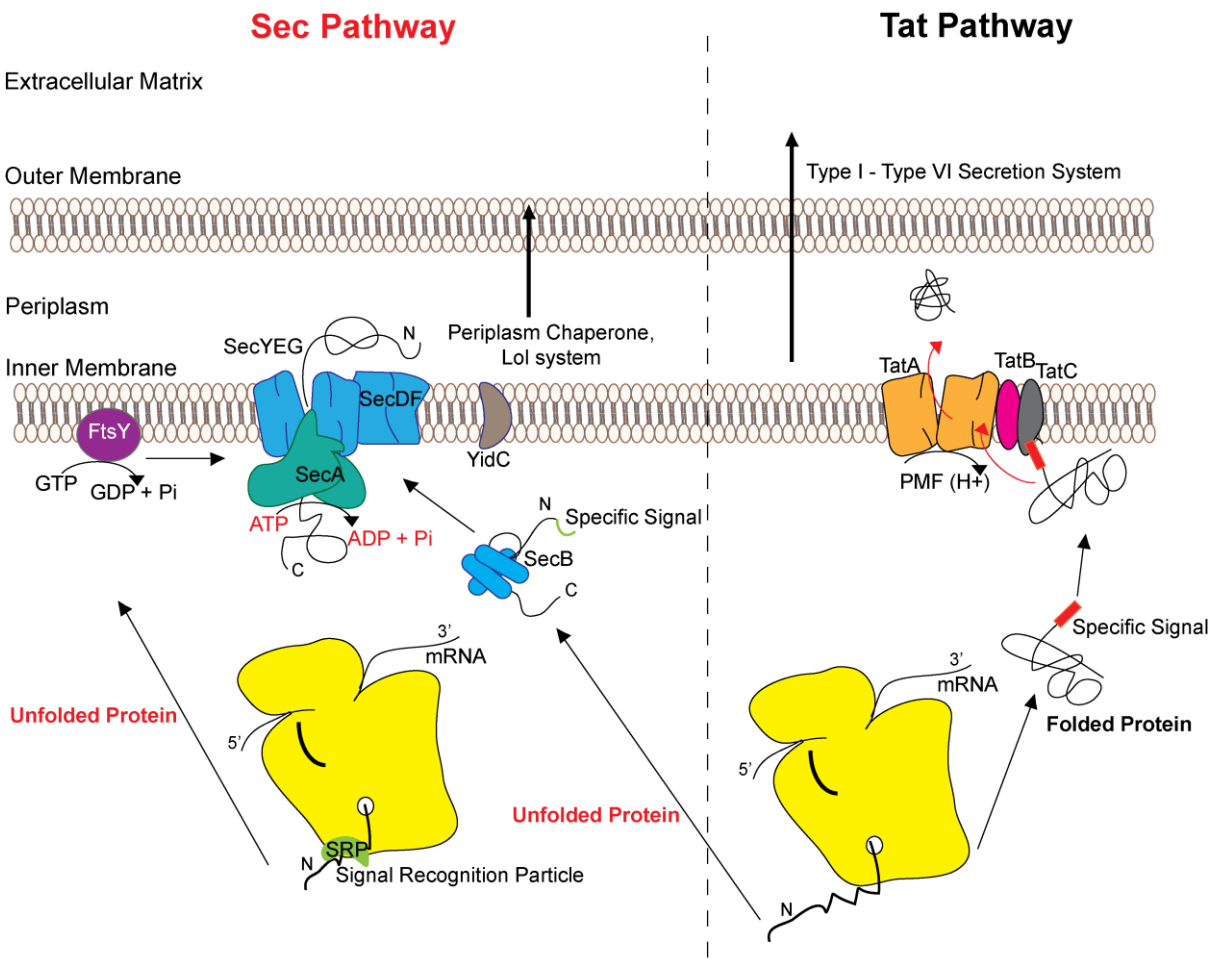

Figure 1.2 **Protein translocation pathways**: There are two different protein translocation pathways in *E. coli* – the Sec and Tat pathways. As shown in the Figure, the Sec pathway usually secretes the primary protein with a specific signal across the inner-membrane. The primary protein with specific signal is associated with SecB and secreted across the SecYEG channel utilising ATP via SecA. Proteins secreted by the Sec pathway are treated by periplasmic chaperones. On the other hand, Tat pathway secretes folded proteins across the inner membrane. Proteins are transported by specific secretion systems, defined as Type I to VI, across the outer-membrane adapted from Driessen and Nouwen, 2008.

These are the main mechanisms for the translocation of the proteins across the IM. However, the Outer Membrane Proteins (OMPs) to be inserted into the OM follow a different pathway. Most of the OMPs are transported into the periplasm in the unfolded state by the Sec pathway, after which the periplasmic chaperones facilitate their folding and transport, but the full mechanism of translocation is not fully known (Mogensen and Otzen, 2005). Characterised periplasmic chaperones include SurA and FkpA. The protein secretion into the extracellular milieu is further mediated by many different kinds of secretion mechanisms. So far, six different types have been characterised in bacteria which are classified as Type I to Type VI secretion systems (TSS). The TSS is essential for pathogenesis and virulence in many pathogenic bacteria, in which the toxins or virulence factors are translocated from cytoplasm by the Sec or Tat pathways. Subsequently, the proteins are exported out using highly complex machinery spanning

the IM to the OM (Filloux *et al*., 2008). All these protein translocation and export pathways across the bacterial membrane can affect the membrane integrity and thereby cause different kinds of envelope stress in the bacteria (De Lisa *et al*., 2004 and Mehner *et al*., 2012).

1.1.4 Envelope Stress Response

E. coli has at least five known stress responses to monitor the envelope homeostasis (see Table 1.1); σ^E, Conjugative pilus expression (CpX), Bacterial adaptive response (Bae), Phage shock protein (Psp) and Regulator of capsular synthesis (Rcs). The Cpx, Bae and Rcs responses are controlled by two-component systems. Two-component based bacterial signal transduction responses to stress are very common (Ruiz and Silhavy, 2005; Rowley *et al.,* 2006 and Darwin *et al.,* 2005). Most of these envelope stress responses are activated by specific signal transducers and involve an array of proteins such as sensor kinases, membrane repair proteins and proteases (Lima *et al*., 2013).

STRESS RESPONSES	STRESS STIMULI	MECHANISM: PROTEINS INVOLVED
σ^E stress response	- Overexpression of OMPs (Outer membrane proteins) such as OmpX, OmpT - Exposure to ethanol, DTT, puromycin - Heat shock, detergents, Osmotic and oxidative stress.	The RseA (Sigma-E factor regulatory protein)-(σ^E)-cytoplasmic-RseB periplasmic, upon stress this complex is cleaved off by the IM protease DegS (Serine endoprotease) to release RseA-(σ^E), which is further sequestered at ClpXP by SspB (Stringent starvation protein B) to release σ^E from RseA to activate the specific genes involved in translating proteins for folding and degradation (Lipinska *et al.,* 1988; Erickson and Gross, 1989 and Danese and Silhavy, 1997). This response is crucial for virulence in some Gram-negative bacteria such as *Salmonella typhimurium, Vibrio cholera* (Dartigalongue *et al.,* 2001)

Rcs- Regulator of capsular synthesis Phosphorelay system	- Overproduction of envelope proteins - Antimicrobials - Biofilm associated stress	The response is mediated by phosphorelay which involves RcsC-RcsD-RcsB. RcsB is a response regulator that activates the target genes with post-phosphorylation (Huang *et al.*, 2006).
Psp response	- Mislocalised secretins such as pIV - Defects in secretion system - Phage invasion - Ethanol treatment. - Ionophore treatment.	An array of proteins are involved in eliciting and establishing the response, signal sensors PspBC, membrane repairing effector PspA and transcriptional activator (bacterial enhancer binding protein) PspF (Brissette and Russe*l* 1990; Becker *et al*., 2005; Darwin, 2005 and Joly *et al.,* 2010).

Cpx system- Conjugative pilus expression	- Cell envelope alterations e.g. cell adhesions. - P-pili synthesis - Misfolded envelope proteins - Overproduction of lipoprotein NlpE - Alkaline pH.	The two-component response system involves - IM sensor kinase (CpxA), cytoplasmic response regulator (CpxR) and an additional cytoplasmic regulator of CpxA called CpxP inhibiting its activity. Under stress states CpxA is released from CpxP, autophosphorylated using ATP, and further activate CpxR which in turn upregulates or downregulates gene expression from the *cpx*-regulon. Upregulated genes include genes involved in protein secretion (*secA*) and protein folding (*dsbA*), lipid biosynthesis and genes involved in virulence or adherence, while downregulated genes include those involved in chemotaxis, motility and cell division (Danese *et al.*, 1995; Raivio and Silhavy, 1997 and Rowley *et al.,* 2006).This response is also essential for pathogenesis for many Gram-negative bacteria as well such as *Salmonella, Shigella, Vibrio and EPEC (*Rowley *et al.,* 2006)
BaeSR system	- Stress such as spheroplast formation - Stress in the presence of Antimicrobials such as novobiocin	The Two-component system comprising IM sensor kinase BaeS and the response regulator BaeR (Baranova and Nikaido, 2002 and Hirakawa *et al.*, 2005)

Table 1.1 The different envelope stresses found in enteric bacteria.

The dissipation of pmf due to extra-cytoplasmic membrane stress and the change in the physical and chemical properties of the membrane activates the Psp stress response. This thesis work elucidates the Psp response and describes its regulation at the single molecule level with fluorescence microscopy in live *E. coli* cells.

1.2 Bacterial Gene Regulation

In a bacterial cell, gene regulation and bacterial cell envelope components are closely correlated with respect to regulation of the stress responses and their subsequent activation with the stress stimuli and therefore have to constantly communicate with each other, especially under environmental stress conditions. The stress responses listed in the Table 1.1 are tightly regulated at the genetic level. Therefore, it is important to understand the role of gene regulation that triggers specific stress responses in the presence of external stimuli. Bacterial cells have exploited these regulatory checkpoints efficiently in order to adapt to changing growth regimes (Buck *et al*., 2000). These highly specific responses not only enable cells to survive in stress-inducing conditions, but also maintain the expression of housekeeping genes. It is vital for cells to conserve energy and resources, whilst managing cell maintenance under stress inducing conditions with the help of specialised pathways.

1.2.1 Bacterial Transcription Initiation

One of the central processes of gene regulation is bacterial transcription driven by multi-subunit RNA polymerase (RNAP) (Friedman and Gelles, 2012 and Lee *et al.,* 2012). In all eubacteria, all transcription uses the evolutionarily conserved catalytically active core RNAP made up of two α, β, β', ω subunits (Buck *et al*., 2000 and Shingler 2010). The most modulated and rate-limiting step of bacterial transcription is transcription initiation, often the target for anti-microbial therapy (Darst, 2004; Friedman and Gelles, 2012). Initiation of transcription is mediated by the dissociable sigma (σ) factor that associates with the core RNAP, resulting in holoenzyme with reprogrammed DNA binding affinity. This is the first step in transcription initiation, called promoter recognition, in which holoenzyme RNAP (closed complex-RPc) recognizes promoter elements upstream to the transcription start site (Shingler 2010; Lee *et al*., 2012 and Friedman and Gelles, 2012).

All bacterial species have a housekeeping σ^{70}-factor responsible for transcription from generic promoters, and some alternate σ-factors that redirect RNAP to the specific promoters required for different cellular functions (Shingler 2010 and Bush and Dixon, 2012). Accessory factors that can modulate RNAP activity include promoter strength, small effector molecules (such as guanosine 3', 5' bisphosphate, ppGpp), particular accessory promoter elements (such as UP elements located 20 bps upstream of the promoter), and some other small proteins such as DksA (RNA polymerase binding

transcription factor) that directly bind to the RNAP (Shingler 2010; Bush and Dixon, 2012 and Zakrzewska and Lavery, 2012).

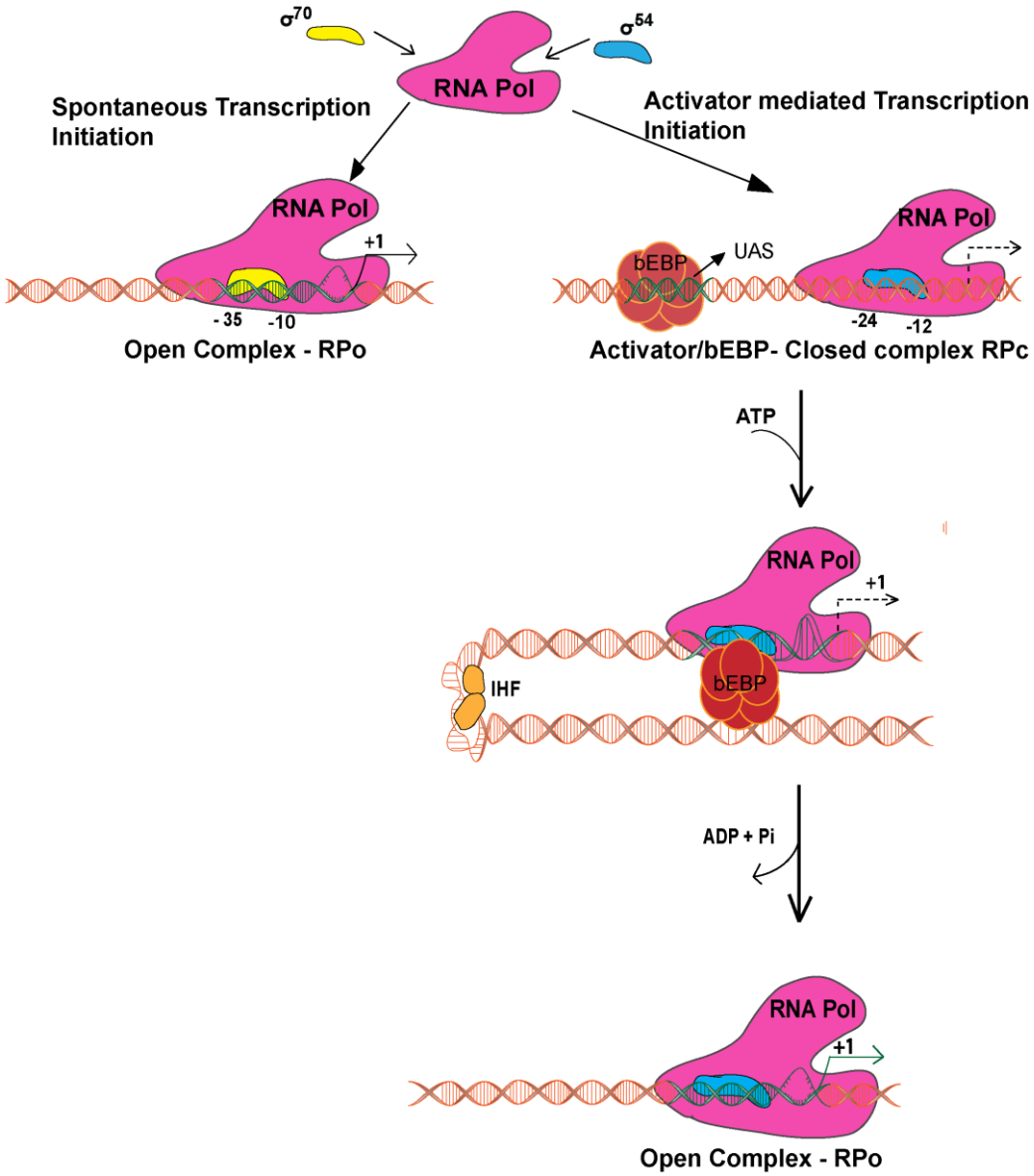

Figure 1.3 **Bacterial Transcription Initiation**: (adopted from Review by Joly *et al*., 2010). The Figure explains the differences between σ^{70} and σ^{54} dependent transcription. σ^{70} dependent transcription is activated by the binding of σ^{70} to the closed complex. σ^{54} dependent transcription resembles eukaryotic transcription with activation of the closed complex facilitated by a bEBP, in this case represented by a hexameric ring, which catalyses change in confirmation of the closed to open complex via ATP hydrolysis.

Since the discovery of σ-factors, it has become very clear that these proteins are central to the function of the RNAP holoenzyme. In addition to double stranded DNA promoter recognition and binding, σ-factors are closely involved in promoter melting and inhibit non-specific initiation (Joly *et al*., 2010; Bush and Dixon, 2012 and Lee *et al*., 2012). Some σ-factors are targets for activators, and control early transcription initiation through promoter clearance and release from RNA polymerase. The principal σ-

factor in *E. coli* is σ^{70}, a 613 – a.a protein (Paget and Helmann, 2003 and Lee *et al*., 2012). The major class of σ^{70}-RNAP holoenzyme (closed complex, RPc) recognizes -35 (TTGACA) and -10 (TATAAT) promoter sequences upstream from the transcription start site +1 and constitutively initiates transcription by forming an RNAP-promoter DNA open complex (RPo) as shown in the Figure 1.3. With the help of single molecule fluorescence resonance energy transfer (smFRET) between the β and β' subunits of RNAP showed that the constitutive conformational changes within the clamp sites are inherent to transcriptional initiation, with DNA-loading propagating DNA interaction with the RNAP holoenzyme active-centre (Chakraborty *et al*., 2012). These mechano-chemical conformational changes within RPo lead to DNA unwinding and formation of a melted DNA bubble between the -10 and +2 elements encompassing the promoter sites (deHaseth *et al*., 1998; Ishihama, 2000 and Shingler, 2010) as shown in Figure 1.3. Besides the σ^{70} factors many more σ factors are present in bacteria usually involved in the activation of stress responses. The presence of alternative σ-factors in bacteria varies widely between species and largely reflects upon the lifestyle of the bacterium. The gut commensal *E. coli* has seven different σ-factors whereas some soil and water bacteria, living in extreme conditions, could possess many more σ-factors. For example, *Streptomyces coelicolor* have in excess of 60 alternate σ-factors (Shingler, 2010). Intracellular pathogens such as *Mycobacterium genetalium*, which occupy a relatively constant environment, possess a single σ-factor.

Besides σ^{54}, all the other σ-factors belong to the σ^{70} class (such as σ^{38}, σ^{32}, σ^{28}, σ^{24} and σ^{18}) (Bush and Dixon, 2012). σ^{54} (also called σ^{N}) differs both in amino acid sequence, promoters and transcription mechanism from the σ^{70} class whilst binding the same core RNA polymerase as shown in Figure 1.3. The σ^{54}-dependent transcription relies on bacterial enhancer binding protein (bEBP) to catalyse the conversion of the RPc to RPo (Morett and Segovia, 1993 and Buck *et al*., 2000; Browning and Busby, 2004; Joly *et al*., 2010; Shingler *et al*., 2010 and Bush and Dixon, 2012). The focus of this report is bacterial σ^{54}-RNA polymerase, which is at the centre-point of sophisticated signal transduction pathways.

1.2.2 σ^{54}-Dependent transcription

1.2.2.1 σ^{54} - its occurrence and importance

The bacterial σ^{54} dependent systems are of general importance because they display some similar functional properties to many eukaryotic RNA polymerase II promoters that are activated through transcriptional enhancers and bacterial enhancer binding proteins (bEBP) (Buck *et al*., 2000; Joly *et al*., 2010 and Mehta *et al*., 2013). σ^{54} dependent promoters are found in 60% of all bacterial species and drive tightly regulated genes used for a wide variety of biological stress associated functions (e.g. pathogenicity, persistence), bio - geo transformations important for the nitrogen, carbon and sulphur cycles in the environment, energy metabolism, RNA modification, chemotaxis, flagellation, electron transport, response to heat shock and phage shock forms of extracytoplasmic membrane stresses and

even expression of alternative σ-factors (Buck *et al*., 2000; Reitzer and Schneider 2001 and Wigneshweraraj *et al*., 2008). Besides being essential to enteric bacteria, various genome-sequencing projects have revealed that the open reading frames encoding σ^{54} are found in diverse bacteria such as Gram-positive *Bacillus subtilis*, to *Planctomyces limnophilus* (Buck *et al*., 2000, Wigneshwaraj *et al*., 2008; Shingler, 2010 and Bush and Dixon, 2012). σ^{54} transcription dependent genes are also found in extreme thermophile, obligate intracellular pathogens, spirochetes and green sulphur bacteria (Bush *et al*., 2000; Joly *et al*., 2010 and Shingler, 2010). σ^{54} is also found in many pathogenic bacteria, such as in *Pseudomonas aeruginosa*, in which σ^{54} gene (*rpoN*) - knockout causes reduced virulence. Even in the plant pathogen *Pseudomonas syringae,* σ^{54} controls virulence related genes called *hrp* (Buck *et al*., 2000; Bush and Dixon *et al*., 2012 and Jovanovic *et al*., 2012). Most bacteria contain several alternative σ-factors belonging to the σ^{70} class, while more than one σ^{54} rarely coexists in the same organism. There are a few exceptions such as *Bradyrhizobium japonicum* and *Rhodobacter sphaeroides* with two *rpoN* genes. Each enhancer protein is induced by a specific signal that further activates the σ^{54}-dependent transcription of specific genes in response to the stress conditions (see Figure 1.3).

1.2.2.2 σ^{54} structural determinants

σ^{54}-RNAP ($E\sigma^{54}$) recognizes distinct promoter sequences located at positions -24 and -12 upstream relative to the +1 transcriptional start site (consensus TTGGCACG-N4-TTGC) (Barrios *et al*., 1998 and Shingler 2010). The σ^{54} has three main regions classified as – Region I (RI), Region II (RII) and Region III (RIII) based on function instead of structure as shown in the (Buck *et al*., 2000; Shingler 2010 and Bush and Dixon, 2012).

The N-terminal of RI is the regulatory domain of σ^{54} that binds to the -12 promoter element to form the RPc (Shingler 2010 and Bush and Dixon, 2012). RI plays an important role in keeping a check on the switch from RPc (closed complex) to RPo in the absence of bEBP (Figure 1.3 and Figure 1.4). Upon activation with the bEBP in the presence of an inducing signal, Region I has been shown to bind to the ATP hydrolysing domain of the activator to catalyse the switch from closed to open complex (Buck *et al*., 2000; Browning and Busby, 2004; Bush and Dixon, 2012 and Lee *et al*, 2012). It has been shown with *in vitro* studies that the deletion of σ^{54} RI bypasses the requirement of an activator if pre-melted DNA template is added in solution (Buck *et al*., 2000 and Bush and Dixon, 2012).

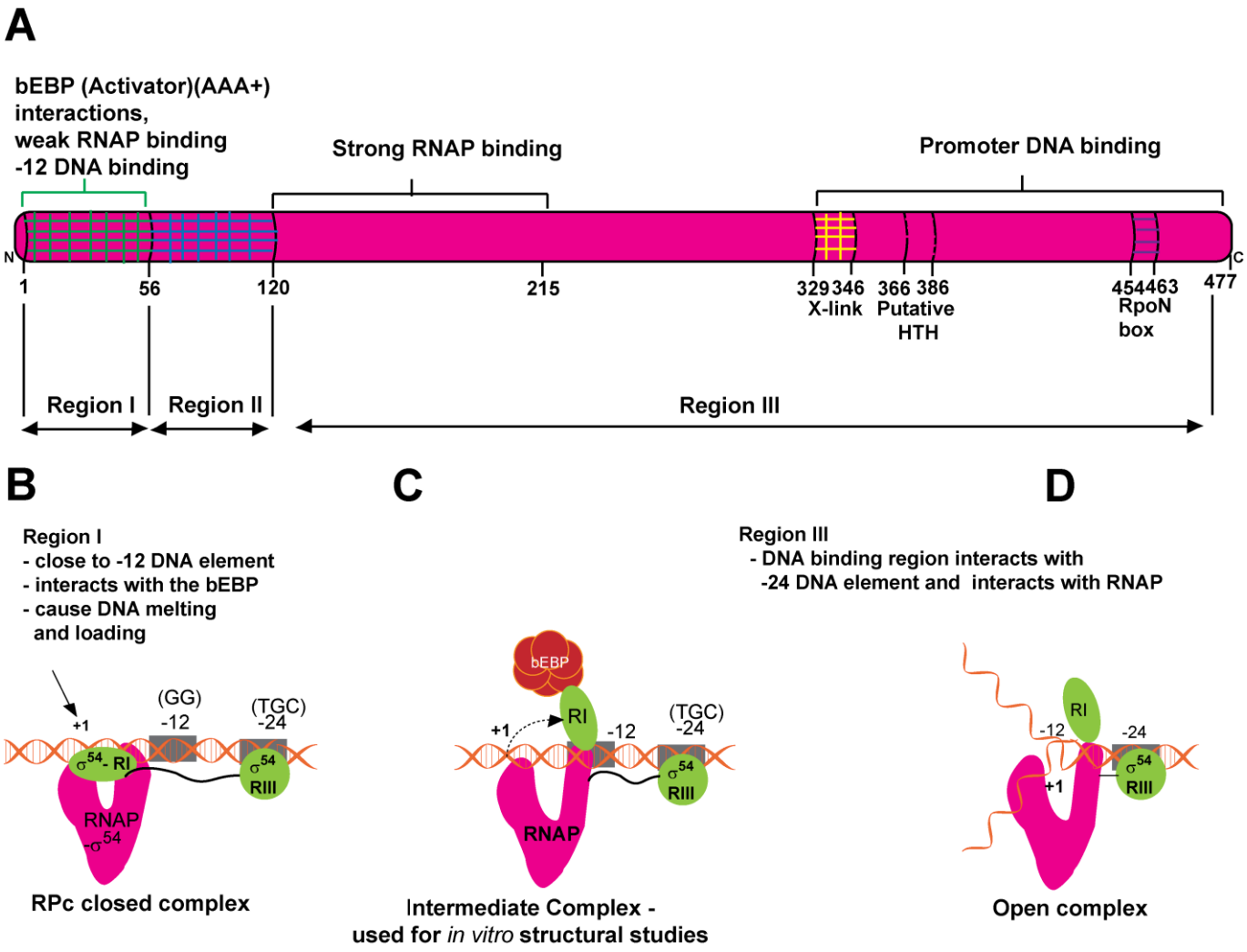

Figure 1.4 **σ^{54} domains and their intracellular interactions:** Adopted from Bush and Dixon, 2012. (A) Domain organisation of *E. coli* σ^{54} - σ^{54} has 477 aa and consists of 3 regions (regions I to III). Region I interacts with the activator of transcription and the -12 DNA elements. Region III has major core RNAP binding regions as defined in the Figure (120a.a to 215a.a). Region III also consists of promoter DNA binding cross-link domain with the putative helix-turn-helix motif and RpoN box. Region II is often acidic and often absent. The schematic diagram represents the movement of the regions of σ^{54} with respect to the closed complex and the bEBP. (B) The diagram represents the closed complex, where the σ^{54} region I (RI - density) binds RNAP and obstructs DNA loading and henceforth melting. (C) Illustrates the intermediate complex, where a bEBP ring binds to σ^{54} relocating the RI. Subsequently region III comes closer; RIII drags the -24 element downstream along with the -12 element. All these movements enable DNA melting and loading into the active centre of RNAP. (D) The formation of open complex catalysed by bEBP with the respective regions of σ^{54} as shown in this schematic diagram.

RII varies in different species and has been shown to play a part in DNA binding and melting (Figure 1.4). The C-terminal of RIII is well conserved across species and binds the promoter DNA. RIII consists of DNA cross-linking motif and RpoN box. Recently nuclear magnetic studies of the RpoN box have identified a specific helix-turn-helix motif that binds the -24 promoter element (Figure 1.4) (Shingler, 2010). RIII also contains determinants that bind to the core RNAP (Ishihama, 2000 and Bush and Dixon, 2012) (Figure 1.4). The spatial rearrangements in RI during activation, including binding to the -12

promoter sequences have been studied using FRET and proximity based assays have confirmed changes in the regulatory centre of σ^{54} at the point of RPo formation (Wigneshweraraj *et al*., 2001;Wigneshweraraj *et al*., 2008; Bose *et al*., 2008 and Bush and Dixon, 2012). All this remodelling with the help of nucleotide binding and ATP hydrolysis, from closed complex to open complex, can be defined as the second paradigm for bacterial transcription (Buck *et al*., 2006).

1.3 bEBP - Dependent Activation

The bacterial enhancer binding proteins (bEBPs also called σ^{54} activators) (Patel & Latterich, 1998; Bose *et al*., 2008; Shingler 2010 and Joly *et al*., 2010) belong to a class of ATPase associated with other cellular activities (AAA^+), also termed mechano-chemical enzymes. This is one of the most abundant classes of proteins, accounting for 10-18% of predicted gene products in prokaryotic and eukaryotic genomes (Iyer *et al*., 2004). bEBPs are modular proteins, usually with three domains, an N-terminal regulatory domain, central AAA^+ domain and C-terminal DNA binding domain (Rappas *et al.,* 2005, 2006; Joly *et al.,* 2010 and Shingler, 2010) (see Figure 1.4). The central AAA^+ core domain has motifs involved in signal responsive control and the C-terminal domain mediates DNA binding. The AAA^+ module is found in a wide range of proteins, converting the energy derived from ATP hydrolysis to mechanical force on the interacting substrates and driving many different processes such as protein refolding and proteolysis, initiation of DNA replication and DNA helicase activity and cellular cargo transport pathways (Shingler 2010 and Bush and Dixon, 2012).

In the case of bEBPs the mechanical force is probably used to cause conformational changes in the RPc to RPo, which is transcriptionally competent (Ogura & Wilkinson, 2001; Chen *et al.,* 2007 and Joly *et al*., 2010). bEBPs possess seven highly conserved regions (C1-C7) (Wigneshwaraj *et al*., 2008; Shingler 2010 and Bush and Dixon, 2012) including Walker A and Walker B motifs for ATP binding and hydrolysis, and the sensor I and sensor II regions (Schumacher *et al*., 2006; Shingler 2010) as shown in the Figure 1.7. In Rappas *et al*., 2005 the interface between $PspF_{1\text{-}275}$ and σ^{54} was studied in detail by structural methods such as cryoelectron microscopy to reveal intramolecular conformational changes driven by ATP hydrolysis in the mobile L1 loop (see Figure 1.7). The L1 loop contains highly conserved GAFTGA-motif; a signature structural element of the bEBPs (Rappas *et al*., 2005; Bose *et al*., 200; Wigneshwaraj *et al*., 2008 and Joly *et al*., 2012). The structural data from the bEBP nitrogen regulatory protein C1 (NtrC1) from *Aquifex aeolicus* bEBP show that the GAFTGA-LI loop forms a raised rim proximal to the active site in the active ATP-bound state and relaxed and flattened in the ADP-bound state (Doucleff *et al*., 2007 and Chen *et al*., 2007; 2010). Similar spatial movement of the GAFTGA-L1 loop has been shown for PspF interacting with σ^{54} in *E. coli*. It has also been shown with structural studies in Rappas *et al*., 2005, 2006 and Bose *et al*., 2008 that at least two GAFTGA-LI regions contact

RPc. Still, the exact stoichiometry and interface of the bEBP with RPc is unknown. bEBPs specifically bind to the upstream activating sequences (UAS) positioned 80 to 200 bps from the promoter (Figure 1.3 and 1.4) through the C-terminal DNA binding domain (Kustu *et al.,* 1989; Jovanovic *et al.*, 1996 and Studholme & Dixon, 2003). This DNA binding domain confers specificity on the bEBP for a specific target enhancer. These enhancer sequences are two adjacent copies of long inverted repeats for binding dimeric bEBPs. It has been established that binding to these target enhancers tends to stimulate the formation of a stable multimeric ring of active bEBP (Rappas *et al*., 2007 and Schumacher *et al*., 2006). The oligomerisation to higher order structures (usually hexamers or heptamers) and nucleotide binding determines the intramolecular and sub-module interactions during structural re-arrangements (Ogura & Wilkinson, 2001; Joly et al., 2006; Schumacher et al., 2006; Burrows et al., 2008, 2009; Joly et al., 2008; Zhang et al., 2012 and Batchelor et al., 2009).The active multimeric complexes also proposed at some promoters to introduce DNA bending around the bEBP-RPc that stabilises the RPc complex (e.g. in E. coli NtrC at the glnA promoter, PspF at the pspA promoter) (De Carlo et al., 2006 and Shingler 2010). Tucker et al., 2010 characterised NorR to be completely dependent on binding to all its three UAS to be able to form an active ATPase competent multimeric ring. However, bEBPs lacking the DNA binding domain are either truncated forms or in nature capable of activating σ^{54}-dependent transcription from solution (Jovanovic et al., 1996, 1997; Joly et al., 2010 and Shingler, 2010). DNA looping and bending is often facilitated by an Integration Host Factor (IHF) that further assists bEBP to contact the RPc (Morret & Segovia, 1993; Jovanovic and Model, 1997; Dworkin et al., 1998 and Huo et al., 2009) and to remodel RPc to RPo as shown in the Figure 1.3 and Figure 1.4 (Morett & Buck, 1989; Buck et al., 2000 and Bose et al., 2008). As reviewed in Shingler 2010, many global regulators such as ppGpp (Guanosine tetraphosphate), DksA (the DnaK suppressor) in addition to bEBPs, IHF and RPc add another layer of signal-responsive input to the σ^{54}-dependent transcription.

1.3.1 Global regulators: positive and negative impact on σ^{54} promoters

Global regulators can regulate the different states of bEBP – RPc such as promoter binding or activation to RPo. There are many different types of global regulators:

- A class of global regulators that naturally interfere with or establish the obligate interactions between σ^{54}-RNAP, target DNA and bEBPs. For example, the cyclic-AMP receptor protein (CRP) binds to the σ^{54}-*glnHp2* promoter of *E. coli* and acts as a negative regulator. CRP in its bound state to the promoter induces DNA bending and prevents the contact between NtrC and RPc (Mao *et al*., 2007).

- The binding of PspF to its UAS within the *psp* promoters auto-regulates its own expression. The PspF binding to the UAS hinders the accessibility of σ^{70}-RNAP to the *pspF* promoter (Jovanovic and Model, 1997 and Dworkin, 1996).
- The Integration Host Factor (IHF) stimulates σ^{54}-dependent transcription via DNA bending at specific sites. IHF-induced DNA bending stabilises the interaction between bEBP and RPc. The DNA bending also adds specificity to the bEBP - catalysed activation from the σ^{54}-specific promoters (Jovanovic and Model, 1997; Shingler, 2010 and Bush and Dixon, 2012). The specificity in transcription initiation mediated by IHF is due to the sharp bend introduced in the DNA that blocks non-specific interactions and thereby ensures activation of only specific promoters. For example, the IHF facilitates topological changes in the DNA - aided binding of PspF to *pspA-E* promoters. As a result, the yield from the *psp* promoters increases (Jovanovic and Model, 1997).
- ppGpp and DksA have also been shown to increase the efficiency of σ^{54}-dependent transcription (Sze and Shingler, 1999 and Shingler, 2010). ppGpp and DksA both bind to the active-centre of RNAP, bringing structural changes within the RNAP (Shingler, 2010). ppGpp binding to RNAP can result in transcriptional inhibition at specific stringent σ^{70} promoters, or stimulate some σ^{54} promoters. DksA can amplify the effect of ppGpp at some specific promoters (Österberg *et al*., 2010 and Shingler 2010). DksA accesses the active site of RNAP where it mediates long-range structural changes within RNAP that alter interactions with the -6 and +6 σ^{70} promoters (Shingler, 2010). The DksA binding to RNAP makes it more susceptible to ppGpp regulation. The DksA amount in the cell is constant, while amounts of ppGpp fluctuate and thus prepare RNAP for specific transcriptional regulation (Shingler, 2010). The intracellular levels of ppGpp increase during amino acid starvation, carbon and nitrogen limitations as well as many environmental physical and chemical stresses that reduce growth rates.

  Many processes and responses that are involved in counteracting nutritional and environmental stresses (e.g. phage shock response, nitrogen starvation) are controlled by σ^{54}-dependent promoters. Thus, ppGpp could have a major impact on σ^{54}-dependent transcription (Sze and Shingler, 1999 and Shingler, 2010). σ^{54}, like any other σ-factor, has to compete fiercely with σ^{70} for the availability of core RNAP (Bernardo *et al*., 2006 and Shingler, 2010). Under stress conditions or stationary phase or slow growth conditions, ppGpp and DksA have known to inhibit transcription from σ^{70}-promoters (Bernardo *et al*., 2006 and Shingler, 2010). Thereby the σ^{54}-RNAP levels would increase, owing to greater availability of core RNAP freed from the σ^{70}-RNAP holoenzyme (Shingler, 2010).

1.4 Signal dependent response of bEBP

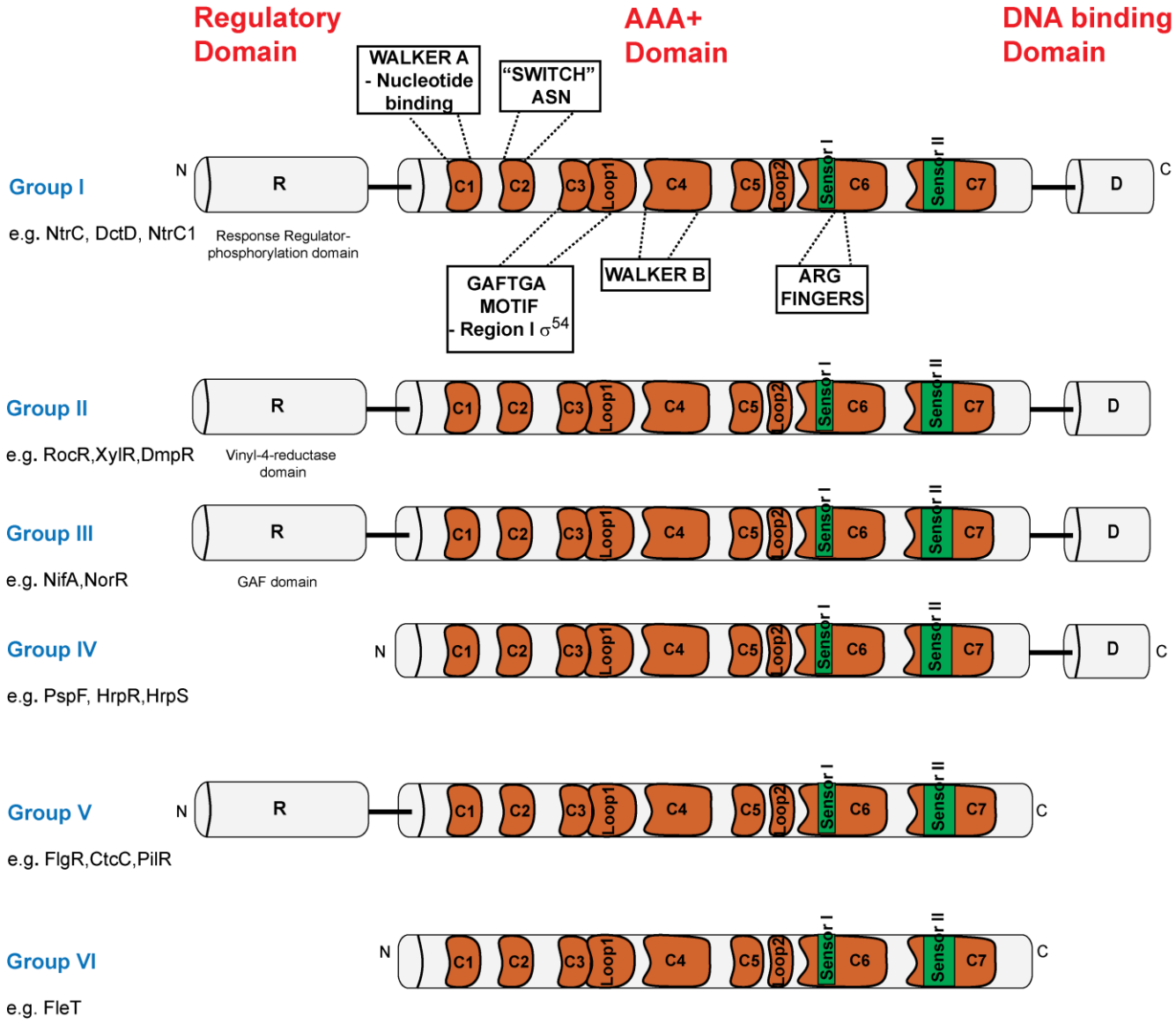

Figure 1.5 **The classification of bEBPs**: The schematic diagram represents the domain architecture of the three specific domains of bEBPs. bEBPs are classified into six groups. The central AAA+ domain is highly conserved and contains the active center that catalyses the formation of RPo. The central AAA+ domain is further divided into more structural conserved domains C1-C7 as described in the Figure. The N-terminal regulatory domain (R) is present in Group I, II, III and V and is not well conserved across all these groups and responds to a specific signal. Group IV and VI bEBPs are regulated *in trans* by specific proteins, for example PspF regulated by PspA. The C-terminus is represented by helix-turn-helix DNA (D) binding motif that binds to the specific enhancer / UAS DNA sequences.

These bEBPs differ in domain architecture and in their regulation as explained in the (see Figure 1.5). The signal responsive function of bEBPs for a specific signal can be found within the regulatory domains or achieved by *trans*-acting proteins as defined in the Figure 1.5 for the different classes of bEBPs. The bacterial proteins like bEBPs respond to the specific signal by direct or indirect detection by specific

structural domains. The three most commonly found signalling mechanisms are vinyl-4-reductase (V4R) motifs, response regulator (RR) motifs or GAF domains (Joly *et al*., 2010; Shingler 2010 and Bush and Dixon, 2012). V4R motif was historically characterised as hydrocarbon binding domain found in proteins across all kingdoms of life. For e.g., DmpR (Dimethyl phenol regulatory protein), XylR (Xylose regulator) from *Pseudomonas putida* are bEBPs with a V4R regulatory motif, which bind aromatic compounds to activate the transcription (O'Neill *et al*., 1998; Shingler, 2010 and Bush and Dixon, 2012) and are part of the Group II (Figure 1.5). The bEBPs that have the RR domain of the two-component regulatory system include *E. coli* nitrogen regulatory protein NtrC (Kern *et al*., 1999), *Sinorhizobium meliloti*, dicarboxylic acid transport regulator DctD (Park *et al*., 2002), Zinc resistance associated (ZraR) regulator of the Zn^{+2} periplasmic binding protein and ZraP of *Salmonella typhimurium* (Sallai and Tucker, 2005 and Shingler 2010) and these mainly belong to Group 1 of bEBPs. The responsive signal originates from the cognate sensory histidine kinases that recognise a diverse array of stimuli. The control of phosphotransfer from the sensory histidine kinases to a conserved Asp residue of the RR domain of bEBPs is the key step that controls conversion from inactive dimers to the ATPase active multimeric form. Phosphorylation stabilises the interaction between the subunits of the multimeric form e.g. NtrC oligomer. On the other hand, for the C-4 dicarboxylic acid transport protein (DctD) and NtrC1 (NtrC homolog) from hyperthermophile *Aquifex aeolicus* (Lee *et al*., 2003), phosphorylation negatively regulates the interaction between the subunits of the oligomer leading to a dimeric reorganisation (Shingler, 2010 and Bush and Dixon, 2012).

The GAF domain derives its name from a common motif of cyclic-GMP specific phosphodiestrase, *Anabaena* adenylate cyclases and *E. coli* – Formate hydrogen lyase (FhlA). FhlA is a specific bEBP that binds to formate and activates the transcription of formate hydrogen lyase (Hopper and Böck, 1995 and Shingler, 2010). GAF motifs are found in the regulatory input domains of bEBPs related to the nitrogen-regulatory protein NifA, which controls the expression of oxygen-sensitive nitrogenases (Studholme and Dixon, 2003).

1.4.1 bEBPs that lack a regulatory domain

Some bEBPs naturally lack the *cis*-acting regulatory domain; instead they are activated by *trans* acting proteins and the nature of the signals and signalling cascades are far less understood. One such example is of Phage shock protein F (PspF) which is inhibited by its regulator, PspA, under non-stress conditions. In the presence of extracytoplasmic membrane stress conditions, the negative regulation imposed by PspA on PspF is relieved and PspF activates the expression of *psp* genes under σ^{54}-dependent transcription (Joly *et al*., 2010). Likewise, the HrpR-HrpS hetero-multimer is regulated by HrpV in *Pseudomonas syringae.* The inhibition of HrpR-S by HrpV is relieved under stress conditions (Jovanovic *et al*., 2012).

1.5 The Phage Shock Response

The Phage shock response (Psp) is a highly specialised and widely distributed response mechanism that helps the cell to survive extracytoplasmic membrane stress (Joly *et al*., 2010) as shown in Figure 1.6. The Psp response and its regulation is the focus of SMI studies reported in this thesis. The Psp response was first reported during studies of filamentous phage infection in *E coli,* where the PspA protein was highly expressed in response to the production of a phage gene IV product, pIV protein (Brissette *et al.,* 1990 and Joly *et al.,* 2010). The pIV forms the OM part of the exit channel for the extrusion of the mature phage particle (Feng *et al.,* 1999). The mislocalisation of pIV in the IM compromises the membrane integrity and activates the Psp response (Joly *et al*., 2010). Transcriptome analysis of *E. coli* cells under pIV-induced stress conditions gave a very specific and restrictive response clustered to the upregulation of *pspABCDE* and *pspG* genes (Lloyd *et al.,* 2004).

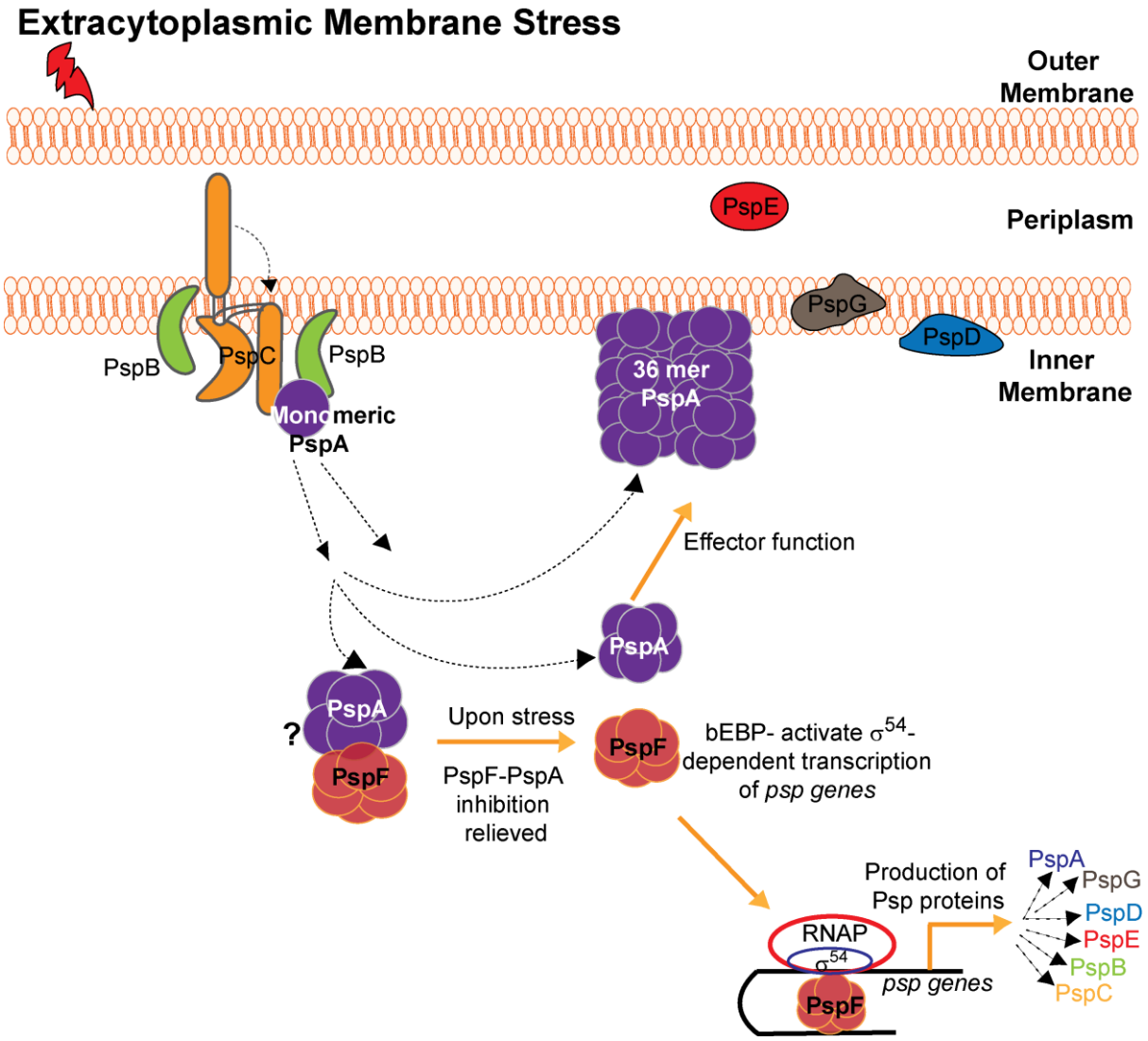

Figure 1.6 **Schematic sketch of the Psp response**. The schematic Figure explains the different proteins involved in the Psp response under stress conditions. Stress inducers range from mislocalised OM secretins such as pIV phage protein, bacterial secretions such as PulD, 10% ethanol, extreme temperature and ionophores. With the onset of stress PspA relieves the negative inhibition on PspF. PspF then activates σ^{54} dependent transcription of *pspA-E* and *pspG* genes. The major effectors during the stress response are PspA (36-mer assembly) and PspG (pentamer/hexamer). PspBC are the signal sensors and transduce the signal to PspA, this signal is somehow relayed to the PspF-PspA inhibitory complex. The localisation of the inhibitory complex in the cell is still unknown and thus the passage of signal relay to the inhibitory complex is also unknown. The precise functions of PspE and PspD have not been exactly characterised with respect to the response.

1.5.1 Phage Shock Protein F

PspF is a bEBP that activates σ^{54}-dependent transcription of *pspABCDE* and *pspG* genes (see Figure 1.6). The Psp response was highly diminished in *ΔpspF* cells, which emphasizes the dependence of the activation of the *psp* genes on PspF as an activator (Lloyd *et al.,* 2004). PspF is one of the very well-studied bEBPs and has helped to understand σ^{54}-dependent transcription in great detail. PspF is a 35kDa (325 amino acids) cytoplasmic protein belonging to the group IV of bEBPs that is characterized

by the lack of regulatory domain and is regulated by PspA in *trans* (see Figure 1.5). The central AAA+ domain is the same as that of all the bEBPs, containing a central AAA+ domain with ATPase activity and a carboxy terminal domain containing Helix-Turn-Helix (HTH) motif (see Figure 1.7) that specifically binds to UAS sequences within *pspA* and *pspG* regulatory regions (Jovanovic *et al.,* 1996; Dworkin *et al.,* 1997 and Lloyd *et al.,* 2004).

As illustrated in the Figure 1.7B with the NTP soaked crystal structure of $PspF_{1\text{-}275}$ monomer defining the tertiary structure of the central AAA+ domain and this protein lacked the C-terminal DNA binding domain. bEBPs consist of conserved structural architectures such as Walker A, Walker B, Sensor illustrated in the Figure 1.7. Loop 1 with the GAFTGA motif structure was not fully resolved due to the highly flexible structure and has been shown by the dotted lines in the Figure 1.7 (Schumacher *et al*., 2006 and Joly *et al*., 2010). The raised GAFTGA motif has been shown to interact with the $E\sigma^{54}$ in the presence of ATP bound state and then flattens following ATP hydrolysis to ADP (Rappas *et al*., 2005 and Bose *et al*., 2008). The spatial rearrangements of the structural domains within the $PspF_{1\text{-}275}$ triggers self-assembly of $PspF_{1\text{-}275}$ into a hexameric ring as predicted by structure prediction software (Pymol) Figure 1.7B. The sequence of events from the assembly of PspF monomers into hexameric ring to binding to the UAS sequences, interaction with the RPc by IHF facilitated DNA looping results in the formation of activation complex and with ATP hydrolysis RPo is formed Figure 1.3 and Figure 1.7.

The expression level of PspF remains constant under stress growth conditions and is independent of PspA, PspB or PspC expression in the cell. The expression of all the other Psp proteins is elevated under the same stress-inducing conditions (Jovanovic *et al.,* 1997; Jovanovic *et al*., 2004 and Lloyd *et al.,* 2004). It has been shown with fractionation experiments in *Yersinia* that the cytoplasmic localisation of PspF does not change with the stress conditions (Yamaguchi *et al*., 2010; Yamaguchi and Darwin, 2012 and Yamaguchi *et al*., 2013) but the interacting proteins switch. Some of the well-studied mutants of PspF are $PspF_{1\text{-}275}$ – with the deletion of the HTH DNA binding domain (does not bind DNA) (Jovanovic *et al.,* 1996, 1997 and 1999) - and $PspF^{W56A}$ (no evident interaction with PspA) (Elderkin *et al.,* 2002 & 2005 and Joly *et al.,* 2009). Only with higher *in-vitro* concentrations (100-fold) the $PspF_{1\text{-}275}$ mutant is able to form a functional hexamer and support transcription of *psp* genes from solution (Jovanovic *et al.,* 1999). The mutant $PspF_{W56A}$ does not bind PspA and so is not negatively regulated by PspA, consequently allowing the constitutive transcription of other *psp* genes (Elderkin *et al*., 2002 and Joly *et al*., 2010) irrespective of the presence of stress.

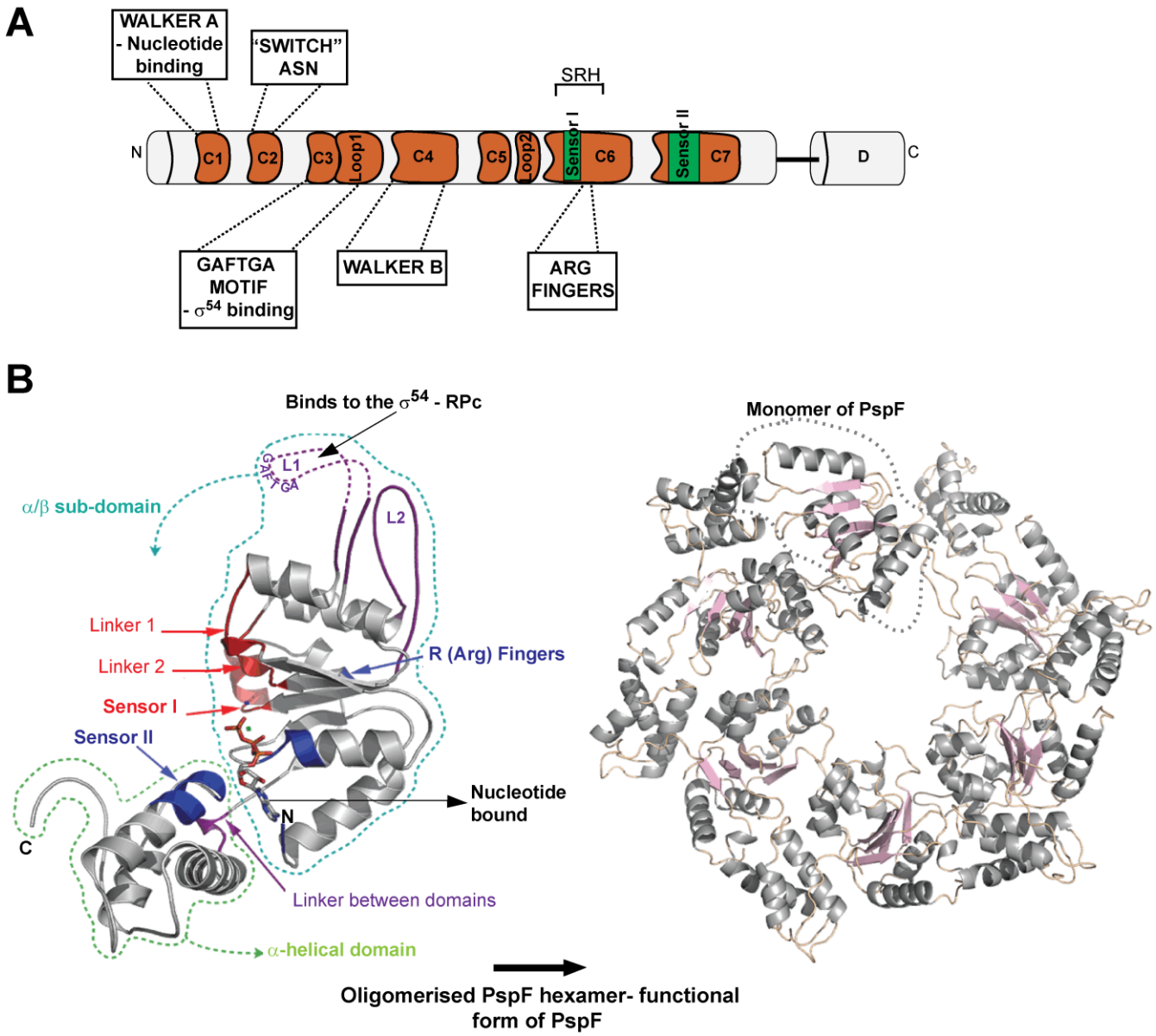

Figure 1.7 **Domain organisation of PspF and Crystal structure of PspF**: (A) The domain organisation of PspF belonging to the Group IV of bEBPs lacking an N-terminal regulatory domain. The central AAA+ domain has the conserved organisation like other bEBPs. It consists of the conserved C1-C7 residues containing the Walker A (GxxxxGK, where x is any residue), Loop1 (L1 contains highly conserved GAFTGA motif), Walker B (hydrophobic residues), Loop2 (L2), Second region of homology (SRH, containing sensor I and putative Arg-fingers and Sensor II. (B) The NTP soaked crystal structure of the $PspF_{1-275}$ monomer showing the structured α/β subdomain and the helical c-terminus domain. The α/β subdomain shows the highly flexible L1 (missing from the crystal structure and so represented with the dotted lines). Linker 1 and 2 (shown in red) are at the end of helix 3 and 4 forming connections between different regions. Sensor I (red), sensor II (blue), Arg fingers (blue) and L1 and L2 loops (purple) have been marked in the Figure (Schumacher *et al*., 2006). With the help of the monomeric $PspF_{1-275}$ structure, the hexameric ring of PspF viewed from the central pore has been reconstituted (adapted from Nan Zhang's PhD thesis).

1.5.2 Phage Shock Protein A

PspA is an IM-associated 26 kDa protein (222 amino acids); it is not an integral membrane protein but is peripheral. It is highly expressed upon stress with the induction of the Psp response, and has been found in all Gram-negative bacteria displaying the Psp response (Joly *et al.,* 2010). PspA plays central regulatory and effector roles in the Psp response (Joly et al., 2009) (see Figure 1.6). Under inducing conditions PspA acts as an effector preventing proton loss during PMF-dissipating conditions and repairing membrane damage (Kobayashi *et al.,* 2007). However, under normal growth conditions PspA acts as a negative regulator that binds using the W56 residue of PspF and inhibits PspF ATPase activity (Joly *et al*., 2010). It has been demonstrated *in vivo* and *in vitro* that PspA does not control the activity of $PspF^{W56A}$ and hence the Psp expression behaves as under stressed growth conditions (Elderkin *et al.,* 2002 & 2005). As mentioned above, PspA is a major effector of the Psp response and is involved in pathogenesis of enterobacteria (Joly *et al.,* 2010).

PspA has been associated with distinct oligomeric states corresponding to specific functionalities. It has been reported that as a negative regulator PspA forms a hexamer, while as an effector it acts as a 36-mer repairing the membrane and so the proton leakage (Kobayashi *et al.,* 2007; Joly *et al.,* 2009 and Lenn *et al.,* 2010) as shown in the Figure 1.6. The purified PspA blocked proton leakage of membrane vesicles reconstituted from total lipids of *E. coli* (Kobayashi *et al*., 2007). Engl *et al*., 2009 reported the subcellular localisation of eGFP-PspA and PspG, which exhibited two classes of eGFP-PspA foci – polar (stationary) and lateral (dynamic). It was hypothesised that the polar complexes could communicate with the pmf- consuming processes such as chemotaxis and reduces the energy consumption, thereby conserving pmf. The lateral, dynamic foci were shown to be cytoskeletal protein MreB dependent. *S*-(3, 4-Dichlorobenzyl) isothiourea (A22), a chemical known to disrupt MreB filaments diminished the lateral PspA and PspG foci (Engl *et al*., 2009). *In silico* analysis predicted that PspA forms a helical coiled coil structure comprising of four α-helical domains, helix domain 1 to 4 (Dworkin *et al.,* 2000; Elderkin *et al.,* 2005 and Joly *et al.,* 2009).

1.5.3 PspF-PspA inhibitory complex

The PspF-A inhibitory complex forms a pivotal point of regulation in the Psp response. It can also be described as the major unknown in this system with respect to its subcellular localisation and communication with the other inner membrane bound or associated proteins. Although PspA imposes negative control upon PspF by inhibiting its ATPase activity (Joly *et al.,* 2009), this inhibition occurs with different degrees of contribution from different PspA helices: PspA full length (FL) > HD1-HD3 > HD2-HD4, with HD4 being dispensable for PspF negative regulation but required for the high order oligomer formation and the effector function of full length PspA (Joly *et al.,* 2009). It was shown with gel filtration that $PspA_{1\text{-}186}$ (HD1-3) forms high order oligomers on its own, but in the presence of PspF it was shown

to be present in the ratio of 1:1 i.e. 6 $PspF_{1-275}$: 6 $PspA_{1-186}$ molecules (Joly *et al*., 2009). Photobleaching studies of eGFP-PspA showed that the stoichiometry of PspA was observed to be heptamer to hexamer, representing the regulatory complexes bound to PspBC or PspF and the higher order oligomers to be the membrane bound effector PspA self-assemblies (Lenn *et al*., 2010). The cell fractionation studies of PspA and PspF from *Yersinia* showed that PspF remains cytoplasmic under non-stress conditions while PspA becomes more membrane bound with the onset of stress conditions (Yamaguchi *et al*., 2010). Recent imaging studies using PspF-GFP and PspA-GFP showed that PspF is highly dynamic and cytoplasmic under both non-stress and stress conditions while PspA was observed to be less dynamic and more membrane-associated under stress conditions (Yamaguchi *et al*., 2013).

1.5.4 Phage Shock Protein B and C

PspB and PspC are integral IM proteins of the Psp response and act as the signal transducers. In *ΔpspBC* cells the Psp response was not mounted under pIV-inducing conditions, emphasizing upon the importance of PspBC as signal transducers (Lloyd *et al.,* 2004). There is strong evidence for PspB, PspC and PspA protein-protein interactions. PspA-C, PspB-C and PspB-A interactions (in the presence of PspC only) (Adams *et al.,* 2003 and Jovanovic *et al*., 2006) using bacterial two hybrid system. It was shown in Jovanovic *et al*. (2010) using affinity chromatography that PspA-PspB-PspG co-purified with $PspC_{6xHis}$ co-expressed with wild type (WT) PspB. The PspG was co-purified with $PspC_{6xHis}$ when expressed in the cells lacking PspA (Jovanovic *et al*., 2010). This showed the formation of an active Psp (B) C regulatory complex in the cells that specifically interacted with PspA and PspG independently. It has also been established that the overexpression of PspC or PspBC induces the Psp system while overexpression of PspB alone does not induce the Psp response (Jovanovic *et al.,* 2010). Overexpression of PspC reduced the PMF in Δ*pspF* cells in the absence of the Psp response while PspBC overexpression did not reduce the PMF (Jovanovic *et al*., 2010).

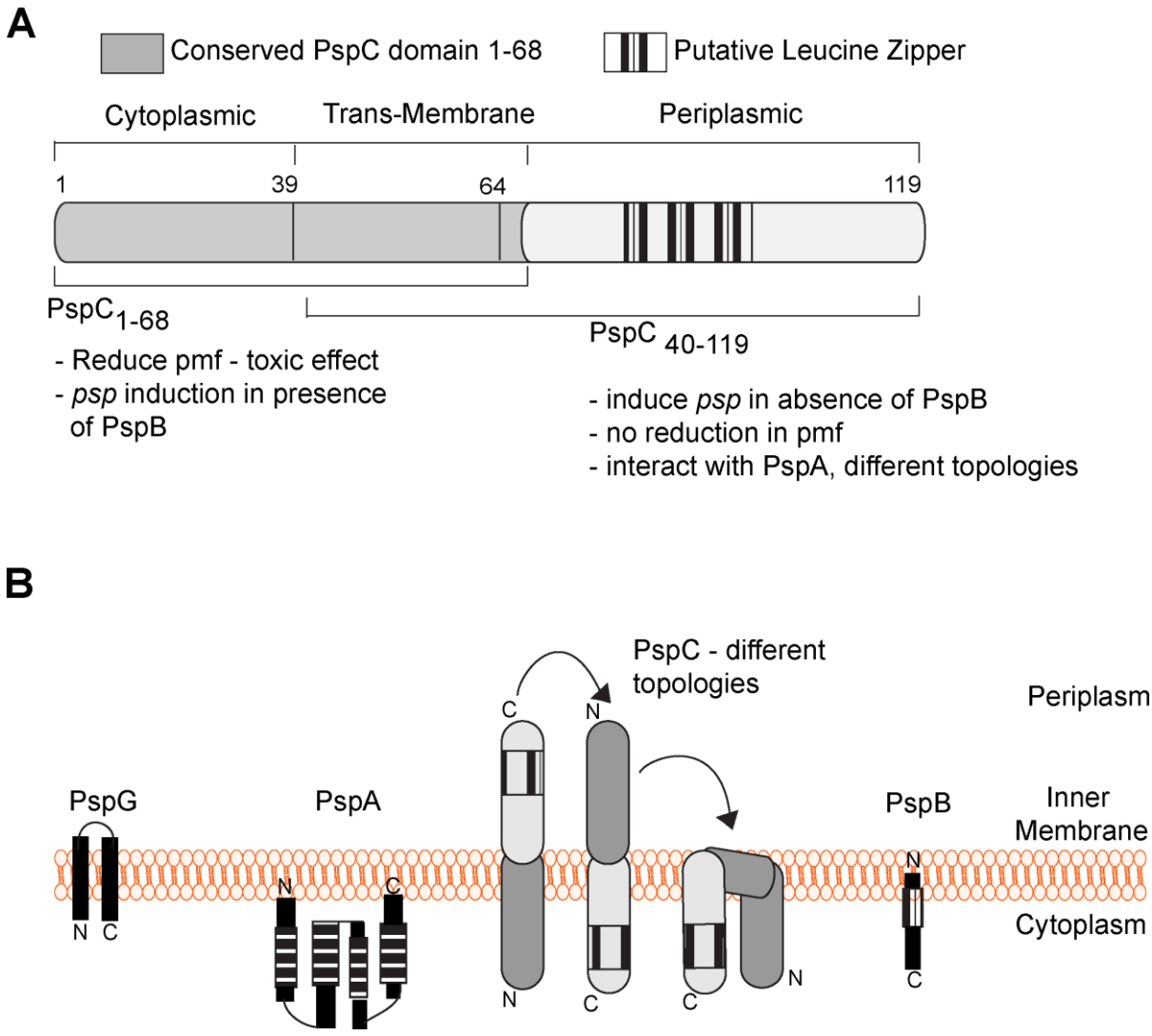

Figure 1.8 **The domain organisation of PspC protein and the possible membrane organisation of Psp proteins**: (Adapted from Jovanovic *et al*., 2010) (A) Schematic representation of the domain architecture of the PspC protein. It has 119 amino acids and it is an integral membrane protein. It is organised into three domains: the Cytoplasmic and transmembrane domains 1-68 a.a and the periplasmic domain 69-119 a.a. $PspC_{40\text{-}119}$, which entails transmembrane and periplasmic inserting regions, can induce the Psp response independent of PspB, while $PspC_{1\text{-}68}$ cytoplasmic domain impairs PMF and has a toxic effect but can only induce the Psp response in a PspB dependent manner. (B) The schematic representation of the possible orientations of the membrane associated Psp protein. PspG, PspBC are integral membrane Psp proteins. The predicted coiled coil structure of four helix domains of PspA, with helix domain 1 and 4 could interact with the membrane. PspC can adopt different topologies depending on functionality. The periplasmic domain has a putative leucine zipper that is known to interact with PspA and confers different topologies to PspC. The periplasmic domain can bend into the IM/cytoplasm in order to interact with PspA (as shown in the figure).

Therefore it has been thought that the PspBC complex behaves somewhat as an antitoxin-toxin pair where PspB stabilizes the expression of PspC and counteracts its toxic effects in both *E. coli* and *Yersinia* (Darwin, 2005 and Maxson and Darwin, 2006). PspBC has been shown to be more crucial for the virulence of *Yersinia enterocolitica* (Darwin, 2005; Maxson and Darwin, 2006 and Gueguen *et al*., 2011) than PspA. PspBC contain putative leucine zipper motifs. The leucine zipper mutant of PspB was

able to induce the Psp response like WT but displayed impaired upstream signalling and did not interact with ArcB (Jovanovic *et al*., 2009 and Engl *et al*., 2011). The structural studies of PspC reported in Jovanovic *et al*., 2010 determined that the putative periplasmic leucine zippers ($PspC_{40-119}$) were essential to establish interaction with PspA and are involved in the Psp signal transduction (as shown in Figure 1.8). $PspC_{40-119}$ was able to induce *psp* response but did not affect the PMF (see Figure 1.8). The cytoplasmic domain ($PspC_{1-68}$) was found to be important to confer the toxic effect to PspC and reduced the PMF in the *ΔpspC* cells when co-expressed with PspB (Jovanovic *et al*., 2010).

1.5.5 Other Phage Shock Proteins

PspD exhibits PspA-like effector function and is localised peripherally at the inner membrane (Jones *et al.,* 2003 and Jovanovic *et al*., 2006). PspE is a bona-fide periplasmic rhodanese with no known function in either the regulation of *psp* transcription or the effect of the Psp response (Adams *et al.,* 2002; Joly *et al.,* 2010). The integral IM protein PspG is an effector of the Psp response (Lloyd *et al.,* 2004). It has been shown to self-associate and can form oligomers up to the pentamer or hexamer (Engl *et al*., 2009 and Jovanovic *et al*., 2010). PspG can colocalize with PspA as an effector protein during the Psp response (Engl *et al*., 2009). It interacts with PspC and was co-purified in complex with $PspC_{6xHis}$ in the cells lacking PspA (Jovanovic *et al*., 2010). At a higher concentration, PspG can also interact with ArcB and upregulated ArcAB - regulated genes involved in micro aerobic and anaerobic respiration (Jovanovic *et al*., 2006).

The functional complexity of signalling during the Psp response and the resulting protein-protein interactions are dependent on the particular stimulus which impairs the IM and the type of growth conditions. In micro aerobic conditions, the signal is distributed via the ArcAB system to the PspBC while under aerobic or anaerobic conditions an Arc-independent pathway follows (Jovanovic *et al*., 2006; Engl *et al.,* 2009; Engl *et al*., 2011 and Joly *et al*., 2010). Thus, the Psp response is viewed as a highly specialised stress response system with highly evolved protein-protein interactions. Where PspBC complex and PspF-PspA inhibitory complex can be considered sensors and response regulators, respectively, of a specialised and unusual system that is not a phosphor relay system (Joly *et al*., 2010).

1.5.6 psp Regulon

In *E. coli*, the *psp* genes are organized within the PspF regulon comprising an adjacent *pspF* gene and the *pspABCDE* operon, and a physically separated *pspG* (Joly *et al*., 2010) as shown in the Figure 1.9. The *pspF* and *pspABC* genes are highly conserved across the enterobacteria family (Huvet *et al.,* 2010). The *pspABCDE* operon and *pspG* gene are co-ordinately regulated by σ^{54}-dependent transcription and activated by transcriptional activator PspF (as shown in the Figure 1.3 and Figure 1.9 (Weiner and Model, 1994; Jovanovic *et al.,* 1996; Jovanovic *et al.,* 1997 and Lloyd *et al.,* 2004). This transcription

activation is facilitated by IHF protein via DNA looping (Morett & Segovia, 1993; Jovanovic and Model, 1997 and Dworkin *et al.,* 1998). The transcription of *pspF* is under the control of a housekeeping σ^{70} promoter and is autogenously negatively controlled (Jovanovic *et al.*, 1996 and Jovanovic *et al.,* 1997).

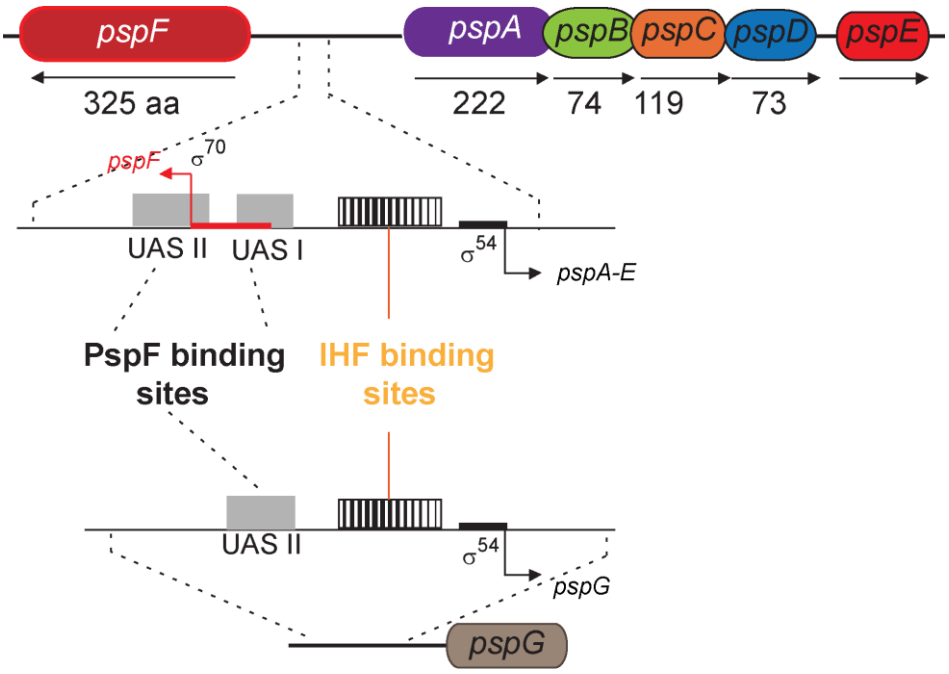

Figure 1.9 **The *psp* regulon in *E. coli***: The schematic representation of the orientation of the genes (Adapted from Joly *et al*., 2010). The *psp* regulon consists of *pspABCDE* operon, *pspG* gene and *pspF*, which is transcribed upstream of the psp operon. The *pspABCDE* operon and *pspG* genes are under the control of σ^{54} promoter. Upstream of the promoter is the binding site for IHF as shown in the schematic representation. The upstream activator sequences (UAS I and UAS II upstream of *pspA* promoter and UAS II upstream of *pspG* are defined in the diagram. PspF binds to these specific UAS sequences. Notably, UAS I & II upstream of the *pspA* promoter partially overlap with the σ^{70}- promoter and the transcription start site of PspF, hence PspF autogenously regulates its own expression by binding to the UAS I & II while activating the σ^{54} dependent transcription of *psp* genes. The *pspA* gene is probably located 29.45 minutes from the origin of replication and *pspG* is 91.84 min (Joly *et al*., 2010).

Therefore, the *psp* regulon is also a good model system to study bacterial transcription regulated by different factors such as external stimuli, sigma factors and bacterial enhancer binding proteins. It has also been identified that 6sRNA also provides another layer of regulation to the expression of *psp* genes. It has been shown that 6sRNA indirectly interacts with RNA polymerase and inhibits transcription of *pspF,* thus subsequently leading to the inhibition of expression of *psp* operon (Trotochaud and Wassarman, 2006). Cells without 6sRNA survive better at elevated pH than WT cells, and the 6sRNA dependent effect is eliminated in *pspF* mutants.

1.5.7 Biological functions of Psp response

1.5.7.1 PMF Maintenance

A stable and conserved PMF within the cell is important for its survival. Cells lacking the Psp response have reduced viability, especially in the stationary phase, on exposure to energy-limiting conditions such as the presence of alkaline pH or bile salts (Weiner and Model, 1994 and Adams *et al.,* 2003). The absence of Psp has a detrimental effect on the efficiency of the pmf and ATP-dependent protein secretion (Joly *et al*., 2010). It is proposed that PspA self-associates to form scaffolds at the cytoplasmic face of the IM, binding to the phosphotidylglycerol and phoshotidylserine under stress conditions thereby changing the rigidity of the lipid bilayer and in turn maintaining the pmf (Kobayashi *et al.,* 2007). Additionally, PMF was not maintained in cells lacking lateral PspA and PspG complexes (Engl *et al*., 2009 and Joly *et al*., 2010). However, there is no direct biochemical or biophysical evidence for any of these PspA membrane repair mechanisms.

Transcriptome analysis showed that the overexpression of Psp effector proteins such as PspA drive the expression of specific genes involved in energy consumption processes (Lloyd *et al.,* 2004). The downregulated genes are involved in chemotaxis, motility and aerobic respiration and some of the upregulated genes were involved in anaerobic respiration, cation (H^+) uptake as well as secretion. In this way, the Psp response indirectly maintains cell viability by switching the metabolism to anaerobic respiration and fermentation as well as downregulating pmf consuming processes (Joly *et al*., 2010; Jovanovic *et al*., 2010 and Engl *et al*., 2011).

1.5.7.2 Pathogenesis in Gram-negative Bacteria

Infection via Gram-negative bacteria usually involves OM secretins that are part of Type II and Type III secretion systems. The secretion systems facilitate cell adherence and the injection of virulence factors in extracellular milieu or into the host cytoplasm. The Psp response is induced by OM secretins, thus the Psp response may stabilise the cell envelope integrity during infection (Joly *et al.,* 2010). A *pspC* mutant strain of *Yersinia enterolitica* displayed attenuated virulence and impaired growth upon Type III secretion (Darwin and Miller, 1999). The *psp* genes expression is elevated during swarming and macrophage infection of *Salmonella typhimurium* and *Shigella flexneri* (Wang *et al*., 2004; Karlinsey *et al*., 2010 and Joly *et al.,* 2010). It has been shown that *pspA* mutation significantly attenuated the virulence of *Salmonella typhimurium* in the mice models expressing a specific divalent metal transporter (Karlinsey *et al*., 2010).PspA helps in the divalent metal transport via the specific divalent metal transporters.

1.5.7.3 Protein Translocation

Proteins are translocated across the bacterial membrane using Sec or Tat pathway as shown in the Figure 1.2. TatA complex can be co-purified with PspA and they form a co-complex observed with a scanning electron microscope (Mehner *et al*., 2012). It was shown that in the absence of PspA the transport of large membrane protein complexes such as TMAO reductase was compromised. Mehner *et al*., 2012 also showed the importance of PspB and PspC in facilitating the contact between TatA and PspA. These studies highlighted the potentially important role of PspA in recruitment at active translocons to keep a check on the membrane stress status. Furthermore, the overexpression of TatA is able to induce Psp response in a PspF, PspB and PspC dependent manner. It was also shown that PspA enables efficient translocation of proteins to the periplasm or across the membrane when overexpressed in the cells (DeLisa *et al*., 2004). Likewise in *Streptomyces lividans*, PspA stimulated the production of homologous and heterologous proteins secreted through either Sec or Tat pathway (Vrancken *et al.,* 2007 and Vrancken *et al.,* 2008). PspA homologue has also been shown to play a vital role under membrane stress conditions in *Streptomyces lividans* (Vrancken *et al*., 2008).

1.5.7.4 Persistence in bacteria

The Psp response has also been shown to have a role in the anti-microbial resistance of cells. This functionality of the Psp response could be exploited to develop medical treatment. In *E. coli* persister cells that form biofilm to develop multi-drug resistance there is evidence of induced *psp* expression (Keren *et al.,* 2004, Joly *et al*., 2010 and Bush and Dixon, 2012). Often the multi-drug efflux pumps in the persister bacteria use pmf to drive the efflux of the drugs out of the cells, highlighting potential induction of the Psp response. Thereby, this can be exploited to mutagenise *psp* and associated genes to develop recombinant pathogenic bacteria to be used as targets for live attenuated vaccines (Joly *et al.,* 2010). Along with the vaccine production, the Psp response can also be a target for potential drugs.

1.6 Inducing Stimuli for the Psp Response

The mislocalisation of OM secretin pIV was the first identified inducer of the Psp response (Brissette *et al.,* 1990; Darwin 2005 and Joly *et al*., 2010). pIV is a filamentous phage outer membrane protein which is required for the assembly and extrusion of the phage particles (Russel and Kazmierczak, 1993 and Kazmierczak *et al*., 1994). Filamentous phage undergoes a concerted assembly and extrusion process in which the capsid proteins in the cytoplasmic membrane polymerise around the viral DNA (Russel and Kazmierczak, 1993 and Kazmierczak *et al*., 1994). The viral particles extrude through the *E. coli* cell without causing cell death. At least three proteins are essential for the assembly and extrusion of viral particles – phage encoded pI and pIV and host encoded thioredoxin (Russel and Kazmierczak, 1993). pI

may initiate the phage assembly by recognizing the packaging signal in phage DNA and further interact with thioredoxin, pIV and major coat proteins (Russel and Kazmierczak, 1993). pIV is an outer membrane protein and has been shown to form multimeric channel of around 10-12 subunits using scanning transmission electron microscopy (Linderoth *et al*., 1997). It was shown with cell fractionation studies that mislocalisation of multimeric pIV in the inner membrane induced the Psp response while the cytoplasmic pIV did not induce Psp response (Russel and Kazmierczak, 1993). pIV is a phage-encoded protein but still exhibits homology to the bacterial OM secretins of the Type II and Type III secretion systems such as PulD from *Klebsiella*, OutD in *Erwinia* or HrpH in *Pseudomonas syringae* and each of these induce the Psp response (Russel and Kazmierczak, 1993). In *Yersinia,* during virulence YscC OM secretin forms a channel through which type III secretion substrates are translocated. The overexpression of YscC has been shown to induce the Psp response (Darwin & Miller, 1999).

A wide array of many other kinds of inducing stimuli has now been shown to induce the Psp response besides the classical mislocalised OM secretins in the IM. These include:

- Treatment with uncouplers of PMF such as CCCP, dinitrophenol or free fatty acids (Weiner & Model, 1994).
- Exposure to the hydrophobic organic solvents such as *n*-hexane or cyclooctane (Kobayashi *et al.,* 1998).
- Inhibition of fatty acid synthesis (Bergler *et al.,* 1994)
- Late stationary growth phase (Weiner & Model, 1994)
- Exposure to extreme heat shock (50^{o}C), 10% ethanol and hyper-osmotic shock (0.75 M NaCl) (Brissette *et al.,* 1990).
- Impaired protein secretion pathways induce the Psp response. These systems are also found in archeae, eukaryotic organelle and thylakoid membrane of plants. The deletion of the Tat pathway (DeLisa *et al.,* 2004) or deletion of components of the Sec pathway (SecA, SecD, SecF, SecM) has been shown to induce the Psp response (Jones *et al.,* 2003).
- The Psp response is also highly upregulated in TolC mutants. TolC forms the multi-drug efflux transporter (Keren *et al*., 2004; Dhamdhere and Zgurskaya, 2010; Kint *et al.,* 2012 and Vega *et al*., 2012).

1.6.1 Relevance of Psp response in different kingdoms of life

The Psp response facilitates pathogenesis of Gram-negative bacteria (for example, - *E. coli, Yersinia, Shigella, and Salmonella*) (Joly *et al*., 2010). Darwin, 2005 found putative Psp systems in Gamma-, Delta- and Alpha-proteobacteria. Additional *in-silico* genome search has revealed that *psp* is not only

conserved in Gram-negative bacteria but also present in all the three kingdoms of life. Huvet *et al.,* 2009 reported evolutionary divergence of the Psp proteins with a high degree of co-conservation of PspF-PspA. However, some species gave reduced limited homology to only PspA. For example, in Gram-positive bacteria such as *Streptomyces lividans*, *Bacillus subtilis,* LiaH has been identified as a PspA homologue. LiaH was also induced by membrane stress or alkaline shock response in Gram-positive bacteria (Darwin, 2005; Huvet *et al*., 2009, 2011 and Joly *et al*., 2010). The halophilic archeae *Haloferax volcanii* exhibited upregulated expression of PspA homologue under high salt conditions (Bidle *et al.,* 2008). Cyanobacteria *Synechocystis* and higher plants have a PspA homologue called Vesicle-inducing protein in plastids, 1 (Vipp1) essential for thylakoid biogenesis and photosynthesis (Westphal *et al.,* 2004, Joly *et al.,* 2010; Vothknecht *et al.,* 2012 and Zhang *et al*., 2012). Vipp1 has been shown to complement the PspA deletion in *E. coli* (DeLisa *et al.,* 2004).

1.7 Single Molecule Imaging

With the advancements in fluorescence microscopy techniques, high spatial resolution images of biomolecular assemblies can be acquired in live bacterial cells. Such imaging methods are employed to study single molecules, single protein molecules or multi-protein assemblies within the cell. With the help SMI bacterial transcription, replication, translation and many other responses, such as those for stress perception and management, can be observed *in vivo* in an intact single bacterial cell (Elf *et al*., 2007; Bustamante *et al*., 2011; Li and Xie, 2011; Roee *et al*., 2011; Di Liberto and Cavalli, 2012; Munsky *et al*., 2012; Kaplan and Friedman 2012; Sánchez-Romero *et al*., 2012; Lenn and Leake 2012 and Dulin *et al*., 2013). Most ensemble-based *in vivo* or *in vitro* assays are limited by averaging and can also mask rare states and cellular heterogeneity, and therefore miss intermediate assemblies and pathway steps (Stower, 2012; Di Liberto and Cavalli, 2012 and Zakarzewska and Lavery, 2012). The live cell single molecule imaging (SMI) circumvents some of these problems and allows detection of complexes refractory to detection by conventional approaches. Figure 1.10 shows the evolution of techniques since the discovery of rod-shaped *E. coli,* ranging from structural studies such as x-ray crystallography and cryoelectron microscopy to single molecule fluorescence microscopy.

In 1976 Thomas Hirschfeld first reported the detection of single molecules of immobilised fluorophore tagged proteins under the optical microscope. Hirschfeld's reported method laid the foundation for the current SMI techniques (Li and Xie, 2012).

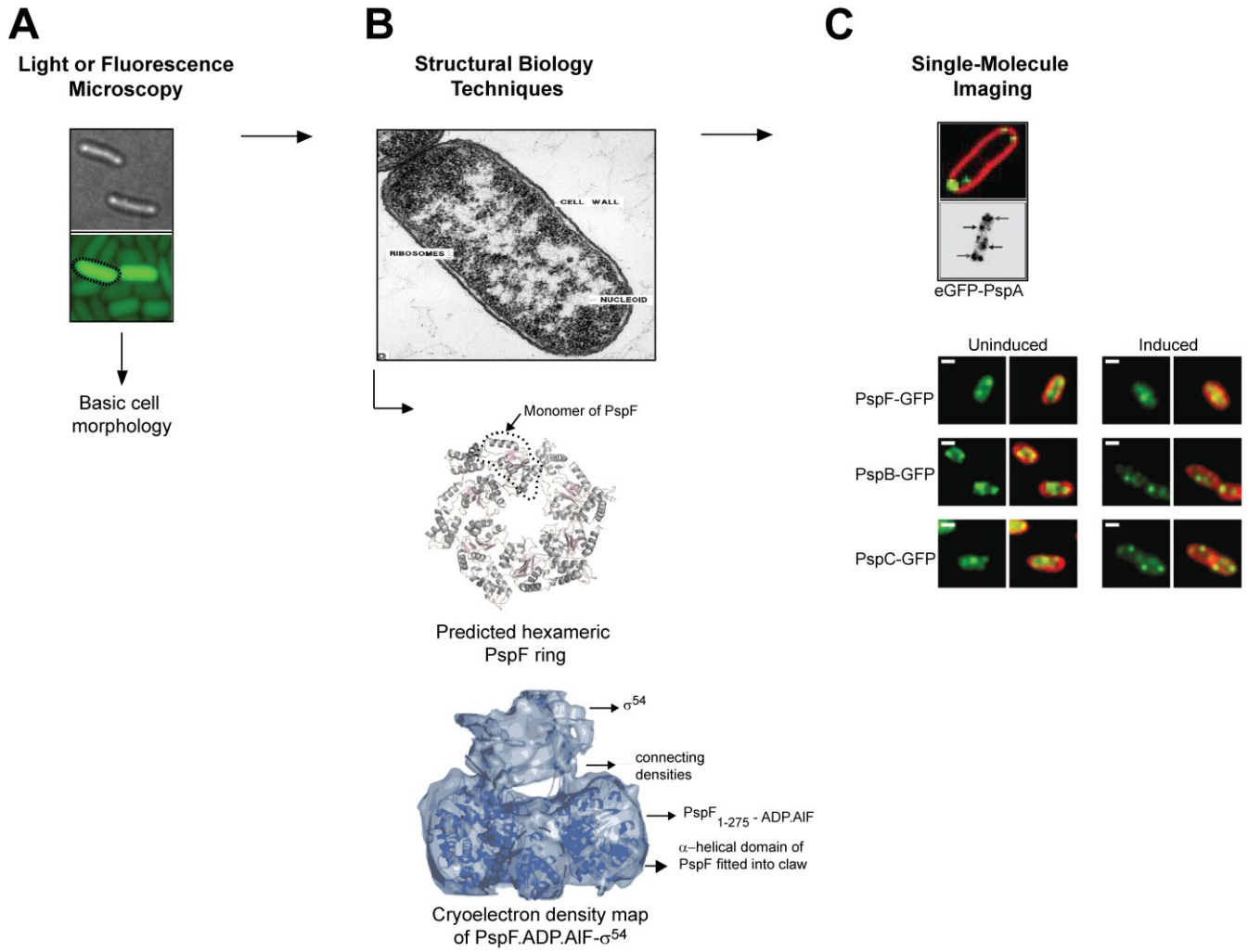

Figure 1.10 **Evolution of different techniques to study *E. coli***: The Figure explains the different types of techniques used such as bright-light and fluorescence microscopy, electron microscopy to elaborate on the cell morphology and protein structures. (A) The bright light image of the rod-shaped *E. coli* cell and the corresponding fluorescence image (adapted from web - http://sys-bio.org/research/). (B) The structural biology techniques such as electron microscopy – to study the subcellular structural details within *E. coli* cell showing the nucleoid, cell wall formation and ribosomes (adapted from web - http://www.ucmp.berkeley.edu/bacteria/bacteriamm.html). The structural studies further evolved and were used to determine the protein structures at Å resolution such as the structure of monomer of PspF, was determined using X-ray crystallography, and the prediction software was subsequently used to produce the hexameric ring from the crystal structure of monomer PspF (Rappas *et al*., 2005 and Joly *et al*., 2010). Cryoelectron microscopy was used to study structural interactions and subunit rearrangements in multi-protein complexes such as PspF-σ^{54} (Rappas *et al*, 2005, 2006). (C) SMI techniques are applied to study a single protein molecule or complexes in the live *E. coli* cells. The proteins or multi-protein complexes can be studied in the native environment as a fusion to fluorescent proteins such as Green Fluorescent Protein (GFP). For example eGFP-PspA was localised at the cell poles and at the lateral membrane localisation (Engl *et al*., 2009). PspF-GFP, PspB-GFP and PspC-GFP have been imaged in *Yersinia enterolitica* to be localised in the cytoplasm or at the membrane respectively under non-stress and stress conditions (Yamaguchi *et al*., 2013).Scale bar = 1 µm

SMI methods vary from force studies using optical tweezers to observe for example DNA repair enzymes (Lord *et al*., 2010; Taniguchi *et al*., 2010; Lenn and Leake, 2012; Li and Xie, 2012; Leake, 2013; Ritchie *et al*., 2013 and Robson *et al*., 2013), to *in vitro* assays of fluorogenic enzyme turnovers (Lenn *et al*., 2008), single particle tracking and photobleaching studies (Chiu and Leake, 2011 and Lenn and Leake, 2012) as explained in detail in 1.7.3. The live cell studies using SMI are also valuable in providing essential recapitulations of the biochemical data generated *in vitro*. Due to the relative ease and non-invasive nature of fluorescence microscopy, live *E. coli* cells have replaced standard laboratory test tubes (Xie *et al*., 2006 and Chiu and Leake, 2011) for the quantitative observation of functional complexes. Recently with the characterisation of GFP and its variants, their optimised genetic expression, fast maturation, pH tolerance and many more useful properties have led to increased focus towards the application of such fluorescent proteins instead of organic dyes (Xiao *et al*., 2008; Gitai, 2009; Lord *et al*., 2010; Chiu and Leake, 2011). The observations in SMI allow detection of stochastic events in the cells of the same population. The spatial and temporal resolution of protein assemblies can give insightful information regarding their coupling with different signalling pathways and response mechanisms (Chiu and Leake, 2011; Li and Xie, 2012 and Mehta *et al*., 2013).

ADVANTAGES OF SMI	DISADVANTAGES OF SMI
Live cell studies	Cellular autofluorescence adds to background noise
Report stochastic cellular events	< 100 nm resolution of the images
Devoid of ensemble averaging	Artefacts due to the fluorescent proteins fused to the proteins of interest
Determine subcellular localisation, intracellular dynamics and functional stoichiometry	Data interpretation can be tricky and requires implementation of novel algorithms
Super resolution imaging	

Table 1.2 Lists the various advantages and disadvantages of SMI techniques

Along with the many advantages of SMI (see table 1.2), there are some critical limitations of the methods, such as autofluorescence that adds to the background noise. It cannot resolve structural features at the scale of X-ray crystallography or cryo-electron microscopy (Figure 1.10B). Additionally, the inherent folding properties of fluorescent protein in the fusion can drive artefactual localisation of fusion protein assemblies or contribute falsely to the quantitative analysis; therefore it becomes

imperative to check the stability and functionality of the fusion before the SMI experiments (Lenn and Leake, 2012 and Swulius and Jensen, 2012). SMI approach is highly data intensive, and thus requires computational expertise in order to analyse an array of images generated. This is a roadblock for a pure biological laboratory (Xiao *et al*., 2008; Lord *et al*., 2010; Chiu and Leake, 2011; Lenn and Leake, 2012 and Leake, 2013). Therefore the SMI approach requires specialised instrumentation and interdisciplinary cooperation in order to confidently interpret the data (Xiao *et al*., 2008; Lord *et al*., 2010; Chiu and Leake, 2011 and Leake, 2013).

Over the past few years, expert laboratories have tried to overcome some of the shortcomings of the SMI methodologies. The problem of autofluorescence has been addressed by using fluorescent proteins with longer wavelengths such as enhanced yellow fluorescent protein (EYFP), Venus or red-emitting fluorophores (Nagai *et al*., 2002; Yu *et al*., 2006 and Xiao *et al*., 2008). The signal can also be improved against cellular autofluorescence by reducing the detection volume and thereby cutting out the autofluorescence. Techniques such as Total Internal Reflection Fluorescence (TIRF) Microscopy have been employed that limit the axial length by lasers penetrating to only a few 100 nm into the bacterial cell. This increases the signal to noise ratio to an extent and is ideally suited to study membrane dynamics (Lord *et al*., 2010 and Chiu and Leake, 2011). The background noise from SMI has been dealt with by modifying the instrumentation of the microscopes, some popular variations to conventional wide-field microscopy is slimfield and stroboscopic microscopy. The slimfield microscopy is useful for studying the rapid temporal resolution because the excitation light is concentrated to a smaller area ($\sim$ 30 μm^2). This mode of illumination increases the strength of excitation of the sample by almost 100 times (Xie *et al*., 2008 and Chiu and Leake, 2011). The comparatively greater excitation intensity can reduce the camera noise by lowering the integration times to millisecond (Chiu and Leake, 2011). Stroboscopic illumination is based on employing short pulse with shutter and camera kept open for longer time (Chiu and Leake, 2011 and Ritchie *et al*., 2013). With the stroboscopic illumination the detection limit of single molecule in live cells is reduced to sub-millisecond levels. This method is not dictated by the shutter speed or camera frame rates but is governed by the laser pulse width. And by varying the laser pulse width and dwell times, dynamics and resident times of single molecules along with the binding constants can be measured (Xie *et al*., 2008, Chiu and Leake, 2011 and Ritchie *et al*., 2013). It has been used to determine the dynamics of transcription factors (Xie *et al*., 2008 and Chiu and Leake, 2011).

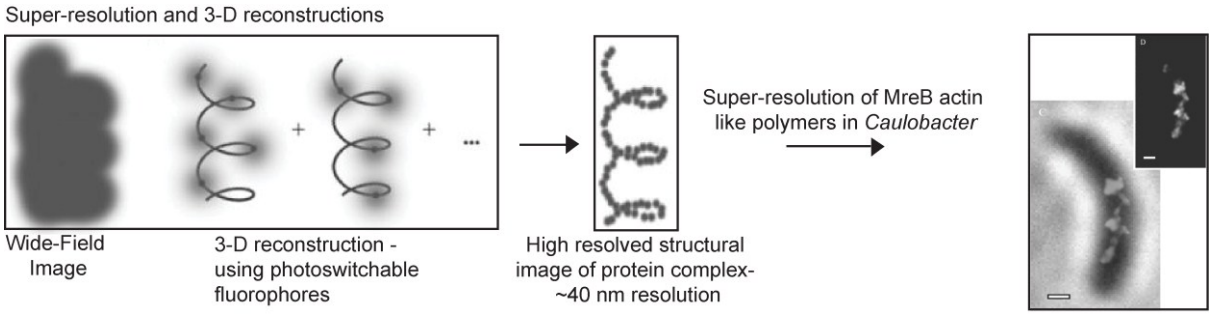

Figure 1.11 **The advantages of super-resolution imaging and 3-D reconstructions**: Standard wide-field single molecule imaging cannot resolve beyond 100 nm while super-resolution imaging and 3-D reconstructions on the wide-field image can resolve to give highly defined structural conformations, as shown in the Figure for MreB filaments in *Caulabacter*. In the wide-field image, MreB filaments appear as a blob which can be resolved to form spiral structures with the help of super-resolution imaging and 3-D reconstructions and achieve 40nm resolutions. The super-resolution technique is evolving rapidly and resolutions lower than 10nm have also been achieved by Kim *et al*., 2006 and Biteen *et al*., 2008.

Resolution limitations have been rectified with the development of techniques such as super-resolution imaging and 3-D reconstructions as shown in the Figure 1.11. The super-resolution imaging is achieved by precise localisation of the readouts from the single molecules of the fused photoactivable or photoswitchable fluorophores for example PAmCherry. The majority of these fluorophores are sent to non-fluorescent states or in case of photoactivable they are activated using for example UV radiation of 405 nm wavelength (Sauer, 2013). This cycle of photoactivation of set of fluorophores and their precise localisation is recorded for few thousand frames in order to obtain precise reconstructions. Some of the methods used to perform super-resolution imaging and analysis are photoactivated localisation microscopy (PALM), or stochastic optical reconstruction microscopy using special photo convertible fluorophores (Sauer, 2013). These are some of the widely used microscopic set-ups used to perform super-resolution imaging. The super-resolution microscopy also relies on very high laser power of around 100 mW in order to obtain precise localisation read out for the fluorophores. However, super-resolution imaging is tedious and expensive and has some fundamental drawbacks (Kim *et al*., 2006; Lord *et al*., 2010; Lenn and Leake, 2012).

- The construction of the super-resolution image requires repeated sampling of the single molecule localised spot with thousands of frames. These increased photon integration times are required in order to obtain images with the weak fluorescent signal. Thus the effective temporal resolution of these images (seconds to minutes) is very low compared to molecular events, consequently failing the purpose of the SMI technique to image nanomachines.
- Most of the super-resolution experiments reported in the literature are done on fixed cells rather than live cells. The bacterial cells are fixed usually with formaldehyde to preserve the protein interactions or complexes in order to be studied using the super-resolution methods

Live bacterial cells are viable and dividing and so the protein complexes and structures are much more transient and dynamic.

- There is also a high risk of artefactual localisation and thereby 3D-reconstructions of these images could be misleading. The ambiguity in localisation is a result of the short wavelength (long UV) illumination along with the long imaging times. The short wavelength is vital for activating the photo-switchable fluorophores or organic dyes. However, the short wavelength lasers could impair cell viability.
- Most of the super-resolution imaging has not addressed the relevant biological question; rather the studies have focused on demonstrating the proof of principle of the technique and advanced mathematical programmes.

Super-resolution imaging, despite all the challenges, has been very important in redefining the imaging of biomolecules and protein assemblies in the cells. The application of super-resolution imaging along with mathematical modelling has enabled the reporting of functional tertiary protein structures *in vivo*. As it has been highlighted in the above section in SMI experiments the microscopic set-up is vital and governs the hypotheses to be tested.

1.7.1 Microscopic set-up

Since the establishment of optical fluorescence microscopy, it has been a vital instrument in cell biology. The light source in form of laser is used noninvasively to probe a sample to study the localisation and dynamics of the internal structures in living cells. Optical microscopy has further advanced into high-resolution fluorescence microscopy, achieving nanometer scale. This technique takes advantage of highly evolved microscopic set-ups consisting of cameras with fast capture rates such as the electron multiplier camera (EMCCD), high numerical aperture objectives and filters. These advanced components within the microscope enable the characterisation of the exact position of the fluorescent molecule in the sample at a single molecule level. Therefore this technique is defined as single molecule epifluorescence microscopy (Xiao *et al*., 2008 and Lord *et al*., 2010). Most commercially available microscopes are confocal, however confocal microscopy is not feasible for SMI of bacterial cells because the entire cell is mostly within the depth of focus of a high numerical aperture (NA) microscope (~300-700 nm) (Lord *et al*., 2010). Due to their small size, the SMI of bacterial cells can be accomplished with the standard wide-field epifluorescence microscopic set-up. TIRF is mainly used to study membrane dynamics or membrane bound proteins in the bacteria.

1.7.2 Single Molecule Imaging methodologies

SMI based experiments have been widely used to study enzyme turnovers, subunit composition and interactions of transcription and translation complexes in *E. coli* (Reyes-Lamothe *et al*., 2008; Lord *et al*., 2010; Reyes-Lamothe *et al*., 2010 and Chiu and Leake, 2011). The next generation sequencing methods also are based on single molecule fluorescence where every nucleotide added to the growing DNA strand by DNA polymerase is marked by specific fluorescent signal corresponding to the added nucleotide. The SMI techniques to be applied for a particular study are highly dependent on the kind of question to be answered; some of the methods mentioned are specific for photobleaching studies and others lay emphasis on protein dynamics.

1.7.2.1 Detection by Localisation

In the bacterial cell, imaging of freely diffusing proteins is difficult because the fluorescent signal diffuses throughout the cell and is beyond the capture rate of the camera. However, if a fluorescent protein (FP) fusion is tethered to the membrane or DNA, it enables the visualisation of the fluorescent protein defined as foci as shown Figure 1.12. Even transient binding to the membrane or DNA can be detected (Kim *et al*., 2006 and Li and Xie, 2011).

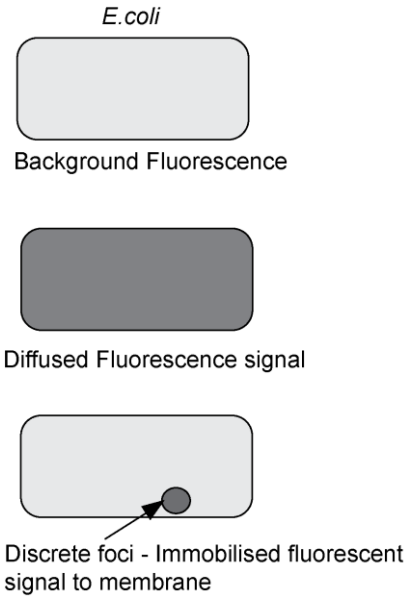

Figure 1.12 **Detection by Localisation** (Adapted from Li and Xie, 2011).The figure explains the principle behind detection by localisation method of SMI. According to this method there are three different forms of fluorescence observed in live *E. coli* cells: inherent background fluorescence observed in *E. coli*; diffused fluorescence signal due to fast diffusion of the fluorescent tagged protein imaged, and the fluorescent tagged protein detected as a defined foci if tethered to the membrane or nucleoid.

Employing this method under wide-field fluorescence microscopy with short exposure time rates and faster EMCCD frame rates can yield images of transcription factors bound to the stationary DNA in contrast to the unresolved and under-sampled free transcription factors. It is also possible to track these factors using custom-generated tracking algorithms to calculate mean square displacement plots and thereby diffusion coefficients for the particular protein (Treanor *et al*., 2009; Leake, 2013 and Ritchie *et al*., 2013). The tracking of these proteins is also possible by using stroboscopic laser illumination, also called slimfield illumination (see above 1.7).

1.7.2.2 Fluorescence Recovery after Photobleaching (FRAP)

Fluorescence recovery after photobleaching (FRAP) involves weak initial imaging with weak laser illumination after which a region of interest (ROI) is selected. This ROI is irreversibly photobleached with a strong laser pulse and the cell is then imaged with the weak laser illumination again. The recovery of the fluorescence from the ROI by the diffusion of the surrounding FP fusion molecules into the region is measured over time. These measurements determine the mobility of macromolecules in both prokaryotic and eukaryotic cells.

FRAP measurements in a small bacterial cell could be challenging and not very sensitive at the single molecule level. There is the danger of photobleaching a larger area with strong laser illumination that might result in underestimating the number of fluorescent molecules diffusing across the ROI (Moerner *et al*., 2007; Darzacq *et al*., 2009 and Mika and Poolman 2011) and time scales of measurements is in seconds unlike ms for SMI measurements.

1.7.2.3 Fluorescence Correlation Spectroscopy (FCS)

Fluorescence correlation spectroscopy (FCS) has been reported as a very powerful tool in determining the diffusion coefficients of FP fusions in solution and in *in vitro* membrane systems such as giant-unilamellar vesicles (GUVs). It is a powerful tool for the binding measurements. A laser beam is focused in the cell, within a volume in the femtoliter range. Fluctuations in the fluorescence signals are measured over a short period of time. The results show the movements of the labelled protein in the specified volume. The FCS measurements for the labelled protein determine concentrations, diffusion coefficients and binding constants (Darzacq *et al*., 2009 and Lord *et al*., 2010).

All these FCS measurements are challenging to obtain in live bacterial cells due to the confined and crowded volume of the cell, low signal to noise ratio and even smaller number of absolute molecules to report the diffusion values with confidence. Generally FCS measurements are suitable for fast processes at microsecond to millisecond scales in solution while FRAP measurements are ideal for slower processes at the scale of seconds.

1.7.2.4 Fluorescence Loss in Photobleaching (FLIP)

Fluorescence loss in photobleaching (FLIP) is used to study the dissociation kinetics of proteins from compartments or specific cellular localisations. A specified area is continuously bleached and fluorescence loss from the surrounding regions is measured. This measurement gives a more exact way to analyse the mobility of proteins that specifically binds to the bleached area.

DETECTION BY LOCALISATION	OTHER SMI TECHNIQUES
Simple microscopic set-up with faster frame rates	Much more tedious microscopic set-up required
Flexible to application of many other image analysis and quantification methods	More specific image analysis and quantification methods required
Single particle tracking of the fluorescent foci to determine dynamics can be used	Dynamics usually determined using photobleaching and recovery methods
Functional stoichiometry can be studied by step-wise photobleaching methods	Difficult to employ step-wise photobleaching on the images acquired by FCS, FRAP etc.
Live and viable *E. coli* cells are immobilised on the microscopic slides and studied	These microscopy techniques rely on high expression of proteins. In the study of Psp response, the amount of PspF in the cells is limiting for FCS or FRAPS studies.

Table 1.3 List of the advantages of using "Detection by Localisation" over the other SMI techniques such as FRAP, FCS etc.

Out of all the methods described in section 1.7.2 detection by localisation will be the chosen method to study the spatial and temporal localisation of PspF and PspA fluorescent fusions in live *E. coli* (see table 1.3). The defined diffraction limited spot of either PspF or PspA, in this research, will be imaged if anchored either to the nucleoid or membrane (see Figure 1.12). The signal from the soluble PspF or PspA fluorescent fusions will not be strong to be captured by the camera and recorded as defined foci. Thus the method of detection by localisation will help in characterising the subcellular localisation of the functional PspF or PspA complexes in the live *E. coli* cells under non-stress as well as stress inducting conditions.

1.7.3 Examples of informative single molecule imaging experiments

This section emphasises on the many different applications and approaches of SMI.

1.7.3.1 Bacterial cytoplasmic crowding and protein dynamics

Mika and Poolman in 2011 reported an interesting aspect of bacterial cell cytoplasm. They showed using fluorescence microscopy that the bacterial cytoplasm is more densely packed than the eukaryotic cell. The paper established the pronounced effect of molecular crowding of the cytoplasm and biological membrane on the functional properties of biomolecules such as activity, the oligomeric states of the proteins, and the dynamics of molecules in the cell cytoplasm (see Figure 1.13). The authors concluded that the transport of molecules in a bacterial cell occurs via simple diffusion that can be greatly influenced by cytoplasmic crowding. They reported that under high osmotic conditions, intracellular concentrations of RNA plus DNA and protein reached up to 400 g/l; close to that in protein crystals (Mika and Poolman, 2011), whereas in the LB media these levels were around 300-370 g/l. Similar crowding studies on the human brain gave intracellular concentrations of 50-100 g/l that were much lower than the bacterial cell. More direct dynamic studies with GFP showed that the molecular crowding of the cytoplasm had a higher impact on the GFP mobility than the molecular weight of the protein itself (Nenninger *et al*., 2010). Elowitz *et al*., in 1999 showed that the apparent diffusion coefficient of GFP was affected by GFP expression: the higher the expression, the slower the diffusion of GFP in the cells. The dynamics of GFP were also influenced by the presence of his-tag i.e. in the presence of charge on GFP. These dynamics studies were performed using FRAP and photobleaching studies.

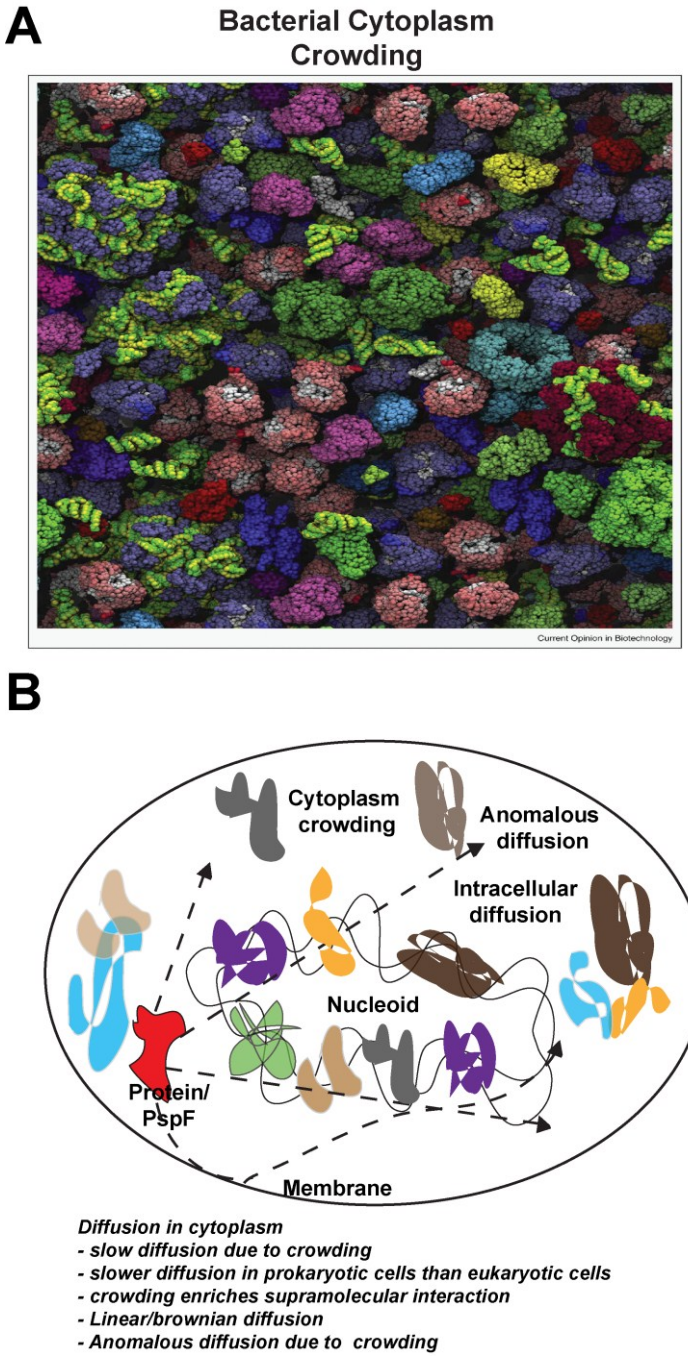

Figure 1.13 **Examples of SMI data from literature**. The images and graphs are obtained from some of the articles published explaining the interesting results that can be attained using SMI. (A) The image of cytoplasm was shown by Mika and Poolman, 2011 by fluorescence microscopy that the bacterial cytoplasm is densely crowded with an intracellular macromolecular concentration reaching up to 400 g/l comparatively much higher than the eukaryotic cells. (B) Schematic structure showing the possible ways of intracellular diffusion in bacterial cytoplasm because of macromolecular crowding. Cytoplasm crowding contributes towards different forms of diffusion such as linear/Brownian diffusion or anomalous diffusion. In return the crowding enriches supramolecular interactions and facilitates multi-protein complexes.

Intracellular crowding reduces the intracellular diffusion but enriched the molecular interactions and in addition the slower diffusion of molecules may promote the formation of supramolecular complexes as shown in the Figure 1.13B (Elowitz *et al*., 1999; Golding and Cox, 2006; Nenninger *et al*., 2010 and Chiu and Leake, 2011). Moreover, due to the unbiased and heterogeneous nature of the cytoplasmic composition and crowding, it may exclude or enrich proteins at specific locations in the cell, such as the nucleoid or the cell pole, establishing different regimes of molecular interactions (Elowitz *et al*., 1999; Golding and Cox, 2006 and Nenninger *et al*., 2010). In the same way, membrane associated or bound proteins would exhibit a combination of movements to find their target binding sites or regions along the membrane.

1.7.3.2 Targeted search for sites on the DNA by transcription factors

The chromosomal fusion of LacI repressor to yellow fluorescent protein (YFP) has been extensively used as a model to report spatial and temporal localisation of DNA binding transcription factors. In Elf *et al*. (2007) the interaction of the LacI repressor on specific operator sequences on the DNA was reported. It was shown that the LacI repressor displays 1D diffusion (D_{1D}=0.046 $\mu m^2/s$) by sliding on the DNA while scanning for the operator sites. However, it also moves within the cytoplasm to bypass the slow DNA sliding movement; this was defined as 3D diffusion (D_{3D}=3 $\mu m^2/s$). It was shown that LacI spends 90% of its time bound to the non-specific sites with D_a=0.4 $\mu m^2/s$. The authors also reported the association and dissociation rates of LacI in the presence of the activator Isopropyl β-D-1-thiogalatopyranoside (IPTG). Later, it was reported that LacI slides along the DNA at about a length of 100 bps at a time (Hammar *et al*., 2012). In the same way it could be possible to describe the DNA dependent dynamics of bEBP-PspF.

1.7.3.3 Imaging of Psp response in *Yersinia enterocolitica*

Yamaguchi *et al* (2013) described the subcellular localisation of Psp proteins fused to GFP under non-stress and stress growth conditions in *Yersinia enterocolitica*. The method of induction of stress in the these cells was by mislocalisation of secretins in the cytoplasmic membrane, secretins are also pIV like bacterial multimeric channels involved in the Type II and III and Type IV pilli secretion systems such as YsaC (Darwin, 2005 and Yamaguchi *et al*., 2013). Chromosomal fusions of PspA-GFP, PspB-GFP and PspC-GFP all showed widely distributed signal under non-stress conditions but in the stress conditions they formed a defined diffraction limited spot at the membrane. PspA-GFP was widely distributed in the cell like PspF-GFP under uninduced (non-stress) conditions but with stress conditions formed brighter larger foci mainly at the cell periphery. PspB and PspC- GFP formed many smaller foci at the cell membrane under uninduced (non-stress) conditions while with stress PspB and C formed larger brighter foci predominantly at the cell poles (see Figure 1.10 C). GFP tagged PspA, B and C were more mobile in

uninduced (non-stress) cells while became much less mobile and more organised with the induction of stress in these cells. PspF-GFP remained cytoplasmic and their organisation and dynamics did not change under non-stress and stress growth conditions (see Figure 1.10 C). It was also shown by co-localisation studies of mCherry and GFP tagged PspA and PspB and C respectively that PspA, B and C localise at the membrane preferentially at the poles during in the uninduced (non-stress) cells (Yamaguchi *et al*., 2013). With the help of SMI methods the PspA and PspF spatial and temporal localisations can be studied in much more detail in *E. coli* that is the focus of research in this thesis.

Objectives

This study focuses on characterisation of the control and regulation of the Psp response with respect to two fundamental Psp response proteins PspF and PspA. The work has two major aspects – The first focuses on illustrating the spatial and temporal localisation of PspF in complex with PspA and or RPc (non-stress conditions; repressed state) or in complex with the RPo (stress conditions; active transcription complex). Study the functional stoichiometry of PspF self-assemblies under non-stress and stress conditions and correlate to its interaction with *pspA* and *pspG* promoters respectively. The interactions between PspF and RPc will be evaluated *in vivo*. The second aspect focuses on understanding the response mechanism mediated by PspA as a major effector. Assign the functional properties of PspA to its uncharacterised structural N-terminal amphipathic helices. Understand novel affiliations of effector PspA with membrane lipids, membrane biogenetic proteins and bacterial cytoskeletal proteins.

1.8 PspF - Master Activator

The precise knowledge of where transcription factors (TFs) reside is important for determining the strategies of gene control (Darzacq *et al*., 2009 and Lee *et al*., 2012). The spatial and temporal localisation of bEBP PspF will throw light on the regulation of the Psp response at the transcriptional level.

In eukaryotic cells, TFs have been shown to move into the nucleus in response to cell injury of the nervous system (Di Liberto and Cavalli, 2012). In the same way bacterial cells have been shown to compartmentalise TFs while switching on the response mechanisms (Di Liberto and Cavalli, 2012 and Zakarzewska and Lavery, 2012). Although most signaling pathways to which TFs respond are cytoplasmic, some are often membrane associated; raising questions about the mechanisms of interplay between membrane and DNA associated TFs (Di Liberto and Cavalli, 2012). The interaction between PspF (transcriptional activator) and PspA (membrane-associated effector) during the Psp response highlights communication between membrane and nucleoid. Therefore detailed understanding of the PspF-PspA inhibitory complex and its spatial and temporal resolution along with the functional stoichiometry will help to characterize the most intricate regulatory mechanisms at the subcellular level. *In vitro* methods are limited by ensemble averaging and devoid of the complete cellular components that could have an influence on the PspF dependent transcription; instead SMI methods will permit the quantitative analysis of functional multi-protein (see Table 1.4).

METHODS USED *Review by Joly et al., 2010*	*METHODS USED IN THE STUDY*
In vitro methods	*In vitro* Methods
Protein Gel based assays determine protein-protein interactions or protein-DNA interactions such as :Mobility shift assays ,Native gels	ChIP-PCR – to study the DNA interaction of V-PspF
Gel filtration to determine oligomeric states	Gel Filtration to determine oligomeric state for PspA mutants
Transcription assays to study mechanism of transcription initiation using intermediate complex using PspF- $E\sigma^{54}$-ADP.AlF	ATPase assays using fluorescence plate reader
Structural biology techniques to define tertiary structures and structural rearrangements, X-ray crystallography	
Cryoelectron microscopy (Rappas *et al*., 2005; Bose *et al*., 2008; Wigneshwaraj *et al*., 2008 and Joly *et al*., 2010).	

In vivo methods	*In vivo* methods
Historical *in vivo* methods such as : β-galactosidase assay, Bacterial two hybrid assays, Western Blotting, Cell fractionation Microscopy to study membrane potential Single Molecule Imaging to study fluorescent protein fusion to the protein of interest such as PspF, PspA in live *E. coli* and *Yersinia enterocolitica*	To determine the spatial, temporal localisation of the fluorescent fusion protein. Diffusion of proteins in the live cells To study the functional stoichiometry of the proteins

Table 1.4 The list of *in vitro* and *in vivo* methods used to study Psp response and the chosen method to study Psp response in this thesis.

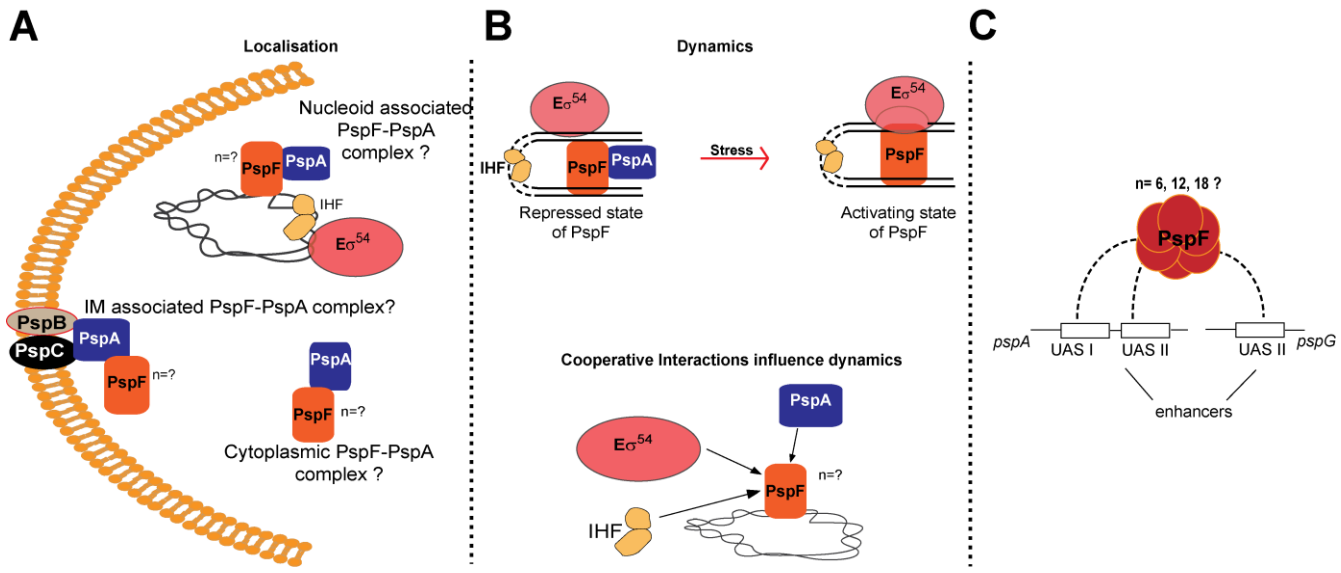

Figure 1.14 **Schematic representation of propositions tested for Venus-PspF.** (A) To determine the subcellular localisation of repressed V-PspF under non-stress conditions and V-PspF under stress conditions.(B) To determine the dynamics of repressed V-PspF and compare it with the dynamics of V-PspF under stress conditions. To establish the vital interactions between V-PspF, RPc and IHF. (C) To determine the functional stoichiometry of V-PspF under non-stress as well as stress conditions and to understand the promoter occupancy of the PspF oligomers to either *pspA* or *pspG* promoters.

1.8.1 Subcellular Localisation of V-PspF

Many different models have been proposed over the years about the localisation of PspF, PspA and the inhibitory PspF-PspA complex in the cell (Darwin *et al.,* 2005, 2007; 2010 and Yamaguchi *et al*., 2013) describing cytoplasmic and membrane bound localisation of Psp response. The SMI approach in live *E. coli* will help to gain insight into the subcellular localisation of PspF-PspA inhibitory complex or PspF self assemblies. In this study a chromosomal fluorescent fusion of PspF Venus fluorescent protein (V-PspF) and some mutants of PspF will be used to perform the SMI approach (2.15 - SMI and image analysis methods). This method will be used to determine if V-PspF is DNA bound or membrane associated in complex with PspA (see Figure 1.14A).

1.8.2 Dynamics of V-PspF

To elucidate the difference between the repressed PspF-PspA inhibitory complex under non-stress conditions from the transcription activating PspF under stress conditions (see Figure 1.14B). Potentially the transcription-activating PspF could be stably bound to its enhancer elements associating with the RPc. In this report the distinction between the repressed and non-repressed states of PspF would be made by measuring the dynamics of V-PspF in the cell, defined by calculating and comparing the different diffusion coefficients.

1.8.3 The interactions between RPc and V-PspF

The importance of interactions of V-PspF with the closed complex will be studied in detail. The changes in the spatial and temporal localisation of V-PspF will be studied in the absence of σ^{54} that results in absence of closed complex. In the same way the effects on the spatial and temporal localisation of V-PspF will be studied in the absence of DNA looping due to the production of truncated IHF. The production of truncated IHF results in the absence of interaction of PspF with the E-σ^{54} complex. The changes in the production of PspF and PspA due to truncated IHF will be studied in detail.

1.8.4 Stoichiometric studies

The functional stoichiometry of PspF under non-stress and stress conditions will be determined using photobleaching experiments. The comparison of the stoichiometry of PspF under non-stress and stress conditions will help in understanding the mechanism of the switch in the functionalities of PspF (see Figure 1.14C). With the transition from non-stress to stress states, PspF goes from repressed by PspA to being the activator of the σ^{54}-dependent transcription of the *psp* genes. The stoichiometry of V-PspF might also help to determine the mechanism of activation of *pspA* and *pspG* promoters. If V-PspF functions as a hexamer *in vivo*, than it would cause simultaneous activation of *pspA* and *pspG* promoters as a higher order oligomer than hexamer. However if it sequentially activates the *psp* promoters than it possibly will be a hexamer (see Figure 1.14C).

1.9 PspA - Master Effector

In many aspects the PspA protein is vital for the adaptive Psp response. PspA is a dual action protein; it functions as a regulator of PspF and an effector during the Psp response (see section 1.5.2- PspA). PspA perceives specific stress stimuli in PspBC dependent manner and relieves the inhibition on PspF (Joly *et al*., 2010). The activation of the Psp response is marked by the higher order oligomerisation of PspA (36-mer) and association with the membrane. However the specific signal and the switch that activates PspA effector function are unknown. The temporal and spatial aspects of the Psp membrane interacting system have been reported in past. The eGFP-PspA fusion was classified into two distinct spatial and functional classes, complexes at the poles proposed to be associated with sensory/regulatory function and motile lateral complexes proposed to be functioning as effectors for maintaining the pmf (Engl *et al*., 2009). The oligomeric state of polar static complexes eGFP-PspA was determined and was found to be hexameric (Lenn *et al.,* 2010). *In vitro* assays have also revealed that hexameric PspA is a regulator and 36-mer acts as an effector (Kobayashi *et al.,* 2007 and Joly *et al.,* 2009).

It has become imperative to characterise the different spatial and temporal properties of PspA-localisation at the membrane, dynamics within the cell, and its lipid binding interactions *in vivo* (see Figure 1.15). In line with the spatial and temporal studies, insights into the structure of PspA especially helix-domain I could lead to a better understanding of the Psp response mechanism. Such PspA structural determinants are implicated in diverse roles - negative control of the Psp response, signal perception via interactions with PspBC, IM-binding and the effector function. These factors also establish the essential link between anionic lipids micro-domains, bacterial cytoskeleton and peptidoglycan biosynthesis machinery and functions of PspA. In addition to revealing the features of PspA functions, it will have an impact on research related to all homologues of PspA.

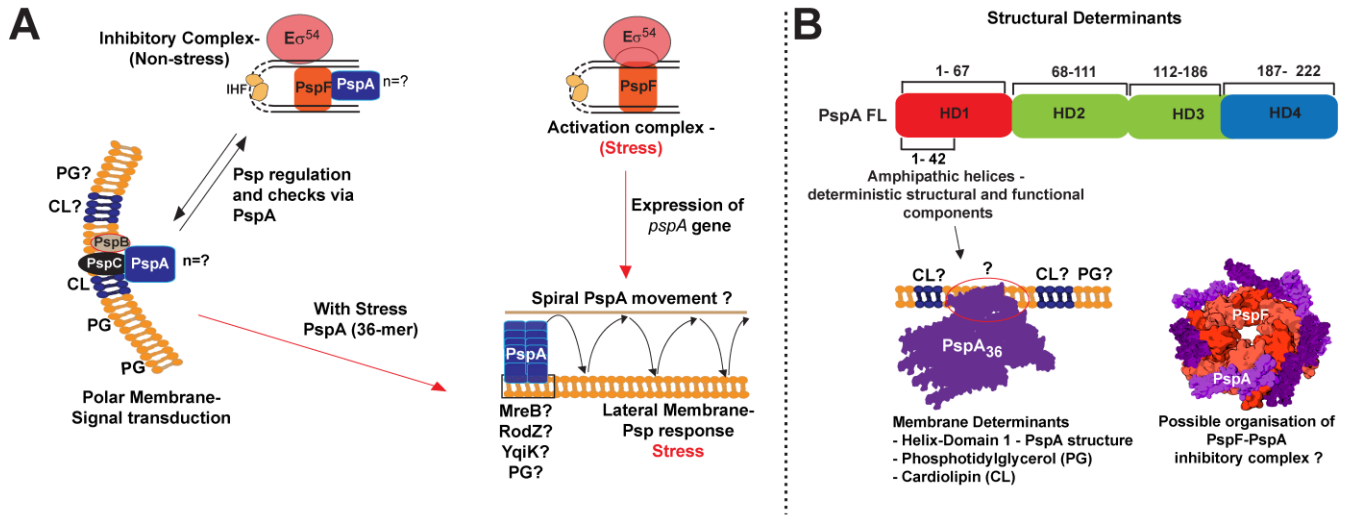

Figure 1.15 **Schematic representation of propositions tested using V-PspA** :(A) The localisation of regulatory V-PspA under non-stress conditions will be studies and the switch in localisation of V-PspA as an effector under stress conditions will be noted. The change in oligomeric state of V-PspA will also be studied from non-stress to stress conditions. The stoichiometry of V-PspA inhibitory complex with PspF will also be determined. Additionally, the interplay between PspA and the cytoskeletal protein such as MreB and cell wall repair protein such as RodZ and potential lipid raft protein YqiK will be reported. All these observations independently will help to derive insights into the mechanism of regulation and activation of Psp response. (B) The structural components of PspA full length protein with its predicted four helix domains (HD). The highlighted HD1 (1-42) will be studied in detail.

The following propositions will be tested in order to unravel effector mechanism of PspA Figure 1.15.The chromosomal fluorescent fusion of full length PspA to Venus - V-PspA will be used for SMI studies to determine the spatial and temporal localisation of PspA.

1.9.1 Mechanism of Regulation and Activation of Psp response by PspA

The observation and correlation of the subcellular localisation, dynamics and the stoichiometry of V-PspA will help to derive a model of the organisation of the PspA as a regulator and effector, and thus the regulation and activation of the Psp response.

Subcellular Localisation: To understand the switch in spatial subcellular localisation of V-PspA in real time from non-stress conditions as a regulator to stress conditions as an effector shown in the illustration in the Figure 1.15A.

Dynamics: The V-PspA fusion will also enable differentiation between the dynamics of PspA under non-stress and stress conditions respectively (as shown in the illustration Figure 1.15A).

Stoichiometry: To classify the shift in oligomeric states of PspA from non-stress to stress growth conditions using photobleaching experiments as shown in Figure 1.15.

1.9.2 Membrane Determinants

Ascertain the role of membrane anionic lipids such as phosphotidylglycerol (PG) and cardiolipin (CL) on the localisation of V-PspA in different growth conditions. Additionally to characterize the role of bacterial actin like MreB, membrane biogenetic protein RodZ and potential lipid raft associated protein YqiK on PspA localisation and effector function during membrane stress as shown in Figure 1.15.

1.9.3 Structural determinants of PspA

Understand the role of N-terminal amphipathic helices within the PspA HD1 and their implications on the structural and biological functions of PspA. To characterise the structural mutants of PspA with respect to their regulatory function, effector function, membrane binding and interaction with the signal sensors PspBC (see Figure 1.15B).

CHAPTER 2

2 Materials and Methods

This chapter includes the materials and methods used for the experiments performed in this work. Standard laboratory methods have been described briefly. The specific methods used for strain constructions such as introduction of fusion proteins into the chromosome, *in vitro* protein work and specific microscopy and image analysis methods are described in detail in separate sections.

2.1 Materials

This section lists the various materials such as media, strains, plasmids, primers, buffers, dyes used in experimental procedures performed in this work.

2.1.1 Media recipes and antibiotics

MEDIUM	COMPOSITION (per litre)
LB (Luria Bertani) broth	10 g peptone, 5 g yeast extract, 5 g NaCl
LB Agar	10 g peptone, 5 g yeast extract, 5 g NaCl, 17 g agar
MacConkey Agar	17 g peptone (Difco), 3 g protease peptone (Difco), 10g Lactose, 5 g NaCl, 1 mg crystal violet, 30 mg neutral red, 1.5 g bile salts, 13.5 g agar
Soft Agar	10 g tryptone, 5 g NaCl and 1.5 g agar
T7 Top Agar	10 g tryptone, 5 g NaCl, 7 g Difco Agar
N^-C^- Minimal media	50 mM MOPS, 2 mM $MgSO_4$, 0.7 mM Na_2SO_4, 1.2mM NH_4NO_3, 0.5 mM KH_2PO_4, 10 mM NH_4Cl, 0.5% w/v Glucose (filter sterilised), (1X) Trace Elements)
Trace Elements (1000X)	5.0 g Na_2EDTA (pH 7.0), 0.5 g $FeCl_3$, 0.05 g $ZnCl_2$, 0.01 g $CuCl_2$, 0.01 g $CoCl_2.6H_2O$, 0.01 g H_3BO_3, 1.6 g $MnCl_2.6H_2O$
SOB (recovery media)	20 g tryptone, 5 g yeast extract, 10mM NaCl, 2.5 mM KCl, 10mM $MgCl_2$, 10mM $MgSO_4$
SOC (recovery media)	SOB + 20mM glucose (filter sterilised)

Table 2.1 The composition of media used to grow bacterial strains.

The following antibiotics were filter sterilised (0.2 µm pore-size) and used at the following concentrations for selection of plasmids and strains.

ANTIBIOTIC	CONCENTRATION
Ampicillin (Amp)	100 µg/ml in water
Kanamycin (Kan)	50 or 25 µg/ml in water
Tetracycline (Tet)	10 µg/ml in water
Chloramphenicol (Cam)	30 µg/ml in ethanol (100 % v/v)
Spectinomycin (Spec)	100 µg/ml in water

Table 2.2 The list of antibiotics used with respective working concentration and abbreviations

2.1.2 Bacterial strains and plasmids

In this section the bacterial strains and plasmids used and engineered for the research are listed in the table with the relevant literature reference. And all these strains and plasmids have been used throughout this work

2.1.2.1 Bacterial strains

STRAIN	RELEVANT CHARACTERISTICS	REFERENCE
MG1655	WT	CGSC#7740
MG1655Δ*pspF*	MG1655 Δ*pspF*	Lloyd *et al.*, 2004
MG1655Δ*pspA*	MG1655 Δ*pspA*	Lloyd *et al.*, 2004
MG1655Δ*pspBC*	MG1655 Δ*pspBC*	Lloyd *et al.*, 2004
MVA27	MG1655Δ*pspA* ϕ (*pspA-lacZ*) (amp^R)	Jovanovic *et al.*, 2006
MVA29	MG1655 Δ*pspABC*::*kan* (kan^R)	Lloyd *et al.*, 2004
MVA44	MG1655 ϕ(*pspA-lacZ*) (amp^R)	Jovanovic *et al.*, 2006
MVA45	MG1655Δ*pspBC* ϕ(*pspA-lacZ*) (amp^R)	Jovanovic *et al.*, 2006

MG1655 V-PspF	MG1655 expressing chromosomal Venus-PspF (kan^S, $sucrose^R$)	Gift from Tchern Lenn This work MG1655 *pspF*::*nptI-sacB kan* /pTKRED(λRed) + *venus-pspF*
MG1655 V-PspF	*ΔrpoN*, *ΔhimA* , *Δcls*	Engineered by P1 transduction
MG1655 V-$PspF^{W56A}$	MG1655*ΔpspF* expressing chromosomal Venus-$PspF^{W56A}$ mutant (kan^S, $sucrose^R$)	Gift from Tchern Lenn Mehta *et al*., 2013 This work MG1655 *pspF*::*nptI-sacB kan* /pTKRED(λRed) + *venus-*$pspF^{W56A}$
MG1655 V-$PspF^{W56A}$	*ΔrpoN*, *ΔhimA*	Engineered P1 transduction
MG1655 V-PspF tet^R	MG1655 V-PspF *venus-pspF::tet* (tet^R)	Mehta *et al*., 2013
MG1655 V-$PspF_{1\text{-}275}$	MG1655 expressing chromosomal Venus-$PspF_{1\text{-}275}$ (tet^S)	Mehta *et al*., 2013 This work MG1655 V-PspF tet/pTKRED(λ Red) + *venus-*$pspF_{1\text{-}275}$ (Stop 276)
MG1655 V-$PspF_{1\text{-}275}$	*Δcls*	Mehta *et al*., 2013
JWK3169	BW25113 *ΔrpoN::Kan* (kan^R)	Baba *et al*., 2006
MC1068	MC1061 *ΔhimA::Tn10* (tet^R)	Laboratory Collection
MVA129 V-PspFΔP*pspG*	MG1655 V-PspF Δ*PpspG*::kan (kan^R)	Gift from Goran Jovanovic (G.J.) This work MG1655 V-PspF/pkD46 (λRed1) + Δ*PpspG*::kan (pKD4 Kan template)
MVA44 (*PpspA-lacZ*) promoter fusion	MG1655 ϕ (*PpspA-lacZ*) (amp^R)	Jovanovic *et al*., 2006

MVA131 V-PspFΔP*pspG*:: (P*pspA-lacZ*)	MVA44 ΔP_{pspG}::*kan* (amp^R kan^R)	Gift from G.J. This work MG1655 V-PspF x P1/MVA129
C600	F^- tonA21 thi-1 thr-1 leuB6 lacY1 glnV44 rfbC1 fhuA1 $\lambda^{-¶}$	Laboratory collection
SA1943	$galK_{am}$ his *rpsL*	Yu and Court 1998
SA1943 λ V-PspA	SA1943 *attB*::P_{pspA}-*venus-pspA* (amp^r)	Gift from G.J. SA1943 x λBDC531 (P_{pspA}-I*venus-pspA*) (amp^r)
DY226	W3110 _*lac*U169 *gal*490 λ[N::*lacZ imm*λ (*cro-bio*) *rnc*14λ^r	Yu and Court. 1998
DY226 λV-PspA	DY226 attB::P_{pspA}-*venus-pspA* (amp^r)	Gift from G.J. DY226 x P1/SA1943 λV-PspA
MVA101 V-PspA with native PspA	MG1655 *attB*::P_{pspA}-*venus-pspA* (amp^r) expressing chromosomal Venus-PspA	Gift from G.J. This work MG1655xMVA127
MVA127 V-PspAΔ*pspA*	MG1655Δ*pspA attB*::P_{pspA}-*venus-pspA* (amp^r), expressing chromosomal Venus-PspA	Gift from G.J.
MVA102 V-PspAΔ*pspBC*	MG1655Δ*pspBC attB*::P_{pspA}-*venus-pspA* (amp^r) expressing chromosomal Venus-PspA	Gift from G.J. This work MG1655Δ*pspBC*xMVA127
JW2500 Δ*rodZ*	Δ*rodZ*::*kan* (kan^r), peptidoglycan biogenesis protein absent	Baba *et al*., 2006
JW1241 Δ*cls*	Δ*cls*::*kan* (kan^r), absent cardiolipin synthase	Baba *et al*., 2006
JW3023 Δ*yqiK*	Δ*yqiK*::*kan* (kan^r), absent bacterial equivalent of lipid rafts	Baba *et al*., 2006

UE54 *Δpgs*	MG1655 *lpp-2* Δ*ara714* *rcsF*::mTn*10cam* Δ*pgsA*::*kan* (cam^r, kan^r) , phosphoglycerol synthase is absent	A gift from W. Dowhan Shiba *et al*., 2004
MC1000	WT	A gift from Y.L. Shih
MC1000 Δ*mreB*	MC1000 Δ*mreB*::*cam* (cam^r), bacterial cytoskeletal protein MreB absent	A gift from Y.L. Shih Engl *et al*., 2009
MVA108 ΔrodZ:: ϕ (*pspA-lacZ*)	MVA44 Δ*rodZ*::*kan* (amp^r, kan^r)	Gift from G.J. This work MVA44xJW2500
MVA109 *ΔpspBCΔrodZ* :: ϕ(*pspA-lacZ)*	MVA45 Δ*rodZ*::*kan* (amp^r, kan^r), RodZ absent in Δ*pspBC* ϕ (*pspA-lacZ*)	This work MVA45xJW2500
MVA27 *ΔpspAΔrodZ* :: ϕ(*pspA-lacZ*)	MG1655Δ*pspA* Δ*rodZ*::*kan* ϕ(*pspA-lacZ*) (kan^r, amp^r)	Gift from G.J. This work MVA27xJW2500
MVA110 V-PspAΔ*rodZ*	MVA101 Δ*rodZ*::*kan* (amp^r, kan^r)	Gift from G.J. This work MVA101xJW2500
MVA111 V-PspAΔ*pspBCΔrodZ*	MVA102 Δ*rodZ*::*kan* (amp^r, kan^r)	Gift from G.J. This work MVA102xJW2500
MVA107 *Δpgs*A-ϕ(*pspA-lacZ*)	UE54 (Δ*pgsA*::*kan*) ϕ(*pspA-lacZ*) (kan^r, amp^r)	Gift from G.J This work UE54xMVA44
MVA115 *Δcls*	MG1655 Δ*cls*::*kan* (kan^r)	Gift from G.J. This work MG1866xJW1241
MVA116 *Δcls*-ϕ(*pspA-lacZ*)	MVA44 Δ*cls*::*kan* (amp^r, kan^r)	Gift from G.J This work MVA44xJW1241
MVA117 *ΔpspBCΔcls* :: ϕ(*pspA-lacZ)*	MVA45 Δ*cls*::*kan* (amp^r, kan^r)	Gift from G.J. This work MVA45xJW1241

MVA27 *ΔpspAΔcls*:: ϕ(*pspA-lacZ)*	MG1655Δ*pspA* Δ*cls*::*kan* ϕ(*pspA-lacZ*) (kan^r, amp^r)	Gift from G.J. This work MVA27xJW1241
MVA118 V-PspAΔ*cls*	MVA101 *Δcls*::*kan* (amp^r, kan^r)	Gift from G.J. This work MVA101xJW1241
MVA119 V-PspAΔ*pspBC*Δ*cls*	MVA102 Δ*cls*::*kan* (amp^r, kan^r)	Gift from G.J This work MVA102xJW1241
MVA120Δ*yqiK*	MG1655 *ΔyqiK*::*kan* (kan^r)	Gift from G.J This work MG1655xJW3023
MVA121 Δ*yqiK*:: ϕ(*pspA-lacZ*)	MVA44 *ΔyqiK*::*kan* (amp^r, kan^r)	This work MVA44xJW3023
MVA117 Δ*pspBC*Δ*yqiK* :: ϕ (*pspA-lacZ*)	MVA45 *ΔyqiK*::*kan* (amp^r, kan^r)	Gift from G.J. This work MVA45xJW3023
MVA27 *ΔpspAΔyqiK*:: ϕ(*pspA-lacZ)*	MG1655Δ*pspA* Δ*yqiK*::*kan* ϕ(*pspA-lacZ*) (kan^r, amp^r)	Gift from G.J. This work MVA27xJW3023
MVA123 V-PspAΔ*yqiK*	MVA101 Δ*yqiK*::*kan* (amp^r, kan^r)	Gift from G.J. This work MVA101xJW3023
MVA124 V-PspAΔ*pspBC*Δ*yqiK*	MVA102 Δ*yqiK*::*kan* (amp^r, kan^r)	Gift from G.J. This work MVA102xJW3023
MVA125 Δ*mreB*Δ*yqiK*	MC1000 Δ*mreB* Δ*yqiK*::*kan* (cam^r, kan^r)	Gift from G.J. This work MC1000 Δ*mreB* xJW3023
MVA126 Δ*mreB*Δ*rodZ*	MC1000 Δ*mreB* Δ*rodZ*::*kan* (cam^r, kan^r)	This work MC1000 Δ*mreB* xJW2500
MVA128 Δ*mreB*Δ*cls*	MC1000 Δ*mreB* Δ*cls*::*kan* (cam^r, kan^r)	Gift from G.J. This work MC1000 Δ*mreB* xJW1241
XL1-Blue	tet^r – Laboratory Collection	Cloning strain

BL21	Laboratory Collection	Expression strain for high level expression of recombinant proteins
BTH101	cya^{-}lac^{+}	Karimova *et al*.,1998

Table 2.3 The table lists the bacterial strains used for the research

2.1.2.2 Plasmids

The plasmids listed in this table have been used throughout this work.

PLASMID	RELEVANT CHARACTERISITICS	REFERENCE
pTKRED	Plac λ-Red P*ara* I-SceI RecA (spc^{r})	Kuhlman and Cox 2010
pTKS	*tetA*-I-*SceI* recognition sites (tet^{r})	Kuhlman and Cox 2010
pUM24	*nptI-sacB kan* cassette (sucrose^{s}, kan^{r}, amp^{r}) cartridge plasmid	A gift from T. Friedrich Pohl et al., 2007
pKD46	Red1 recombinase expressing plasmid (amp^{r})	Datsenko and Wanner 2000
pKD4	FRT-Kan-FRT cassette template plasmid (kan^{r})	Datsenko and Wanner 2000
pCS2	Plasmid expressing fast maturing fluorescent protein Venus (amp^{r})	A gift from T. Nagai to lab
pCG65	Venus/pCS2 carrying Venus-PspA fusion (amp^{r})	Gift from G.J This work
pRS415	Transcription fusion vector (amp^{r})	Simons *et al*.,1987
pCG66	pRS415 carrying P_{pspA}-Venus-PspA fusion (amp^{r})	Gift from G.J.
pCP20	*FLP*$^{+}$, λ *cI*857^{+}, λ p_R Rep^{ts}, (amp^{r}, cam^{r})	Cherepanov and Wackernagel 1995
pGJ4	P_{lacUV5}-*gIV*(pIV) (tet^{r})	Jovanovic *et al*., 2006

pBR325D	Cloning vector, *colD* ori (cam^r, tet^r, amp^r)	Laboratory collection
pGZ119EH	IPTG-inducible *tac* promoter expression vector, (cam^r)	A gift from M. Russel
pMJR129	pGZ119EH harbouring *gIV* (pIV), (cam^r)	A gift from M. Russel
pBAD18-cam	Expression vector, pBAD *ara* promoter (cam^r)	A gift from J. Beckwith
pPB10	pBAD18-cam harbouring wild type (WT) $PspA_{WT/FL}$ (cam^r)	Jovanovic *et al*., 2006
pPB11	pBAD18-cam harbouring $PspA_{1-67}$ (cam^r)	Gift from G.J.
pPB13	pBAD18-cam harbouring $PspA_{1-186}$ (cam^r)	Gift from G.J.
pPB15	pBAD18-cam harbouring $PspA_{68-222}$ (cam^r)	Gift from G.J.
pGJ62	pBD18-cam harbouring $PspA_{\Delta 25-40/ahII}$ (cam^r)	Gift from G.J.
pGJ63	pBAD18-cam harbouring $PspA_{+P33}$ (cam^r)	Gift from G.J.
pGJ64	pBAD18-cam harbouring $PspA^{V29E}$ (cam^r)	Gift from G.J.
pGJ65	pBAD18-cam harbouring $PspA^{V29F}$ (cam^r)	Gift from G.J.
pGJ67	pBD18-cam harbouring $PspA_{\Delta 2-19/ahI}$ (cam^r)	Gift from G.J.
pGJ68	pBAD18-cam harbouring $PspA^{F4E}$ (cam^r)	Gift from G.J.
pGJ69	pBAD18-cam harbouring $PspA^{V11E}$ (cam^r)	Gift from G.J.

pGJ89	pBAD18-cam harbouring $PspA^{P25A}$ (cam^r)	Gift from G.J.
pKT25	IPTG-inducible vector containing the T25 domain of Cya upstream of the MCS (kan^r)	Karimova *et al*., 1998
pUT18C	IPTG-inducible vector containing the T18 domain of Cya upstream of the MCS (amp^r)	Karimova *et al*., 1998
pKT25zip	GCN4 leucine zipper fusion to the C-terminus of the T25 domain of Cya in pKT25 (kan^r)	Karimova *et al*., 1998
pUT18Czip	GCN4 leucine zipper fusion to the C-terminus of the T18 domain of Cya in pUT18C (amp^r)	Karimova *et al*., 1998
T18-PspC	pUT18C harbouring $PspC_{WT/FL}$ (amp^r)	Jovanovic *et al*., 2010
pUT18C-PspF	pUT18C harbouring $PspF_{WT/FL}$ (amp^r)	This work
T25-PspA; (pAJM26)	pKT25 harbouring $PspA_{WT/FL}$ (kan^r)	Jovanovic *et al*., 2010 Engl *et al*., 2009
pAJM26-V11E	pKT25 harbouring $PspA^{V11E}$ (kan^r)	Gift from G.J.
pAJM26-P33	pKT25 harbouring $PspA_{+P33}$ (kan^r)	Gift from G.J.
pAJM26-V29E	pKT25 harbouring $PspA^{V29E}$ (kan^r)	Gift from G.J.
pAJM26-V29F	pKT25 harbouring $PspA^{V29F}$ (kan^r)	Gift from G.J.
pAJM26-ΔahA	pKT25 harbouring $PspA_{\Delta 2\text{-}19/ahI}$ (kan^r)	Gift from G.J.
pAJM26-ΔahB	pKT25 harbouring $PspA_{\Delta 25\text{-}40/ahII}$ (kan^r)	Gift from G.J.
pAJM26-P25A	pKT25 harbouring $PspA^{P25A}$ (kan^r)	Gift from G.J.

pPB1	pET28b+ harbouring $PspF_{1-275}$ (kan^r)	Bordes *et al*., 2003
pSLE18 A	pET28b+ harbouring $PspA_{WT//FL}$ (kan^r)	Elderkin *et al*., 2002
pPM1	pET28b+ harbouring $PspA_{\Delta 2\text{-}19/ahI}$ (kan^r)	This work
pPM2	pET28b+ harbouring $PspA^{V11E}$ (kan^r)	This work
pPM3	pET28b+ harbouring $PspA_{\Delta 25\text{-}40/ahII}$ (kan^r)	This work
pPM4	pET28b+ harbouring $PspA_{+P33}$ (kan^r)	This work
pPM5	pET28b+ harbouring $PspA^{V29E}$ (kan^r)	This work
pGJ91	pET28b+ harbouring $PspA^{P25A}$ (kan^r)	Gift from G.J.
pDSW209	P_{trc} promoter *gfpmut2*-MCS fusion vector (amp^r)	Weiss *et al.*, 1999
pEC1	pDSW209 expressing eGFP-$PspA_{WT/FL}$ (amp^r)	Engl *et al*., 2009
pGJ70	pDSW209 expressing eGFP-linker-$PspA_{\Delta 2\text{-}19/ahI}$ (amp^r)	Gift from G.J.
pAD1	pDSW209 expressing eGFP-linker-$PspA_{\Delta 25\text{-}40/ahII}$ (amp^r)	Gift from G.J.
pGJ90	pDSW209 expressing eGFP-linker-$PspA^{P25A}$ (amp^r)	Gift from G.J.
pCG66	pRS415 harbouring P_{pspA}-Venus-$PspA_{WT/FL}$ fusion (amp^r)	Gift from G.J.

pEXT22	Expression vector, P_{tac} promoter, *lacI*^{q} (kan^r)	Dykxhoorn *et al.*, 1996
pEXT22V-PspF	pEXT22 expressing Venus-PspF $_{WT/FL}$ fusion protein (kan^r)	This work, Gift from Tchern Lenn
pCE2	σ^{54}-YFP; medium copy plasmid	Gift from Christoph Engl
pCA24N	Expression vector, $P_{T5/lac}$ promoter, *lacI*^{q} (cam^r)	Kitagawa *et al.*, 2005
JW1897(-)	pCA24N harbouring PgsA (cam^r)	Kitagawa *et al.*, 2005
JW1241(-)	pCA24N harbouring Cls (cam^r)	Kitagawa *et al.*, 2005
JW2500(-)	pCA24N harbouring RodZ (cam^r)	Kitagawa *et al.*, 2005
JW3023(-)	pCA24N harbouring YqiK (cam^r)	Kitagawa *et al.*, 2005
JW3023(+)	pCA24N harbouring YqiK-GFP fusion protein (cam^r)	Kitagawa *et al.*, 2005
pGEM-T Easy	Cloning vector (amp^r)	Promega

Table 2.4 The list of plasmids used in the research.

2.1.3 General Lab Buffers and Chemicals

The table lists some standard laboratory buffers, chemicals and dyes used in this work.

BUFFER	COMPOSITION	USE
Tris.HCl	121 g Tris Base in 800 ml water, pH adjusted. Volume to 1L water	Standard buffer
Stripping buffer	100 mM 2- Mercaptoethanol, 2 % (w/v) SDS, 62.5 mM Tris-HCl pH 6.7)	Western blot membrane stripping buffer

Z-buffer	60 mM Na_2HPO_4 , 40 mM $NaH_2PO_4.2H_2O$, 10 mM KCl, 1 mM $MgSO_4.7H_2O$, 38 mM of 2-Mercaptoethanol was added per litre just before use	β-Galactosidase Assay
Acrylamide (National Diagnostics)	30 % (w/v) acrylamide 0.8 % (w/v) bis-acrylamide	Protein Gels
Solution II	1.5 M Tris-HCl (pH 8.8) 0.3 % (w/v) SDS	Protein Separating Gel
Solution III	0.5 M Tris-HCl (pH 6.8) 0.4 % (w/v) SDS	Protein Stacking Gel
De-stain	45 % (v/v) methanol, 10 % (v/v) acetic acid	De-staining of Comassie stained protein gel
TBE Buffer	89 mM Tris Borate pH 8.3, 2 mM Na_2EDTA	Agarose DNA gels, loading buffer
Transblot Buffer	10 mM Tris, 100 mM glycine, 10 % v/v methanol	Western Blot transfer buffer
TBS	Sigma-Aldrich	Western Blot transfer buffer
TBSTT	Sigma Aldrich- TBS, 0.1 % (w/v) Tween 20	Western Blot transfer buffer
5X Native loading dye	10% (v/v) Glycerol, 0.5mg Bromophenol Blue	

Table 2.5 The list of buffers used in the different experimental procedures.

CHEMICAL/DYE	SUPPLIER	USE
SYBR® Safe	Invitrogen	DNA gel stain
6X DNA loading dye	Fermentas	DNA gel sample loading buffer
2X Laemmli	Sigma	SDS-PAGE sample loading buffer

Isopropyl β-D-1-thiogalactopyranoside – IPTG (1 M)	Sigma	Induction of protein expression from *lac*
5-bromo-4-chloro-3-indolyl-β-D-galactopyranoside- Xgal (0.1M)	Sigma	Blue/white screening
Ortho-Nitrophenyl-β-galactoside ONPG (1 M)	Sigma	β-galactosidase activity assay substrate
Comassie Blue Stain/Bromophenol Blue	Sigma	Staining SDS protein gel
Sypro Ruby	Invitrogen	Staining SDS protein gel
Ponceau Stain	Sigma	Western Blot membrane staining
Silver Staining	Fixer – 40 % (v/v) ethanol , 10 % (v/v) acetic acid , 50 % (v/v) H_2O Stain – 0.1 % (w/v) Silver Nitrate solution (0.2 g $AgNO_3$, 200 ml H_2O, 0.02 % formaldehyde) Developer – 3 % Na_2CO_3 (w/v) solution in H_2O (Sigma chemicals)	Staining SDS protein gel
1 Kbp ladder	Promega	DNA bp ladder
220 kDa Protein Ladder	Invitrogen	Protein size ladder
Magic Marker	Invitrogen	Western blot ladder

Table 2.6 The list of chemicals and dyes used in the experimental procedures.

2.1.4 Kits

TYPE OF KIT	SUPPLIER	USE
QIAprep Spin Miniprep Kit	Qiagen	Isolation of plasmid DNA
QIAquick PCR Purification Kit	Qiagen	PCR purification
QIAquick Gel Extraction Kit	Qiagen	Gel Extraction
GoTaq DNA Polymerase	Promega	PCR
Peq Taq Polymerase Pfu Phusion	Peq Labs Invitrogen	Mutagenesis
Amersham ECL Western Blotting Detection Reagents	GE Healthcare	Detection of HRP conjugated 2^{o} Antibody for Western Blotting
Modified Lowry Protein Assay	Thermo Scientific	Protein Quantification

Table 2.7 The table lists the commercially available kits used for the research

2.1.5 DNA Primers

PRIMER NAME	SEQUENCE	USE
Δ25-40 Fw Rv	CGC TCT GTT AGA GAA AGC GGA AGA TGT TGA AGT ACG TTC TAC TTC GGC GCG CGC G CGC GCG CGC CGA AGT AGA ACG TAC TTC AAC ATC TTC CGC TTT CTC TAA CAG AGC G	Δ25-40 deletion in His-PspA FL and eGFP-$PspA^{\Delta 25\text{-}40}$ fusion
V/E Fw Rv	GCG GAA GAT CCA CAG AAA CTG GAA CGT CTG ATG ATC CAG GAG ATG G CCA TCT CCT GGA TCA TCA GAC GTT CCA GTT TCT GTG GAT CTT CCG C	V-E mutation in His-PspA $pET28B^{+}$
V/F Fw	GCG GAA GAT CCA CAG AAA CTG TTT CGT CTG ATG ATC CAG GAG ATG G	V-E mutation in His-PspA

Rv	CCA TCT CCT GGA TCA TCA GAC GAA ACA GTT TCT GTG GAT CTT CCG C	pET28B^{+}
Δ2-19 Fw Rv Δ2-19 Fw Rv	GCG GCC TGG TGC CGC GCG GCA GCC ATA TGG AGA AAG CGG AAG ATC CAC AGA AAC TGG CCA GTT TCT GTG GAT CTT CCG CTT TCT CCA TAT GGC TGC CGC GCG GCA CCA GGC CGC GCC TGG TGC CGC GCG GCA GCC ATA TGG AGA AAG CGG AAG ATC CAC AGA AAC TGG CCA GTT TCT GTG GAT CTT CCG CTT TCT CCA TAT GGC TGC CGC GCG GCA CCA GGC	Δ2-19 in His-PspA pSLEA Δ2-19 mutation in eGFP-PspA
+Pro Fw Rv	CTG GTT CGT CTG ATG CCA ATC CAG GAG ATG GAA G CTT CCA TCT CCT GGA TTG GCA TCA GAC GAA CCA G	+ Pro mutation in His-PspA pET28B^{+}
Venus+ Linker Rv	GAA TTC ACC AGA ACC ACC CTT GTACAG CTC GTC CAT G	PCR 1 with pCP2 as Venus-template
pspFKO^{-} Rv	AGC CCA ACG CAA TAA TGT C	PCR1
pspFVenus -ext	AAG ATC TGA TTG AAG AAT CAA CAT GCC AGG ATG AGT TAG CGA ATT ACA CTA ACA	PCR2 -overlap PCR to introduce V-F
F-Venus Fw1	GTT AGC GAA TTA CAC TAA CAA GTG GCG AAT TTC ATC ATC GTG AGC AAG GGC GAG GAG C	PCR1
Linker - pspF Fw	GGT GGT GGT TCT GGT GAA TTC ATG GCA GAA TAC AAA G	PCR1
W56A Fw Rv	GCA TTA TCT CTC CTC CCG TGC GCA AGG GCC GTT TAT TTC GAA ATA AAC GGC CCT TGC GCA CGG GAG GAG AGA TAA	Introduce W56A mutant in V-F fusion

	TGC	
*Kpn*IVenus Fw	GCG GGTACC ATG GTG AGC AAG GGC GAG G	Check V-F fusion
*Xba*IPspF Rv	GCT CTA GAG CAT CCG GCA AGT TGT ATT GC	Check V-F fusion
Recom-Tet cassette Fw	CCT TTA AAC GGC GTC CGC CTG AAG ACG CTA TCG CCG TTT CAG AAA CCA CCT CGC TTC CAA CAC TGT ACG GCC CCA AGG TCC AAA CGG TGA	*ΔpspF* knockout- Tet^R
Recom-Tet cassette Rv	TCC CTT GTT GCA AAC TGA GTT GCA GCA ACT CTT TTT CCT GCT GCA TCT GAA ACT CAC GTA AAT CCT TGG CTT CAG GGA TGA GGC GCC ATC	*ΔpspF* knockout- Tet^R
Fw1-flanking *pspF*	GAA TTG AAA AAC GTG GTG GAAC	Overlap PCR to make $PspF_{1-275}$
Rv1-flanking *pspF*	GCG CGG AAC TGA TGA TAAG	Overlap PCR to make $PspF_{1-275}$
mut Fw mut Rv	C TCG CTT CCA ACA CTG TAG CTG GAT TTA CGT GAG TTT C GAA ACT CAC GTA AAT CCA GCT ACA GTG TTG GAGCG AG	Engineer $PspF_{1-275}$
ΔP*pspG* Fw ΔP*pspG* Rv	TGC TGG AAC ACG CGC TCA AAC TGG TGG CGG ATA AGC GTT AAC TTT TCA CCT GTG TAG GCT GGA GCT GCT TCG CGG TGA CCA TCA GCA TGA CAA AAA AGC CAA TCA CAA AAA GTA GTT CCA GCC ATA TGA ATA TCC TCC TTAG	Introduce *pspG* promoter deletion
ΔP*pspG* check Fw ΔP*pspG* check Rv	TGCTGGAACACGCGCTCAAACTGG CGGTGACCATCAGCATGACAAAAAAGCC	To check for the deletion of *pspG* promoter
CHIP Fw	TTCGCCACTTGTTAGTGTAATTCGC	ChIP for V-

CHIP Rv	CCTGGATCATCAGACGAACCAGTTTCTGTGG	PspF

Table 2.8 The list of primer names, their sequence used. All sequences provided in 5'- 3' direction

2.2 Methods

2.2.1 Generation of bacterial strains

The *E. coli* strain MG1655 was used in this study, in which the chromosome was modified to express fluorescent fusion proteins using Venus as the fluorescent protein. Several different chromosome modification methods were used such as red-recombineering, λ-phage and $P1_{vir}$ phage based transductions. All these different methods resulted in the similar successful introduction of the recombinant gene into the chromosome. The method of choice for recombination also was governed by the starting recombinant gene template. The details are explained below.

2.2.1.1 P1 Transduction

P1 transduction is mediated by infection of the donor bacterial cell and depends on accidental packaging of bacterial DNA by the phage during infection. A subpopulation of such mutant $P1_{vir}$ phage enters into lytic cycle upon infection and ensures replication and cell lysis. The lysate made from the donor strain is then be used to infect a recipient strain and in this process small number of phage transfer the desired gene onto the recipient at its *att* site. The recombined strain is selected for by antibiotic resistance. This method was used to replace LacI-GFP in WT cells, to introduce *ΔrpoN* and *ΔhimA* in cells expressing V-PspF and V-$PspF^{W56A}$, to introduce *Δcls* in V-PspF and V-$PspF_{1-275}$, *pspG* promoter was deleted in V-PspF and also the native *pspA* was deleted in V-PspA using P1 transduction (as shown in Table 2.3).

2.2.1.1.1 $P1_{vir}$ bacteriophage lysate preparation

The bacteriophage lysate was prepared from the donor strain (JWK3169, MC1068, MVA131 – see Table 2.3). For the lysate preparation 0.2 ml of an overnight culture (5 ml) of the donor strain was incubated for 25 minutes with 0.2 ml of a $P1_{vir}$ bacteriophage lysate to allow phage binding to the bacterial cell for infection depends on the phage titre. Then 9.25 ml of LB, 0.25 ml of 40% glucose (w/v) and 0.50 ml 0.1 M $CaCl_2$ was added to the 0.4ml of the above solution in a 100 ml sterile flask for uniform aeration. The cells were incubated at 37°C for around 5-6 hours with shaking until the suspension became clear (upon phage replication, bacterial cells are lysed and can be seen as debris). 2 ml chloroform was added to kill any remaining unlysed bacteria. After 30 minutes incubation at room temperature (RT), the lysate was centrifuged at 16,278 x g at RT for 10 minutes. The supernatant contained the P1*vir* phages including a sub-population of phage containing the bacterial DNA of interest. This lysate solution was subsequently used to infect the recipient strain (*E. coli* MG1655 Venus-PspF/$PspF^{W56A}$ fusion proteins).

2.2.1.1.2 Infection of the recipient strain

Cells from a 5 ml overnight culture of the recipient strain were harvested by centrifugation (5 minutes, RT, 3100 x g) and primed for transduction by 20 minutes incubation in 4.75 ml 0.1 M $MgSO_4$, 0.25 ml 0.1 M $CaCl_2$ at 37°C with shaking. Then, 0.2 ml of the recipient strain was mixed with 0.2 ml of the P1*vir* bacteriophage lysate and incubated for 20 minutes at 37°C without shaking (during this time transduction occurs). Transduction was terminated with 0.4 ml 1 M Na-citrate. The suspension was mixed with 3 ml soft agar and poured onto LB plates containing specific antibiotic and then the transductants were selected.

2.2.1.2 Red-Recombineering Technique

2.2.1.2.1 Construction of strain expressing chromosomal V-PspF, V-PspF^{W56A} and V-PspF$_{1-275}$

The strains expressing Venus-(linker)-PspF (V-PspF) and Venus-(linker)-PspF^{W56A} were constructed using the Red recombineering method for gene replacement (Kulhman and Cox, 2010 and Datsenko and Wanner, 2000) and antibiotic/sucrose counter-selection using the (nptl-sacB) system (Reid and Collmer 1987). The V-PspF and V-PspF^{W56A} were constructed by Dr. Tchern Lenn (ex-laboratory member) and he guided me with the construction of V-PspF$_{1-275}$. The *pspF* gene in MG1655 was first replaced with the *nptl-sacB::kan* cassette, with kanamycin resistant/sucrose sensitivity selection and later replaced with *venus-linker-pspF*/*pspF*^{W56A} fusions selecting for resistance to 5% sucrose (w/v) and kanamycin sensitivity (see Table 2.3). The overlap PCR method was used to place together *venus* and *pspF/pspF*^{W56A} genes with a linker of 7 a.a (3G-1S-1E-1F) (Engl *et al*., 2009). The flanking primers to *pspF* or *pspF*^{W56A} genes using the (see Table 2.8) pPB8-WT or pPB8-W56A (see Table 2.4) template respectively were used for overlap PCR using Pfu Ultra polymerase. Then fusion gene carrying *venus-(linker)-pspF/pspF*^{W56A} DNA were produced by first generating *venus* gene from pCS2 plasmid with flanking *pspF* genes to later stich with the *pspF/pspF*^{W56A} with the linker (as shown in Figure 2.1)
In the first step, the allelic exchange was performed between the MG1655 chromosomal *pspF* and the PCR amplified [Pfu ultra II (HS) (Stratagene)] *nptl-sacB kan* cassette containing 5' and 3' *pspF* flanking DNA sequences by using kanamycin (resistance)-sucrose (sensitivity) counter-selection. MG1655 carrying pTKRED (plasmid expressing the Red recombinase; spectinomycin resistant, 100 µg ml^{-1}) was transformed with the *nptl-sacB kan* linear DNA cassette by electroporation. The pTKRED plasmid facilitates the recombination between the *pspF* gene and *nptl-sacB::kan* cassette. The electroporation was carried out with 1 mm gap cuvettes and Ec1 setup on Bio-Rad micropulser; after electroporation cells were recovered for 3 hours in SOC media at 30^{o}C. The transformants were selected on LA+kanamycin (25 µg ml^{-1}) plates at 42^{o}C to eliminate the pTKRED plasmid which is temperature sensitive. Kanamycin-resistant colonies, arising by integration of the *nptl-sacB kan* cassette into the

pspF gene on the chromosome of strain MG1655, were grown overnight in liquid culture without selection and plated onto glucose and then by replica plating onto sucrose plates to select for sucrose-sensitive candidates. Colonies were checked by performing PCR using flanking primers specific for the *nptI-sacB kan* cassette.

In the second step, MG1655 *pspF::nptI-sacB kan*^{R} now carrying pTKRED where transformed by *venus-(linker)-pspF* or *venus-(linker)-pspF*^{W56A} linear DNA by electroporation and the *nptI-sacB kan* was excised from the chromosome through a second recombination event being replaced by *venus-(linker)-pspF/pspF*^{W56A} as shown in the Figure 2.1A. The desired sucrose-resistant kanamycin sensitive phenotype of candidate recombinants (MG1655 V-PspF or MG1655 V-PspF^{W56A}; see Table 2.3) was verified by replica-plating and candidate colonies were screened for the desired genotype by colony PCR with primers designed to anneal outside the sites of recombination.

PCR products were sequenced to check that the Venus-(linker)-PspF or Venus-(linker)-PspF^{W56A} was correctly inserted and for point mutations. To obtain MG1655 V-PspF lacking DNA binding domain (helix-turn-helix motif) - Venus-(linker)-PspF$_{1-275}$, the red recombineering method and the pTKRED plasmid were used to replace the V-PspF with the V-PspF$_{1-275}$ as shown in Figure 2.1B. A stop codon at the 276th amino acid of V-PspF was introduced to express V-PspF$_{1-275}$ using PCR amplification using specific primers *venus::pspF* fw and mut rv primers see Table 2.8.The tet-cassette containing the *pspF* flanking primers see Table 2.8 (PCR amplified from the plasmid pTKS) was first introduced into the MG1655 V-PspF recipient. In the second step Tet cassette was replaced with the Venus-(linker)-PspF$_{1-275}$ and selected for the tetracycline sensitive MG1655 V-PspF$_{1-275}$ recombinants (see Table 2.3).

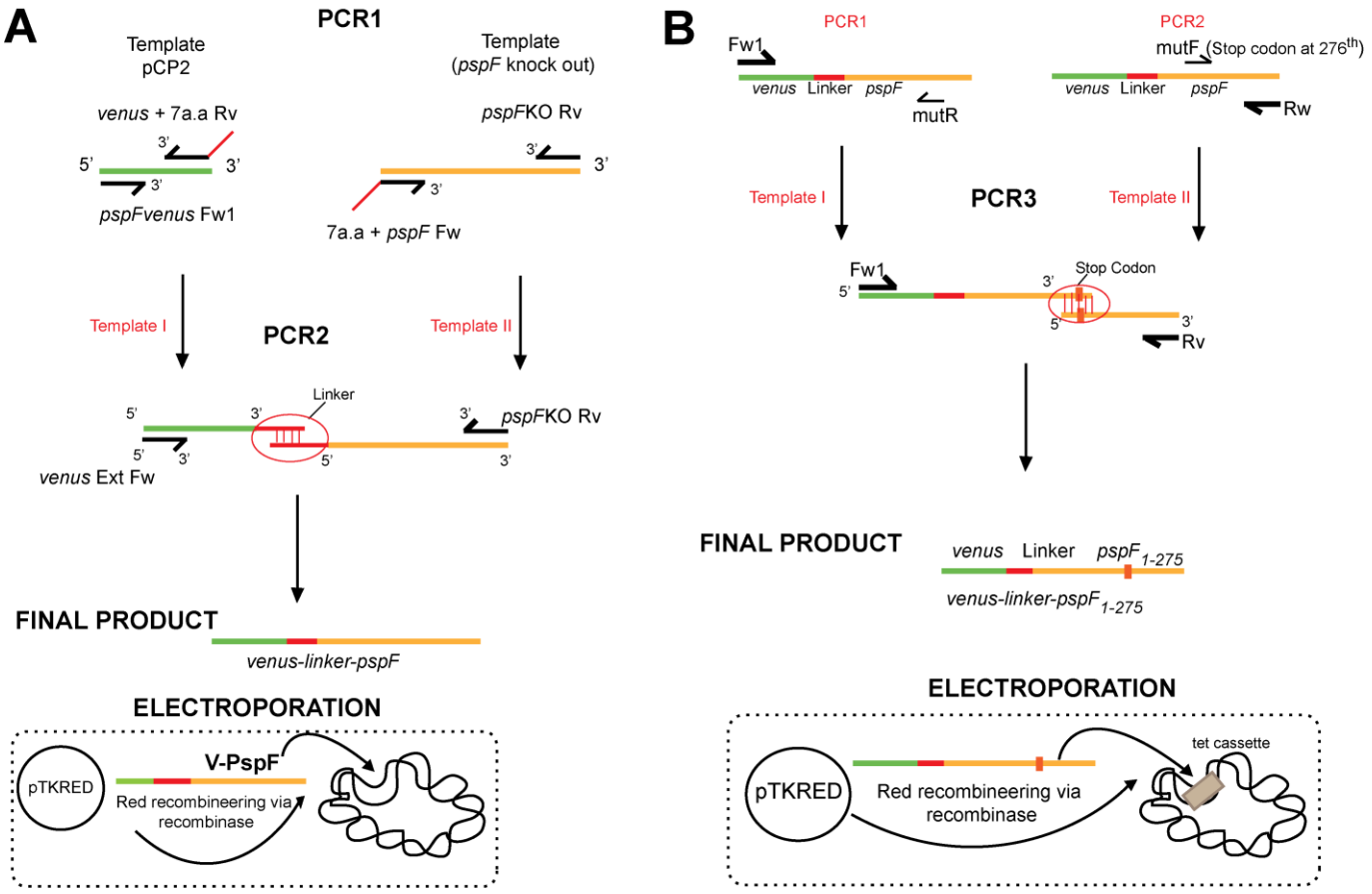

Figure 2.1 **Schematic explaining the red recombineering technique:** (A) The recombination of *venus-linker-pspF* gene replacing the WT *pspF* gene in MG1655 *E. coli* cells. The recombination was achieved by a Red recombineering technique facilitated by pTKRED specialist plasmid. The *venus linked pspF* gene is produced by two – step PCR reactions and the linear PCR product is electroporated in the cells containing the pTKRED plasmid to mediate the recombination with the *pspF* knock out strain and the insertion of the fusion gene in the cells was selected by sucrose resistance and kanamycin sensitive colonies. (B) The schematic explains the construction of V-PspF$_{1-275}$ using two step PCR and red recombineering technique. In the first step of recombination Tet cassette was introduced into the *venus-pspF* region and in the second step the *venus-pspF* carrying the stop codon was introduced replacing the Tet cassette and selected using tetracycline sensitive colonies.

2.2.1.3 λ-phage Recombination

2.2.1.3.1 Construction of strain expressing chromosomal V-PspA

V-PspA was constructed by Dr. Goran Jovanovic (a post-doc in the lab). The Venus-(linker)-PspA (V-PspA) fusion was constructed by cloning the (linker: ggt ggt ggt ggt tct ggt ggt tct gag ttc)-*pspA* DNA *Eco*RI-*Xba*I fragment into Venus expressing plasmid pCS2 and then excising the Venus stop codon and *Eco*Ri site using site specific mutagenesis, creating pCG65 (see Table 2.4). The P*pspA-venus-pspA* (Venus-PspA fusion under control of the *pspA* promoter) was constructed by separately amplifying 0.3 kb of the *pspA* promoter region as an *Eco*RI-*Nco*I fragment from MG1655 *E. coli* genomic DNA and 1.3 kb of the *venus-(linker)-pspA* fusion *Nco*I-*Bam*HI fragment from pCG65, ligating, and then sub-cloning

1.6 kb *Eco*RI-*Bam*HI fragment into pRS415 (Simons *et al*., 1987), creating pCG66 (Table 2.4). This construct was verified by sequencing. The single-copy chromosomal fusion of P*pspA-venus-pspA* was constructed as described (Yu and Court 1998) (see Table 2.3). Briefly, phage λBDC531 (imm21) was grown in a C600 strain carrying pCG66. The resulting λ phages were used to generate lysogens in SA1943 and screened for a Gal^- phenotype on MacConkey galactose agar plates supplemented with ampicillin (40 μg ml^{-1}). P1 phage were grown on the SA1943 λV-A lysogens and the resultant lysates were used to transduce the recipient strain DY226, which was screened for ampicillin resistant transductants at 42°C. The constructed strain carrying the P*pspA-venus-pspA* fusion inserted into *attB* was then screened for the Bio+ phenotype and the presence of prophage (sensitivity to λ phages). Finally, P*pspA-venus-pspA* fusion was moved by P1 transduction (Miller, 1992) into strain MG1655Δ*pspA*, generating ampicillin resistant strain MVA127 (see Table 2.3).

2.2.1.4 Construction of strain lacking the *pspG* regulatory region

This was constructed by Dr. Goran Jovanovic (a post-doc in the lab). A deletion of the *pspG* promoter (ΔP*pspG*) in MG1655 expressing V-PspF cells was constructed using NanoBio protocol for gene knockout based on method developed by Datsenko and Wanner, 2000. Hybrid primers containing the flanking sequences of the *pspG* promoter region and sequence homology to 5' or 3' of the FRT-Kan-FRT cassette were used to amplify 1.1 kb linear DNA fragment from pKD4 that substituted the 226 bps long P*pspG* on the chromosome. Target strain MG1655 V-PspF was transformed by pKD46 expressing the Red recombinase and cells were grown at 30°C. The amp^r transformants were selected and electroporated using the linear DNA PCR product. The electroporation was carried out with 1 mm gap cuvettes and Ec1 setup on Bio-Rad micropulser. After electroporation cells were recovered for 3 hour in SOC media at 37°C and grown on LB+kan (25 μg ml^{-1}) plates for 24 hour at 42°C [loss of temperature sensitive pKD46 (Red1)] and then the kan^r and subsequently kan^r amp^s recombinants were selected. The presence of FRT-Kan-FRT replacing the P_{pspG} was verified with colony PCR using pair of primers containing the flanking sequences of the *pspG* promoter region and PhusionTaq polymerase (Fermentas) and the verified strain was named MVA129. The antibiotic cassette was not removed with allowing P1 transduction (Miller, 1992) to move ΔP_{pspG}::Kan into strains of interest.

2.2.2 Curing Kanamycin Resistance

Introduction of mutations by $P1_{vir}$ phage transduction resulted in the insertion of kanamycin resistance cassette flanked by two flippase recognition targets (FRTs). The excision of the Kan cassette was accomplished by plasmid pCP20, which contains FLP recombinase, the recombinase mediates ejection of the FLP sequences flanking the Kan cassette leaving FLP scar sequence. pCP20 plasmid is an amp^R and cam^R that shows temperature-sensitive replication and thermal induction of FLP synthesis.

Transformants for pCP20 were selected for amp^R at 30°C; colonies were restreaked and grown twice at 42°C without antibiotics to cure for pCP20 plasmid. The strains were replica plated on the LB-agar plates and plates with ampicillin or kanamycin. Colonies that did not grow on antibiotic selective plates were deletion strains.

2.3 Competent cells

2.3.1 Chemically competent cells

The standard protocol for making chemically competent cells was followed from Sambrook *et al*, 1989. But briefly chemically competent bacterial cells were prepared using calcium chloride. The overnight culture of the single colony with the required antibiotic was used for serial dilution of day cultures. From the night culture 500 µl was added to 10 ml LB and then 1 ml into 9 ml of LB. Cells with final OD_{600} of 0.4 were pelleted at 3100 x g (Eppendorf 5810R centrifuge) for 10 minutes at 4°C. After 10 minutes the pellet was resuspended in 5 ml of 1M $CaCl_2$ incubated on ice for 20 minutes, followed with addition of 1 ml 0.1 M $CaCl_2$ + 15 % (v/v) glycerol. Aliquots of 100-200 µl volume were stored at -80°C.

2.3.2 Electrocompetent cells

The standard protocol from Sambrook *et al*., 1989 was followed but briefly. An overnight culture containing specific antibiotic was used to inoculate a day culture with single colony, IPTG (if needed) and 0.5% (w/v) glucose and grown until OD_{600} of 0.5. Simultaneously the microcentrifuge, 10 % glycerol (v/v) solution, electroporation cuvettes and the eppendorf tubes were pre-chilled. The culture was then chilled with ice-water slurry for 10 minutes, and then centrifuged at 3100 x g at 4°C for 7 minutes. The pellet was resuspended with 20 ml chilled 10 % (v/v) glycerol; this was repeated for 9 times. The same step was repeated with 10 ml 10 % (v/v) chilled glycerol before resuspending the pellet in 1ml of chilled 10 % (v/v) glycerol. This suspension was transferred into a sterile eppendorf and centrifuged at top speed for 1 minute at room temperature on bench top microcentrifuge (Eppendorf 5810R). These electrocompetent cells were subsequently used for electroporation.

2.4 Transformation

2.4.1 Heat Shock Transformation

2-4 µl of Plasmid DNA (50 ng/µl) was added to 100 µl of chemically competent cells and incubated on ice for 45 minutes. The cells were heat shocked at 42°C for 2 minutes and then the cells were recovered by addition of 250 µl of LB at 37°C for an hour. The cells were then plated on LB-agar plate with a specific antibiotic.

2.4.2 Electroporation

Electroporation was carried out with 1 mm gap, pre-chilled cuvettes using the Ec1 setup on Bio-Rad Micropulser™. After electroporation cells were recovered for 3 hour in SOC media (see Table 2.1) at 37°C with gentle shaking and then grown on antibiotic selective LB-agar plate.

2.5 Molecular Biology techniques: DNA methods

This section explains the various molecular biology methods used for DNA related studies such as plasmid isolation, PCR, mutagenesis and various other methods, with brief explanation of protocol and components.

2.5.1 Plasmid Isolation

Plasmid DNA was isolated from 10 ml overnight culture supplemented with appropriate antibiotic in LB. QIAprep Spin Miniprep Kit (Qiagen) was used to isolate the plasmid DNA from the night culture see Table 2.7. This kit is based on alkaline lysis method for DNA isolation from bacterial cells. The cleared bacterial lysate is loaded on anion-exchange column to which DNA selectively binds under appropriate salt and pH conditions. RNA, proteins and other low-molecular weight impurities are removed by salt wash, and ultra-pure DNA is eluted with a high salt wash. The plasmid DNA was eluted in a final volume of 50 µl or 30 µl in ultra-pure water or elution buffer and according to manufacturer's guidelines.

2.5.2 DNA Sequencing

Isolated plasmids were sent for sequencing if needed to check for the correct gene sequence to DNA Core Laboratory of the Medical Research Council (Clinical Sciences Centre, Hammersmith Hospital, London), or to Eurofins MWG Operon. 7 µl of plasmid with 3 µl of specific primer were sent in an eppendorf for sequencing. The sequencing results were analysed using BioEdit Alignment Editor Version 7.0.5.3.

2.5.3 Polymerase Chain Reaction (PCR)

2.5.3.1 PCR for molecular cloning

The desired gene of interest was cloned from the chromosome or plasmid DNA using specific set of primers depending on the gene (see primer Table 2.8).The PCR reaction and recipe are listed in the table below, and Taq Polymerase (Dream-Taq® or Peqlab) or Cloned Pfu (Stratagene) was used for the reaction using Eppendorf Thermocycler PCR machine.

COMPONENT	FINAL CONCENTRATION	VOLUME
Template strand	100 ng	2 µl
10 X Dream Taq Buffer (Fermentas) 10 X HF Buffer (Peq Lab) 5X HF Buffer (Stratagene)	1X 1X 1X	5 µl 5 µl 10 µl
Fw Primer Rv primer	1 µM 1 µM	1 µl 1 µl
dNTPs mix 5µM (Roche)	0.1 µM	1 µl
Dream Taq / Peq Lab Taq/ Pfu Cloned	0.1 u/µl	1 µl
Milliq Water		39 µl
Total Reaction Volume		50 µl

Table 2.9 The PCR reaction components

STEPS	TEMPERATURE AND DURATION
Denaturation	94°C for 1minutes
Denaturation Annealing Extension	94°C for 30 seconds 51°C for 1 min 68-71°C for 1 minutes Repeated for **24-35** cycles
Final Extension	71°C for 12 minutes

Table 2.10 The table gives the list of PCR script used on the machine

2.5.3.2 Colony PCR to check for gene deletions

PCR was performed to check for gene deletions by using antibiotic cassette specific primers or primers homologous to flanking regions in comparison to the parent strain to confirm the deletion. The PCR was performed using a single mutant colony, suspended in 10 µl of sterile water.

COMPONENT	FINAL CONCENTRATION	VOLUME
Colony suspension	1 colony in 10 µl Milliq water	2 µl
10 X Dream Taq Buffer (Fermentas) 10 X HF Buffer (Peq Lab)	1 X 1 X	5 µl 5 µl
Fw primer Rv primer	1 µM 1 µM	1 µl 1 µl
dNTPs mix 5µM (Roche)	0.1 µM	1 µl
Dream Taq / Peq Lab Taq	0.1 u/µl	1 µl
Milliq Water		39 µl
Total Reaction Volume		50 µl

Table 2.11 The table lists the PCR reaction components

STEPS	TEMPERATURE AND DURATION
Denaturation	94°C for 2.5 minutes
Denaturation Annealing Extension	94°C for 1seconds 55°C for 1 min 68-71°C for 1 minutes Repeated for **24-35 cycles**
Final Extension	71°C for 12 minutes

Table 2.12 The list of PCR recipes

2.5.3.3 Site-directed Mutagenesis

Site-directed mutagenesis was used to exchange or insert nucleotides in the plasmid template to either mutate genes or cause gene deletions. The DNA modification was performed on plasmids using PCR with *Pfu Turbo* high-fidelity DNA polymerase and primer pairs containing the desired mutation with the flanking regions to the gene interest of interest. Following PCR amplification of the plasmid, the PCR mix contained the parental template sequence and the newly synthesised mutant fragments. The parental

template was degraded using restriction enzyme *DpnI* as selectively preserving the modified templates. In the final step, an aliquot of the modified plasmid was transformed into *E.coli* XL1-blue cells to propagate the mutant plasmid. 8-10 colonies were used to make overnight cultures for isolating the plasmid using the QIAquick® plasmid purification kit, and the sequences confirmed with plasmid sequencing.

COMPONENT	FINAL CONCENTRATION	VOLUME
Template	100 ng	2 µl
Cloned Pfu 10X buffer (Stratagene)	1 X	5 µl
dNTP mix	100 µM	1 µl
Fw primer Rv primer	1 µM 1 µM	1 µl 1 µl
Cloned *Pfu* Enzyme	0.1 u/µl	1 µl
Milliq Water		39 µl
Total		50 µl

Table 2.13 The table lists the reagents and components of the PCR reaction for site-directed mutagenesis

STEPS	TEMPERATURE AND DURATION
Denaturation	95°C for 1 minutes
Denaturation Annealing Extension	95°C for 30 seconds 55°C for 1 min 68-71°C for 1 minutes Repeated for **16 cycles**
Final Extension	68°C for 12 minutes

Table 2.14 Details of steps of a PCR cycle for site-directed mutagenesis

COMPONENT	FINAL CONCENTRATION	VOLUME
PCR purified product		50 µl
10X Fast digest buffer	1 X	6 µl

DpnI (Fermentas)	0.05 u/µl	3 µl
Milliq Water		1 µl
Total		60 µl

Table 2.15 The details of *DpnI* treatment protocol

2.5.3.4 Agarose Gel Electrophoresis / Gel Extraction

Agarose gel electrophoresis was used to analyse DNA fragments from PCR reactions or other DNA methods. Agarose gel was prepared by microwave heating 0.8 or 1.2 % agarose (w/v) in 30 ml or 80 ml 1X TBE (National Diagnostics, see Table 2.5) depending on the DNA fragment size. SYBR® Safe (Invitrogen) DNA gel stain was added to 1:10,000 final dilution with the solution set in a gel-casting tray. The samples were loaded with 6X DNA loading dye and run at 80-100V for 25-30 minutes in 1X TBE running buffer. The gel was visualised using blue light transilluminator and the image was captured with the camera. The DNA fragments of interest from the agarose gel can be excised and purified using a Gel Extraction Kit (Qiagen) see Table 2.7. The DNA was eluted in final volume of 30-50 µl in elution buffer or ultra-pure water for various DNA modification methods.

2.5.3.5 Restriction Modification

Plasmid DNA was restriction digested in a reaction volume of 10 or 20 µl with Fermentas Fast Digest ® or NEB endonucleases at 1/20 dilution. The reactions were incubated for 30 minutes at 37°C before being visualised on an agarose gel. The manufacturer's protocol was followed for the specific enzyme.

PCR purified product/ plasmid	7 µl
Restriction Enzyme	1 µl
10X FastDigest Buffer	1 µl
Total	10 µl

Table 2.16 The protocol for the restriction digestion modification of plasmid DNA or PCR product

2.5.3.6 DNA Ligation

Ligations were performed using NEB Quick T4 DNA ligase, the mixture was diluted at 37°C for an hour.

Quick T4 DNA ligase	1 µl
2X Quick Ligation Buffer	10 µl

Vector DNA	2 µl
Insert DNA	6 µl
Milliq Water	1 µl
Total	20 µl

Table 2.17 Components of typical DNA ligation mixture

2.6 Cell Fractionation

The Figure 2.2 schematically explains the protocol in detail. The strains were grown overnight in LB at 37°C. Day cultures were made by 1:50 dilution from the overnight culture and were grown until OD_{600} of 0.2-0.3. The cells were induced with 12.5 µl of 40 % (w/v) L-arabinose for an hour. The volume of cells was normalised to OD_{600} of 0.8 and equivalent volumes of cells was taken for each of the samples. The culture was pelleted at 9632 x g for 5 minutes. The pellet was then resuspended in 20 µl of 200 mM Tris.HCl-pH8 with 5 µl of 10 mM EDTA. After thorough vortexing, 40 µl of 30 % (w/v) sucrose and 5 µl of 5 mg/ml egg white lysozyme (Sigma-Aldrich) were added to the solution. The lysed cells were left at room temperature for 10 minutes and then cells were lysed using repetitive freeze-thawing (freezing in dry ice ethanol followed by thawing at 42°C). After cell lysis with freeze-thawing 400 µl of H_2O, 12 µl of $MgCl_2$ and 10 units of DNAse I (GE Healthcare) were added, after 20 minutes incubation at room temperature soluble and insoluble (membrane and aggregate proteins) were separated via centrifugation at 16,278 x g for 5 minutes. The supernatant contained soluble fractions while the pellet contained insoluble fractions.

2.6.1 Isolating Soluble Fractions (Supernatant)

500 µl of trichloracetic acid (TCA) was added to the supernatant containing soluble proteins and left at 4°C for 10 minutes. This was centrifuged at 16,278 x g for 10 minutes; the pellet was washed with 500 µl acetone and centrifugation was repeated. The supernatant was removed, and the pellet was air-dryed before being resuspended in 30 µl Laemmli buffer (Sigma-Aldrich) and 30 µl 4 % SDS (w/v).

2.6.2 Isolating IM fraction (Pellet)

The pellet containing insoluble proteins was resuspended in 100 µl of 1 % (w/v) Triton with 10 mM $MgCl_2$ and 50 mM TrisHCl-pH8, incubated for 20 minutes at 37°C and then centrifuged for 5 minutes at 16278 x g at room temperature. The supernatant was added to chloroform and methanol premix and pellet was discarded.

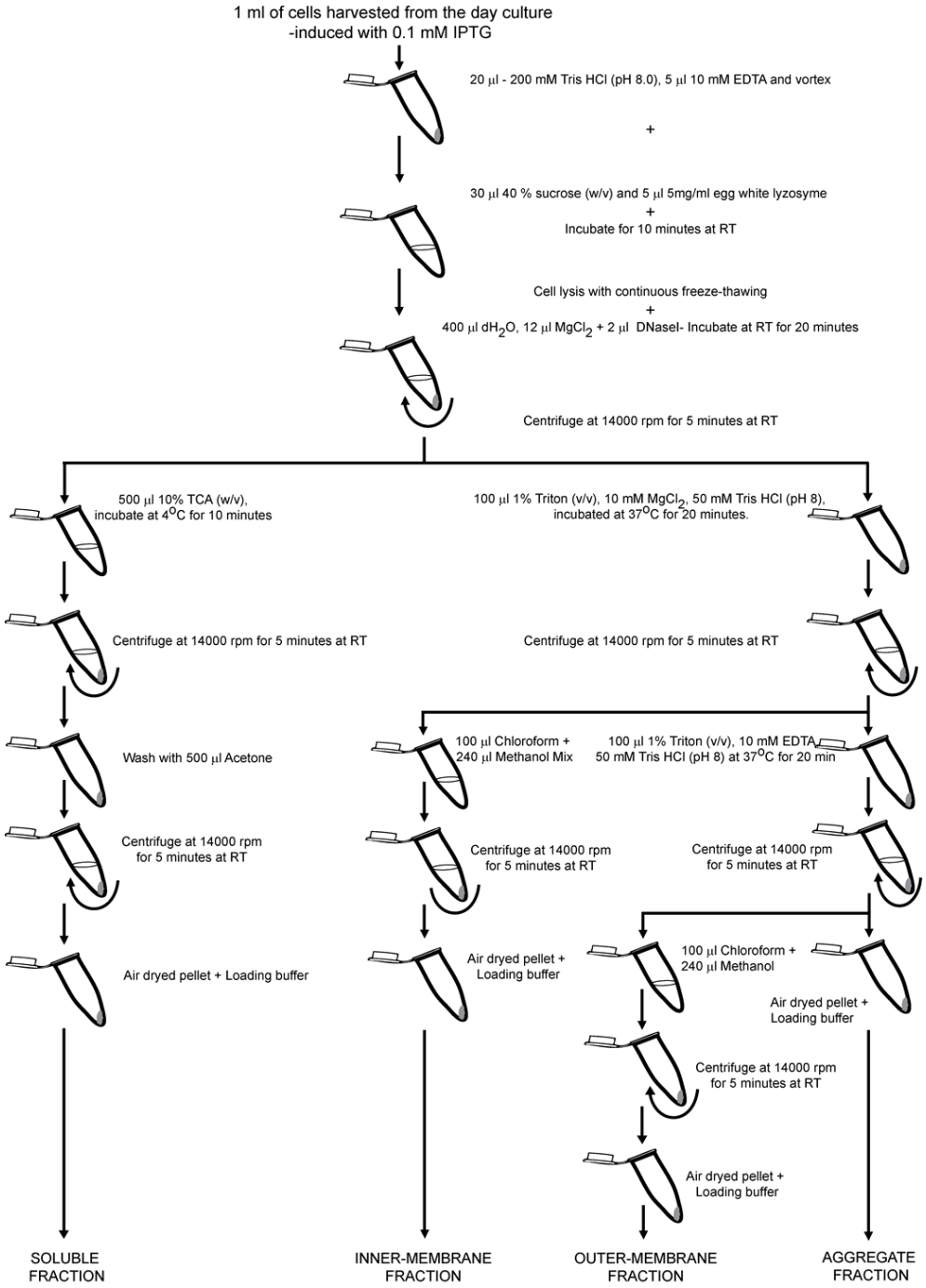

Figure 2.2 **Cell fractionation technique:** The cell fractionation method is used to differentiate between cytoplasmic protein, inner-membrane associated protein, outer-membrane protein and protein aggregate. The schematic shows the steps and chemicals involved in the fractionation method. In order to obtain inner-membrane fraction the supernatant was treated with chloroform and methanol pre-mix.

Centrifugation was repeated and the resulting pellet was air dryed before being resuspended in 30 µl Laemmli buffer and 30 µl 4 % (w/v) SDS. These fractions were boiled at 100°C for 2 minutes and loaded onto 12.5 % (w/v) SDS gel for Western Blotting.

2.7 Protein gels

2.7.1 SDS-PAGE

SDS-PAGE (Sodium dodecyl sulphate-Polyacrylamide Gel Electrophoresis) was used to visualise proteins. The samples for SDS-PAGE were made in Laemelli buffer and 4% (w/v) SDS and were boiled at 100°C for 2 min. 20 µl of samples were loaded on 12.5% (w/v) SDS polyacrylamide gel. The gel was run using the Bio-Rad mini-protein gel II system. The gel was run at 100 volts for 45 minutes in 1X Tris/SDS/Glycine (National Diagnostics).

SEPARATING GEL	STACKING GEL
30% (v/v) Acrylamide - 4.1ml	30% (v/v) Acrylamide – 600 µl
Solution II, pH8.8 - 2.5ml	Solution III, pH 6.8 – 1 ml
Filtered Water - 3.4ml	Filtered Water – 2.4 ml
10% APS w/v - 100 µl	10% APS (w/v) – 40 µl
TEMED – 10 µl	TEMED – 4 µl

Table 2.18 Recipe for 12.5% SDS PAGE protein gel

2.7.2 Native PAGE

Native PAGE was used to visualise protein in their native conformation with intact charge and structural conformation. 4.5% (w/v) acrylamide native gels were used to study native interactions between different proteins such as PspF-PspA interaction.10 µl of protein sample is loaded on the gel with 5x Native loading dye (10% (v/v) Glycerol, 0.5mg Bromophenol Blue).

COMPONENT	VOLUME
30 % (v/v) Acrylamide	0.75 ml
10 X Tris/Glycine Buffer	0.5 ml
Filtered Water	3.75 ml
10% APS (w/v)	50 µl
TEMED	5 µl

Table 2.19 The table lists the components of 4.5 % (w/v) acrylamide native gel

2.7.3 PspF-PspA interactions: Native gel mobility shift assays

To detect the protein-protein interactions, the native gel mobility shift assays were performed. Reactions (at a final volume of 10 µl) were set up with final concentration of 10 µM $PspF_{1-275}$ and 5 µM PspA and PspA mutants. The sample is made in 1X STA Buffer [2.5mM Tris-acetate (pH 8.0), 8 mM Mg-acetate, 10mM KCl, 1mM DTT, 3.5% (w/v) PEG 8000) and incubated for 15 min at room temperature. 2.5 µl of 5X Native loading dye was added to the protein sample before loading. The native gels were visualised with Comassie or SYPRO Ruby (Invitrogen), visualised using Fujifilm FLA5000 and image reader software and analysed using AIDA software.

2.7.4 Western blotting

Following SDS-PAGE, the gels were either stained with Comassie Blue to quantify protein bands or used to perform Western Blot. The proteins from the gel were transferred onto a methanol-activated-ImmunoBlot™ PVDF membrane (BIO-RAD) using a Trans-Blot® Semi-Dry Transfer Cell (BIO-RAD) for an hour at 100-150 mA. The transfer was carried out by making a sandwich of four Whatman filter papers, activated PVDF membrane, SDS-PAGE gel and four more Whatman filter papers equilibrated with transblot buffer as shown in Figure 2.3.

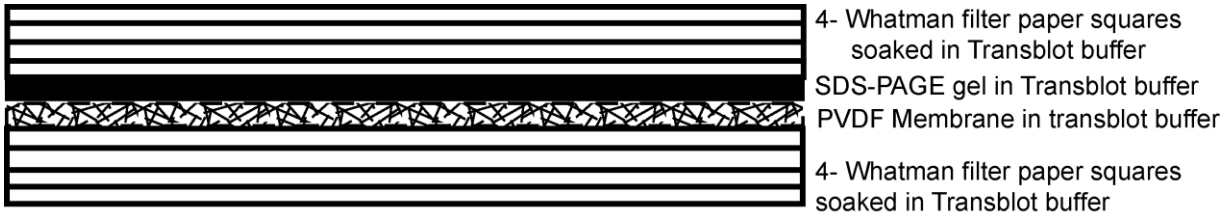

Figure 2.3 **The Western Blot sandwich:** The diagram shows the placement of Whatman filter paper, SDS gel, PVDF membrane and filter papers. All these are first equilibrated in transblot buffer.

The transfer of the proteins on the membrane was checked by staining with Ponceau S stain (Sigma-Aldrich). The blocking, washing and incubation with primary and secondary antibodies were performed using a BenchPro™ 4100 Western Processing System (Invitrogen). The same procedure was also occasionally performed manually where the membrane after the transfer was washed with 2X TBS or 2X TBS-TT. The membrane was then incubated with 5 % (w/v) milk powder (Marvel) solution in 2X TBS. Next the membrane was incubated with specific primary antibody (diluted in 5 % milk powder (w/v) + TBS solution) overnight at 4°C. The following day it was incubated for an hour at room temperature with a Horseradish-Peroxidase (HRP)-conjugated secondary antibody, and then thoroughly washed with 5 X TBS-TT. Following the automated membrane treatment or manual washing the proteins were detected using ECL-Plus Western Blotting Detection System (GE Healthcare) and was digitally acquired using

Bio-Rad GelDoc™ and ChemiDoc™ Imaging system with the Image Lab software and analysed using Adobe Photoshop CS3.

STEP	TIME (MINS)
Blocking 5 % (w/v) milk-powder in TBS	60
Washing 2X in TBS-TT	2 X 10
Washing 1X in TBS	10
Incubation with primary antibody diluted in 5% (w/v) milk-powder in TBS	720 (12 hours)
Washing 2X TBSTT	2 X 10
Washing 1X TBS	10
Incubation with Horseradish peroxidase (HRP) conjugated secondary antibody	60
Washing 5X TBSTT	5X10

Table 2.20 Western Blotting protocol using the BenchPro 4100 Western Processing System Recipe was called "PspF"

PRIMARY ANTIBODY AND DILUTION	SECONDARY ANTIBODY AND DILUTION
Anti-Venus/GFP – 1:1000, JL8 Living Colours (Clontech)	Goat-Anti-Mouse-HRP – 1:5000, GE Healthcare
Anti-GFP Antibodies – 1:10000, Invitrogen	Goat-Anti-Rabbit-HRP – 1:10000, GE Healthcare
Anti-PspF Antibodies – 1:1000, (Jones *et al.*, 2003)	Goat-Anti-Rabbit-HRP – 1:5000, GE Healthcare
Anti-PspA Antibodies – 1:1000, (Jones *et al.*, 2003)	Goat-Anti-Rabbit-HRP – 1:5000, GE Healthcare
Anti-pIV Antibodies – 1:1000 (Jovanovic *et al.*, 2010)	Goat-Anti-Rabbit-HRP – 1:10000, GE Healthcare
Anti-PspB Antibodies – 1:1000 (Engl *et al.*, 2010)	Goat-Anti-Rabbit-HRP – 1:10000, GE Healthcare

Anti-PspC Antibodies – 1:1000 (Engl *et al*, 2010)	Goat-Anti-Rabbit-HRP – 1:10000, GE Healthcare

Table 2.21 Antibodies used with their respective concentration and corresponding secondary antibody

2.8 β-Galactosidase Assay

β-Galactosidase assay is a colorimetric test employed in this study to determine the activity of the P*pspA* promoter fused to *lacZ* gene. *lacZ* is the most widely used reporter gene encoding β-galactosidase enzyme which splits lactose into glucose and galactose.

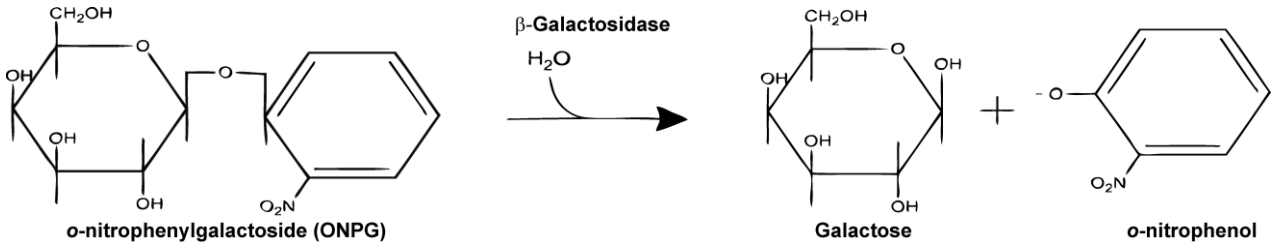

Figure 2.4 **β-Galactosidase assay:** The chemical equation showing the breakdown products of ONPG into *o*-nitrophenol and galactose

The β-galactosidase can utilise artificial galactoside such as ONPG (*o*-nitrophenylgalactoside) that is split into *o*-nitrophenol and galactose - *o*-nitrophenol is yellow at cellular pH and soluble which is measured quantitatively (Miller, 1972) as illustrated in the Figure 2.4.The amount of *o*-nitrophenol per unit time is proportional to the concentration of β-galactosidase (*lacZ* gene product) when ONPG is in excess to the enzyme.

2.8.1 Cuvette based Assay

An overnight culture of 5 ml of LB containing appropriate antibiotic(s) with a single transformed colony was incubated at 37°C shaking at (220 x g). In the morning, a day culture of 5 ml LB with appropriate antibiotic(s) was inoculated with 50 µl of the overnight culture, this was shaken at 37°C until an OD_{600} of 0.2. If required, protein expression was induced by the addition of either IPTG (1 or 0.1 mM) or arabinose (0.02% w/v) was added to culture, which was shaken for a further 3 hours at 37°C (220 x g). The growth was stopped with cold shock treatment and OD_{600} measured at a dilution such that the reading fell within the spectrophotometer linear range. The assay was performed in triplicates. To the 200 µl of the day culture, 800 µl Z-buffer and 50 µl chloroform were added; the sample was vortexes for 30 seconds and placed 30°C in a water bath. To each triplicate 200 µl of pre-warmed ONPG in Z-buffer (4 mg/ml) was added and the time of addition noted. When the solution had turned a pale yellow, Na_2CO_3 (500 µl, 1M) was added to stop the reaction and the time recorded. Measurements of OD_{420} and OD_{550} were made and the Miller Units calculated using the following Equation 2.1. The Miller units value

gives an estimate of the promoter activity (P*pspA* promoter) fused to the *lacZ* gene expressed in Miller Units (below is the equation).

$$\text{Miller Units (MU)} = \frac{(OD_{420} - 1.75 \times OD_{550}) \times 1000}{OD_{600} \times t \times v}$$

$OD_{\mathbf{420}} = \text{absorbance of reaction at } 420\text{nm}$

$OD_{550} = \text{absorbance of reaction at } 550\text{nm}$

$OD_{600} = \text{absorbance of culture at } 600\text{nm}$

$t = \text{reaction time (minutes)}$

$v = \text{volume of cells used in the assay (ml)}$

Equation 2.1 The formulae for the classic cuvette based β-Galactosidase activity assay to calculate the Miller units

2.9 Bacterial Two Hybrid (BACTH) System

The adenylate-cyclase based bacterial two-hybrid (BACTH) system described in Karimova *et al.*, 1998 uses inactivated T18 and T25 fragments of adenylate-cyclase from *Bordetella pertussis*. These fragments can only form the active enzyme when in close proximity, and this interaction can be facilitated by two proteins fused to T18 and T25, respectively.

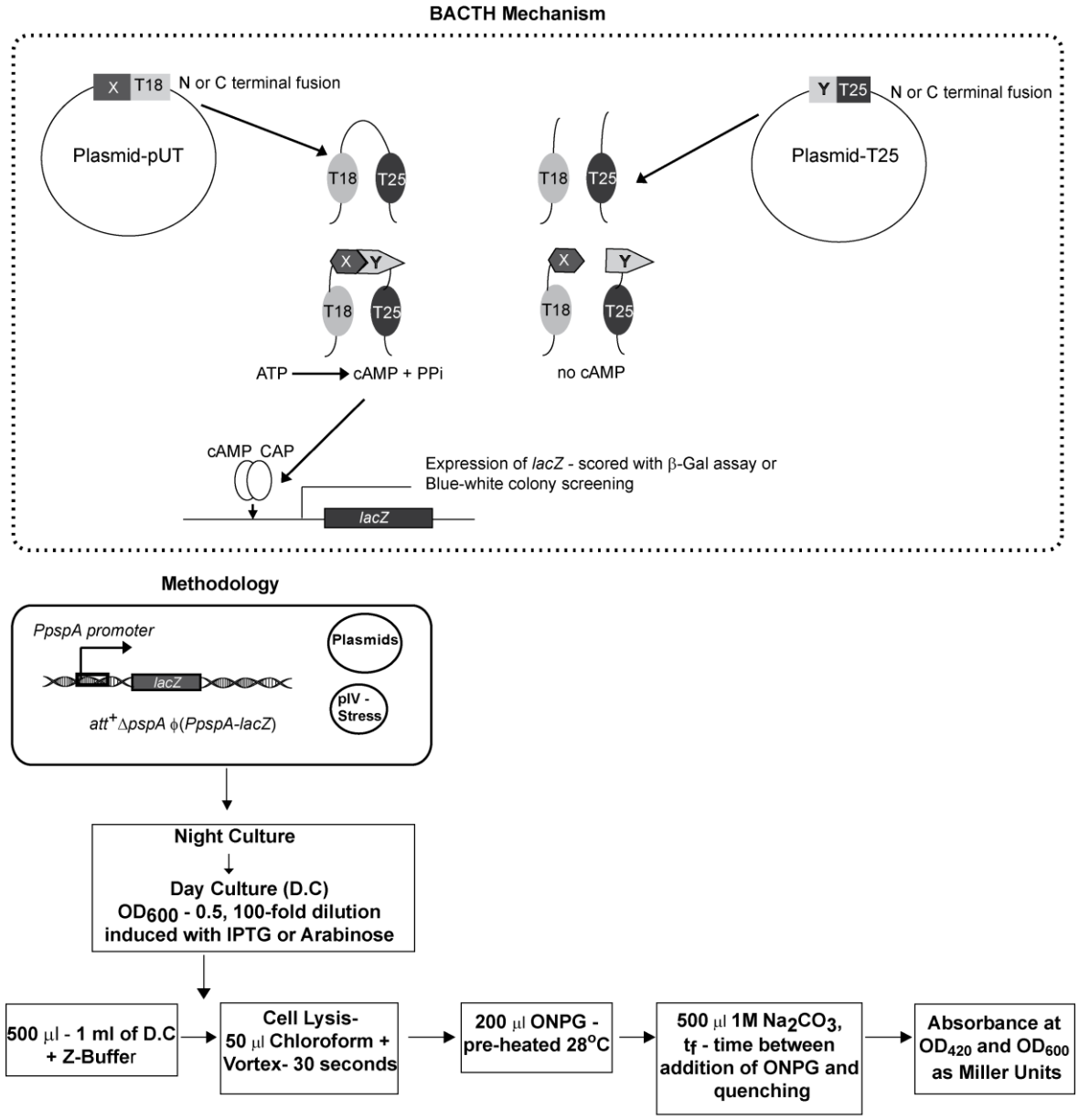

Figure 2.5 **Schematic showing the mechanism and protocol of BACTH method:** The diagram shows the mechanism of the BACTH based on T18 and T25 plasmid system; in the presence of positive interaction cAMP is released that activates the expression from the *lacZ* promoter. The flow chart explains the procedure of the BACTH experiment.

The positive interaction between the two proteins of interest is reported by the lacZ expression, which can be analysed in the BTH101 (cya-) strain either by using blue-white screening on X-Gal plates or in a β-Galactosidase assay. The BACTH system and its mechanism has been described the Figure 2.5.

2.10 Motility assay

For the motility assays the MG1655*ΔpspF* strain was used a background strain into which specific plasmids were transformed. The motility assays were performed as described (Lloyd *et al*., 2004) to

estimate the PspA effector function in these strains in form of bacterial motility. 2 µl of the overnight culture of MG1655*ΔpspF* expressing WT-PspA or mutant forms was spotted on soft agar plates and incubated at 30°C for 18 hours until rings showing bacterial mobility spread on the plates. These rings were measured in millimetres and the same experiment was repeated for biological replicates to obtain mean diameter of the rings with standard error.

2.11 *In vitro* protein studies

2.11.1 Expression of Proteins

In this thesis protein such as PspA full length, its structural mutants along with $PspF_{1-275}$ were purified using 6x-His tag. A $pET28b^+$ based plasmid was used to fuse PspA full length with N-terminal 6X His tag called pSLEA (Elderkin *et al*., 2006). pSLEA was subsequently used as a template to introduce the various structural mutations in the HD1 of PspA full length by site directed mutagenesis (see 2.5.3.3-Site-directed Mutagenesis). The various plasmids were introduced into the BL21 *E. coli* expression strain by heat shock transformation selected with kanamycin LB-agar plates (see Table 2.4-plasmid). One or two of the transformed colonies were used to make an overnight culture in 20 ml LB-kanamycin broth culture incubated at 37°C under shaking conditions. The night culture was used to inoculate 1L LB broth and shaken at 120 x g at 37°C until an OD_{600} of 0.5 was reached. Then the culture was treated to cold shock treatment for 20 minutes in a water-bath at 4°C. The culture was then induced with 0.1mM or 0.5 mM IPTG and incubated at 30°C for 3 hours with shaking. The cells from the culture were then harvested at 4844 x g for 15 minutes at 4°C. The cell pellet was the resuspended in resuspension buffer (5 ml per centrifugation tube) for PspA or PspF and stored at -80°C. This cell extract was used to purify the specific protein and the protein purification procedure varied depending on whether PspA or PspF was purified.

2.11.1.1 PspA Purification

RESUSPENSION BUFFER	EXTRACTION BUFFER	BUFFER A	BUFFER B	DIALYSIS BUFFER
100 mM Tris-HCl pH 7.5	100 mM Tris-HCl pH 7.5	100 mM Tris-HCl pH7.5	100 mM Tris-HCl pH 7.5	20 mM Tris-HCl pH7.5
50 mM NaCl	500 mM NaCl	500 mM NaCl	500 mM NaCl	200 mM NaCl

75 mM NaSCN	75 mM NaSCN	75 mM NaSCN	75 mM NaSCN	75 mM NaSCN
5% (v/v) glycerol	1% (w/v) CHAPS		1M Imidazole	0.01% (w/v) CHAPS
				5% (v/v) glycerol

Table 2.22 Table lists PspA purification buffers

Purification was performed using Ni-chelate affinity chromatography using a 5 ml HiTrap™ Chelating HP column (GE Healthcare) charged with $NiCl_6$ (20 mg/ml) (hereafter called as activated column). An AKTA (GE Healthcare) FPLC system was used to carry out the Ni- affinity chromatography for his-tagged proteins. The cell extract stored at -80°C was used for purification; a sample was kept for SDS-gel before sonication. For purification the cell extract was defrosted on ice and to it a tablet of protease cocktail inhibitor (Roche) was added. The cells were lysed by sonicating for 2x10 mins (40% power, 2 sec pulse) with a 5 min interval between consecutive sonication and the cell debris was pelleted by centrifuging at 17418 x g for 15 mins at 4°C. A sample of the supernatant was reserved for the protein gel, and the cell pellet was resuspended in PspA extraction buffer with CHAPS detergent. The cell suspension was gently agitated at 4°C typically for an hour, but up to overnight for some of the PspA mutants for complete solubilisation of the pellet. Next the cell extract in the extraction buffer was spun down at 17418 x g for 45 minutes. This second supernatant was loaded on to the activated column equilibrated with PspA Buffer A using a superloop (GE Healthcare) at a rate of 0.5 ml/min. Non-His tagged proteins were first removed by washing the column with PspA buffer A (2ml/min) and the flow through was collected. The column was also washed with 7% PspA buffer B (+ 1 M imidazole), and the wash was also collected. PspA was eluted with a 0% - 100% gradient with PspA Buffer B containing 1 M imidazole over 40 mins. The 1000 ml eluted fractions contributing to the peak during elution were stored on the ice. The fractions containing protein (after analysis by SDS-PAGE) were combined and dialysed overnight at 4°C using PspA dialysis buffer using dialysis membrane (Spectra/Por) with 12-14 kDa molecular weight cut off. The protein solution after dialysis was collected and spun down in 4°C on a table top eppendorf centrifuge at 20442 x g for 5 minutes. The supernatant was collected and distributed into 100 µl aliquots and stored at -80°C freezer.

2.11.1.2 $PspF_{1-275}$ Purification

LYSIS BUFFER	BUFFER A	BUFFER B	DIALYSIS BUFFER
20 mM TrisHCl pH 8	25 mM Sodium Phosphate buffer (pH7)	25 mM Sodium Phosphate buffer (pH 7)	20 mM Tris-HCl (pH 8)
500 mM NaCl	500 mM NaCl	500 mM NaCl	50 mM NaCl
5% (v/v) Glycerol	5% (v/v) Glycerol	5% (v/v) Glycerol	1 mM DTT
		1M Imidazole	0.1 mM EDTA
			5% (v/v) Glycerol

Table 2.23 Table lists PspF purification buffers

The cells were harvested from a 1L of LB culture inoculated with 20 ml of overnight culture of strain expressing $PspF_{1-275}$. The cells harvested by centrifugation (4355 x g at 4°C for 15 min) and were resuspended in Lysis Buffer. The cell extract was further lysed by two rounds of sonication performed as for PspA, and the soluble fraction was extracted by centrifugation at 17418 x g for 45 minutes. This was loaded onto an activated 5 ml Hi-Trap column using a superloop at 0.5 ml/min. Non his-tagged proteins were washed with Buffer A and 7 % (v/v) Buffer B and 1000 ml protein fractions were eluted with a linear gradient of Buffer B containing 1M imidazole from 1-100% over 40 minutes. The fractions were analysed on SDS-gel and dialysed with the dialysis buffer using dialysis membrane (Spectra/Por) with 12-14 kDa cut off overnight at 4°C.

2.11.2 Folin-Lowry Protein Quantification

The Folin-Lowry method was used for protein quantification (Lowry *et al.*, 1951). A serial dilution of BSA was made from known concentration of 10 mg/ml to make standard curve to estimate the protein concentration. The Solution A and B provided in the DC™ Protein Assay (Bio-Rad) were added to the 5 µl of each BSA serial dilution made in duplicate, for the standard curve. 5 µl of protein sample from two different undermined concentrations were was used to which Folin reagents were added on a 96-well plate. 50 µl of the following Folin reagents form the kit were added to 5 µl of the BSA dilutions in a 96-well plate and the plate was incubated for 30 mins at room temperature. The colorimetric changes were measured at 750 nm. The protein concentration was measured from the BSA standard curve corresponding to the absorbance value measured for the protein samples.

2.11.3 His-Tag Cleavage

The His-tag from $PspF_{1-275}$ was cleaved by biotinylated-thrombin (Thrombin Cleavage Kit, Novagen) for 3 hours at room temperature around 20-25°C under shaking conditions. The residual uncleaved proteins and biotinylated thrombins were removed by Ni-NTA agarose beads (Qiagen) and streptavidin agarose beads (Novagen) respectively and the cleaved protein fraction was confirmed with SDS-gel and was dialysed using the same PspF dialysis buffer (see Table 2.23).

2.12 Gel filtration

Gel filtration is also referred as size exclusion chromatography that separates molecules on the basis of size as they pass through the stationary phase in the column. Gel filtration is used to purify proteins especially proteins sensitive to pH and other metals or co-factors. It can also be applied to regain protein folding with optimised buffer compositions (Amersham Biosciences – handbook). It is also readily used to estimate the oligomerisation state of proteins. PspA WT and variants were used in order to determine their oligomeric states as compared to WT using gel filtration. The gel filtration method was performed as described in Joly *et al.*, 2009. The PspA protein samples were pre-incubated for 10 min at 4°C in a gel filtration sample buffer containing 20 mM Tris HCl (pH 8.0), 50 mM NaCl and 15 mM $MgCl_2$. 50 µl of sample (concentration of around 20 µM) was injected into the column. A Superose 6 column (10 mm X 300 mm, 24ml; GE Healthcare) was used for the PspA and mutants. The column was installed on an AKTA system (GE Healthcare), equilibrated with sample buffer and the sample loaded. The chromatography was performed at 4°C at a flow rate of 0.4 ml/min. The column was calibrated with the protein standards as listed in Table 2.24.

MARKER	MOLECULAR WEIGHT	ELUTION TIME
Blue Dextran	2000 kDa	10.22 ml
Thyroglobulin	669 kDa	11.97 ml
Apoferritin	443 kDa	13.90 ml
β-Amylase	200 kDa	14.92 ml
BSA	66 kDa	16.08 ml
Carbonic Anhydrase	29 kDa	17.75 ml

Table 2.24 The table lists the protein standards run on Superose 6 column

2.13 ATPase Assay

In this study steady state ATPase assay was performed to determine the inhibition of ATPase activity of $PspF_{1-275}$ by PspA WT and variants. The steady state ATPase assay protocol was first published by Norby in 1988 and has been a useful substitute for radioactive ATPase assay and can be performed on a 96-well plate using automated plate reader Fluostar (BMG-Labtech). The principle behind the NADH-coupled regeneration system is briefly described below in Figure 2.6. The ATPase activity was measured at 37°C in a 100 µl final volume using following solutions. The readings were taken in an interval of every minute for 2 hours using a recipe on the plate reader.

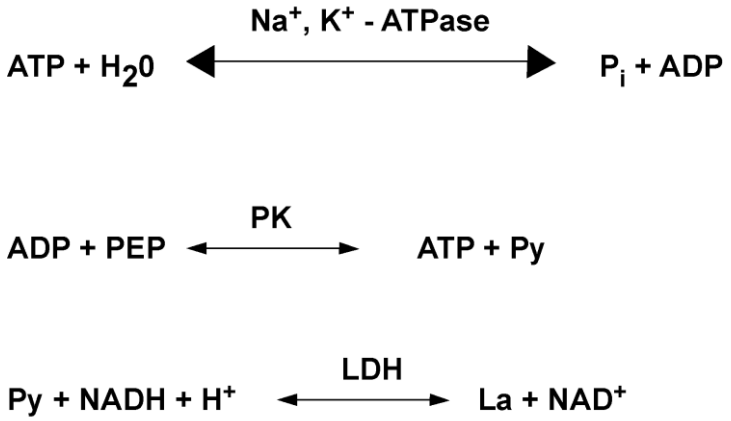

Figure 2.6 **The ATPase assay equations:** The formation of NAD^+ is detected in the assay. Pi- inorganic phosphate; PK- pyruvate kinase, Py- pyruvate, LDH- Lactate dehydrogenase and La- lactate.

ATPASE BUFFER (10X)	CONCENTRATION
Tris HCl pH8	250 mM
KCl	1 M
$MgCl_2$	100 mM
DTT	10 mM

Table 2.25 The composition of ATPase buffer

COMPONENTS	STOCK	FINAL CONC.	VOLUME – 100 µl
ATPase Buffer	10X	1X	10 µl
Pyruvate Kinase	1000 units/ml	10 units/ml	1 µl
Phosphoenol pyruvate	300 mM	10 mM	3.3 µl

L-Lactate dehydrogenase	5500 units/ml	20 units/ml	0.36 µl
NADH	200 mM	1 mM	0.5 µl
MilliQ Water			64.84 µl

Table 2.26 Table lists the buffer composition and components of the reaction mastermix

$PspF_{1-275}$	0-10 µM	10 µl
PspA and mutants	0-30 µM	10 µl
ATP	100 mM	10 µl

Table 2.27 Table lists ingredients added to the 96-well plate before adding the mastermix

The rate of decrease of NADH absorbance at 340 nm is proportional to the rate of steady-state ATP hydrolysis.

$$\Delta A = \frac{OD_{340-start} - OD_{340-end}}{T_{end} - T_{start}}$$

OD_{340} = absorbance of reaction at 340nm at start at the start of reaction

OD_{340} = absorbance of reaction at 340nm at the end of the reaction

T_{end} = reaction end time in minutes

T_{start} = reaction start time in minutes

Equation 2.2 The formula to calculate the amount of decrease in ATP hydrolysis over time with the increase in concentration of PspA

2.14 ChIP-CHIP

ChIP-CHIP using PCR was employed to characterise the DNA binding of V-PspF *in vivo* and also to describe the binding sites. The ChIP technique relies on 1 % (v/v) formaldehyde fixing of the protein-DNA interactions, this interaction is later enriched with the specific anti-GFP antibody. The Figure 2.7 below explains the principle behind the ChIP-CHIP.

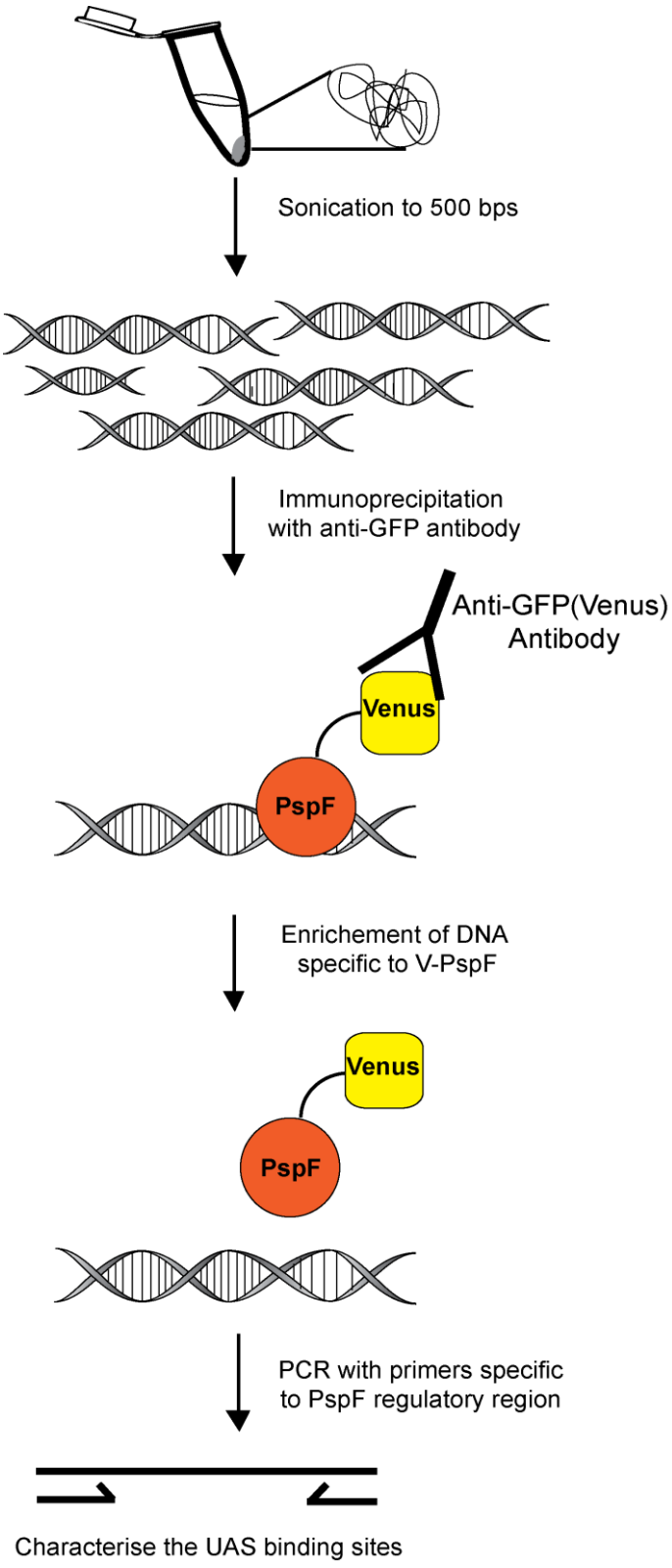

Figure 2.7 **The principle of ChIP-CHIP method:** The ChiP-CHIP based on PCR was used to consolidate the DNA binding property of V-PspF *in vivo*. Formaldehyde is used to fix the cells and thereby preserve the protein-DNA interactions.

2.14.1 ChIP (IP) Buffers

IP BUFFER	WASH II \ IP SALT BUFFER	WASH III	WASH IV	ELUTION BUFFER
50 mM HEPES-KOH pH7.5 150 mM NaCl 1 mM EDTA 1%(w/v) Triton X-100 0.1% (w/v) Sodium Deoxycholate 0.1% (w/v) SDS	IP buffer + 500 mM NaCl	10 mM Tris pH8 250 mM LiCl 1 mM EDTA 0.5% (w/v) Nonidet-P40 (Sigma-Aldrich) 0.5% (w/v) Sodium Deoxycholate	Tris-EDTA pH7.5	50 mM Tris-HCl pH7.5 10 mM EDTA 1% (w/v) SDS

Table 2.28 Lists the buffer used during the ChIP protocol at different points

Figure 2.8 explains briefly the protocol for the Chip-PCR technique that was employed for the work described in this thesis.

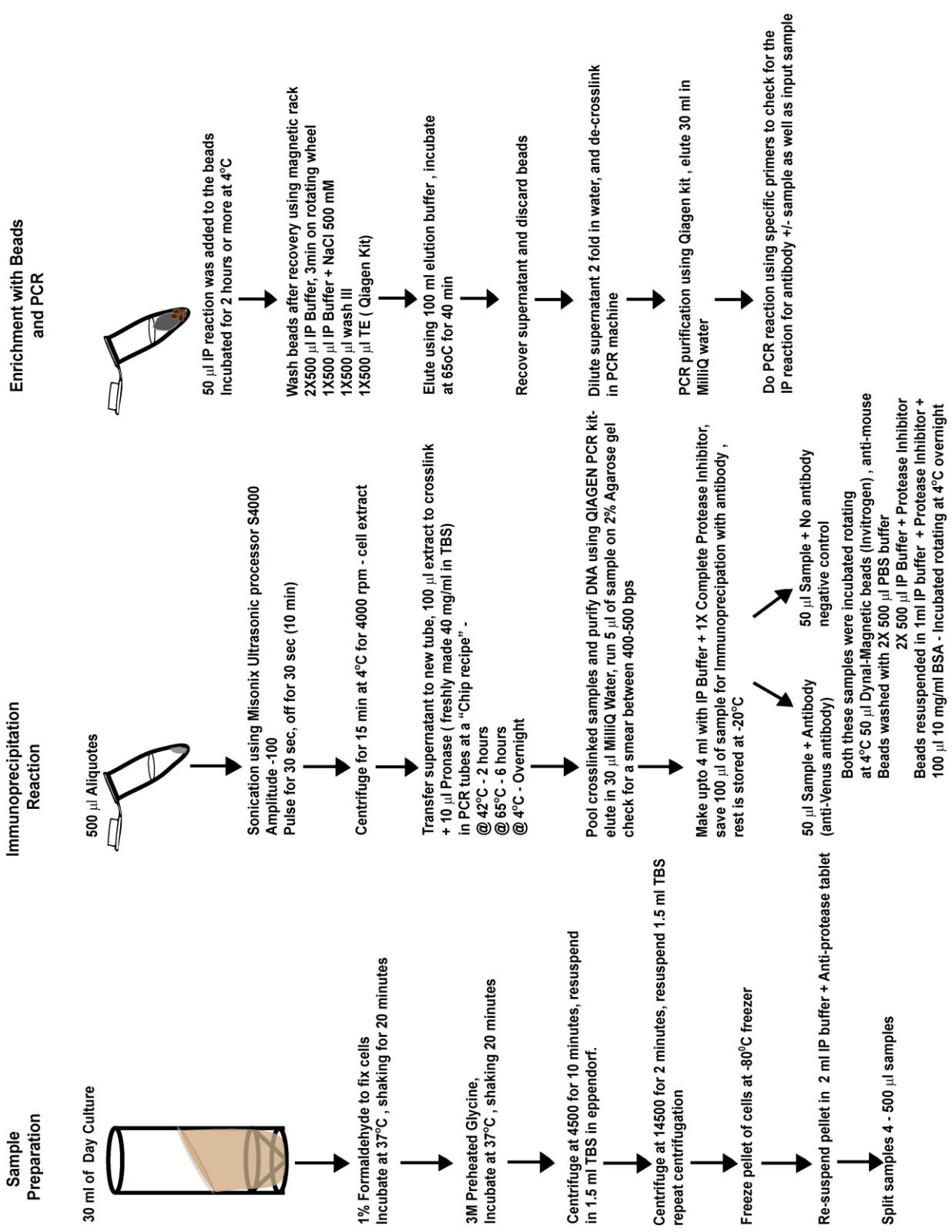

Figure 2.8 **Chip-PCR protocol:** This protocol was followed to perform Chip-PCR using V-PspF under non-stress and stress conditions and V-PspF$_{1-275}$ was used as non-DNA binding control. The immunoprecipitation was done using anti-GFP (Venus specific) antibodies (Clontech).

2.15 SMI and image analysis methods

2.15.1 Milli-second time-scale single molecule fluorescence microscopy

SMI compliments the ensemble biochemical characterisation and consequently further advances the studies by reproducing near native conditions during experimentation, capturing transient multi-protein complexes, and determining the stoichiometries of functional complexes can be determined (Biteen and Moerner, 2010; Li and Xie, 2012). For any single molecule fluorescence studies a fluorescent protein fusion is imperative, the fusion can be achieved in form of chromosomal fusion under native promoter, or under inducible promoter or plasmid-borne FP fusions.

In 2012 published work reported localisation artefacts (Swulius and Jensen, 2012; Margolin, 2012) dependent on the placement of the fluorescent tag to MreB, thus showing that single molecule fluorescence studies requires an extra measure of proof. It is vital to perform extensive stability and functional tests with the fluorescent fusions. It has also been shown that these artefacts are also dependent on the protein concentrations, thus it is important to perform these studies with close to physiological concentration of the protein (Biteen and Moerner, 2010 and Li and Xie, 2012). It is recommended to select the fluorescent molecule for fusion to be spectrally separated from the cellular autofluorescence that is mainly in the blue-green range. Therefore yellow or red emitting fluorescent proteins are favoured for single molecule fluorescence microscopy.

Moreover to optimize the number of photons detected, the single molecule microscope should be equipped with a high-Numerical Aperture oil-immersion objective (NA = 1.49), narrow and carefully chosen filters, and modern sensitive photon detectors such as electron-multiplying charge-coupled detector (EMCCD) (Moerner *et al*., 2007; Biteen and Moerner, 2010 and Li and Xie, 2012). The high background issue in the cells can also be addressed by using Total Internal Reflection Fluorescence Microscopy (TIRF) set-up, which limits the penetration to about 100 nm because of the evanescent wave. TIRF mode is ideal to study membrane-associated protein dynamics and localisation. In bacterial cells, proteins are freely diffusing around in the cytoplasm within < 5 milliseconds (Li and Xie, 2012), and such fast frame rates cannot be achieved by the microscopic set-up and the protein complexes cannot be resolved to form defined foci due to poor fluorescent signal from these proteins. . Thus only tethered PspF or PspA fusion proteins will be visualised with wide-field or TIRF illumination mode. Another important criterion for efficient imaging of the live *E. coli* cells was its stable immobilisation and observation in the same focal plane. This was achieved by mounting the culture samples on a 1% (w/v) agarose (in N^-C^- minimal media) pads set on glass slides.

2.15.1.1 Imaging conditions and slide preparation

The *E. coli* cells were grown at 30°C in N^-C^- minimal media supplemented with 0.4 % (w/v) glucose and 10 mM ammonium chloride until grown to exponential phase with OD_{600} = 0.4. The microscopy was done in a temperature controlled room at 20-25°C. The cells imaged were viable because they were observed in the exponential phase of growth and in the field of view many of the cells were observed to be dividing. The dividing cells were not used for the localisation data analysis. 1% (w/v) agarose solution was made in N^-C^- minimal media, boiled for 30 seconds until all the agarose dissolved. 100 µl of the boiling agarose solution was dropped on a glass slide securely placed using masking tape under sterile bench top conditions with the flame. The agarose solution was then flattened, sandwiched between the two slides in order to obtain a very thin layer of 1% agarose pad (see Figure 2.9). The vertical dimension of the agarose pad was 0.13 mm equivalent to the dimension of the masking tape used to separate the agarose layer between the glass slides. The agarose pads is left to dry for 2-3 hours after which when the sample is ready for imaging. Around 20 µl of the sample is placed on the agarose pads and covered with a coverslip. The N^-C^- minimal media is ideal for imaging because the FP fusion is relatively stable in minimal media instead of LB growth media and also less autofluorescence is recorded with minimal media.

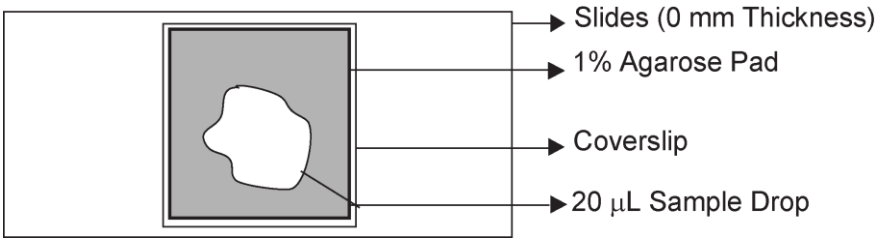

Figure 2.9 **Agarose Pads:** The diagram of a typical slide with the sample used for imaging experiments where the thin layer of agarose pads immobilises the live *E. coli* cells.

2.15.1.2 Induction of stress in the cells

The stress in the cells was induced using the over-production of phage pIV protein in the *E. coli* cells using pGJ4 or pMJR129 plasmids (see Table 2.4). The pGJ4 plasmid was mostly used unless specified where pIV was continuously produced in the cells under leaky promoter expression. In the cells the mislocalised multimeric pIV protein in the inner membrane resulted in the induction of Psp response. pMJR129 was IPTG inducible expression of pIV which was only used to study real-time change in the production of Venus-PspA with the different IPTG (0.1mM) induction times (Russel and Kaźmierczak, 1993).

2.15.1.3 Fluorescent Proteins and fluorophores

The fluorophores used in the SMI vary from small organic fluorescent dyes, autofluorescent proteins and even small genetically encoded tags. The organic fluorescent dyes have enhanced brightness and emit millions of photons before bleaching and are very photostable, e.g. - Cy3 and other carbocyannine dyes, rhodamines fluoresceins (Moerner *et al*., 2007). The major drawback of small organic fluorescent dyes is the lack of specificity and the requirement for exogenous labelling of the sample. The quantum dots are also used, these are semiconductors that photophysically act like fluorescent molecules (Rekas *et al.*, 2002; Moerner et al., 2007 and Lord *et al.*, 2010). The most commonly used and developed fluorophores used in SMI are genetically encoded autofluorescent proteins. The demonstration of GFP as a fluorescent tag, which can be encoded genetically has revolutionised *in vivo* labelling. Since then, many mutants of GFP have been identified; characterised and crystal structures have been published (as listed in the Table 2.29). Now a broad range of fluorescent proteins are available spanning the entire visible spectrum some which are listed in the table with their excitation/emission wavelengths and oligomeric state. Photoswitchable fluorescent proteins are also available which can be reversibly or irreversibly switched on and off, or converted to different colours which have proved to be very useful in super-resolution imaging. The fluorescent proteins are usually genetically fused to the gene of interest for the specific protein via an artificial linker which is either chromosomally expressed or is plasmid borne.

FLUOROPHORE	λ_{ex} _excitation (nm)	λ_{em} - emission (nm)	OLIGOMERISATION AND CHARACTERISTICS
<u>Green</u>			
GFP	475	509	Monomer
eGFP	488	507	Monomer
Superfold GFP	485	510	Monomer – fast folding, highly stable, fast maturation time
Emerald	487	509	5x-times brighter

Yellow			
YFP	514	527	Monomer, GFP derivative, less sensitive to pH and Cl^- and faster maturation
eYFP	513	527	Derivative of YFP
Venus	515	528	
Citrine	516	529	30x-times brighter, fast maturation at 37°C
Red			
mCherry	587	610	Monomer; 15 min maturation time
mRaspberry	598	625	Monomer, 55 min maturation time
Blue/UV			
TagBFP	402	457	Monomer
mTagBFP2	399	454	Monomer
EBFP2	383	448	Monomer

Table 2.29 The table lists some fluorescent proteins with different wavelength ranges (Adapted from web source http://nic.ucsf.edu/dokuwiki/doku.php?id=fluorescent_proteins)

In this study Venus has been chosen as the fluorescent protein used to fuse with PspF and PspA. Venus is a derivative from yellow fluorescent protein. Yellow fluorescent protein was derived from GFP with a key mutation of threonine residue 203 to tyrosine. Venus contains a novel mutation F46L which accelerates oxidation of the chromophore thus reducing the maturation time at 37°C. Some other series of mutations enabled better folding and increased acid tolerance to pH and Cl^-.

2.15.2 *Microscopic set-up*

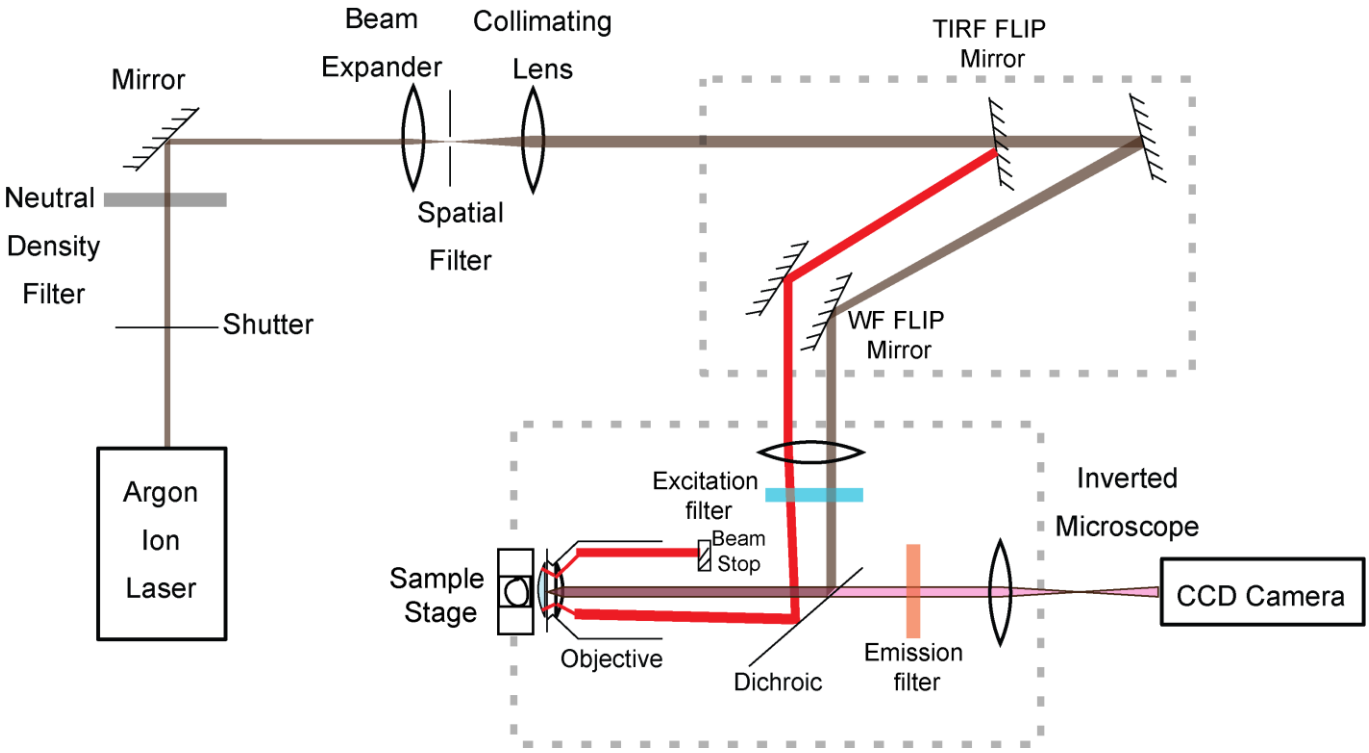

Figure 2.10 **Schematic showing the microscopic set-up of wide-field and TIRF used in the experiments:** The *E. coli* cell is only 2 µm x 1 µm in dimension which is enough to be studied under wide-field illumination. The microscopic set-up is highly sensitive and fast enough to capture single molecule events in the cell. The camera has fast capture rates; there are a number of filters to improve laser power in order to achieve a higher signal to noise ratio. The brown line represents the laser beam path for the wide-field (WF) mode of illumination and red represents the TIRF mode of illumination with the respective positions of the FLIP mirrors. The critical angle in order to achieve TIRF illumination is defined by arcsin (1.37/1.49) where 1.37= refractive index of the cells and 1.49 = NA of the microscope which is around 66.9° for this microscope. The reflected beam is collected using a beam stop within the microscopic set-up.

The microscopic set-up and the components are essential in order to achieve millisecond capture rates, diffraction limited spots and high signal to noise ratio to observe the fluorescent protein fusion. In this work two different imaging systems have been used depending on the kind of image analyses required (see Figure 2.10).

The first system was a custom-built inverted epifluorescence microscope that was used in both wide-field (WF) or total internal reflection fluorescence (TIRF) mode of illuminations, and based on a Nikon TE2000 optical microscope. The microscope was fitted with tuneable argon ion laser that could be used to excite at 488 and 514 nm wavelengths depending on the fluorophore (see Figure 2.10). The Venus/YFP fused proteins were excited with 514 nm line of argon ion laser (35LAP321-230, Melles Griot) and a corresponding dichroic filter set (zt154 TIRF, Chroma Technology).The numerical aperture of the microscopic set-up was 1.49, 100 x oil-immersion objective was used and the final magnification of the sample is 200 X. The laser power used for Venus fused to V-PspF was around 5 mW and the images

were captured as a video of 100-400 frames, with frame rate of 30 frames/second. All these images were taken with 2X2 binning with 500X500 pixel area at 15 milliseconds exposure time.
488 nm line of argon ion laser was used to excite eGFP/GFP fusions and specific dichroic filter (XF2010, Omega Optical) was used. The laser power was 1.5 mW or lowered to 0.5 mW for specific photobleaching experiments. The images were captured as a video with 100-1000 frames with frame rates of 25.6 frames/second and 2x2 binning. The quantum yield from either Venus or eGFP tagged fusion proteins was around 60% with the current set up of the EMCCD camera. The temperature in the room with the microscopes was maintained to around 20-25°C. The third system was Deltavision OMX V3 (Applied Precision, Washington and used at CR-UK London) in which imaging was done with 3 ms exposure time (44 frames/second) and was mainly used for photobleaching experiments using 10% laser power at 514 nm. The microscopic sample stage was temperature controlled to around 22°C and the microscopy room was also temperature controlled at 22°C. The quantum efficiency of the OMX microscope at 514 nm is around 85 %. The stage drift of the OMX microscope should be approximately 0.75 X 10^{-4} microns for a second long video or 0.5 X 10^{-4} microns due to temperature drifts for a second long video which is insignificant for a 2 micron X 1 micron *E. coli* cell. The microscopic experiments referred to in this thesis were based on taking a second long video and therefore the stage drifts for video sequences lasting for seconds would be approximately 10,000 fraction of the cell length (on custom built microscopy set up), which will have insignificant contribution to the dynamics for 2 micron X 1 micron *E. coli* cell.

2.15.3 Image Analysis

The images were analysed and displayed using image analysis software ImageJ (www.rsbweb.nih.gov/ij/) and FiJi (http://fiji.sc/Fiji- Schindelin *et al*., 2012). The images of all the fluorescent fusion samples used in this study were illustrated using ImageJ software. The quantitative analysis of foci localisation for V-PspF or V-PspA in the cell, the quantification of number of foci/cell and the total raw intensity profiles were also performed using ImageJ software.

2.15.3.1 Cell Intensity Analysis

The *E. coli* cells expressing eGFP-PspA or V-PspA were analysed to determine the intensity of eGFP-PspA or V-PspA foci intensity at the respective cellular location. This intensity analysis in context to foci localisation was performed using ImageJ software. For the analysis a box of around 18 pixel width was drawn across the cells of similar lengths so that it covered the whole cell and the intensity values were obtained as shown in the Figure 2.11.

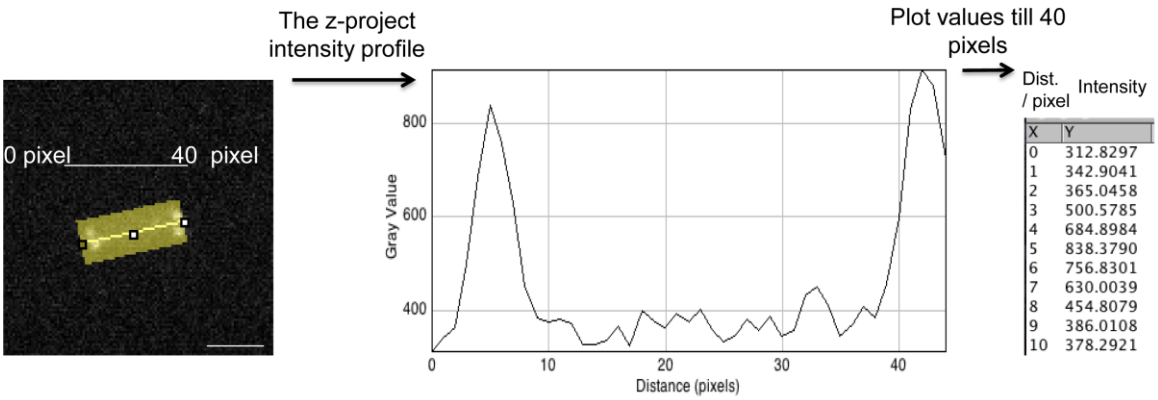

Figure 2.11 **Cell Intensity analysis across the cell length**: The schematic shows the steps in the measurement of the intensity per pixel along the cell length starting from the left pole as 0 pixels till the right pole of the cell calculated with the yellow box in the image covering the cell. The scale bar is equal to 1 µm. This measurement along the cell gave rise to a z-project profile of intensity across the cell length (in pixels on x-axis). From the profile the plot values starting from 0 pixels to 40 pixels (in this case) were recorded for 'n" number of foci and represented as mean intensity per pixel along the whole cell length with corresponding error bars or total fluorescence intensity of the cell.

This analysis tool gives pixel by pixel intensity value across the cell length starting from the left pole of the cell. In this way we were able to establish differences in the intensity at the poles vs. the lateral membrane for the different PspA structural and functional mutants such as eGFP-PspA$_{\Delta 2\text{-}19}$ and eGFP-PspA$_{\Delta 25\text{-}40.}$ Using this analysis tool the total fluorescence intensity of the cells expressing eGFP-PspA WT and mutants was also measured. The same analysis was also performed to study the real time induction of Psp response with the varying amounts of mislocalised pIV at different time intervals.

2.15.3.2 Diffusion analysis

The dynamics of biomolecules can be studied using single particle tracking which is a powerful tool to study dynamics in heterogeneous environment such as in live cells and it was pioneered by Gelles *et al*., 1988. Single particle tracking is a generic term which describes methods to study the dynamics of individual particles as opposed to an ensemble average (Saxton, 2008). A particle can be a plastic or gold bead or an individual fluorescent molecule (organic dye or fluorescent protein) attached to a biomolecule. In general the particle can be located with higher resolution than the Rayleigh limit using single particle tracking (Saxton, 2008). The diffusion analysis for V-PspF, V-PspA, GFP-LacI and σ^{54}-YFP under different growth conditions was performed using Matlab Image analysis algorithms (written in Matlab Mathworks). These diffusion analysis scripts have been described in (Treanor *et al.*, 2009) based on the algorithms published by Crocker and Grier (1996). The algorithm by Crocker and Grier (1996) filters the image to remove noise, thresholds the image and uses image segmentation to identify the individual particles as areas above threshold. Then it determines the centroid of each particle with sub-pixel accuracy. The localised fluorescent protein molecules mostly protein assemblies or self-

assemblies of Venus-PspF or Venus-PspA can be identified as diffraction limited spot called as foci. The algorithm is based on ascertaining the foci observed above the threshold values and tracking the specific foci over time with sub-pixel accuracy. Around 100-1000 foci were tracked using 1.5 second long video sequence referred for the purpose of single particle tracking described in this work. However the single particle tracking method did not distinguish between central-nucleoid, lateral membrane or polar membrane associated V-PspF or V-PspA foci or between single protein complex or self-assemblies, which were further described using photobleaching studies. The localised tracks over time were used to calculate mean square displacement (MSD). Mean square displacement was calculated by averaging all one-time-step displacements along the whole trajectory to give the first time point on the MSD curve, then all 2-time step displacements along the whole trajectory to give the second time point and then all three-time steps to give the third point and so on. This was done until the last point minus one was obtained, which was the length of the whole trajectory. However variations between displacements for the proteins in the study were large because the trajectory was short and there were few displacements for the average, so the error was very large, therefore points 1-3 were used to determine the slope and from this the diffusion coefficient. As the fit to the first three data points of the MSD curve was used this covered the time range of 50 – 150 ms instead of specific time window.

The MSD curves were linear in this range which justifies this method. Important is that the points on the MSD curve are time-lags and each represents the whole trajectory and not the time points of the image sequence. The MSD for an individual particle can be calculated with step sizes, which are one step less than the trajectory length, for example a trajectory of 15 steps will have the largest time lag of 14. When calculating this for many particles we chose length of the shortest trajectory –1 as the length for the MSD for all trajectories. The shortest trajectory length was given by the minimum length which we regarded as a trajectory (5 in the case of these experiments) and this was not limited by photobleaching. The diffusion coefficient was calculated as $1/4^{th}$ of the slope of the linear MSD curve. The diffusion coefficient was calculated based on the assumption that the particle diffuses in 2D (More details of equations in Appendix-8). Thereby with the diffusion coefficient the characteristics of dynamics of PspF or PspA proteins were determined in live *E. coli* cells. The microscope stage is fairly stable for the time scales in which these images were captured, and thus internal mechanical instability of the microscope did not contribute to the dynamics of the proteins that were tracked in the cells. The dynamic data would be presented as distribution of 2D diffusion coefficients and with the diffusion coefficient distribution the foci were classified as slow if the diffusion coefficient was between 0 - 0.15 $\mu m^2/s$ and fast diffusing with > 0.15 $\mu m^2/s$ because equal frequency of data gave 0 - 0.15 $\mu m^2/s$ and > 0.15 $\mu m^2/s$ diffusion coefficients for V-PspF under non-stress condition and this cut-off was easy to compare with all the other V-PspF variants and V-PspA. The apparent 2D diffusion coefficient stated for all the protein samples was calculated to be the median of the n values of diffusion coefficients.

2.15.3.3 Photobleaching studies

Photobleaching analysis was employed in order to establish the stoichiometry of the Venus-PspF and Venus-PspA foci characterised spatially and temporally. Photobleaching analysis was done according to the published methods (Lenn *et al.*, 2011 and Mehta *et al.*, 2013) for V-PspF and eGFP-PspA respectively. The fairly static foci were analysed to obtain intensity profile over 400-1000 frames depending on V-PspF or V-PspA foci respectively using ImageJ stack measure plug-in. The intensity profile was treated with the Chung-Kennedy algorithm employed specifically to remove the statistical noise and reveal photobleaching using filtered trace. The output of this filter is a smoother and clearer signal, with an improved signal to noise ratio. This signal was subsequently used to calculate the PDDF (Pairwise Difference Distribution Function) and its power spectrum. Finally, peaks in the power spectrum are detected and the number of steps present in the original photobleaching trace is determined. The step size (I_s) from the power spectrum was used to finally determine the stoichiometry using the difference between the initial (I_i) and the final intensity (I_f) of the foci as shown in the Equation 2.3.

$$\text{Stoichiometry} = \frac{I_i - I_f}{I_s}$$

$I_i = \text{Initial intensity}$

$I_f = \text{Final intensity}$

$I_s = \text{Intensity sample size}$

Equation 2.3 The formula to calculate the stoichiometry of proteins using the edge preserving algorithm from the intensity trace and the power spectrum generated from the PDDF values

The intensity traces were also analysed using manual counting methods by either counting the number of blinking or bleach steps which will correspond to the stoichiometry or by calculating the average sample intensity size and then calculating the stoichiometry using the difference in the initial and final intensity.

2.15.3.3.1 Chung-Kennedy Algorithm

The Chung-Kennedy Algorithm (Chung and Kennedy, 1991; Leake *et al.*, 2006 and Lenn *et al.*, 2011) is a noise-removal filter that preserves the steps in step-wise signals. A forward and backward window is generated from any given data point to sample the same number of points before and after the point from which the windows are generated. The number of points sampled (i.e. the window size) is variable. The mean and variance of each window is calculated and the output (filtered) value is the one with the smaller variance. This preserves steps as the variance of a window straddling points on both sides of a step-change will be larger than a window with points on only one side. The window size is selected to give the smallest standard deviation between the raw and filtered signals. The window size was kept as

2000. Only one pass of the filter was applied to the data. Blinking and association of new monomers in the photobleaching time-course did not affect the determination of step size, on the other hand actually helped instead. However blinking at t=0 of the photobleaching trace could have underestimated the stoichiometric analysis.

2.15.3.3.2 Pairwise Difference Distribution Function:

The pairwise difference distribution function (PDDF) (Kuo *et al*., 1991 and Lenn *et al*., 2011) for each filtered bleaching trace was calculated as follows. For every data point, its value is subtracted from all data points that follow. For a signal having n data points, the total number of pairwise differences will be equal to n (n − 1)/2. Subsequently the distribution of these pairwise differences can be calculated using a user-defined number of bins, in this case 2000. The PDDF is then normalised by dividing each bin count with the total number of pairwise differences to give the percentage of the total number of pairwise differences in each bin. The power spectrum of the PDDF was then calculated by fast Fourier transform using the Hanning window.

2.15.4 Di-4-ANEPPDHQ staining

The cells were grown in the same N^-C^- minimal media up till OD_{600} of 0.3 to 0.4. The dye was diluted to 2 mM using 1M dimethyl sulphoxide (DMSO). 1 µl of the dye (2 mM) was added to the diluted 1 ml of the day culture to a final concentration of 2 µM. The cells with the dye were incubated at the room temperature for 20 minutes. These cells were then mounted in the agarose pads and imaged using 488 nm in the TIRF mode of illumination. These images were then analysed using Image J software to calculate the total cell fluorescence intensity and the intensity of the localised dye with respect to the cell length (see Section 2.15.3.1 and Figure. 2.11). The preferential binding of this dye to inner-membrane or outer membrane is not specifically known.

RESULTS

CHAPTER 3

3 Spatial and temporal localisation of Venus-PspF fluorescent fusion protein under different growth conditions

This result chapter describes the successful construction and production of the Venus- Phage shock protein F (V-PspF) fluorescent protein (FP) fusion. It establishes that the FP fusion is stable and functional like the WT PspF. Subsequently V-PspF protein assemblies were imaged in live *E. coli* cells using single molecule imaging (SMI). The precise localisation of V-PspF under non-stress and pIV mislocalised induced stress conditions would lead to an understanding of where functional PspF assemblies reside in the cell (see Figure 3.1). Figure 3.1 pictorially illustrates the possible subcellular localisation of V-PspF in the cell ranging from nucleoid bound, membrane bound or freely diffusing in the cytoplasm as V-PspF-PspA inhibitory complex under non-stress conditions.

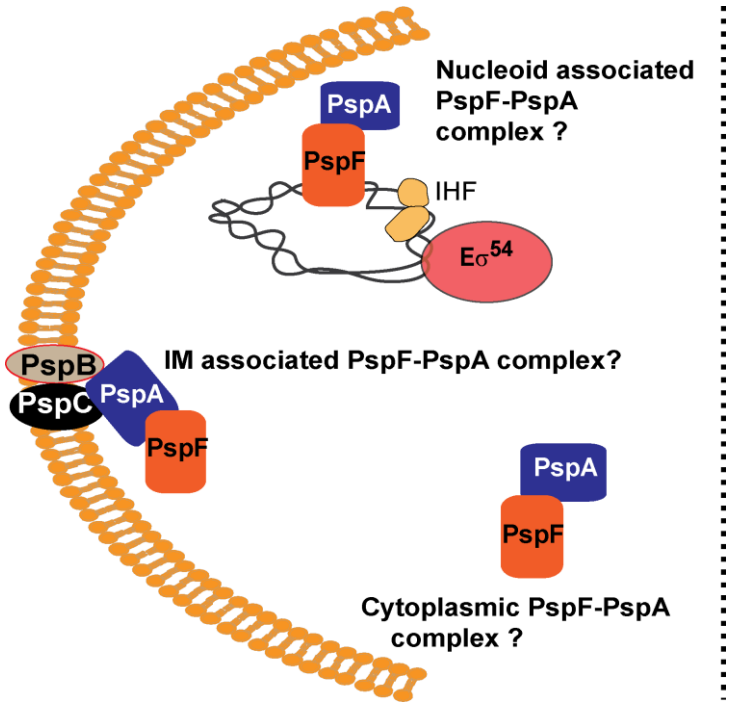

Figure 3.1 **The possible spatial localisation of PspF in *E. coli*:** The spatial localisation of PspF will be studied by expressing and imaging V-PspF in live *E. coli* cells. V-PspF could be either nucleoid associated bound to the specific DNA sequences, diffused in cytoplasm (Yamaguchi *et al*., 2013) or bound to the membrane via PspA specifically at the poles (Engl *et al*., 2009).

The cytoplasmic PspF-PspA complex could be associated with upstream activating sequences (UAS) or associated with the membrane via PspA. After resolving the spatial localisation of V-PspF under non-stress as well stress conditions, the V-PspF foci will be studied to determine their subcellular dynamics.

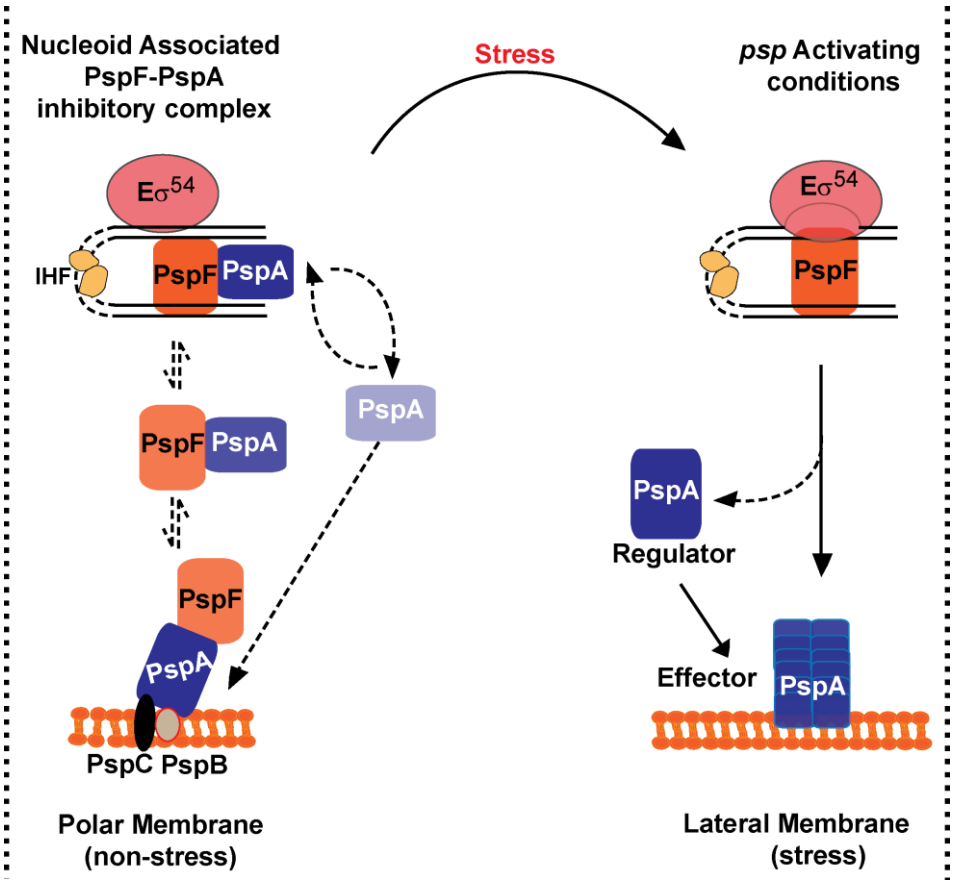

Figure 3.2 **The potential temporal localisation of V-PspF**: The schematic representation shows the potential temporal localisation of repressed V-PspF that could be nucleoid associated, cytoplasmic or membrane associated. The activating V-PspF could be at the nucleoid part of the open complex (RPo) and PspA functions as an effector at the lateral stressed membrane.

Dynamic studies would enable differentiation between the repressed state of PspF and the non-repressed transcription activating PspF complexes as shown in Figure 3.2.

3.1 Introduction

3.1.1 PspF: bEBP of the Psp response

As mentioned in (1.5.1-PspF protein) PspF is the bacterial enhancing binding protein (bEBP-master activator) for the σ^{54} dependent transcription of the *psp* genes. The mislocalisation of outer membrane (OM) secretin protein such as pIV in the inner membrane is a well-studied inducer of the Psp response in *E. coli* (Brissette *et al*., 1990 and Joly *et al*., 2010) and has also been used as inducer during the experiments of this research. The transcriptome analysis of *E. coli* under pIV induced stress conditions showed many fold increase in the expression of *pspABCDE* and *pspG* genes while the expression of the *pspF* gene was constant (Lloyd *et al*., 2004). σ^{54}- dependent transcription of *psp* genes is tightly regulated, with no leaky PspF-independent expression, compared to the σ^{70}-dependent transcription

machinery. The PspF dependent activation of *psp* genes is highly stochastic that goes from basal level expression to very high expression of *psp* genes upon stress induction (Buck *et al.*, 2000). Transcription factors such as LacI and PspF are expressed in low copy numbers in the cells. The low copy number is an essential characteristic of biomolecules which can impart stochasticity. From Western blot analysis the amount of PspF was estimated to be 120 molecules (approximately 20 hexamers) in the cell (Jovanovic *et al.*, 1997) which was much lower, as compared to RNAP enzyme that forms around 14-16 % of the total protein content in the bacterial cell (Shepherd *et al*., 2001). Thus the study of transcription factors such as PspF becomes much more reliable with SMI, because the data can be collected reliably for low copy number proteins than the high copy number proteins. Real-time single cell measurements can reveal stochastic events driven by transcription factors and capture events eluded by averaging in ensemble studies of synchronized cell cultures (Wang *et al.*, 2012 and Li and Xie, 2012).

3.1.2 Studying Transcription factor like PspF by SMI

A single fluorescent protein fusion can be detected above the cellular background (see Figure 1.12; page number 68) by spatial confinement of the fusion molecules within the data collection timescales (Xiao *et al*., 2008) – this method is described as “detection by localisation”. The same method has been convincingly used to study binding of transcription factors such as LacI to specific operator sites (DNA sequences). A SMI technique like millisecond (ms) time-scale fluorescence microscopy takes advantage of fluorescent proteins such as GFP and its derivatives to capture protein machineries and assemblies and rare events in live *E. coli* cells. For live cell SMI it is imperative that the fluorescent protein matures fast enough to capture fast dynamics of cellular processes. Another criterion for the fluorescent protein is that it should be bright enough to be distinguished above the cellular autofluorescence. In this study a variant of yellow fluorescent protein (YFP) called Venus was chosen to fuse with PspF and PspA because it fulfilled all the above requirements. It was reported that Venus has fast maturation time (t = 7min) inside *E. coli* cells (Yu *et al*., 2006) and is 80% brighter than the organic dye fluorescein (Shaner *et al*., 2005). Table 3.1 shows the advantages of live cell imaging as compared to imaging of fixed cells, and imaging of PspF and PspA in live *E. coli* cells was preferred form of sample preparation for SMI studies.

LIVE CELL IMAGING	FIXED CELL IMAGING
Real time measurements	No real time measurements can be made
Native environment	Cells treated chemically such as with formaldehyde

Dividing and healthy cells	Fixed cells
Autofluorescence	Less autofluorescence
Usually higher signal	Signal could be lower but can be multiplied by 3-D reconstructions
Super-resolution microscopy and 3-D reconstructions are difficult to achieve	Super-resolution and 3-D reconstruction are better if performed on fixed cells

Table 3.1 List of characteristics of live cell imaging as compared to imaging of fixed cells.

SMI with Venus-protein fusions in live *E. coli* cells will capture temporal and spatial differences in V-PspF complexes under different growth conditions in real time, which are very relevant to gain insight into the mechanism of activation of Psp response. The spatial and temporal characteristics of V-PspF are studied using millisecond fluorescence microscopy in wide-field and total internal reflection (TIRF) illumination modes. TIRF mode will to distinguish between nucleoid-associated complexes and membrane associated V-PspF-PspA complexes.

3.1.3 Mobility of protein complexes in cells

The bacterial cell cytoplasm is overcrowded (see Figure 1.13A, B; page number 72) because of the absence of compartmentalisation of cellular processes as occurs in eukaryotic cell cytoplasm (Mika and Poolman, 2011). All the macromolecules such as DNA, RNA, proteins and lipids are constantly interacting and influencing the viscosity and the physical space in the cytoplasm and thereby the movement of these macromolecules (Mullineaux *et al.*, 2006; Magdziarz *et al*., 2009; Nenninger *et al*., 2010 and Mika and Poolman, 2011). Diffusion is the major mode of intracellular movement for proteins. The diffusion of proteins in the overcrowded bacterial cytoplasm governs the rates of cellular processes and also facilitates efficient interaction between different macromolecules. The cellular diffusion of proteins can either be normal, or Brownian/anomalous (Mika and Poolman, 2011). The Brownian diffusion of proteins follows a linear path depending on the time. Anomalous diffusion is more complex and depends on more complex interactions between multiple proteins and subsequent interactions with the nucleoid and membrane (Mika and Poolman, 2011). The proteins may have to hop between domains, search and slide on specific sites on the nucleoid or follow a more defined path along the membrane and these miscellaneous diffusion paths contribute to anomalous diffusion of proteins (Kim *et al*., 2006; Elf *et al*., 2007 and Mika and Poolman, 2011). The dynamics of proteins in the cell has been defined as apparent 2D diffusion coefficient and the value of diffusion coefficient can be obtained using many different techniques as mentioned in (Section 1.7-Single Molecule Imaging). The most common method of measuring diffusion coefficient (D) of fluorescent-tagged protein is by single particle tracking

in which the fluorophore tagged biomolecule can be located with higher resolution than the Rayleigh limit and tracked over time (more details see Methods section 2.15.3.2, Gelles *et al*., 1988 and Saxton, 2008). DNA binding proteins including transcription factors such as LacI have been studied in great detail in order to understand the DNA-facilitated movements of LacI. LacI as explained in detail (Section 1.7.3.2- Targeted search for sites on the DNA by transcription factors) exhibits many different types of cellular dynamics each characterised by specific diffusion coefficients.

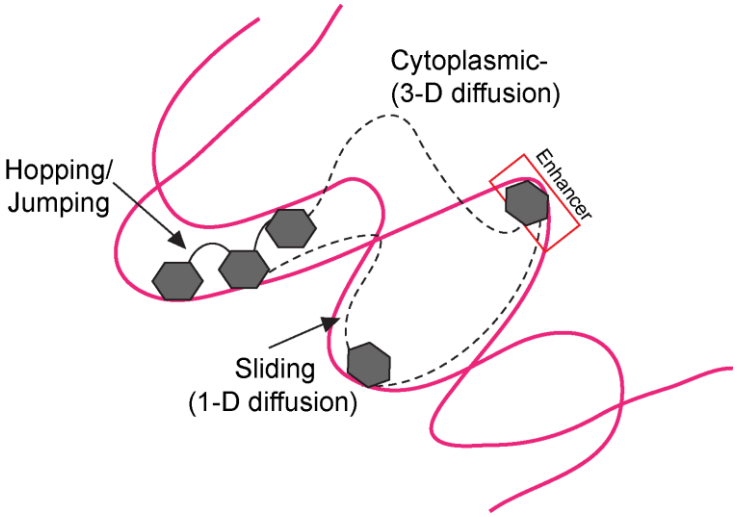

Figure 3.3 **Different diffusion exhibited by a transcription factor**: A transcription factor such as LacI displays a range of diffusion when in search of the operator sites. It can either slide along DNA (1-D diffusion), usually spanning 100 bps at a time, or hop from one stretch of DNA site to another, or it can even diffuse across cytoplasm (3-D diffusion) in search of the operator sites. Therefore transcription factor such as LacI show anomalous diffusion (adapted from Chapter 2 Wang and Austin, 2011).

LacI has been shown to exhibit anomalous diffusion with the combination of sliding along the DNA sites, hopping between the sites on DNA and cytoplasmic 3-D dynamics as shown in the Figure 3.3 (Elf *et al*., 2007; Biebricher *et al*, 2009; Wang and Austin, 2011 and Hammer *et al*., 2012). A similar approach and set of propositions could be true for PspF since it can bind specific enhancer sites on the chromosome and possibly occasionally interact with the membrane.

By the estimating of diffusion coefficients for V-PspF under different growth conditions and for different functional mutants, it will be possible to report for the first time the temporal localisation of the different partnering Psp proteins in the cell (see below 3.9). The comparison of diffusion coefficients of the different states of PspF would also help to highlight the importance of interplay between the nucleoid and membrane during the membrane stress responses.

3.2 Stable and functional V-PspF fluorescent protein

The V-PspF fusion was tested for its stability and functionality in the cells to show that it successfully complimented wild type PspF with respect to its cellular functions.

3.2.1 Gene replacement and construction of V-PspF fusions

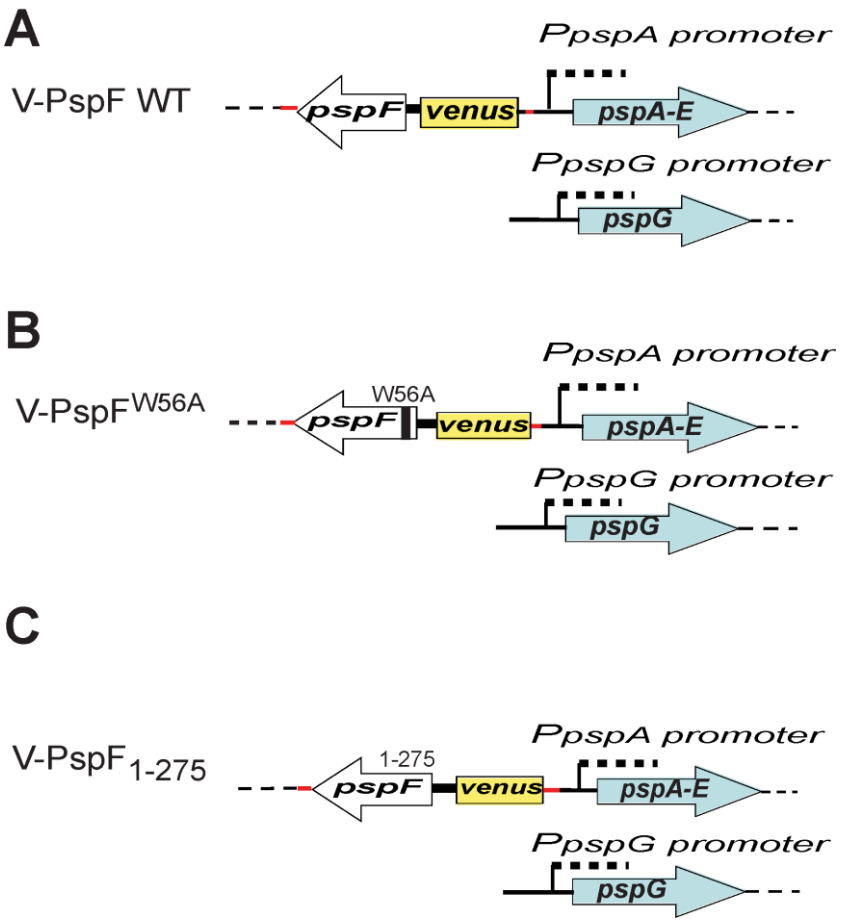

Figure 3.4 **Schematic organisation of the *psp* genes.** The organisation of fusion genes expressing V-PspF and the various mutants. The *venus* gene and the linker are fused to the N-terminus of *pspF*, retaining the other *psp* genes at their native locations. (A) V-PspF WT; (B) V-PspF^{W56A} mutant, lacking the repressive binding interaction with PspA and (C) V-PspF$_{1-275}$, with a deletion of the DNA binding domain.

The fluorescent fusion of V-PspF/V-PspF mutants was constructed using red recombineering technique (see Figure 3.4 for schematic outline of the fusion proteins and their genomic position), where the native *pspF* gene was replaced with the N-terminal of *venus*-linker-*pspF* gene fusion. A seven amino acid long linker 3G-1S-1G-1E-1F (Engl *et al*., 2009) fusing the *venus* and *pspF* genes governed the stability of the FP fusion. The detailed methodology of the red recombineering technique is described in (see Methods 2.2.1.1). The background strain used for all experimental purposes was MG1655 (Joly *et al*., 2010) (see Table 2.3). The mutant PspF^{W56A} has a single amino acid substitution of alanine instead of tryptophan and PspF^{W56A} escapes negative control by no binding of PspA to PspF. So consequently the transcription of *psp* genes is constitutively active in the cells expressing PspF^{W56A} mimicking stress states of the cells (Elderkin *et al*., 2005). The V-PspF^{W56A} mutant with the single amino acid substitution

(W56A), as shown in Figure 3.4B, also escaped negative control by PspA through reduced binding of PspA to PspF (Elderkin *et al*., 2005 and Joly *et al*., 2009). This well-characterised mutant of PspF that does not bind PspA was ideal to study the influence of PspA on the localisation and the dynamics of the PspF. The other PspF mutant was $PspF_{1\text{-}275}$ that lacks the DNA binding helix-turn-helix motif (Jovanovic *et al*., 1997) and cannot bind UAS sequences in the *psp* regulatory regions. Most literature reported studies of PspF have been *in vitro* biochemical assays using this non-DNA binding variant of PspF-PspFΔHTH functionally similar to $PspF_{1\text{-}275}$ (referred in this thesis). The $PspF_{1\text{-}275}$ was a useful mutant to characterise the specific UAS binding property of Psp. V-$PspF_{1\text{-}275}$ where the C-terminal DNA-binding domain (Jovanovic *et al*., 1996) was deleted through the introduction of a stop codon at position 276 of PspF WT is shown in Figure 3.4C. The presence of the chromosomal *venus-pspF* fusion was confirmed by colony PCR. The colony PCR was performed using primers specific for the *venus–pspF* gene locus using Venus-Fw and PspF-Rv primers listed in Table 2.8 - (KpnI Venus-fw and XbaI PspF-Rv).

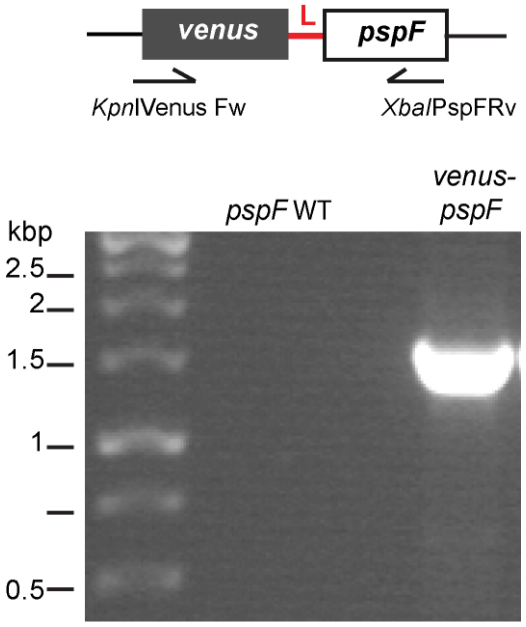

Figure 3.5 **Agarose gel of a colony PCR gel to check for the presence of chromosomal *venus-pspF***: The gel showed the presence of band corresponding to the gene fusion of *venus-pspF* by colony PCR. The colony PCR was performed with the specific primers (see Table 2.8) as shown in the diagram. L - corresponds to the linker that fuses *venus* and *pspF* genes.

The gel shown in Figure 3.5 represents the PCR product obtained from the colony PCR of the *venus-pspF* fusion constructs. The expected band size for the fused *venus-pspF* genomic construct was around 1.5kbp. The presence of the chromosomal fusion construct in the *E.coli* cell was further confirmed with the sequencing of the PCR product of the *venus-linker-pspF*.

3.2.2 *V-PspF FPs were functional*

The production, stability and functionality of the V-PspF/ V-PspF mutants was tested using Western Blotting (see Method 2.7.4-Western blotting) of the crude cell extracts, using specific anti-Venus antibodies, anti-PspF antibodies and anti-PspA antibodies. The MG1655 cells expressing V-PspF or V-PspF mutant's cells were grown in N^-C^- minimal media, supplemented with 0.4% (w/v) glucose-carbon source and 10 mM ammonium chloride-nitrogen source along with trace elements at 30°C. The N^-C^- minimal media was specifically the chosen growth media because the V-PspF fusion would be much more stable in minimal media instead of rich LB media. The growth at 30°C was important because it was an ideal temperature for the maturation of Venus fluorescent protein and also reduced the activity of proteolytic enzymes during cell growth. The stress was induced in these cells using leaky plasmid expression from pGJ4 for continuous pIV production and consequently mislocalisation of pIV protein in the inner-membrane resulted in induction of Psp response (see Table 2.4 and Section 2.15.1.1) and in this thesis *psp on* denotes pIV mediated stress inducing conditions while non-stress conditions denote as *psp off* state.

The production and ability to activate *psp* gene expression, and regulation by master regulator PspA was studied to confirm the functionality of the V-PspF FPs. The presence of PspA protein was studied as a measure of functionality of V-PspF using anti-PspA antibodies. PspA was found to be produced at native physiological levels under physiologically normal conditions (non-stress conditions) while its production increases almost 100-fold in stress conditions induced by mislocalisation of secretin pIV in the inner-membrane (IM) (Brissette *et al*., 1990).

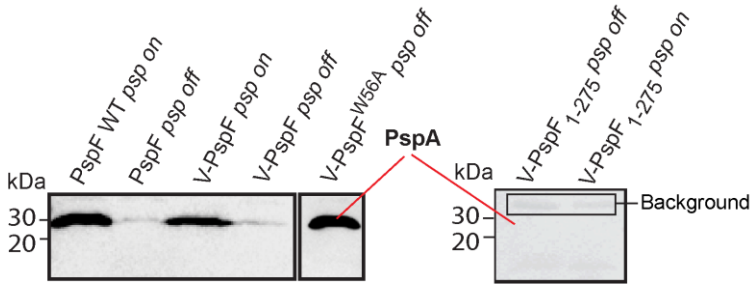

Figure 3.6 **Western blot to test functionality of V-PspF**: The Western blot was performed to show the functionality of different V-PspF proteins (by their ability to activate the of *pspA* gene) using PspA antibodies; as shown the V-PspF WT fusion behaved as native PspF, supporting a basal level production of PspA under non-stress conditions (*psp off*) which was activated by V-PspF with the onset of stress (*psp on*); transcription of the *psp* genes is constitutively switched on in V-$PspF^{W56A}$ (*psp off* conditions) and in cells expressing V-$PspF_{1-275}$ in non-stress (*psp off*) and stress conditions (*psp on*) no PspA was detected.

$PspF_{WT}$ (MG1655) and V-PspF were shown to activate basal level production of PspA (26kDa) under non-stress conditions (*psp off*) as shown in Figure 3.6. The production of PspA was induced in both the strains expressing $PspF_{WT}$ and V-PspF in the presence of stress (*psp on*). The comparable intensity of PspA bands observed with $PspF_{WT}$ and V-PspF expressing strains respectively under non-stress as well

as stress conditions confirmed the functionality of the fusion similar to WT. The V-PspF^{W56A} mutant was shown to strongly induce the production of PspA even under non-stress growth conditions (*psp off*) (see Figure 3.6). V-PspF$_{1-275}$ mutant without the C-terminal DNA binding helix-turn-helix motif showed the expected behaviour of failing to activate *psp* expression *in vivo* as shown in Figure 3.6 (Jovanovic *et al*., 1996). Thus no PspA was detected on the blots in the cells expressing V-PspF$_{1-275}$ because this mutant does not bind the specific UAS sites and therefore does not activate the transcription of *psp* genes *in vivo* at physiological level in non-stress conditions or in stress activating conditions (Jovanovic and Model, 1997).

3.2.3 V-PspF FPs were stable

The stability of the V-PspF fusion was investigated prior to imaging in order to confidently attribute the fluorescent foci observed to an assembly of V-PspF rather than Venus fluorescent protein aggregates. Western blotting using anti-Venus or PspF primary antibodies was performed to assess the stability of V-PspF. Western blot should detect high molecular weight bands (63kDa) for the fusion with minimum background bands (~35kDa PspF or ~28kDa Venus, as proteolytic products of the fusion).Western blot of the V-PspF and mutants was challenging, as PspF protein is inherently present in very low amounts in the cell, which is at the detection limits of the technique. It has been reported in Jovanovic *et al*., 1997 that around 120 molecules of PspF are present in *E. coli* cells.

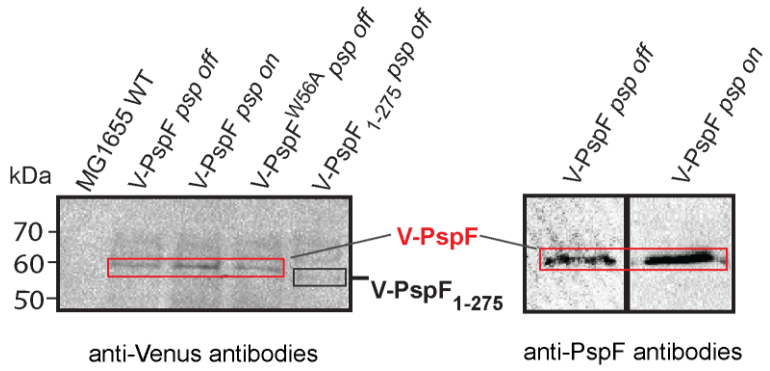

Figure 3.7 **Western Blot to show expression and stability of V-PspF and mutants using Venus specific GFP antibodies and anti-PspF antibodies**: Western blot was performed to show the production and stability of the V-PspF (non-stress, *psp off*, and stress *psp on*, conditions), V-PspF^{W56A} (*psp off*) (~64 kDa) and V-PspF$_{1-275}$ (*psp off*) (~60 kDa) using Venus specific GFP antibodies. Western blot was also performed to show the production and stability of the V-PspF (non-stress, *psp off*, and stress *psp on*, conditions) using anti-PspF antibodies.

Figure 3.7 shows blots of V-PspF under non-stress growth conditions (*psp off*) and with pIV stress growth conditions (*psp on*). V-PspF under non-stress and stress conditions gave band around 63kDa (~35kDa PspF + ~28kDa Venus), while the MG1655 *E.coli* strain expressing PspF$_{WT}$ gave no high molecular weight band with anti-Venus antibodies. The band representing V-PspF^{W56A} was also

observed around 63kDa as illustrated in Figure 3.7. The V-PspF$_{1-275}$ band was observed at a lower molecular weight (~ 58kDA) as compared to the V-PspF WT (see Figure 3.7). Also the gels in Figure 3.7 showed that the production of PspF in the cells remained constant as the intensity of the bands of V-PspF were similar for cells grown under non-stress as well as stress growth conditions.

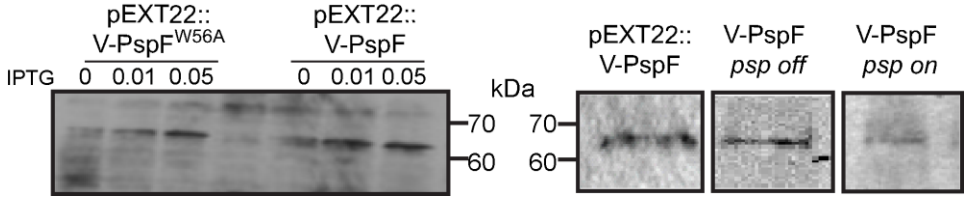

Figure 3.8 **Western Blot to show that the chromosomal expression and plasmid borne expression of V-PspF is similar**: The Western blot to validate the ideal inducing concentration of the pEXT22 plasmid to attain near physiological expression of V-PspF. The 0.01 mM IPTG was used to induce the plasmid and then the expression of V-PspF FPs from plasmid was compared with the chromosomal expression of V-PspF. The plasmid borne expression (pEXT22) of V-PspF was induced by 0.01mM IPTG.

Additionally V-PspF/V-PspF^{W56A} was produced from low copy plasmid-pEXT22 (see Table 2.4). The Western blot in Figure 3.8 detected a 63kDa band representing V-PspF under both non-stress and stress growth conditions, and confirmed its stable production. The inducing conditions were selected to be 0.01mM IPTG after testing the different concentration of IPTG in order to obtain near physiological expression of V-PspF (see Figure 3.8). Thus V-PspF and its mutants were established to be functional and stable under the growth conditions to be used to harvest cells for single-molecule epifluorescence microscopic studies.

3.3 SMI microscopy of Venus and V-PspF

Similarly for microscopy cells were grown at 30^{o}C in N^{-}C^{-} minimal media, supplemented with 0.4% (w/v) glucose, 10 mM ammonium chloride and trace elements. The growth in minimal media instead of rich media reduced the background autofluorescence contributed by LB broth media, the fusion was less susceptible to proteolysis and the cell divided with slower division rate ideal for optimum fluorescent protein maturation. The overnight culture grown in N^{-}C^{-} minimal media was diluted 40 times for day culture in N^{-}C^{-} minimal media that was grown up till exponential OD_{600}= 0.4-0.6 and then immobilised on a 1% agarose pad on the microscopic slides (see for details Methods 2.15.1.1). The agarose pads immobilised sufficient number of cells in the imaging plane of which a convincing number of cells exhibited bright fluorescent spots that could be used for image analysis to estimate spatial and temporal localisation. The cells imaged were viable as some cells observed in the field of view were dividing and the Western blotting (see Section 3.2) were done on the cell extracts from the samples used for imaging studies. The microscopy was performed on a custom-built inverted epifluorescence oil-immersion microscope (see for details Methods – 2.15.1 and 2.15.2) in the wide-field and TIRF illumination mode,

TIRF modes enable to differentiate between cytoplasmic or membrane associated localisation. The excitation wavelength was set at 514 nm with specific dichroic mirror and laser power of 5 mW. The imaging was done at 15 ms exposure time with 30 frames/s frame rate.

3.4 SMI of Venus fluorescent protein on its own

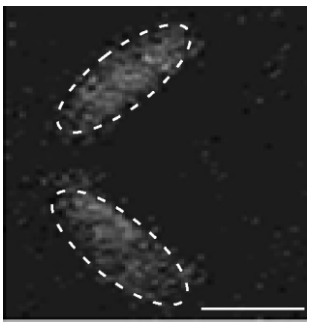

Figure 3.9 **Venus fluorescent protein observed with the microscope**: The fluorescent wide field image of MG1655 cells expressing Venus alone from the pCS2 plasmid. Scale bar = 1µm

It is important to establish the experimental evidence from the imaging of Venus on its own before imaging the Psp protein fusions to Venus. Because Venus monomer can form aggregates and drives localisation of the proteins in the cell (personal correspondence with Meriem El Karoui (University of Edinburgh and Landgrof *et al*., 2012). The Venus fluorescent protein produced from pSC2 plasmid in MG1655 cells was observed in the wide-field microscopic set-up. In *E.coli* the Venus fluorescent protein alone displayed no defined foci as shown in the Figure 3.9. The cell showed a more diffused fluorescence signal due to the fast diffusing Venus monomers in the cell. These highly mobile Venus molecules could not be captured with the exposure time of 38 milliseconds (ms). Foci could be defined as localised bright fluorescent spots of the fluorescent fusion which are diffraction limited spots. The images of Venus alone showed that it does not form defined foci, and so any foci observed with Venus-PspF imaging would be PspF driven localised spots.

3.5 Distribution of foci/cell

Prior to understanding the spatial localisation of V-PspF in *E.coli* cells under non-stress or stress conditions, it is essential to define the number of foci observed per cell. The number of potential PspF binding sites (3 UAS sequences to bind to) on the chromosome is small and so the number of V-PspF foci observed per cell offers an inferential indication of the localisation of the V-PspF-PspA inhibitory complex. There are 120 molecules of PspF in *E. coli* cells (Jovanovic *et al*., 1997) with no more than 3 DNA binding sites on the nucleoid. It is speculated that not more than 3 foci of V-PspF assemblies can be detected in the cells at a time.

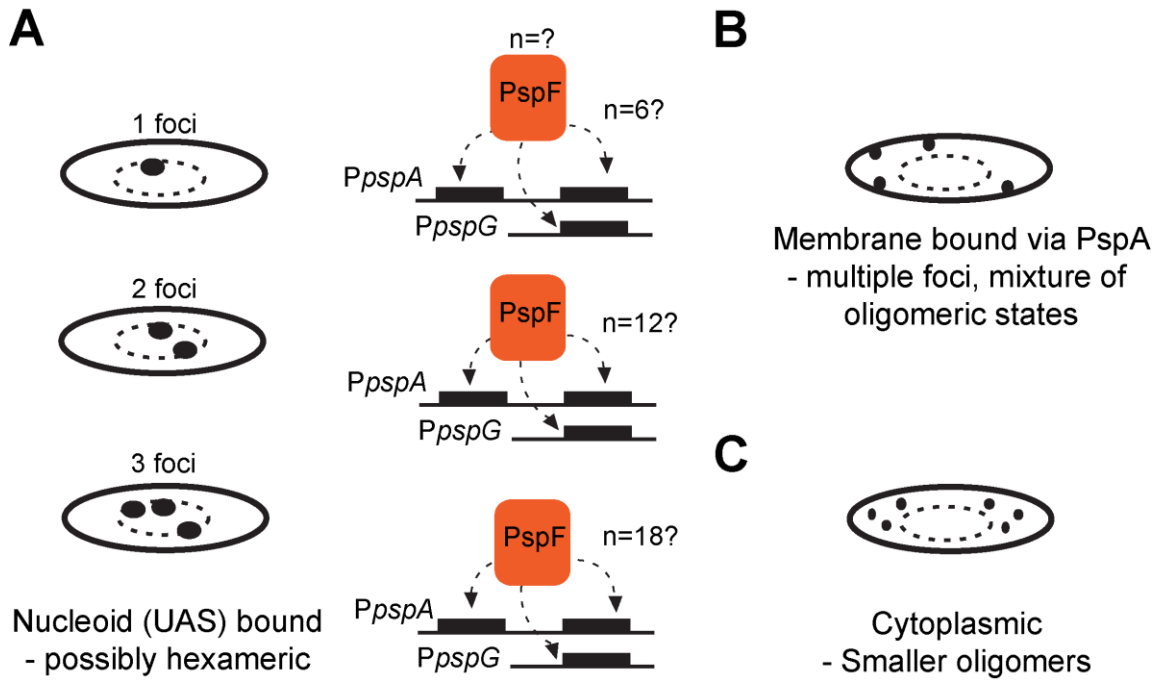

Figure 3.10 **The predicted models for the distribution of number of foci/cell**: The number of V-PspF foci/cell is a very good indication of the potential localisation and potential functional stoichiometries. (A)The observation of more than one foci per cell is either due to the replicating chromosome with multiple binding sites or it might be that PspF binds more than one UAS sequences in *pspA* and *pspG* promoters in the cells. More than one foci might also reflect on the functional stoichiometry of PspF which could be 6-mer (when one foci observed); 12-mer (when 2 foci observed bound to 2 UAS) and 18-mer (when 3 foci observed bound to 3 UAS). (B) V-PspF foci might also be observed as membrane proximal foci as part of PspF-PspA inhibitory complex, and such PspF self-assemblies might have a range of oligomeric states. (C) V-PspF could be cytoplasmic diffusing as PspF-PspA inhibitory complex.

In the same way a single foci or maximum of 3 V-PspF foci per cell would suggest that these foci are nucleoid associated bound to UAS at either *pspA* or *pspG* promoters as shown in the Figure 3.10. It is possible that the resolution that can differentiate between all three foci bound to the UAS cannot be achieved easily or it is also formally possible that more than one foci observed could be due to the replicating chromosome (Bates and Kleckner, 2010). More than three V-PspF foci observed might suggest membrane association of V-PspF-PspA inhibitory complexes via PspA as shown in Figure 3.10B. Along with the potential localisation, the number of foci data can also be used to speculate on the possible stoichiometries of the foci as shown in Figure 3.10. The UAS bound state of PspF is likely to be a hexameric self-assembly, as it has been reported for $PspF_{1\text{-}275}$ *in vitro*, which forms concentration dependent hexameric species (Joly *et al.*, 2006). One diffraction-limited spot might indicate a single hexamer of PspF is active at any given time in the cell. The estimated 120 molecules of PspF can form 20 hexamers of PspF, which could be a thermodynamic requirement for UAS occupancy in the cell (Elf *et al.*, 2007). Whether the number of diffraction limited spot of V-PspF changes from non-stress to stress conditions will also be worth noting.

The estimation of number of foci was done using the video sequence of 100 frames; however the calculations were done on the first frame when the foci first appeared in the sequence. The foci number distribution was calculated for all the cells in the field of view.

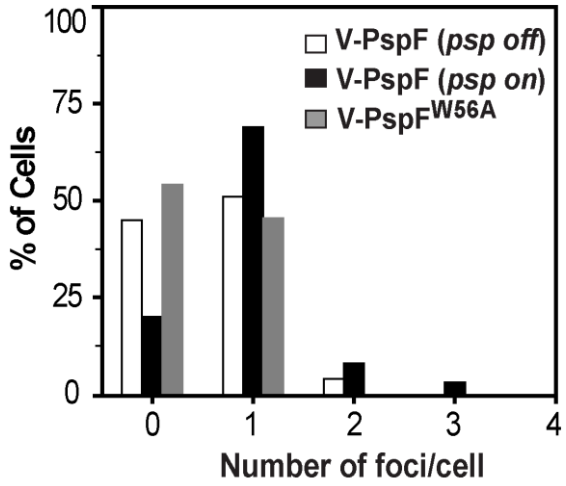

Figure 3.11 **The distribution of number of foci/cell**: Graph of the number of V-PspF foci [number of cells (n) =314 (non-stress- *psp off*), n=197 (stress, *psp on*)] or V-PspF^{W56A} (n=185) per cell where x-axis represents number of foci and y-axis represents total percentage of cells. The sample images have been shown in the following Figures 3.12, 3.13 and 3.14 and the analysis was done on images taken in wide-field mode.

3.5.1 Foci Distribution of repressed V-PspF- non-stress conditions

For non-stress conditions 314 cells were studied in total out of which 51 % cells displayed one foci, 4 % had two foci and in the rest 45 % of cells no discernible foci was detected as shown by white columns in Figure 3.11. The 45% cells where no foci were observed could be either due to the cells being out of the focal plane or DNA bound PspF foci was not established during the time of observation. The two foci observed in the cells could be due to the replicating chromosome with multiple UAS sites (Bates and Kleckner, 2010). The two foci could also represent the two different forms of PspF self-assembly- one bound to the DNA and the other bound to the membrane via PspA because the second foci was not observed for longer frames and usually disappeared into the cytoplasm. The second foci were less transiently observed, typically for 5 to 10 frames (about 300 - 400 ms), which could indicate transient membrane interaction of V-PspF.

3.5.2 Foci Distribution for activating V-PspF – stress conditions

The foci distribution per cell was calculated for V-PspF, expressed from cells grown under stress conditions. In stressed cells (*psp* on) from a field of view of 197 cells, 69% of cells with single foci, 8% with two foci, 3% with 3 foci and 20% of the cells with no foci were detected as shown by black columns in Figure 3.11. In the stressed cells the V-PspF foci were more stably observed for 30 frames (observed

up to 1s) in the video sequence of 30 frames/second. This could be due to a more pronounced DNA binding interaction of PspF as part of the activation complex under stress inducing conditions. In some cells even 3 foci were observed which could be due to the replication of the chromosome (Bates and Kleckner, 2010).

3.5.3 Foci Distribution of V-PspF^{W56A} – no binding to PspA

The cells expressing V-PspF^{W56A} were grown under non-stress conditions. However, this is a functional mutant which does not bind PspA, thus is not regulated leading to constitutive expression of *psp* genes. In these conditions, 45% cells gave one foci and in the rest (55 %) no discernible foci was observed (as shown by grey columns in Figure 3.11). The V-PspF^{W56A} foci were also observed for longer times (25-30 frames, up to 1s) as compared to V-PspF under non-stress conditions The V-PspF^{W56A} mutant behaves like non-repressed V-PspF, activating the transcription of *psp* genes under the non-stress conditions.

3.5.4 Inferences from the number of foci/cell results

Comparing the foci distribution of V-PspF under non-stress and stress conditions and for V-PspF^{W56A} (non-stress) showed that the majority of the cells showed single foci per cell (Figure 3.11A). The observation of more than one foci in some cells could be due to the presence of several DNA binding sites, because of the replicating chromosome in the cells in the log phase, as observed in cells under stress (Bustamante *et al*., 2011). Alternatively it could also be due to V-PspF–PspA complex being observed in a different form in the cell such as transiently bound to the membrane under non-stress conditions.

PspF contains a DNA binding helix-turn-helix motif that assists in binding to the UAS sequences. The interactions of PspF at the membrane or cytoplasm via PspA are more likely to be less specific than binding to UAS, thus leading to higher numbers of PspF (lower order forms) to be observed in the imaging. Therefore the observation of single foci/cell strongly indicates that the PspF-PspA inhibitory complex is formed at the nucleoid, specifically bound to the UAS DNA at either of its *psp* promoters. It also represents that the amount of PspF is limiting in the cells and thus governs its spatial localisation. The distribution of the number of foci/cell strongly argues towards nucleoid localisation of V-PspF.

3.6 Subcellular Localisation of V-PspF

3.6.1 V-PspF is nucleoid associated under non-stress conditions

The PspF full length protein is known to bind specifically to the enhancers (UAS) of the *pspA* and *pspG* promoters on the *E. coli* chromosome (Dworkin *et al*., 1997, Jovanovic *et al*., 1999 and Lloyd *et al*., 2004), and *in vitro* the AAA+ domain of PspF forms hexameric self-associated complexes competent to

activate transcription (Rappas *et al*., 2005; Joly *et al*. 2006.; Bose *et al*. 2008 and Joly *et al*., 2009). It is important to understand the regulation and activation of the Psp response with full length PspF. The V-PspF fusion with the help of SMI will help to estimate the precise localisation of repressed PspF self-assemblies (Figure 3.1). The V-PspF fluorescent protein was observed as defined foci which were diffraction limited and not aggregates of Venus alone (Figure 3.9). V-PspF foci were predominantly (~60%) localised in the nucleoid (central/lateral) as stable foci (observed for 30 frames = 900 ms) as shown in Figure 3.12B. Most of the nucleoid-associated foci bleached after 900 ms. Amongst the nucleoid associated foci two types of subcellular localisation were observed central foci or lateral foci. The remaining 40% of foci were observed at the polar periphery of the cell, possibly membrane associated. These foci were relatively transient, observed for 10 frames=150 ms and most times disappeared into the cytoplasm (Figure 3.12). The TIRF microscopy was used to differentiate between DNA bound PspF and membrane associated PspF, possibly via PspA. The TIRF mode preferentially imaged the fusion protein localised at the membrane proximal region of the immobilised cells. Only the V-PspF polar local foci were evident in TIRF mode as shown in the Figure 3.12A. The membrane proximal foci were observed for 250 ms in the TIRF mode as seen with wide-field illumination. The cytoplasmic/nucleoid foci were not evident in the TIRF mode, whilst they were stably observed for 900 ms in the wide-field mode.

3.6.1.1 Native interactions of V-PspF were detected using SMI

The repressed V-PspF was predominantly nucleoid associated and showed intermittent interaction with the membrane. It was important to ascertain that the functional equivalent of native PspF, V-PspF exhibited the localisation associated with its function. This was the premise behind overproducing PspF from pBAD based plasmid (high copy number plasmid) to check if the native interactions of V-PspF were disrupted. Non-tagged native PspF was induced in the presence of 0.2% (w/v) arabinose cells expressing fluorescent V-PspF; all the foci were lost Figure 3.12A-iii. This showed that native interactions between V-PspF – itself and potential interacting and tethering partners such as DNA and PspA were out-competed by native PspF. Therefore SMI of assemblies of V-PspF allowed investigation of the native bEBP system in live cells.

The subcellular localisation data strongly suggested that the V-PspF-PspA repressive complex is present in the nucleoid and that only transiently V-PspF-PspA complex (or self-assembled PspF) communicated with the IM by direct juxtaposition to polar regions of the cell. Yamaguchi *et al*. (2013) have made a similar conclusion on the cytoplasmic localisation of PspF but the specific nucleoid association of PspF was not fully characterised. The TIRF microscopy observation of only membrane proximal V-PspF at the

poles and titration of the V-PspF foci with native PspF indicated that the diffraction-limited foci were native self-assemblies of V-PspF and not artefacts driven by Venus assemblies.

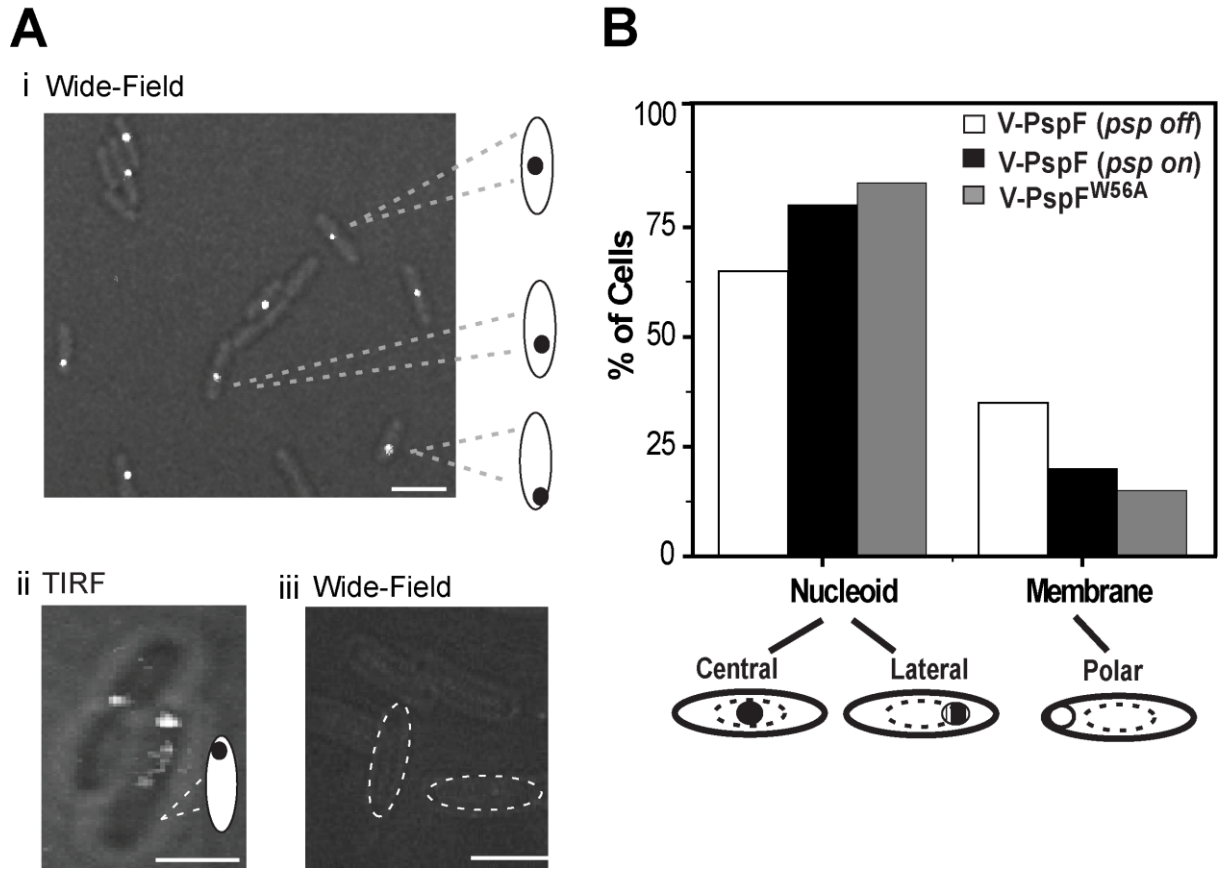

Figure 3.12 **Spatial localisation of V-PspF under non-stress conditions**: (A-i) V-PspF proteins are shown as white bright spots within the live *E. coli* under non-stress conditions (*psp off*). The image is a merge of fluorescent and bright field images of cells to illustrate specific localisations (scale bar = 1µm). The example of V-PspF localisation such as central nucleoid, lateral nucleoid and membrane proximal has been shown by cartoons alongside the image. (A-ii) The TIRF image shows the membrane proximal localised V-PspF foci. (A-iii) The merged image of fluorescent and bright field shows the disappearance of V-PspF foci when native PspF is overproduced from the plasmid. (B) The sub-cellular localisations of the foci on x-axis (cartoon schematically presents the localisation for the V-PspF foci studied) and percentage of cells on y-axis [n=100 (non-stress- *psp off*), n=99(stress- *psp on*) and n=99 (V-PspF^{W56A})].

3.6.2 Activating σ^{54} dependent transcription augments nucleoid association

Next, V-PspF localisation was examined in cells undergoing induction of *psp* gene expression, through application of IM stress caused by synthesis and mislocalisation of the pIV secretin protein (Model *et al*., 1997; Darwin *et al*., 2005; Joly *et al*., 2010). σ^{54} - dependent transcription heavily relies on the bEBP (PspF) for isomerizing the formation of open complexes, very similar to eukaryotic RNA polymerase II (Freidman and Gelles, 2012, Section 1.4). The activator such as PspF interacts with the closed promoter complex (RPc) as well as the open complex (RPo). It was reported that an activator increases the formation of an open complex by > 300 fold (Friedman and Gelles, 2012). The interaction between PspF

and σ^{54} may persist under activating conditions and lasts for 100 s (Friedman and Gelles, 2012). The overall interactions between PspF and RPc, the intermediate closed complex-PspF-with nucleotide bound state (RPi) and activation complex (RPo) under stress inducing conditions are all sufficiently long lived and stable to be effectively studied using single molecule imaging studies at millisecond time scales. With the help of SMI some of the transient interactions between PspF and closed complex can be studied in much greater detail.

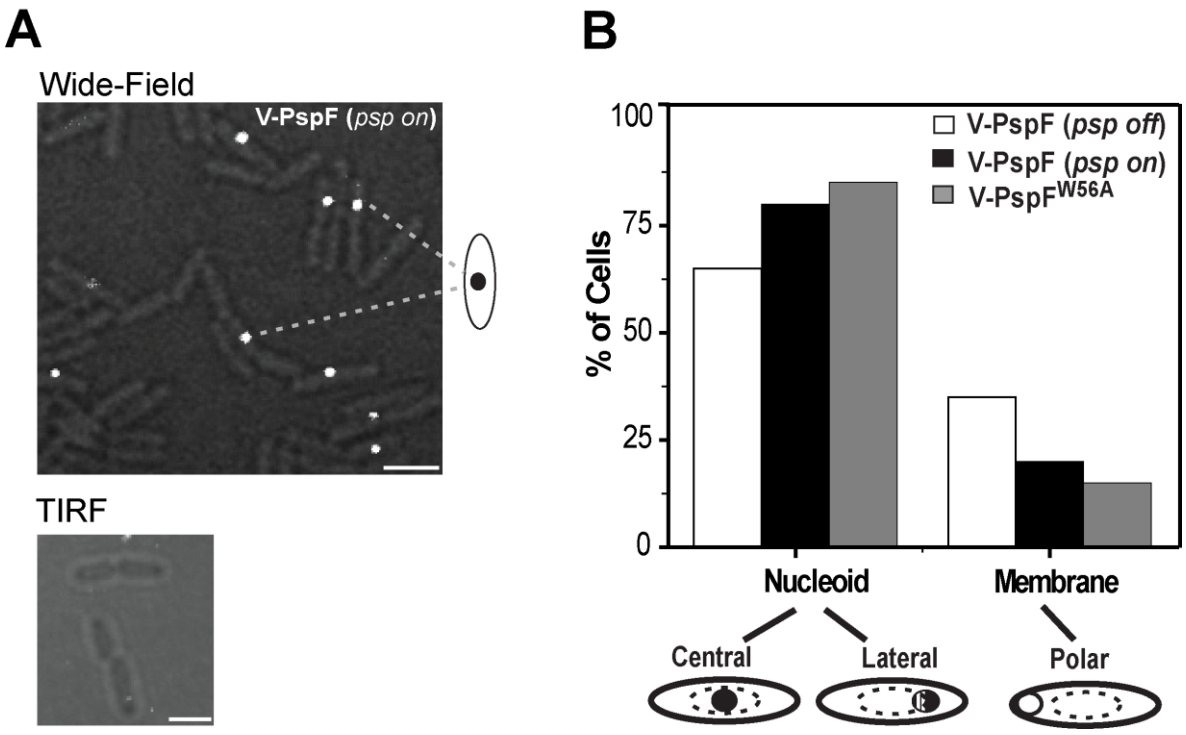

Figure 3.13 **Spatial localisation of V-PspF under stress conditions**: (A) V-PspF proteins are shown as white bright spots within the live *E. coli* under stress conditions (*psp on*). The image is a merge of fluorescent and bright field images of cells to illustrate specific localisations (scale bar = 1µm). The V-PspF foci under stress conditions are predominantly central nucleoid as shown in the image and cartoon. No foci were observed in the TIRF mode. (B) The sub-cellular localisations of the foci on x-axis with the cartoon schematically showing the localisation for the V-PspF foci studied and percentage of cells on y-axis [n=100 (non-stress- *psp off*), n=99 (stress - *psp on*) and n=99 (V-PspF^{W56A})].

In line with these findings, the majority of foci (~80%) were stably observed for 35 frames = 1050 ms central/lateral-nucleoid associated, with some transient polar membrane foci as shown by Figure 3.13. Most of the foci observed in the *psp on* state at the nucleoid were not imaged in the TIRF mode (see Figure 3.13). The PspF under stress conditions actively interacted with the enhancer DNA and RPc to form RPo. Thus the V-PspF foci observed in the stress conditions were mainly nucleoid-associated, as part of the active transcription complex.

3.6.3 PspA drives membrane-associated localisation of PspF

V-PspF^{W56A} mutant bypassed negative regulation by PspA, mimicking stress conditions.185 cells producing the V-PspF^{W56A} were analysed to study the localisation under non-stress conditions (*psp off*).

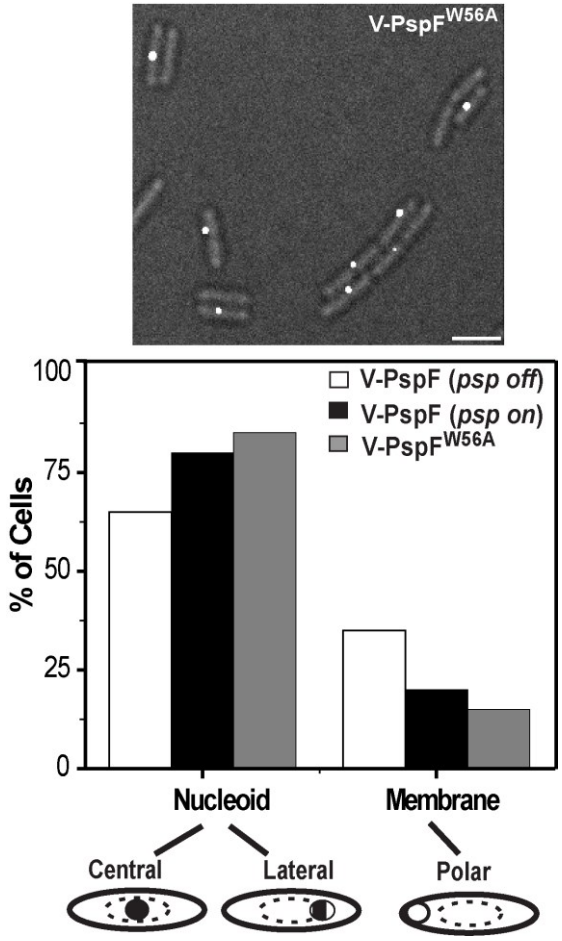

Figure 3.14 **Spatial localisation of V-PspF^{W56A} under non-stress conditions**: V-PspF^{W56A} proteins are shown as white bright spots within the live *E. coli* under non-stress conditions (*psp off*). The image is a merge of fluorescent and bright field images of cells to illustrate specific localisations (scale bar = 1µm). The V-PspF^{W56A} foci under stress conditions are predominantly central nucleoid as shown in the image and cartoon. The sub-cellular localisations of the foci on x-axis (cartoon schematically presents the localisation for the V-PspF foci studied) and percentage of cells on y-axis [n=100 (non-stress- *psp off*), n=99(stress- *psp on*) and n=99 (V-PspF^{W56A})].

85% of the foci were nucleoid associated and only 15% were observed at the poles. The predominant localisation of V-PspF^{W56A} in the nucleoid under non-stress conditions affirms the participation of V-PspF^{W56A} with the active transcription complex. These findings indicate that PspA possibly drives the polar membrane proximal localisation of PspF. The TIRF microscopy of V-PspF^{W56A} foci under non-stress conditions did not show any polar proximal – membrane associated foci. The imaging of V-PspF^{W56A} under pIV inducing stress conditions didn't show any change in the localisation as this particular PspF mutant is constitutively activating the expression of *psp* genes.

3.6.4 PspF is nucleoid bound

A comparison of wide-field and TIRF imaged V-PspF provided strong support for its predominant nucleoid rather than stable membrane association. V-PspF did not form a membrane proximal boundary on summation of images. It is concluded that under non-stress conditions V-PspF is nucleoid-associated with intermittent polar membrane localisation, while under stress V-PspF is predominantly nucleoid bound to its specific UAS DNA. The polar proximal localisation of V-PspF is PspA dependent as part of the V-PspF-PspA inhibitory complex.

3.7 DNA binding Properties of V-PspF

The spatial localisation studies of V-PspF showed that the PspF-PspA inhibitory complex is nucleoid associated and the regulation of Psp response is mediated from the nucleoid with intermittent movement to the membrane. However in order to verify the nucleoid association of V-PspF and back up the imaging data, an *in vitro* technique of Chromatin Immuno Precipitation (ChIP) was used to confirm the UAS bound state of V-PspF. Additionally, a non DNA binding variant of V-PspF – V-PspF$_{1\text{-}275}$ was also studied.

3.7.1 ChIP-PCR of V-PspF

ChIP has been used to characterise DNA binding properties and DNA binding sites for transcription factors and sigma factors. ChIP can either be combined with PCR, microarray or even sequencing in order to report the exact DNA binding sequences (Grainger *et al*., 2006 and Northrup and Zhao *et al*., 2011). The ChIP-PCR method was employed to ascertain DNA binding properties of V-PspF under non-stress and stress conditions. Immunoprecipitation was achieved using anti-Venus antibodies (2.14, Figure 2.7 and Figure 2.8) and DNA was sheared using a highly sensitive water-bath sonicator. The cross-linked anti-Venus antibody-PspF-DNA was purified using magnetic beads coated with the secondary antibody (anti-mouse antibodies). The cross-linked DNA fragments were separated out from the complex with high temperature treatments. No specific product was obtained with PCR using specific primers for the UAS within the *pspA* and *pspG* promoters. The ChIP technique was not successful despite many attempts with V-PspF. The failure of this technique could be because of multiple reasons – such as inefficient fixing of V-PspF at the specific UAS or at the DNA with formaldehyde because V-PspF is produced at very low levels in the cells (Jovanovic *et al.*, 1996). Also the anti-Venus antibodies may not be sensitive enough to enrich fixed and DNA bound V-PspF complexes. After the failure of ChIP method to establish the DNA binding properties of V-PspF under non-stress as well as stress conditions, it was important to obtain the non-UAS binding variant of PspF-PspF$_{1\text{-}275}$. The PspF$_{1\text{-}275}$ has been

extensively studied *in vitro* and many structural studies reporting its interaction with σ^{54} have been reported (Rappas *et al*., 2005 and Bose *et al*., 2008).

3.7.2 Non-DNA binding variant of V-PpsF

The V-PspF$_{1-275}$ fusion was stably expressed in the cells (as shown in Figure 3.6), but no discernible foci could be imaged under the wide-field or TIRF illumination mode in the microscope. The PspF$_{1-275}$ self-assembles into a hexamer and also interacts with PspA as a hexameric assembly *in vitro* (Rappas *et al.*, 2005; Joly *et al.*, 2006). The failure to detect foci with V-PspF$_{1-275}$ could be because of the fast diffusion of the soluble non UAS-bound PspF variant, which supports the idea that the nucleoid associated V-PspF foci are specific *psp* UAS DNA-bound complexes (see Section 3.6). When V-PspF$_{1-275}$ is produced from the chromosome PspA and other Psp proteins are not produced (Jovanovic *et al.*, 1996 and Figure 3.6), and so the V-PspF$_{1-275}$-PspA complex is not formed *in vivo*. Accordingly, no IM associated V- PspF$_{1-275}$ was detected, as illustrated in the Figure 3.15A.

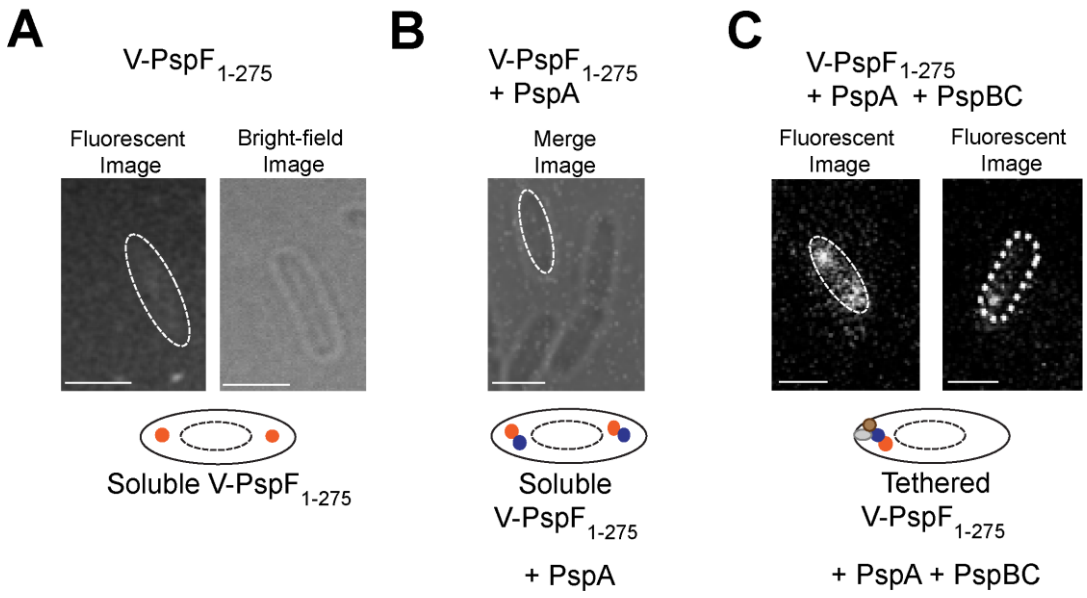

Figure 3.15 **Titration of V-PspF$_{1-275}$-PspA complex at the membrane by PspA and PspBC**: (A) The fluorescent and bright field image of the MG1655 cells producing V-PspF$_{1-275}$. No discernible foci is observed in these cells indicating that the deletion of DNA binding domain renders V-PspF$_{1-275}$ soluble and fast diffusing in the cytoplasm. The cartoon of the cell shows the soluble V-PspF$_{1-275}$ in orange circles localised in the cytoplasm of the cells instead of bound to the nucleoid. (B) PspA was overproduced from a plasmid pPB9 to titrate V-PspF$_{1-275}$ at the membrane as an inhibitory complex, but no foci were observed again. As shown in the cartoon of the cell the PspF-PspA inhibitory complex with PspF as orange circle and PspA as blue circle are also soluble and were not detected by the imaging. (C) Along with PspA, PspBC (brown circle and grey circle) was also expressed from pAJM3 plasmid to show if localised V-PspF$_{1-275}$ foci are recovered. V-PspF$_{1-275}$ was recovered to an extent and foci were observed at the polar membrane localisation. The V-PspF$_{1-275}$ confirmed that the localised V-PspF foci were indeed nucleoid bound and PspBC sensors recruit the polar membrane localisation of V-PspF-PspA inhibitory complex. Scale bar = 1µm

3.7.2.1 Does PspA overproduction make V-PspF$_{1-275}$ observable?

It has been shown that PspF$_{1-275}$ as a hexamer binds six molecules of PspA and is negatively controlled by PspA *in vitro* (Elderkin *et al.*, 2005; Joly *et al.*, 2009). Therefore, in principle V-PspF$_{1-275}$ would associate with PspA *in vivo* and might be visible in polar IM-associated regions of the cell. In order to prove this, PspA was overproduced from the pPB9 plasmid in cells producing V-PspF$_{1-275}$ (Material - Table 2.4). The pPB9 plasmid (see Table 2.4) is a high copy plasmid induced with 0.2 % (w/v) arabinose. But again no V-PspF$_{1-275}$ foci were observed in these cells under wide-field and TIRF mode as shown in Figure 3.15B. A possible reason for not observing V-PspF$_{1-275}$ in the presence of PspA could be the absence of other Psp proteins such as the IM sensors PspBC that interact with PspA (Jovanovic *et al.*, 2010 and Yamaguchi *et al.*, 2010). The V-PspF$_{1-275}$-PspA inhibitory complex therefore remains soluble and thus cannot be observed under the microscope with 15 ms exposure time.

3.7.2.2 Does PspA and PspBC overproduction make V-PspF$_{1-275}$ observable?

In cells producing V-PspF$_{1-275}$ no other Psp proteins were produced. Therefore in the presence of only PspA without PspBC no foci were imaged. PspBC are the integral membrane proteins and are signal sensors of Psp response and relay the stress signal to PspA. And PspBC have been shown to play regulatory role during the Psp response (Engl *et al.*, 2009 and Jovanovic *et al.*, 2012). The overproduction of PspA (pPB9) and PspBC proteins from pAJM3 plasmid in the cells might help to capture the soluble V-PspF$_{1-275}$ at the membrane see Figure 3.16C. The imaging of the cells overproducing PspA and PspBC with V-PspF$_{1-275}$ was done in the TIRF mode. The V-PspF$_{1-275}$ foci were observed but for a very short period (4-5 frames=150 ms). This showed that the imaging of soluble V-PspF$_{1-275}$ was difficult and the tethered foci as shown in Figure 3.12 could not be observed easily or only observed for a shorter period of time (see Figure 3.15).

The nucleoid association of V-PspF potentially plays an important role in the establishment of the PspF-PspA inhibitory complex. Therefore in cells producing V-PspF$_{1-275}$, the inhibitory complex with PspA is not observed, as this complex is not tethered at the nucleoid, but instead is soluble in the cell. The presence of PspBC proteins enabled the capture of the V-PspF$_{1-275}$-PspA complex, but the complex could not be stably observed for a longer time interval. Alternatively the V-PspF$_{1-275}$ cannot associate with the PspA *in vivo* when DNA binding ability is lost; however, this is speculation for which there is no experimental evidence.

3.8 Inferences drawn from localisation studies

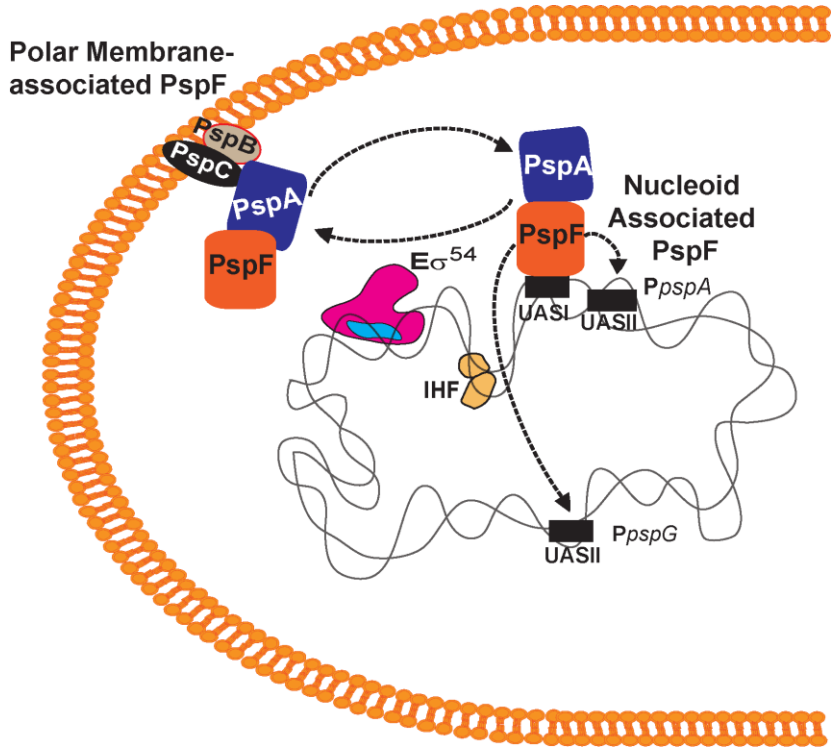

Figure 3.16 **The nucleoid associated V-PspF-PspA inhibitory complex**: The schematic illustration shows the model explaining the spatial and temporal localisation of the Psp response. The nucleoid association of PspF-PspA inhibitory complex that binds to the UAS DNA sequences at *pspA* and *pspG* promoters. The V-PspF might bind to the UAS at the same time or move between the UAS. The PspF-PspA inhibitory complex also moves within the cytoplasm to associate with the membrane to check for the membrane stress status.

Under physiologically repressive conditions or activating conditions PspF is clearly nucleoid-associated. A comparison of wide field and TIRF imaged V-PspF foci provided strong argument for their predominant nucleoid association rather than a stable membrane association as shown in Figure 3.16. In the non-stress conditions some PspF-PspA complexes probably would be more dynamic because of a PspA driven membrane association. Meanwhile in stress conditions PspF self-assemblies would be less dynamic with respect to limited membrane association, and instead associate with the RPc for making RPo. However the distinction between these different states of V-PspF could not be fully derived by simply comparing the spatial localisations. Therefore temporal localisations of V-PspF foci could be used to examine the differences between the repressed and non-repressed states of V-PspF.

3.9 Temporal Localisation of V-PspF

Temporal localisation is described for mobile foci observed in the cells. V-PspF that was localised in the cytoplasm was predominantly bound to the nucleoid but still displayed varying degrees of local or long distance dynamic movement. Such measure of dynamics of V-PspF will be very crucial to distinguish

between its different functional states under non-stress or stress growth conditions. The temporal localisation or dynamics of V-PspF is estimated by comparing the total raw intensity of the V-PspF foci under non-stress and stress conditions. Then more conclusively the dynamics are reported in the form of a diffusion coefficient obtained by single particle tracking algorithms.

3.9.1 Quantification of intensities of V-PspF foci

The preliminary diffusion analysis of the V-PspF foci under different growth conditions was measured by comparing the intensities. Intensity of V-PspF foci imaged under non-stress and stress conditions and for V-PspF^{W56A} (non-stress conditions) were analysed as shown Figure 3.17. The intensity analysis of the foci helped to compare approximately the amounts of V-PspF in the foci and estimate their dynamics. The fast moving complexes often move out of focus during the acquisition and that resulted in reduction of the overall intensity.

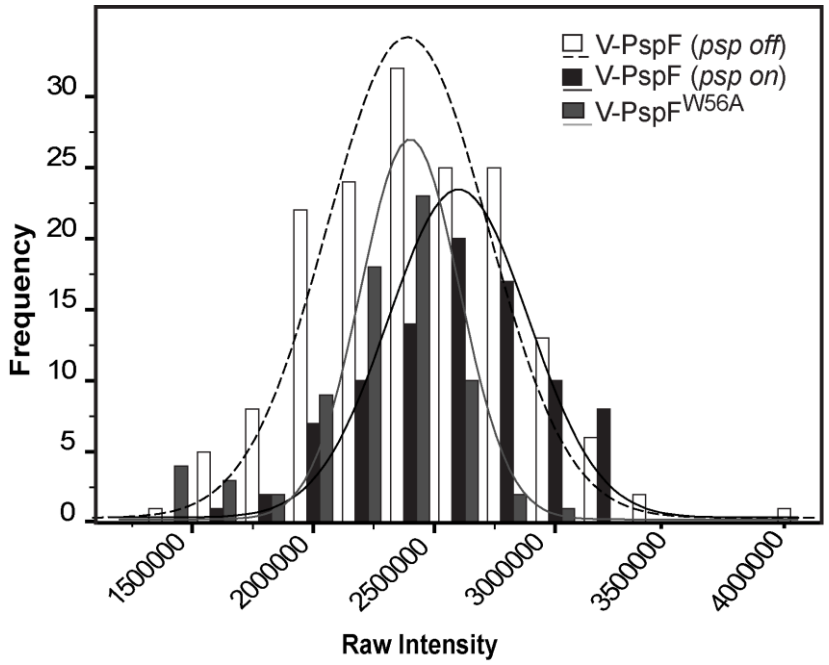

Figure 3.17 **The raw intensities of V-PspF (*psp off/on*) and V-PspF^{W56A}.** The image sequence of 100 frames (1.5 s long) were added together to obtain a summed image, where the intensity for each of the foci was calculated and called the raw intensity. The raw intensity was calculated for 100 foci of V-PspF under non-stress or stress conditions, and for 60 foci of V-PspF^{W56A} under non-stress conditions. The graph presents the distribution of the raw intensity on x-axis against the frequency distribution on the y-axis; V-PspF non-stress (white), V-PspF stress (black) and V-PspF^{W56A} (grey). Gaussian curves show a moderate shift of the raw intensity to the right for V-PspF under stress compared to other two data sets. Immobile complexes were excited in the centre of the focus plane. It was estimated that the mean displacement of the V-PspF complex in non-stress cells is about 125 nm in 15 ms exposure time, suggesting that the mobile complexes could move out of the focal plane within one frame, giving apparent lower intensity.

Also the small differences in the intensity could also be due to an underestimation of the fluorescence intensity. The acquired image of the fast moving foci could be more diffuse which makes it difficult to

calculate the precise fluorescence intensity of the foci minus the background. The 100 frames video sequence of V-PspF [(*psp*-off) and (*psp*-on)] and V-PspF^{W56A} (non-stress, *psp off*) states were added to generate an average image. These images were used to manually analyse the spots, in order to determine integrated intensity of a defined area. The comparisons of raw intensity distribution for V-PspF non-stress, V-PspF stress and V-PspF^{W56A} (non-stress) foci were very similar as shown in the Figure 3.17. The similar intensities of the foci showed that the PspF amounts were unaltered irrespective of the growth conditions and mutant type. This inference was consistent with the Western blot analysis (see 3.2.3 - V-PspF FPs were stable) with constant PspF production detected under all conditions. The 10% reduction in intensity of V-PspF under non-stress conditions could be the consequence of underestimation of the fluorescence intensity for fast moving complexes (Figure 3.17). The intensity analysis of the foci is not the most accurate measurement to differentiate the different dynamic properties of V-PspF foci. There upon the dynamics of V-PspF was defined by the Mean square displacement (MSD) over time and the apparent diffusion coefficients values were calculated as described below 3.9.2.

3.9.2 Cellular dynamics defined by Diffusion coefficient values

The diffusion analysis was performed using Matlab (Mathwork) scripts based on the tracking algorithm by Crocker and Grier (1996). The scripts were custom built and provided by Dr. Andreas Buckbauer (CR-UK, London), which have been described in Treanor *et al*., 2009 (see Methods 2.15.3.2). The analysis of the dynamics of the foci was based on tracking the V-PspF foci (between 200-1000 foci tracks) with sub-pixel accuracy. As shown in Figure 3.18, the tracks of the foci over the 100 frames, i.e. 3s long, were used to calculate the MSD curve of the foci over time and for each 1/4th of the gradient of the MSD curves gave diffusion coefficient values.

3.9.2.1 V-PspF as a repressed complex with PspA is more dynamic

The nucleoid associated V-PspF under non-stress is possibly more dynamic due to its widespread subcellular localisation (see Figure 3.12) as is also seen with the intensity measurements (See section 3.9.1). V-PspF like LacI could also show different types of dynamics being the DNA binding protein (see Figure 3.3). Therefore dynamic studies of V-PspF will help to characterise the different dynamic classes of V-PspF and also differentiate between nucleoid associated and the membrane associated V-PspF. The nucleoid associated V-PspF would be much more stably bound to the UAS with reduced dynamics in the cell as compared to the transiently membrane associated V-PspF, which would be much more dynamic and diffuse in the cytoplasm as shown in Figure 3.2.

Under non-stress conditions PspF usually exists with PspA in the form of an inhibitory complex (Joly *et al.*, 2010). The spatial localisation of V-PspF was found to be predominantly nucleoid associated with transient membrane interaction via PspA as a PspF-PspA inhibitory complex. The different classes of foci observed in the cell either associated with nucleoid or membrane and even the rarely observed freely diffusing foci were all tracked using the single particle tracking and all the diffusion coefficients recorded (See Methods 2.15.3.2) without any classification based on the localisation of the foci in the diffusion coefficient distribution. All the V-PspF foci observed in the cells were tracked to obtain tracks, mean square displacement curve and diffusion coefficient (Crocker and Grier, 1996). Figure 3.1818A illustrates example of the tracks obtained for the foci localised at the nucleoid and poles under non-stress conditions. The individual tracks showed that the movement exhibited by the foci localised either in the nucleoid or membrane were restricted to local movements, however, these small movements could be enough to show efficient diffusion within the *E. coli* cells. *E. coli* cells have very small in dimensions (2 µm x 1 µm) as shown in (Figure 3.18. The nucleoid-localised foci could form intermittent association with the membrane via PspA even with small movements. And the foci at the poles show comparatively small tracks because the transiently membrane associated foci would just disappear into the cytoplasm as soluble foci with short track and high errors in the MSD values (See Methods 2.15.3.2). The 82 tracks of V-PspF foci in non-stress conditions were used to calculate the Mean Square Displacement curve as shown in graph Figure 3.18B. The MSD curve plot shows that V-PspF foci under the non-stress conditions are more dynamic.

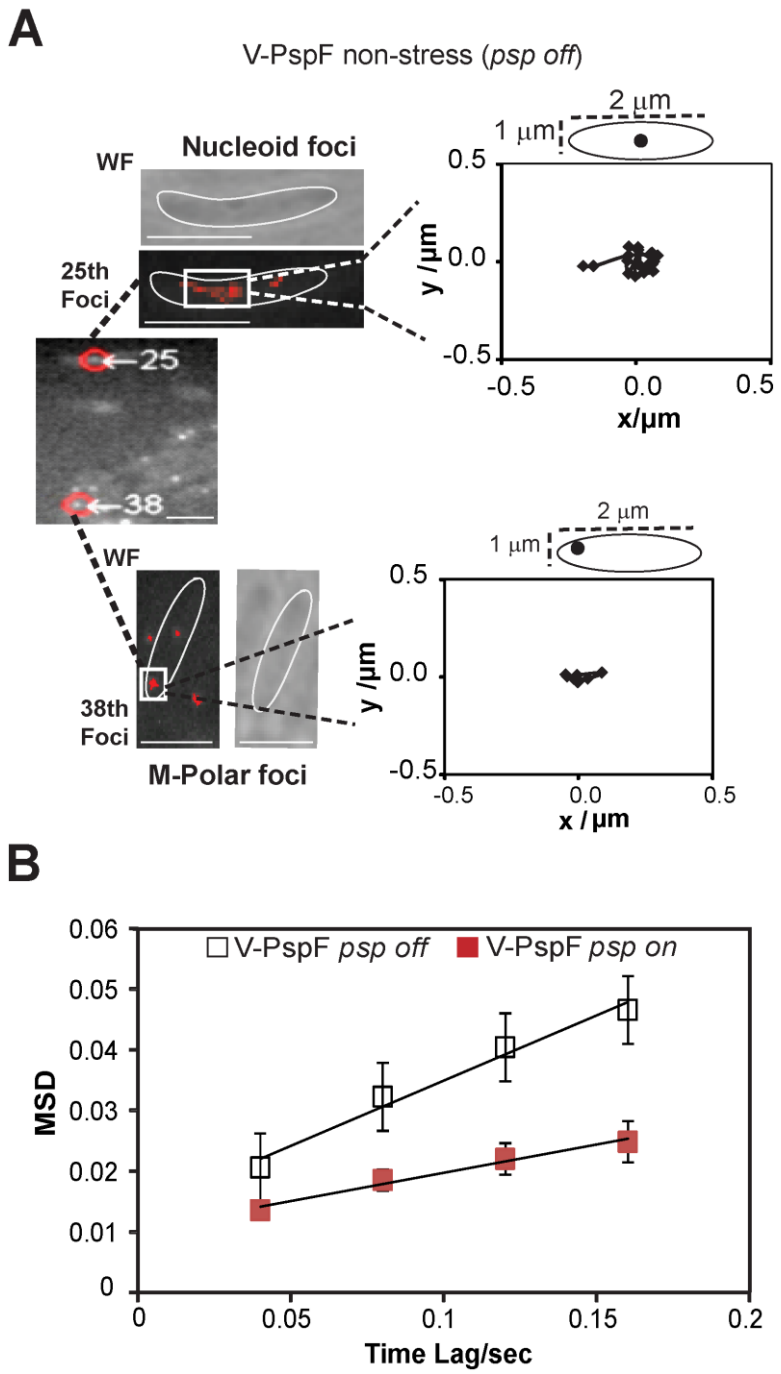

Figure 3.18 **Measuring the apparent two-dimensional diffusion coefficient for V-PspF (*psp off*).** (A) The schematic shows individual tracks obtained by the single molecule tracking algorithm for V-PspF foci in cells under non-stress (*psp off*) conditions. The tracks for specific foci localised in central and polar regions were plotted with respect to *E. coli* cell dimensions (in µm). These tracks were used to generate MSD curve plots and diffusion coefficients for the foci. The images have a scale bar=1µM. (B) An example of a typical MSD curve plot (mean values with standard errors) obtained for V-PspF foci in non-stressed cells (white, n=82) compared to stressed cells (red, n=71) using special algorithm.

The V-PspF foci tracked over 3 seconds gave 1423 foci tracks, for which diffusion coefficients were calculated for each track. The distribution of diffusion coefficients as shown in Figure 3.19 showed that the V-PspF foci mainly diffused tethered to the nucleoid with 93% foci displaying dynamics less than 1 $\mu m^2/s$ and only 7 % displayed dynamics more than $1\mu m^2/s$. A maximum diffusion coefficient value of 1.6 $\mu m^2/s$ was obtained. These comparatively fast moving foci could possibly be the PspF-PspA complex either dropping off from the UAS DNA or moving across the cytoplasm to check for the membrane status.

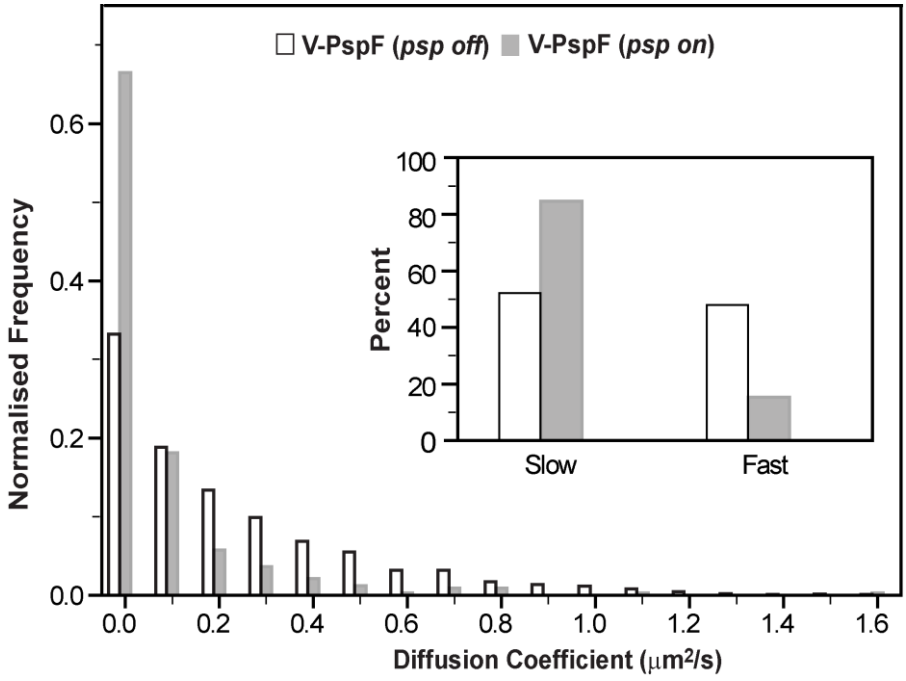

Figure 3.19 **More dynamic V-PspF under non-stress *psp off* conditions**: Dynamics of V-PspF under different growth conditions (non-stress-, *psp off*, n=1423 or pIV induced stress-, *psp on*, n=331) are presented as normalised distribution of the diffusion coefficients ($\mu m^2/s$) obtained (see details 2.15.3.2). The apparent diffusion coefficient of V-PspF (*psp off*) was 0.134 $\mu m^2/s$ and 0.018 $\mu m^2/s$ for V-PspF (*psp on*). Inset: the slow/fast foci are classified according to distribution of diffusion coefficients with cut off at 0-0.15 $\mu m^2/s$ - slow and >0.15 $\mu m^2/s$ - fast.

In order to understand and compare V-PspF dynamics across all the conditions and mutants, a classification of foci into slow diffusing and fast diffusing states was obtained (see Figure 3.19). The classification was made according to the diffusion coefficient distributions obtained for V-PspF for all the different conditions studied, with 0-0.15 $\mu m^2/s$ classified as slow diffusing foci and >0.15 $\mu m^2/s$ as fast diffusing foci (see Methods section 2.15.3.2). The V-PspF foci under non-stress conditions gave 52% as slow diffusing and 48 % as fast diffusing, showing an equal distribution across the two sets of classification

In addition to the classification of the foci, apparent diffusion coefficients were calculated as median of all the diffusion coefficient values (n=1423). The apparent diffusion coefficient of V-PspF under non-stress conditions was calculated to be 0.134 $\mu m^2/s$ (derived from Figure 3.19). The apparent diffusion

coefficient value indicates that V-PspF is more likely to be DNA bound rather than freely diffusing in the cell (apparent diffusion coefficient of free diffusion >2.5 $\mu m^2/s$) (Elowitz *et al*, 1999; Millneaux *et al*, 2006 and Nenninger *et al*, 2010). LacI has been shown to have an apparent diffusion coefficient of D_a - 0.4 $\mu m^2/s$ (Elf *et al*, 2007), taking into account the 1D diffusion of sliding on the non-specific DNA sites and 3D diffusion through the cytoplasm to find specific operator sites. PspF like LacI also showed mostly DNA-facilitated dynamics. PspA assisted in membrane associated dynamics at the polar regions and also possibly free cytoplasmic 3D diffusion (see Figure 3.19). Thus it suggests that repressed V-PspF-PspA complex is dynamic and forms the crucial connection between the nucleoid and membrane status. Using the diffusion coefficient distribution and by comparing the apparent diffusion coefficients it could be speculated that V-PspF foci displayed a range of dynamics possibly a combination of Brownian or linear motion along the DNA, along with the dynamics through the cytoplasm or associated with the membrane. The different classes of apparent diffusion coefficients could be like that obtained for LacI dynamics, which were divided into 1D, 2D and 3D dynamics (Elf *et al*, 2007).

3.9.2.2 Comparisons with other relevant DNA binding proteins

It is apparent from the dynamic studies of V-PspF under non-stress conditions that it is primarily DNA associated. In this section, the focus is going to be redirected from V-PspF to understanding the dynamic properties of some other relevant DNA binding proteins such as LacI – a classically studied transcription factor, and σ^{54} – the target for bEBPs such as PspF to isomerise closed complex (RPc) to an open $E\sigma^{54}$-DNA complex (RPo).

LacI and its binding to operators has been studied in detail with single molecule imaging and has led to many novel findings regarding the properties of DNA binding, binding constants, and diffusion dynamics (as explained in Introduction 1.7.3.2).

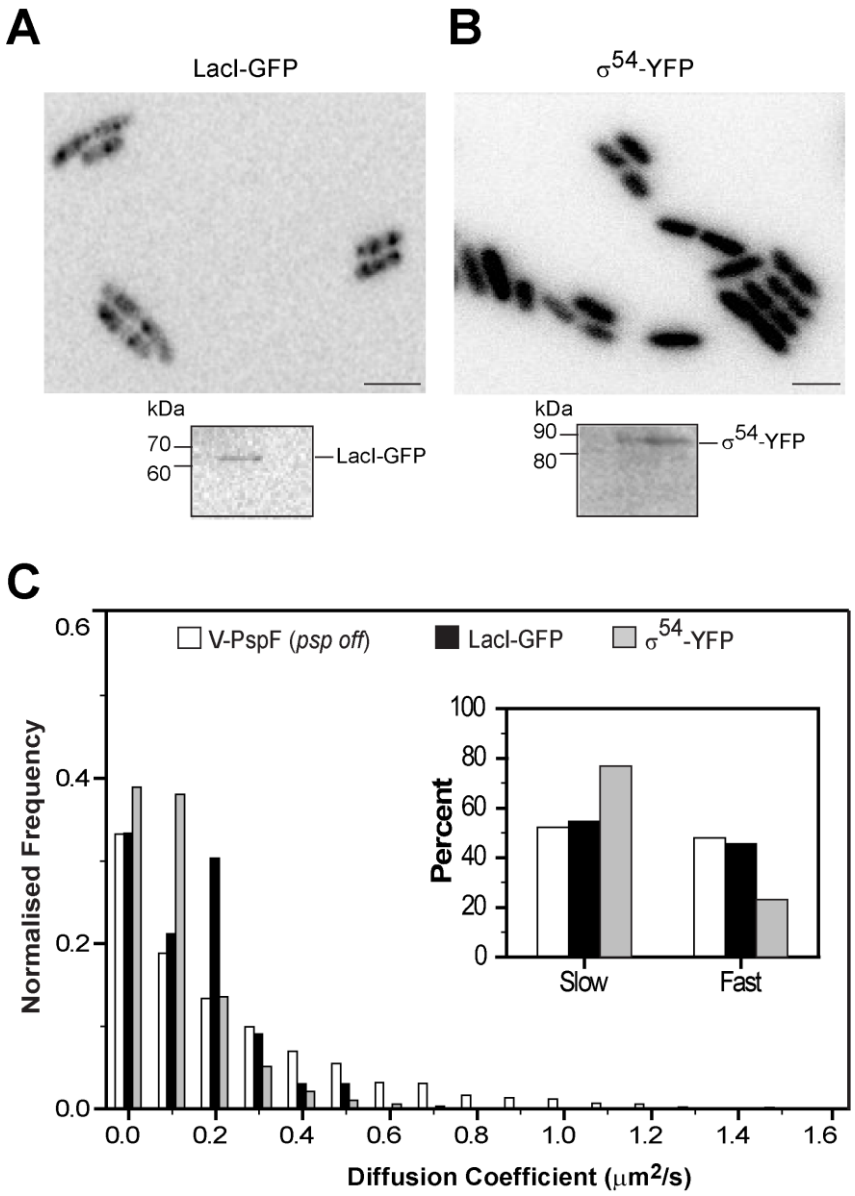

Figure 3.20 **Spatial and temporal localisation of other relevant DNA binding proteins such as LacI and σ^{54}**: (A) The merge image of bright field and fluorescent image showing LacI-GFP foci (black). There were around 1-2 foci per cell. The figure also shows the corresponding Western blot of the stable LacI-GFP fusion (around 66 kDa) using anti-GFP antibodies. (B) The merge image of bright field and fluorescent image showing σ^{54}-YFP in the cell. It was produced from a medium copy plasmid. The images show that it was produced in very high amounts seen in the totally diffused signal in the cells (black), scale bar = 1μm. The figure also shows the corresponding Western blot of the stable fusion σ^{54}-YFP (around 82 kDa) using anti-GFP (specific for YFP/Venus antibodies). (C) The magnitude of the diffusion coefficient obtained for V-PspF is similar to that of a DNA binding protein as reported in literature for e.g. LacI. In order to confirm these findings, diffusion coefficients of LacI-GFP expressed from the chromosome in MG1655, and σ^{54} (σ^{54}-YFP expressed from the plasmid pCE2); σ^{54} is direct PspF interacting partner in the RPc and/or RPo were determined. The normalised distribution of apparent diffusion coefficients for LacI-GFP (black, n=39), σ^{54}-YFP (grey, n=12624) and V-PspF (white, n=1423) is shown. The apparent diffusion coefficient of V-PspF was 0.134 $\mu m^2/s$; apparent diffusion coefficient of LacI-GFP was 0.13 $\mu m^2/s$ and σ^{54}-YFP was 0.071 $\mu m^2/s$.

A chromosomally expressed LacI-GFP fusion in MG1655 was used for the dynamics studies (a gift from Steve Busby's lab) with the native operator sites available for binding. Many more LacI-GFP foci were

observed in the cells as compared to V-PspF (see Figure 3.20A). σ^{54}-YFP fusion was also studied independently to compare its spatial and temporal localisation with V-PspF. It was produced from the plasmid in the MG1655 WT cells without IPTG induction (pCE2, medium copy plasmid and Table 2.4). σ^{54} is physiologically expressed in higher amounts as compared to transcription factors such as PspF or LacI (Wigneshwaraj *et al*., 2008) and therefore many σ^{54}-YFP foci were observed in the SMI illustrated by diffused signal across the cells in Figure 3.20B.

The LacI-GFP foci were tracked over the 100-frame video and the data was treated in the same way as the V-PspF foci in order to obtain the diffusion coefficients. This would validate the methodology and further confirm the DNA binding property of PspF. Figure 3.20C shows the distribution of diffusion coefficients of the LacI-GFP compared to V-PspF under non-stress conditions. The inset also shows the classification of foci into slow diffusing and fast diffusing foci. The distribution between LacI-GFP and V-PspF was very similar with just a small proportion of V-PspF foci showing faster dynamics. This is possibly due to the movement of PspF-PspA complex to the membrane, as the maximum value recorded for LacI-GFP foci was 0.5 $\mu m^2/s$ as opposed to 1.6 $\mu m^2/s$ for V-PspF. The classes of slow diffusing as well fast diffusing foci were also very similar for LacI-GFP and V-PspF see inset Figure 3.20C. The apparent diffusion coefficient calculated for LacI-GFP was 0.13 $\mu m^2/s$ (n=66) same as that observed for V-PspF. The similar dynamic behaviour of V-PspF and LacI-GFP reinforced the DNA associated movement of V-PspF bound to its specific UAS DNA sequences.

In the same way, the dynamic behaviour of σ^{54} was also studied to directly correlate with the dynamics of V-PspF. It would be interesting to study the dynamics of σ^{54} in the cells and factor in the dynamics of σ^{54} with that of PspF. The σ^{54}-YFP was produced in much higher amounts as compared to V-PspF and LacI-GFP so the threshold was chosen to be much higher during the single particle tracking so that only the very bright foci were tracked (see Section Methods 2.15.3.2). The diffusion coefficient distribution of σ^{54}-YFP showed that σ^{54} also shows predominantly DNA associated dynamics (see Figure 3.20). It is possible that $E\sigma^{54}$ as part of RPc are bound to the DNA specifically or non-specifically while searching for the specific promoter targets. The apparent diffusion coefficient calculated for the σ^{54}–YFP was 0.071 $\mu m^2/s$. The inset of graph Figure 3.20 showed that >70 % were slow diffusing foci and <30 % fast diffusing, with a maximum diffusion coefficient value calculated to be of 1.5 $\mu m^2/s$. The dynamic studies of σ^{54}-YFP showed that σ^{54} has a more restricted dynamics in the cell, possibly due to its constant interaction with multiple proteins such as RNAP, various bEBPs and the nucleoid. Thus the study of dynamics of some of the relevant DNA binding proteins and correlating with V-PspF was very insightful and supportive of the inferences for V-PspF dynamics. The data shown in Figure 3.20 added confidence to the diffusion analysis technique used for V-PspF. The dynamic studies showed that the diffusion coefficients displayed by DNA binding proteins are reproducible and characteristic for DNA binding transcription factors.

3.9.2.3 Nucleoid associated PspF is less dynamic

The more prolonged observation and predominant nucleoid localisation of the V-PspF foci hints at the less dynamic nature of the V-PspF foci under stress conditions. The isomerisation step leading to formation of RPo is mediated by PspF and is the rate-limiting step of transcription initiation.

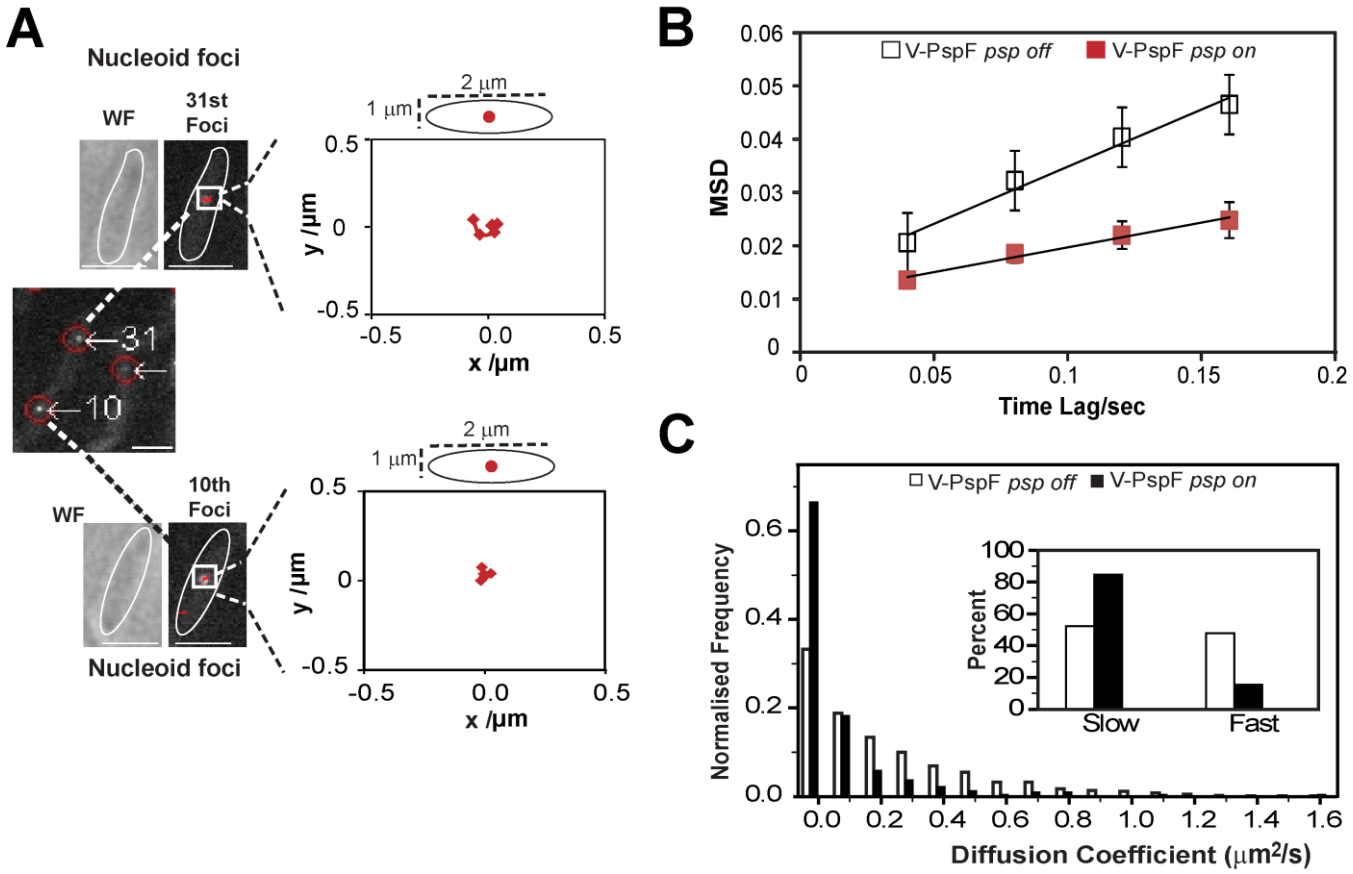

Figure 3.21 **The dynamics of non-repressed activating V-PspF**: The schematic shows individual tracks obtained by the single molecule tracking algorithm and diffusion analysis for V-PspF foci in cells under stress (*psp on*) conditions. The tracks for central foci (*psp on*) were plotted with respect to *E. coli* cell dimensions (in μm). These tracks were used to generate MSD curve plots and diffusion coefficients for the foci. The images have a scale bar=1μM. (B) An example of a typical MSD curve plot (mean values with SD) obtained for V-PspF foci in non-stressed cells (white, n=82) compared to stressed cells (red, n=71). The data are the mean values with standard error bars. (C) Dynamics of V-PspF under different growth conditions (non-stress-, *psp off*, n=1423 and pIV induced stress-, *psp on*, n=331) are presented as normalised distribution of the diffusion coefficients ($\mu m^2/s$) obtained as described in (Methods section- 2.15.3.2). Inset of the graph gives the slow/fast foci classified according to distribution of diffusion coefficients with cut off at 0-0.15 $\mu m^2/s$ - slow and >0.15 $\mu m^2/s$ - fast. The apparent diffusion coefficient of V-PspF under stress conditions was 0.018 $\mu m^2/s$.

Substantial level of interaction between the activator-PspF and $E\sigma^{54}$ occurs for successful formation of open complexes which can last up to 100 seconds (Friedman and Gelles, 2012). This shows the extent of stability of the activator- σ^{54} interactions (Friedman and Gelles, 2012). Even then, many open

complexes may not result in successful transcript formation (Friedman and Gelles, 2012). The V-PspF foci in stressed cells were tracked using the tracking algorithm (Crocker and Grier, 1996) in the 100 frame sequence for 3 seconds (see Figure 3.21). The Figure 3.21A shows an example of the individual tracks obtained for central nucleoid foci and the foci showed much more compact movement within the cell as compared to non-stress conditions. The corresponding MSD curve for the 71 tracks showed that the foci were less dynamic as compared to non-stress Figure 3.21B.

The distribution of diffusion coefficients showed that the non-repressed V-PspF foci under stress conditions are much more stable and less dynamic (see Figure 3.21C). The V-PspF under pIV induced stress conditions is associated with the activation complex. The distribution showed 99% of the foci had diffusion coefficient of ≤ 1 $\mu m^2/s$ while only 1 % had > 1 $\mu m^2/s$ and the maximum value of diffusion coefficient was 1.6 $\mu m^2/s$. The foci showed a significant shift from almost equal percentages of slow and fast diffusing foci in non-stress (median diffusion coefficient of 0.134 $\mu m^2 s^{-1}$) to 85 % slow diffusing under stress conditions (see Figure 3.21-inset). The apparent diffusion coefficient for V-PspF foci under stress conditions was calculated to be 0.018 $\mu m^2/s$, - seven times less for V-PspF foci in non-stress conditions.

The diffusion coefficient data implies a more stably DNA-bound state of the non-repressed-activating V-PspF compared to the PspA-repressed V-PspF. So far the results of number of foci distribution (see Section 3.5 and Figure 3.11), subcellular localisation (see Section 3.6 and Figure 3.13) and dynamics (see Section 3.9 and Figure 3.21) have established that the V-PspF foci in stressed cells are predominantly less dynamic and single foci centrally located in nucleoid. The spatial shift to a more central nucleoid, and less dynamic V-PspF foci in stress conditions compared to non-stress conditions, is likely to be due to lack of PspA interactions and/or the participation of PspF in the activation of the RPc formed at the *psp* promoter(s). Consequently, the nucleoid-associated lateral foci seen in non-stressed cells may be related to the repressed V-PspF, likely to be V-PspF-PspA co-complexes. The repressed and the activating states of PspF self-assemblies illustrate different DNA binding states of PspF, which is reflected in the different foci characteristics.

3.9.3 PspF shows PspA dependent dynamics

It has been established by both the distribution and spatial localisation of V-PspF^{W56A} foci (see Figure 3.11 and Figure 3.14) that it closely resembles that of the V-PspF WT foci under stress conditions. This proves that the interaction with PspA plays a crucial role in asserting PspF localisation. In the same way the V-PspF^{W56A} mutant was used to study the contribution of PspA in the dynamics of PspF. The distribution of diffusion coefficients of V-PspF^{W56A} showed that the dynamics of non-PspA binding mutant was similar to the V-PspF under stress conditions (see Figure 3.22). All the V-PspF^{W56A} foci tracked over the 100 frames gave diffusion coefficients of ≤ 1$\mu m^2/s$ and no foci were recorded with > 1 $\mu m^2/s$ and the maximum diffusion coefficient value of 0.8 $\mu m^2/s$.

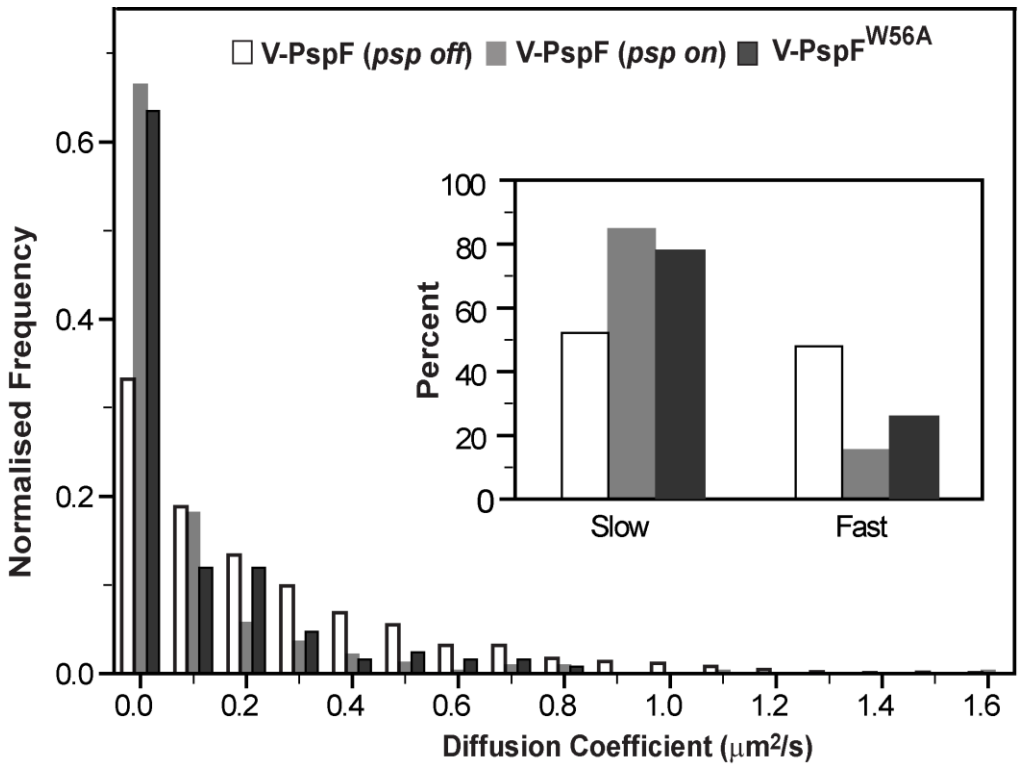

Figure 3.22 **Dynamics of V-PspF is PspA dependent**: The V-PspF^{W56A} mutant of V-PspF was used to determine the dependence of V-PspF dynamics on PspA. V-PspF^{W56A} under non-stress conditions (n=126) are presented as normalised distribution of the diffusion coefficients (μm^2/s). Inset: the slow/fast foci are classified according to distribution of diffusion coefficients with cut off at 0-0.15 μm^2/s - slow and >0.15 μm^2/s - fast. The distribution of V-PspF^{W56A} is compared with that of V-PspF under non-stress and stress conditions. The distribution of V-PspF^{W56A} is very similar to that of V-PspF under stress conditions. The apparent diffusion coefficient of V-PspF^{W56A} was 0.017 μm^2/s similar to apparent diffusion coefficient of V-PspF under stress conditions of 0.018 μm^2/s.

The inset of graph Figure 3.22 shows that 75% of the foci were slow diffusing with 15 % fast diffusing. The apparent diffusion coefficient for V-PspF^{W56A} was calculated to be 0.017 μm^2/s. The distribution of diffusion coefficient in the V-PspF^{W56A} mutant shows the importance of PspA interaction and binding to PspF. This mutant helps to characterise the role of PspA in setting PspF localisation and dynamics. It suggests that the central nucleoid less dynamic species V-PspF foci in stress conditions or in the PspF^{W56A} mutant in non-stress conditions represents activating PspF in complex with the RPo rather than the comparatively faster moving nucleoid associated V-PspF-PspA inhibitory complex. This data also establishes that PspA does not define the binding of PspF to the specific UAS sequences. However the polar proximal membrane interactions of PspF as observed in non-stress conditions for WT V-PspF is purely PspA driven.

3.9.4 The dependence of V-PspF dynamics on membrane determinants

The bacterial membrane performs many critical functions in *E. coli* (as explained in 1.2.1- *E. coli* cell envelope). It recruits the bacterial cytoskeletal network maintained by proteins such as MreB. MreB has been shown to play a critical role in protein trafficking and directing their movement along the membrane for example effector PspA, RNaseE, degradosome and bacterial motility factors (Taghbalout and Rothfield 2007; Engl *et al*., 2009 and van den Ent *et al*., 2010). Engl *et al* (2009) showed that PspA localised as distinct static foci in the MreB mutant and did not have effector functions. Therefore it was important to investigate if MreB has similar kind of effect on the dynamics of V-PspF. In order to determine the effect of MreB on dynamics of V-PspF, the pEXT22 (Table 2.4 of plasmids) plasmid producing low copy of V-PspF were transformed in the *ΔmreB* cells (Table 2.3 of strains) and studied by SMI. The SMI showed that V-PspF foci were observed at the nucleoid position (see Figure 3.23A) and no change in its dynamics appeared in the absence of MreB. This result also showed that the V-PspF does not follow a diffusion path organised by the bacterial cytoskeleton MreB.

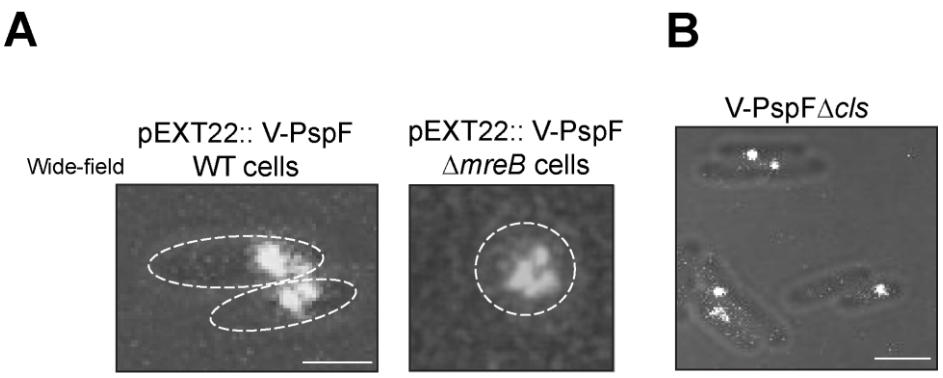

Figure 3.23 **The images to show effects of membrane determinants on V-PspF**: (A) The merged image of bright field and fluorescent image of the V-PspF produced from low copy plasmid pEXT22. The plasmid expressing V-PspF was introduced in the WT MC1000 cells and *ΔmreB* cells, the V-PspF foci retained its nucleoid localisation and dynamics in the absence of MreB. (B) The absence of cardiolipin does not affect the membrane proximal polar localisation of chromosomal V-PspF foci. Scale bar = 1µm

Next, the effect of cardiolipin on the membrane association of V-PspF via PspA was also evaluated. Cardiolipin (CL) is an important anionic lipid mainly localised at the curved poles of the *E. coli* cells (Renner and Weibel, 2012). It has been speculated that CL could have a role to play in organisation of PspBC sensors at the poles (discussed in later section of this thesis). A deletion of cardiolipin synthase (*cls*) gene was introduced in the cells producing chromosomal V-PspF and V-PspF$_{1\text{-}275}$ and the effect on the polar localisation of V-PspF was studied by SMI in the *Δcls* (bacterial strains Table 2.3) background cells. The chromosomally produced V-PspF foci in *Δcls* cells showed membrane proximal polar localisation in the wide-field mode like the V-PspF expressed in WT MG1655 cells under non-stress conditions (Figure 3.23B). This showed that the absence of cardiolipin does not hamper the localisation

of V-PspF. The absence of cardiolipin also did not have an effect on the observation of foci in the V-$PspF_{1-275}$ foci in the presence of overproduced PspA and PspBC from the plasmid.

3.10 Conclusion

The spatial and temporal studies of the repressed as well as non-repressed V-PspF demonstrate that the control of the pervasive Psp stress response operates through a post-DNA binding repression of PspF. The SMI imaging of V-PspF has allowed previously elusive interactions to be studied and suggests regulatory PspF-PspA complex is nucleoid associated. The PspF-PspA complex also intermittently interacts with the membrane. The interaction of PspF in RPc / RPi (intermediate complex in process of formation of open complex with bound PspF and ATP) / RPo complexes at the nucleoid is on the time scales of SMI and very stable and long-lived. The repressive complexes of V-PspF-PspA reside in the nucleoid (see Figure 3.16, page 24) are dynamic as highlighted in their broad distribution of diffusion coefficients, thereby indicating a capacity to communicate with the IM. The proposed occasional excursions of repressive complexes away from the nucleoid towards the IM allows the system to switch from the repressed "off" state to the gene activating "on" state upon stress. The V-PspF movement from the nucleoid to the IM is PspA-dependent (see Figure 3.22).

PspA plays a crucial role in signal transduction that has been reported for the first time. PspF-PspA inhibitory complex appears to travel from the nucleoid to survey the membrane status transiently and in the presence of membrane stress this complex resolves at the membrane. With relieving of the inhibition, PspA stays at the membrane while PspF binds to UAS to activate the σ^{54}-dependent transcription of *psp* genes. Unpublished data from our laboratory has shown that the presence of lipids resolves the PspF-PspA inhibitory complex thereby supporting the model for the resolution of the PspF-PspA complex at the membrane from the SMI studies. The V-PspF dynamics in the non-stress conditions was observed to be MreB independent. Unlike PspA, that shows MreB dependent lateral dynamics as an effector (Engl *et al*., 2009). The membrane polar localisation of V-PspF was not mediated by cardiolipin. SMI studies also revealed the importance of PspBC in facilitating the interaction of PspF-PspA inhibitory complex with the membrane, as shown with V-$PspF_{1-275}$ (refer to 3.7.2).

In the gene activating states V-PspF was more stably bound to the central-nucleoid position with a 7-times reduction in dynamics, reflecting a loss of PspA binding to PspF and gain of highly stable PspF binding to the UAS and σ^{54}. PspF as part of the activation complex during stress conditions closely interacted with proteins such as $E\sigma^{54}$ (RPc) and the DNA looping protein IHF (Integration Host factor). These proteins could strengthen or even facilitate the interaction of the PspF with its enhancer elements or with the RPc. The next chapter explores interactions of PspF with σ^{54} and IHF. These studies would enable to report protein interactions *in vivo* that are beyond the scope of detection with the *in vitro* ensemble based experiments.

CHAPTER 4

4 To delineate the interactions between PspF and the closed promoter complex

This chapter reports on the existence of vital interactions of PspF assemblies with the basal transcriptional complex. Basal transcription complexes are formed with the assembly of multiple protein complexes; here σ^{54} and the core RNA polymerase (RNAP), often afford a primary example of the importance of cooperative interactions in transcription (Buck *et al*., 2000; Browning and Busby, 2004; Friedman and Gelles, 2012 and Bush and Dixon, 2013). Similarly σ^{54} dependent bacterial transcription initiation is also driven by numerous interactions between many different protein complexes (Buck *et al*., 2000 and Joly *et al*., 2010). An intimate interaction exists between σ^{54} and PspF during the formation of the basal transcription complex with the onset of membrane stress (Joly *et al.*, 2010). SMI technique has been used for the first time to report the impact of the closed complex on the spatial and temporal resolution of V-PspF. Many a time, highly sensitive cooperative multi-protein interactions can escape detection with standard ensemble biochemical assays.

The SMI technique enabled to report the importance of continuous communication between the nucleoid and the cell membrane, in order for the cell to combat external stress stimuli (details in Chapter 3). The successful mounting of a stress response heavily relies on accessory proteins and protein assemblies cooperating. For example in the Psp response the PspF-PspA inhibitory complex interacts with membrane, PspA interacts with PspBC regulatory signal sensors and PspF interacts with the RPc or UAS sequences. Such multi-protein assemblies and crowding is known to strengthen and further initiate protein-protein interactions (Mika and Poolman, 2011). Therefore, characterising the engagement of factors impacting the regulated activator function of PspF during the Psp response such as σ^{54} and the Integration Host Factor (IHF) could be crucial as shown in the Figure 4.1.

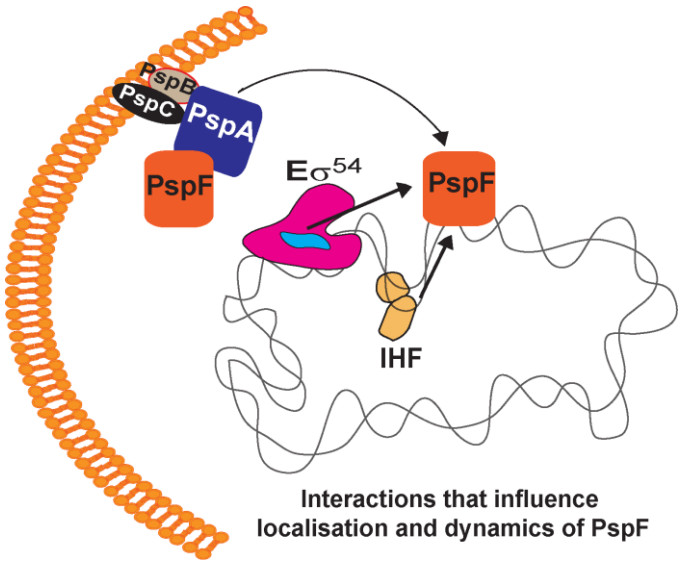

Figure 4.1 **Concerted interactions between PspF and the closed transcription complex**: The localisation and dynamics of V-PspF can be influenced by its interactions with the IHF (DNA bending protein) and σ^{54} as part of the closed complex (E σ^{54}).

Since the activator driven RPc to RPo isomerisation step limits the overall rate of transcription initiation in the σ^{54}-dependent Psp response. The regulation by PspA impacts on PspF activities, for example the alteration of PspF ATPase activity by PspA is crucial in controlling *psp* gene expression. Additional factors include for example σ^{54} and IHF (a DNA bending protein) to strengthen the contact between PspF and the closed complex (RPc) or PspF and UAS DNA sequences respectively (Jovanovic *et al*., 1997; Huo *et al*., 2009 and Friedman and Gelles, 2012).

4.1 Introduction

4.1.1 σ^{54}: unique prokaryotic sigma factor

σ^{54} is a very unique class of sigma factor because it does not share any sequence homology with any other prokaryotic sigma factor belonging to the σ^{70} class (Morett and Segovia, 1993), and it can bind promoter DNA without the core RNA polymerase. σ^{54} dependent initiation can vary the transcriptional efficiency of a wide range of genes without the need for additional repressors (Buck *et al*., 2000). Furthermore, σ^{54}-dependent transcription regulates the gene expression very tightly with very limited leaky expression from the σ^{54} promoters (Shingler, 2010 and Bush and Dixon, 2012) (Section 1.3.2- σ^{54}-dependent transcription). σ^{54} from *E. coli* is a 54 KDa protein (~ 400 amino acids) and has three major functional regions that help to establish interactions with the RNA polymerase, activator and promoter DNA (Hong *et al*., 2009). Detailed study of the structure of σ^{54} revealed that it shares several functional motifs such as leucine zipper, acidic region and glutamine rich regions with eukaryotic transcriptional factors (Morett and Segovia, 1993; Buck *et al*., 2000; Shingler, 2010 and Bush and Dixon, 2012). Thus it

can be studied as a simple system to understand eukaryotic RNAPII promoters, which are also activated by transcriptional activators (Friedman and Gelles, 2012 and Friedman *et al*., 2013). In both the σ^{54}-system and eukaryotic RNAPII, binding of the RNA polymerase to the promoter DNA is not enough to cause activation of transcription. However there are some very fundamental disadvantages of the σ^{54} system compared to the σ^{70} system. The σ^{54} system requires large stretches of intergenic DNA sequences for specific binding of the bEBP to activate the initiation and specific DNA sequences are required for binding of DNA bending proteins such as IHF (Buck *et al*., 2000; Lee *et al*., 2012 and Bush and Dixon, 2012).

Studies with mutations in σ^{54} (*rpoN* gene) showed that the N-terminal region I is very important for its function and that the deletion of region I bypasses bEBP dependent activation of the closed complex (Buck *et al.*, 2000; Cannon *et al.*, 2000; Browning and Busby, 2004 and Bush and Dixon, 2012). However the consequence of deletion of the *rpoN* gene where cells do not produce σ^{54} has not been studied *in vivo* in *E. coli* cells. Genome wide studies in *Listeria* with *rpoN* gene knockout resulted in pleiotropic effects with a major effect on carbohydrate catabolism (Arous *et al.*, 2004). In this chapter the effect of deletion of *rpoN* gene on the bEBP PspF is studied in great detail *in vivo* using SMI studies. σ^{54} is the remodelling target for PspF in the RPc, the deletion of σ^{54} abolishes the assembly of RPc. It has been shown by *in vivo* expression studies that in the absence of σ^{54} there is no activation of the *psp* genes and thus no Psp proteins are produced in the cell (Jovanovic and Model, 1997). However PspF production being under σ^{70} dependent transcription is not hampered in the *ΔrpoN* cells. It has also been shown *in vitro* that PspF binding to the specific UAS DNA sequences is not dependent on the presence of σ^{54} (Jovanovic and Model, 1997).

4.1.2 IHF: an important DNA bending protein

The long stretches of intergenic DNA includes some specific sequences to which DNA bending proteins such as IHF can bind. IHF in *E. coli* is a small (21.8 kDa) DNA binding protein with two non-identical subunits encoded by unlinked *himA* and *himD* genes (Freundlich *et al.*, 1992). IHF is known to share strong sequence homology with HU, which is classified as histone-like protein forming the bacterial nucleoid (Freundlich *et al.*, 1992). IHF is also known to compact DNA, but unlike HU it binds to specific DNA sequences. The IHF heterodimer binds to a 35bp specific DNA sequence, and 70 such IHF binding sites have been identified on the *E. coli* nucleoid (Freundlich *et al.*, 1992). IHF has been identified as one of the most abundant DNA binding protein in *E. coli* with an intracellular concentration of up to 20,000 to 100,000 molecules per cell (Freundlich *et al.*, 1992). IHF shares homology in the DNA binding domain with the eukaryotic transcription factor TFIID (Freundlich *et al.*, 1992). *In vitro* assays showed that IHF is required for the activation of transcription from σ^{54} promoters in solution. The activator specific DNA binding sites are 100-200 bps upstream (UAS sequences) from the promoter on the nucleoid. The

contact between the activator and promoter is facilitated either by native DNA bending or in many cases, by IHF (Freundlich *et al.*, 1992; Jovanovic and Model, 1997). For example, IHF induces a sharp DNA bend (>160°) in order to bring the PspF and σ^{54} together (Rice *et al.*, 1996 and Jovanovic and Model, 1997). Thus IHF plays a crucial role in the activation of *psp* genes as the DNA bending increases the accessibility of PspF to the RPc (Jovanovic and Model, 1997). Unlike a typical regulatory factor, the IHF in *E. coli* is not just limited to regulating gene expression; it has also been shown to play role in site-specific recombination, transposition and DNA replication (Freundlich *et al*., 1992). This shows that the IHF plays a more global function in nucleoid structural organisation (Wang *et al.*, 2011). It has been also shown that the amount of IHF increases during the stationary phase (Freundlich *et al.*, 1992).

As discussed in (section 1.5.1- PspF Protein) PspF binding to UAS autogenously represses its own production. The effect of the absence of IHF mediated DNA bending was studied by measuring the production of PspF in an IHF null mutant. In the *himAhimD* (IHF null mutant) the PspF production increased to five-fold as compared to wild type cells (Jovanovic *et al*., 1997 and Jovanovic and Model, 1997). Thus the interaction between PspF binding and IHF binding was very evident. In the *himD* mutant, HimA can still cause DNA bending but it is not very efficient and the production of PspF was restored to an extent in the *himD* mutant as compared to the IHF null mutant but was still comparatively higher than wild type cells (Jovanovic *et al.*, 1996 and Jovanovic and Model, 1997). The absence of the HimD subunit of IHF affected the expression of *psp* genes (Jovanovic *et al*., 1997) due to impaired DNA bending and thus resulting in reduced interaction of PspF and RPc in order to activate the transcription of *psp* genes.

The interactions of PspF with RPc reported in the literature were studied using gel shift assays and Western blot analysis. In this thesis the concerted interactions between PspF and closed complex are characterised with respect to changes in subcellular localisation and dynamics of PspF.

4.2 σ^{54} is the remodelling target of PspF in the RPc

4.2.1 The stability and functionality of V-PspF in ΔrpoN cells

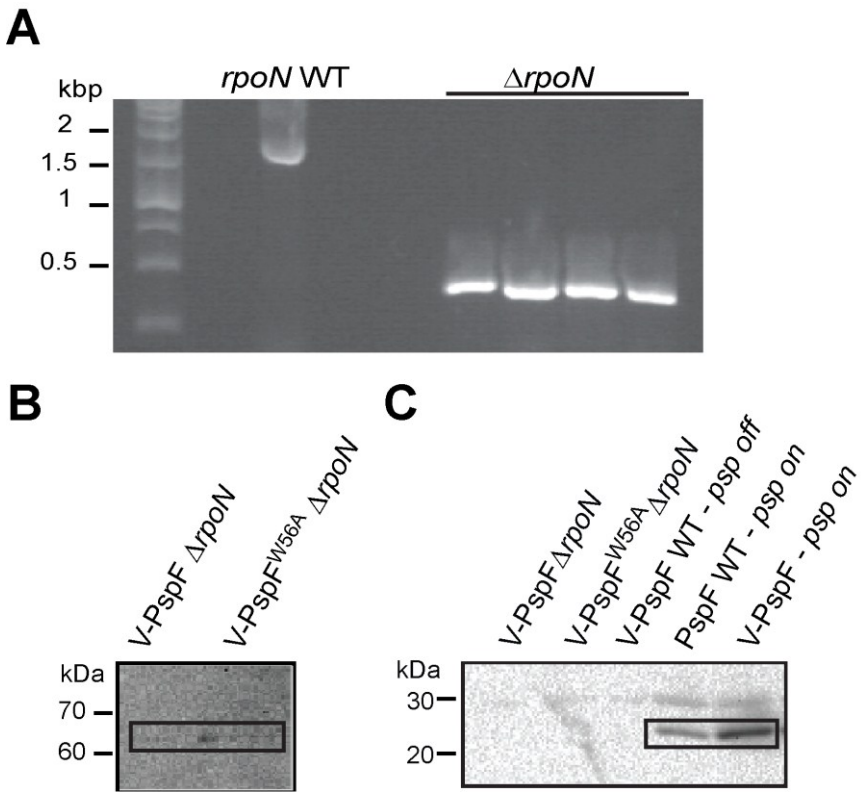

Figure 4.2 **The PCR confirmation of *rpoN* deletion, its stability and functionality**: (A) Agarose gel of the colony PCR shows successful deletion of *rpoN* gene in four different biological samples as compared to WT cells. (B) Western Blot confirms the stability of V-PspF/ V-PspF^{W56A} in the *ΔrpoN* cells using anti-GFP antibodies. (C) The functionality of V-PspF/V-PspF^{W56A} was confirmed by Western blotting against anti-PspA antibodies. No PspA was detected in *ΔrpoN* cells in V-PspF and V-PspF^{W56A}.

The interactions between the RPc and PspF were studied by deleting the *rpoN* gene responsible for σ^{54} expression. An *rpoN* gene knockout was introduced by P1 phage transduction into the MG1655 cells producing chromosomal V-PspF/V-PspF^{W56A} fusion protein (Methods - 2.2.1.1). The absence of the WT *rpoN* gene was confirmed with colony PCR using the specific primers for the *rpoN* knockout gene locus (Methods 2.5.3.2). No band corresponding to the *rpoN* gene was detected in *rpoN* knockout cells while the WT cells gave 2 kbp size band as shown in Figure 4.2A. The stability and functionality of V-PspF/V-PspF^{W56A} fusion in *ΔrpoN* strain was evaluated using Western Blotting with anti-GFP (Venus specific) and anti-PspA antibodies respectively (see Methods section 2.7.4). The stability of V-PspF/V-PspF^{W56A} was studied using anti-GFP (Venus specific) antibodies as shown in Figure 4.2B, both V-PspF and V-PspF^{W56A} were stably produced with minimum background bands (28kDa for Venus or 35kDa for PspF). This showed that the absence of σ^{54} did not impair the production of the fusion of V-PspF or the V-PspF^{W56A} mutant. The *ΔrpoN* cells yielded no Psp proteins due to the absence of σ^{54} to initiate the transcription of *psp* genes (Jovanovic *et al*., 1997 and Buck *et al.*, 2000). Thus no basal level production of PspA was detected on the Western Blot using anti-PspA antibodies in *ΔrpoN* cells producing V-PspF (see Figure 4.2C). V-PspF^{W56A} (negative control) producing *ΔrpoN* cells also gave no band

corresponding to PspA as shown in Figure 4.2C. The stable production of V-PspF fusion in the *ΔrpoN* cells, along with the confirmation of the functional phenotype due to the deletion of the *rpoN*, encouraged us to proceed to the study of V-PspF in *ΔrpoN* cells by SMI studies.

4.2.2 Subcellular Localisation of V-PspF in the absence of RPc (closed promoter complex)

The effect on the spatial localisation and dynamics of V-PspF/V-PspF^{W56A} were measured by SMI studies in *ΔrpoN* cells as explained in Methods section 2.15. The *ΔrpoN* cells expressing V-PspF were immobilised on 0.1% (w/v) agarose pads and imaged with the custom built microscope set-up in wide-field as well as TIRF mode (Methods 2.15.1). The imaging of the *ΔrpoN* cells was performed under non-stress conditions.

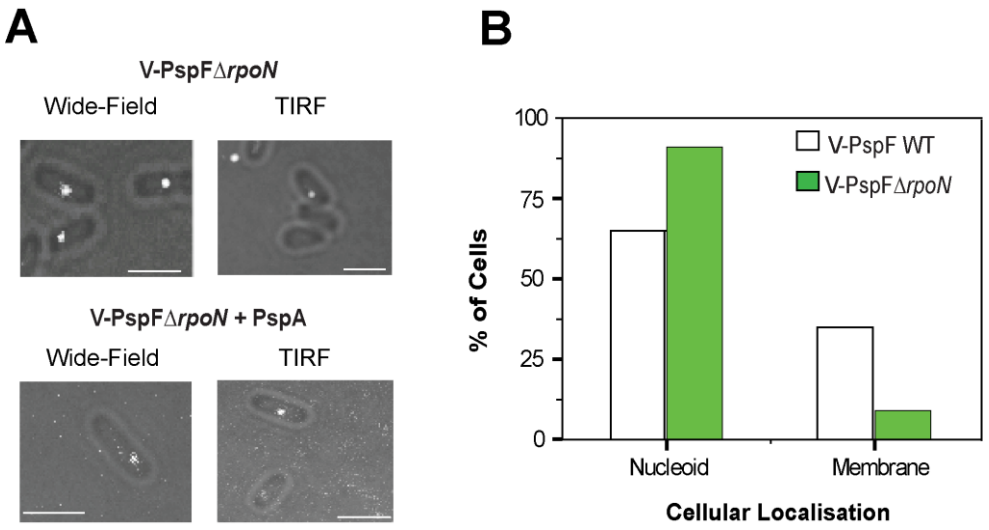

Figure 4.3 **The V-PspF foci and its localisation in *ΔrpoN* cells**: (A) V-PspF foci in *ΔrpoN* cells (no σ^{54}) are predominantly localised as central nucleoid foci in the wide-field mode and foci were not easily observed in the TIRF mode. The overproduction of PspA resulted in observation of V-PspF foci at the membrane proximal regions and could be observed in the wide-field as well as TIRF mode (observed for 3-4 frames, 90-120 ms). Scale bar = 1µm. (B) The summary of V-PspF localisations in wild type (WT, white, n=100 cells with foci) and σ^{54} mutant (*ΔrpoN*, green, n=54 cells with foci) backgrounds.

In the *ΔrpoN* cells effectively no PspA and PspBC sensors were produced (Jovanovic *et al*., 1997). V-PspF localised as diffraction limited bright fluorescent spot in the *ΔrpoN* background strain (see Figure 4.3A). The foci were observed for around 18 frames (522 ms) centrally localised in the cells. In *ΔrpoN* cells 91% of V-PspF foci were localised in the nucleoid with only 9% localised at the membrane proximal region as shown in Figure 4.3B (Methods section 2.15.3). In contrast, WT MG1655 cells showed 35% membrane-proximal V-PspF foci. And in the TIRF mode V-PspF foci were not observed evidently in *ΔrpoN* cells Figure 4.3A. The localisation data shows that the UAS binding of V-PspF was not hampered in the absence of σ^{54}, and so in the absence of RPc. However the membrane association

of V-PspF was curtailed. In the absence of σ^{54} (hence no RPc), no PspA or PspBC is expressed for localisation at the membrane and therefore no PspF-PspA inhibitory complex is formed to drag V-PspF to the membrane proximal localisation. This shows that interactions between different functional proteins lend a high level of communication to the network between multi-protein complexes.

In order to confirm the role of PspA in establishing diverse spatial localisation of V-PspF. PspA was overproduced from a plasmid pPB9 (see plasmids Table 2.4) in *ΔrpoN* cells to mimic the presence of PspA in WT cells. The presence of PspA should suffice for the membrane localisation of V-PspF foci. The overproduction of PspA in *ΔrpoN* cells led to formation of the V-PspF-PspA inhibitory complex and was transiently observed at the membrane (3-4 frames = 90-120 ms) in wide-field as well as TIRF mode (see Figure 4.3A). The production of PspA was enough to drive the membrane localisation of V-PspF in the cells, but the foci were observed for a brief time. As shown with DNA binding mutant –V-PspF$_{1\text{-}275}$ (explained in the Section 3.7.2, page number 154), PspA along with PspBC titrated the PspF-PspA inhibitory complex at the membrane. In the *ΔrpoN* cells no PspBC was expressed so it is possible that the overproduction of PspA alone is not sufficient to establish a very stable membrane association for V-PspF. Jovanovic *et al*., 1997 had shown that UAS assembles together monomeric PspF in cells increasing its local concentration and thereby increases the probability of its engagement with other Psp proteins. The V-PspF foci in the *ΔrpoN* cells did not appear very bright and defined as compared to the V-PspF foci in the WT cells. This could be due to the absence of RPc, which could affect the local interactions of V-PspF at the nucleoid. Consequently the DNA binding of V-PspF self-assemblies under non-stress conditions is hampered. It has been established with many SMI experiments that local protein crowding affects the formation of supramolecular complexes (Nenninger *et al*., 2010 and Mika and Poolman, 2011). Next the dynamics of V-PspF were observed in the *ΔrpoN* cells and compared with the V-PspF dynamics observed in the WT non-stressed cells.

4.2.3 Dynamics of V-PspF in ΔrpoN cells

The V-PspF dynamics were studied in the same way as explained in (Methods 2.15.3.2- Diffusion Analysis) by single particle tracking and the diffusion coefficients were compared. The changes in the characteristics of the V-PspF foci reflect the importance of interactions between σ^{54} and PspF. The effect of absence of σ^{54} will be compared in the cells producing V-PspF^{W56A}, where the expression of *psp* genes is constitutively active due to no inhibition of PspA. These cells are a good control for V-PspF WT to show the consequence of absence of σ^{54} on the transcription of *psp* genes.

The spatial localisation of V-PspF in *ΔrpoN* cells is predominantly nucleoid associated and no polar membrane proximal foci were observed as compared to MG1655 WT cells. Therefore it is interesting to compare the cellular dynamics of V-PspF between MG1655 WT cells and *ΔrpoN* cells. The diffusion coefficient distribution of V-PspF in the *ΔrpoN* cells is shown in the Figure 4.4A. No foci were observed

with ≥ 1 $\mu m^2/s$ diffusion coefficient (n=272). The maximum diffusion coefficient was obtained to be 0.79 $\mu m^2/s$ and the apparent diffusion coefficient was calculated to be 0.008 $\mu m^2/s$. The absence of σ^{54} reduced the dynamics of V-PspF as compared to the WT cells, with 95% foci were slow diffusing (Figure 4.4A-inset). The cellular dynamics of V-PspF^{W56A} was twice as slow in the absence of a PspF-PspA interaction, while the V-PspF dynamics was reduced by 16 times in the σ^{54} deletion mutant cells (absence of RPc). This showed that the absence of σ^{54} i.e. no RPc and hence no PspA had pronounced effect on the V-PspF dynamics.

The absence of RPc could lead to a more stable UAS association for the V-PspF. It is formally possible that PspF interaction with RPc and PspA contributes to its local movements. Such local protein movements might contribute substantially towards the cellular dynamics of V-PspF. As is often the case for multi-protein complexes, the V-PspF self assemblies could dissociate from the UAS sequences. This dissociation could lead to more localised movements such as sliding along the non-specific DNA sites in search for the specific UAS sequences. This is a very likely preposition but difficult to generate any direct evidence for. The local architecture of the nucleoid could also be different in the absence of RPc. These results imply that the σ^{54} transcription machinery (RPc, possibly RPi and then RPo) affects subcellular localisations and dynamics of PspF, possibly by constraining the V-PspF assemblies to the nucleoid as a consequence of the absence of RPc. Such an effect of RPc and/or RPo upon PspF has escaped biochemical detection and emphasizes on the significance of SMI experiments in studying these systems *in vivo* in the presence of all the native components.

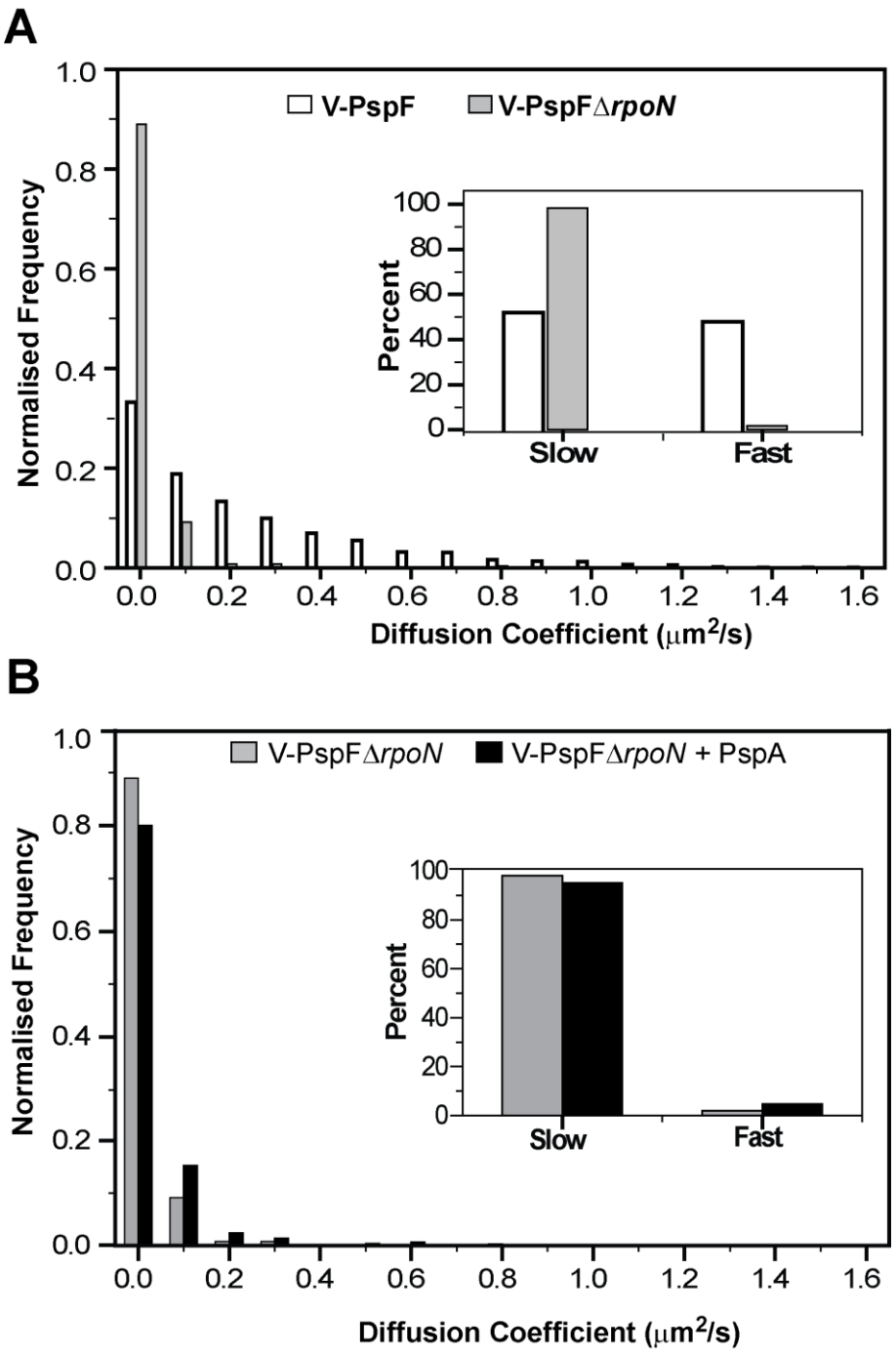

Figure 4.4 **The σ^{54} transcription machinery affects dynamics of bEBP PspF**: (A) Normalised distribution of diffusion coefficients ($\mu m^2/s$) representing dynamics of V-PspF in *ΔrpoN* cells (no σ^{54}) (grey, n=272). Inset gives the percentage of foci with slow (0-0.15 $\mu m^2/s$) and fast (>0.15 $\mu m^2/s$) diffusion. (B) The normalised distribution of diffusion coefficients comparing the V-PspF dynamics in *ΔrpoN* cells and in *ΔrpoN* cells overproducing PspA (n = 271). The inset shows the percentage of slow vs. fast diffusing foci. The apparent diffusion coefficient of V-PspF in *ΔrpoN* was 0.008 $\mu m^2/s$ while for V-PspF in *ΔrpoN* with overproducing PspA was 0.014 $\mu m^2/s$.

4.2.4 Addition of PspA to the ΔrpoN cells

In the section 4.2.2 above the change in the spatial localisation of V-PspF in *ΔrpoN* cells with overproduction of PspA was studied. Now the change in the dynamics of V-PpsF in the presence of overexpressed PspA in *ΔrpoN* cells is determined.

The dynamic studies of V-PspF in *ΔrpoN* cells showed that the absence of RPc aggravated the effect of the absence of PspA on the mobility of V-PspF foci. No foci were observed to have a diffusion coefficient of ≥ 1 $\mu m^2/s$ and a maximum diffusion coefficient for V-PspF foci in the presence of PspA was very similar to the maximum diffusion coefficient value obtained for V-PspF foci in *ΔrpoN* cells. However the apparent diffusion coefficient for the V-PspF foci (*ΔrpoN* cells) in the presence of PspA was 0.014 $\mu m^2/s$, which was 1.75 times higher than the apparent diffusion coefficient in the absence of PspA (see Figure 4.4B). Therefore PspA contributed to the faster dynamics of V-PspF and enabled its association with the membrane. The PspA produced in the cells is able to associate with V-PspF to form the V-PspF-PspA inhibitory complex at the UAS sites and then transiently interact with the membrane. However the localisation and dynamics of V-PspF in *ΔrpoN* cells with PspA overproduction was not retained like in the wild type cells possibly due to the absence of sensors PspBC. PspBC plays a significant role in the membrane association of the inhibitory complex as shown in the V-$PspF_{1-275}$ (Section 3.7.2).

4.3 Interactions between IHF and V-PspF

4.3.1 Stability and Functionality of V-PspF in ΔhimA cells

In the same way as described for the WT cells, the interactions of PspF with IHF were analysed in *ΔhimA* background cells. In *ΔhimA* cells only the HimD subunit of IHF was expressed, the truncated IHF has limited DNA bending abilities, disrupted autoregulation of PspF production and impaired activation of *psp* genes (Jovanovic and Model, 1997). However, lack of HimD does not have any effect on the binding of PspF to its specific UAS sequences (Jovanovic and Model, 1997). The *himA* knockout was introduced in the V-PspF/V-$PspF^{W56A}$ expressing cells by P1 transduction (Methods section 2.2.1.1). Western blot using anti-GFP (Venus specific) antibodies showed a band corresponding to 63kDa (see Figure 4.5A), which is the estimated molecular weight of the V-PspF fusion and no lower molecular weight bands were observed in this gel (see Methods 2.7.4).

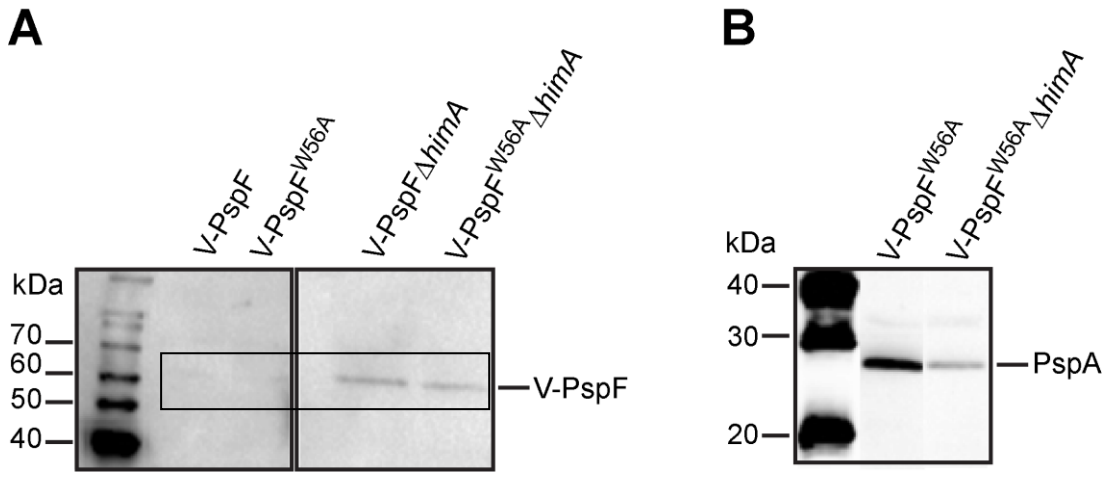

Figure 4.5 **The stability and functionality of V-PspF in *ΔhimA* cells**: (A) The production levels of V-PspF and V-PspF^{W56A} in WT or *ΔhimA* cells were determined using Western blot under non-stress conditions. (B) Western blot was performed to show the induction of PspA production using PspA antibodies in WT or *ΔhimA* (IHF mutant) cells expressing V-PspF^{W56A} (no interactions with PspA and constitutive production of PspA) grown in non-stress conditions.

The Western blot was not only an indication of the stability of the V-PspF in *ΔhimA* cells but also showed that the production of the V-PspF fusion is slightly higher in *ΔhimA* compared to WT cells. The functionality of V-PspF in *ΔhimA* was determined by anti-PspA antibodies as shown in Figure 4.5B where the blots were compared between V-PspF^{W56A} produced in WT vs. *ΔhimA* cells. The V-PspF^{W56A} mutant of V-PspF is constitutively active and PspA is produced under non-stress conditions. Figure 4.5B showed that PspA was produced in lesser amounts in *ΔhimA* cells than the WT cells. Thus with the help of Western Blot studies it was clear that loss of IHF caused imbalance in the *psp* regulon with higher production of the V-PspF fusion and lower production of PspA protein. Next the subcellular localisation and intracellular dynamics of V-PspF in *ΔhimA* cells were determined and compared with those from WT cells. As shown with the *rpoN* mutants (above 4.2) the absence of RPc had severe effects on the localisation and dynamics of V-PspF. It was important next to examine if the absence of IHF and thus the RPc had a similar effect on the V-PspF characteristics and correlated with the Western blot studies.

4.3.2 IHF affects the subcellular localisation of V-PspF

The *ΔhimA* cells were immobilised on 0.1% (w/v) agarose pads and the imaging was done under non-stress growth conditions (see Methods section 2.15.3.1 and 2.15.3.2). The number of foci, spatial localisation and dynamic studies were used to classify the effects of the absence of IHF on the V-PspF interaction with the RPc. It has been shown using gel mobility shift assays that IHF and PspF together account for 48-times more retardation of the UAS DNA than these proteins individually, but that PspF is capable of binding to DNA irrespective of the presence of IHF (Jovanovic *et al*., 1996 and Jovanovic and Model, 1997). It is also formally possible that binding of the IHF to the specific sites on the nucleoid

presents the UAS sequences to PspF to bind to (Jovanovic and Model, 1997). In line with these arguments the effect of truncated IHF in *ΔhimA* cells was studied for changes in the subcellular localisation of the nucleoid associated V-PspF and V-PspF^{W56A}. In comparison to σ^{54} null mutants, in *ΔhimA* cells some low levels of PspA and PspBC proteins were produced that can facilitate PspF-PspA binding to other regions in the cells besides the nucleoid (Figure 4.2 and Figure 4.5; Jovanovic and Model, 1997).

Firstly a comparative increase in the production of V-PspF in *ΔhimA* cells was reflected in the increase in number of foci per cell. With the wide-field as well as TIRF microscopy the numbers of V-PspF and V-PspFW56A foci were determined as shown in the Figure 4.6A images.

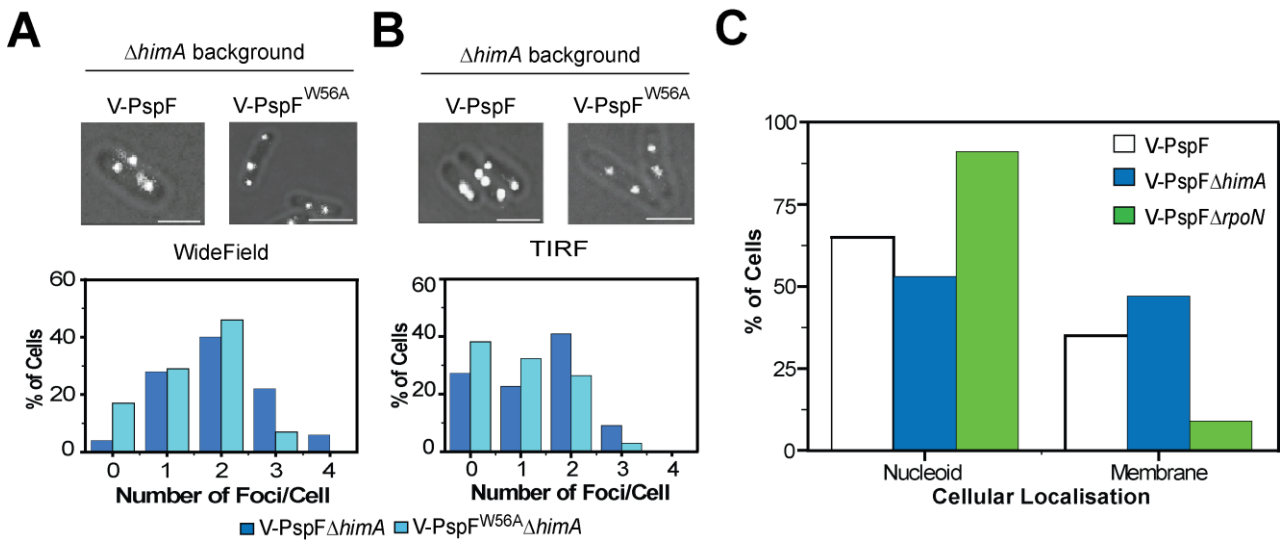

Figure 4.6 **The number and localisation of V-PspF foci in *ΔhimA* cells**: The merge fluorescent and bright field images of V-PspF foci comparing Wide field (A-WF) and (B-TIRF) i in Δ*himA* cells (IHF mutant), foci were predominantly localised at polar and lateral membrane proximal positions; V-PspF^{W56A} foci in Δ*himA* localise similarly to V-PspF. (A-Graph) The distribution of number of foci per cell determined in the widefield illumination mode for V-PspF foci (n=50, dark blue) compared to V-PspF^{W56A} foci (n=52, light blue). (B- Graph) The distribution of number of V-PspF (n=44) and V-PspF^{W56A} foci in TIRF mode (n=34). (C) The summary of V-PspF localisations in wild type (WT, white, n=100), IHF mutant (*ΔhimA*, blue, n=57) and σ^{54} mutant (*ΔrpoN*, green, n=54) backgrounds. (scale bar in the images =1 μm).

The foci distribution per cell showed an increased number of foci observed in *ΔhimA* cells as compared to WT cells. The majority of cells (40%) displayed 2 foci/cell of V-PspF or V-PspF^{W56A} as compared to a maximum of 4-6% of cells with 2 or more V-PspF foci in WT cells. Some cells even showed 4 foci/cell (see graph Figure 4.6A). The increase in the number of foci observed per cell in *ΔhimA* could be due to the combination of reasons, more V-PspF produced and more UAS sites available for binding due to a replicating chromosome (Bates and Kleckner 2005). The number of foci observed per cell was similar in wide-field as well as TIRF modes, with 4 foci observed only in *ΔhimA* producing V-PspF (see Figure 4.6A and B). The greater number of foci observed was independent to the PspA binding and interaction

because V-PspF^{W56A} also gave similar foci distributions see graphs Figure 4.6A and B. The foci distribution per cell illustrates that the DNA binding ability of V-PspF is not damaged in the absence of intact IHF protein. The next study was to observe whether changes occurred to the otherwise predominant nucleoid bound state of V-PspF. In *ΔhimA* cells the V-PspF foci were localised 53% on the nucleoid and 47% on the membrane as shown in the Figure 4.6C. The V-PspF foci were observed in the TIRF mode for a longer period of time frames (10 - 20 frames = 290 - 480 ms) as compared to 120 ms in MG1655 WT cells see images Figure 4.6B. This could be either due to prolonged and stable membrane association of V-PspF foci. It is also plausible that the nucleoid has a different architecture in the absence of the IHF with much closer proximity to the membrane in these cells and therefore nucleoid associated V-PspF foci are observed for a longer time in *ΔhimA* cells than WT cells in the TIRF.

4.3.3 Dynamics of V-PspF in ΔhimA cells

The dynamics of V-PspF in *ΔhimA* were determined and compared with the WT and *ΔrpoN* cells. The comparison with *ΔrpoN* cells was important to establish, as the absence of σ^{54} and IHF both resulted absence of RPc. The absence of σ^{54} was much more severe due to the absence of other Psp proteins while in the *ΔhimA* cells other Psp proteins were present, albeit in smaller amounts. Shown in the Figure 4.7A is the distribution of the diffusion coefficient of V-PspF foci in WT and *ΔhimA* cells. Most of the foci showed < 1 $\mu m^2/s$, the maximum diffusion value was 1.56 $\mu m^2/s$ and the apparent diffusion coefficient was calculated to be 0.015 $\mu m^2/s$.

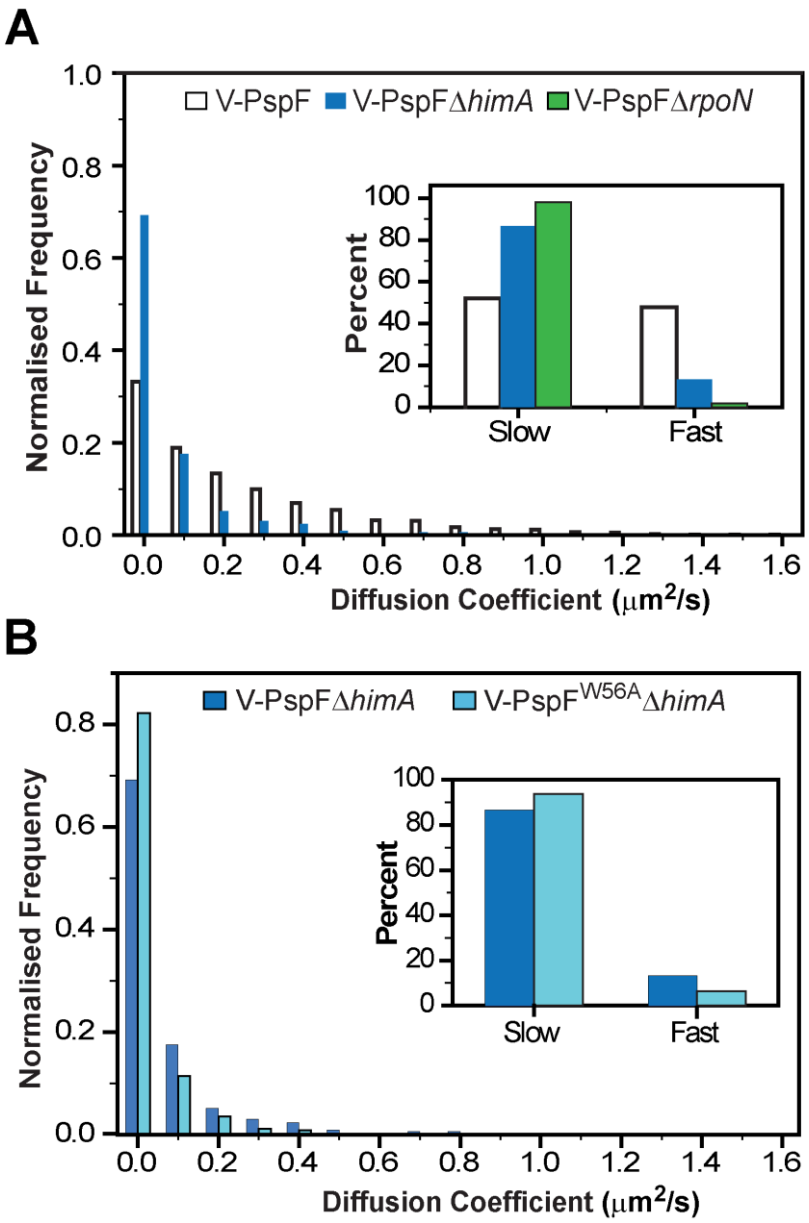

Figure 4.7 **The distribution of diffusion coefficient of V-PspF and V-PspF^{W56A} in *ΔhimA* cells**: (A) The normalised distribution of diffusion coefficients (μm^2/s) comparing dynamics of V-PspF in either WT MG1655 cells (n=1423, white bars) or *ΔhimA* (IHF mutant) cells (dark blue, n=331). Inset: illustrates the percentage of foci with slow (0-0.15 μm^2/s) and fast (>0.15 μm^2/s) comparing between WT MG1655 cells, *ΔhimA* cells and also *ΔrpoN* cells. (B) The dynamics of V-PspF (dark blue, n=331) and V-PspF^{W56A} (light blue, n=445) in *ΔhimA* strain represented by normalised distribution of diffusion coefficients showed very similar distribution for the two proteins. Inset: the slow/fast foci are classified according to distribution of diffusion coefficients with cut off at 0-0.15 μm^2/s - slow and >0.15 μm^2/s - fast. The apparent diffusion coefficient of V-PspF in *ΔhimA* cells was 0.015 μm^2/s, while for V-PspF^{W56A} was 0.01 μm^2/s.

There were 87% slow diffusing foci and only 13 % fast diffusing as shown in inset of Figure 4.7A. The dynamics studies showed that the V-PspF foci in the *ΔhimA* cells were less dynamic as compared to V-PspF in WT cells. However, the dynamics of V-PspF foci in *ΔhimA* was faster than in the *ΔrpoN* cells (see 4.2.3 - Dynamics of V-PspF in *ΔrpoN* cells and 4.3.3 - Dynamics of V-PspF in *ΔhimA* cells). The

IHF facilitated the contact between PspF and RPc via DNA bending. In the absence of native IHF, the DNA bending at the *psp* promoter is reduced and the interaction with RPc would be less frequent. However the transcription of the *psp* genes was not completely abolished because some amounts of PspA were detected in the V-PspF^{W56A} in *ΔhimA* cells (see Figure 4.5B). Thus it is formally possible that V-PspF remained bound to the UAS sequences with restricted local movement. However the dynamics of V-PspF in *ΔhimA* cells were still twice as fast as those observed in the *ΔrpoN* cells. The IHF therefore functions as an architectural element that initiates changes in the nucleoid structure leading to the formation of intimate multi-protein complexes.

4.3.3.1 The contribution of PspA in the dynamics of V-PspF in *ΔhimA* cells

In order to establish that the changes in the dynamics of V-PspF were due to the absence of full length IHF rather than the absence of PspA, it was important to estimate the changes in the dynamics of V-PspF in the non-PspA binding mutant – V-PspF^{W56A}. The dynamics of V-PspF and V-PspF^{W56A} seemed to show PspA independent characteristics as shown in the Figure 4.7B. The median diffusion coefficient of V-PspF in *ΔhimA* cells was 0.01 μm^2/s with maximum diffusion coefficient of 0.66 μm^2/s. The cells producing the V-PspF^{W56A} mutant behave like cells exposed to stress conditions. In *ΔhimA* cells possibly no activation complex was formed in the V-PspF^{W56A} producing cells. The dynamics of V-PspF and V-PspF^{W56A} are similar in the IHF mutant indicating that the interaction of V-PspF with the RPc (and possibly RPi) is highly dynamic and imparts mobility to the V-PspF self-assemblies, and such intimate cooperativity is absent in the absence of native IHF.

These results taken together imply that the σ^{54} transcription machinery effects subcellular localisation and dynamics of PspF, possibly as a consequence of constraining at least local DNA architecture. The V-PspF is influenced by the RPc and IHF, suggesting an intricate balance between nucleoid and membrane associations of PspF reinforced by layers of cooperativity between the Psp system components and the local architectural elements such as IHF. These interactions have escaped standard biochemical detection in *in vitro* assays.

4.4 Conclusion

V-PspF: MUTANT AND BACKGROUNDS	SPATIAL LOCALISATION	DIFFUSION COEFFICIENT (D) ($\mu M^2/s$)	INFERENCE
V-PspF in WT, *psp off*	Single foci, rarely more than two	$D_{apparent}$ - 0.134 (x) D_{max} – 1.6	Most dynamic, Interacts with PspA and membrane
V-PspF in WT, *psp on*	Single foci Nucleoid Not observed in TIRF	$D_{apparent}$ - 0.0183 (7x - less) D_{max} – 1.6	Less dynamic, transcription activation complex
V-PspF^{W56A}	Single foci Nucleoid	$D_{apparent}$ - 0.0174 (8x - less) D_{max} – 0.8	Non-PspA binding Mimics stress state
V-PspF$_{1-275}$	No foci observed	Not measured	No DNA binding
V-PspF in *ΔrpoN*	Single foci Nucleoid, no polar membrane foci	$D_{apparent}$ - 0.008 (16x – less) D_{max} – 0.79	Slow diffusing No RPc interaction
V-PspF in *ΔrpoN* + plasmid borne PspA	Single foci More polar Observed in TIRF	$D_{apparent}$ - 0.014 (9.6x – less) D_{max} – 0.79	PspA imparts dynamics to PspF
V-PspF in *ΔhimA*	More than 2 foci More Lateral and polar Observed in TIRF	$D_{apparent}$ – 0.015 (8.9x – less) D_{max} – 1.56	Imbalance in production of PspF and PspA

V-PspF^{W56A} *ΔhimA*	More than two foci Lateral and Polar	$D_{apparent}$ – 0.01 D_{max} – 0.66	

Table 4.1 The table summarises the major differences between different V-PspF mutants and differences between V-PspF in different cellular background strains.

In this chapter it was determined that the σ^{54}-dependent RPc and DNA bending factors such as IHF play a crucial role in the regulation, localisation and dynamics of the Psp response (see Table 4.1). The absence of σ^{54} not only led to the shutdown of the transcription of *psp* genes, but also effectively stalled the V-PspF self-assemblies to almost immobile complexes on the bacterial nucleoid (see Figure 4.8A).

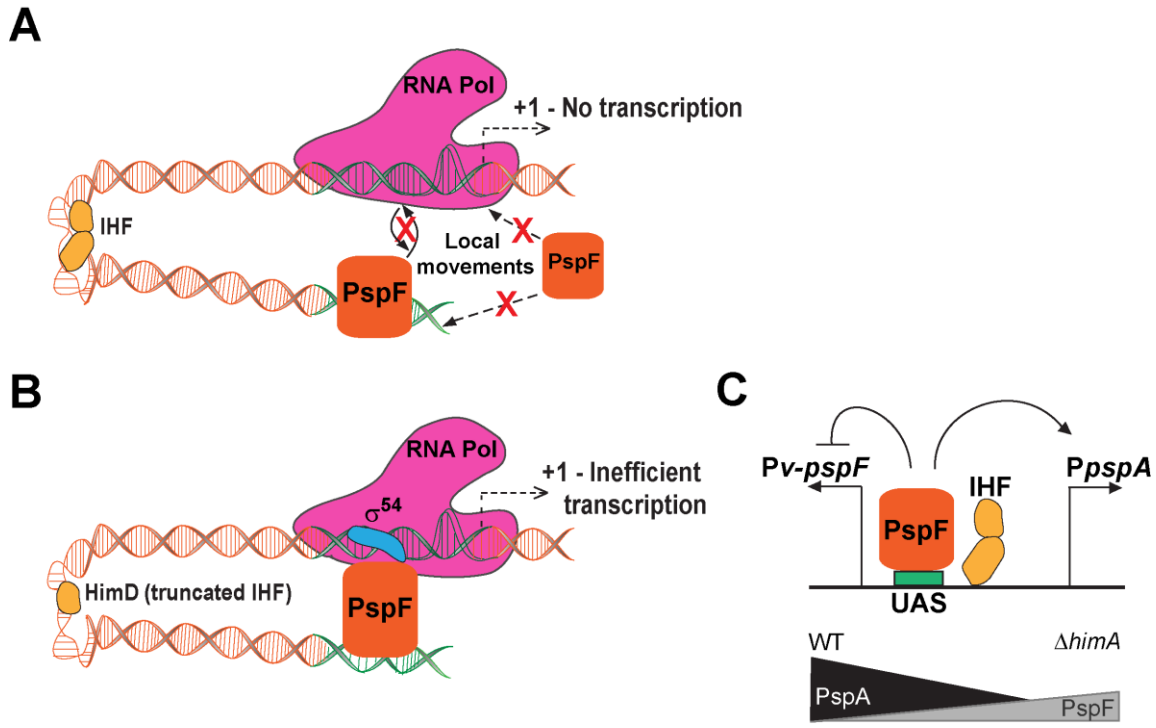

Figure 4.8 **The schematic diagram to explain the consequence of absence of closed complex and interactions between V-PspF, σ^{54} and IHF**: (A) The absence of σ^{54} and so RPc restricted V-PspF interactions with the RPc and showed no local movements around the nucleoid. The reduced local movements have been confirmed with the mainly localised nucleoid V-PspF foci that gave very slow diffusion coefficients. The transcription from the psp promoters was shut down. (B) The diagram shows the effect of truncated IHF on V-PspF and how the incompetent DNA bending changes the interaction between PspF and RPc. More V-PspF foci were observed localised at the nucleoid and membrane proximal regions and were comparatively slower. (C) Schematic presentation of transcription control of *pspF* and *pspA* promoters by V-PspF and IHF. In a WT cell, the IHF assists binding of V-PspF to the UAS in pspA (*PpspA*) and pspF (P*v-pspF*) promoter regulatory region by DNA bending resulting in activation of σ^{54}- driven pspA transcription (arrow) and negative control (footed arrow) of σ^{70}-driven v-pspF transcription. In a *ΔhimA* cells (IHF mutant) these controls are diminished leading to decreased activation of PspA and increased production of V-PspF.

In the same way, the absence of the HimA subunit of IHF caused imbalance in the production of PspF and PspA proteins as shown in the (Table 4.1 and Figure 4.8C). The PspA and PspF proteins display a seesaw effect where increase in PspA production inevitably leads to decrease in PspF production (see Figure 4.8C).

Due to the impaired DNA bending the transcription from the σ^{54} *psp* promoters was reduced and the expression from the *pspF* promoter comparatively increased (see 4.3.1 Stability and Functionality of V-PspF in ΔhimA cells). Additionally, the increase in the amount of V-PspF was also reflected in a higher number of foci observed in the *ΔhimA* cells with up to 4 foci per cell. Even the localisation of the V-PspF differed in the mutant backgrounds, in σ^{54} mutant the V-PspF foci localised predominantly in the nucleoid and in the IHF mutant V-PspF foci were almost equally found in the nucleoid or the membrane proximal region (see Figure 4.6). The dynamics of V-PspF foci were also reflective of the localisation of the foci. In the σ^{54} mutant the V-PspF foci were very slow, while in IHF mutant they were comparatively more dynamic. Such interactions were eluded from *in vitro* studies between RPc and PspF and DNA looping IHF. These interactions were observed *in vivo* assigned with the changes in the subcellular localisation and intracellular dynamics of V-PspF. The faster dynamics of V-PspF in the presence of RPc and IHF helps in spontaneous formation of activating complexes to combat the stress response and such interactions also enable the anchoring of PspF to the specific UAS sites.

The chapter will describe the number of PspF molecules that bind to the UAS *in vivo* under non-stress and stress conditions. The AAA+ domain of the PspF functions as a hexameric ring, (Rappas *et al*., 2005; Joly *et al*., 2010), but the functional stoichiometry of the full length PspF is unknown. The stoichiometry of the repressed PspF AAA domain has been estimated by gel filtration in Joly *et al*., 2006 to be 1:1 ratio with hexamer of PspF AAA domain associated with 6 molecules of PspA. It is essential to elucidate the functional stoichiometry of repressed and non-repressed PspF in order to understand whether the change in oligomerisation is a mechanism for activation of Psp response. It is also formally possible that the binding to either of the *pspA* or *pspG* promoter defines the stoichiometry of PspF assemblies in the cell.

CHAPTER 5

5 To determine the stoichiometry of V-PspF under non-stress and stress conditions, and address whether the activation of *pspA* and *pspF* promoters is simultaneous or sequential

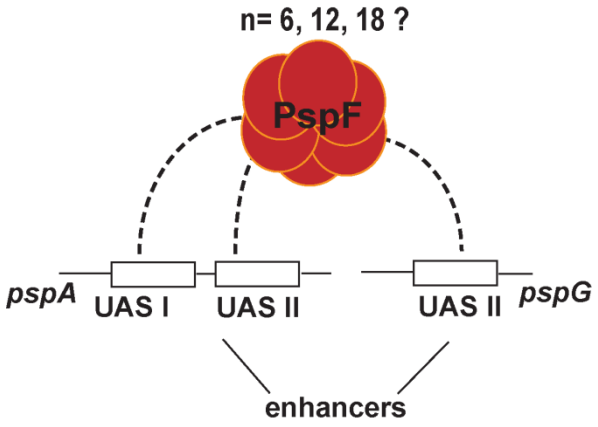

Figure 5.1 **Stoichiometry of V-PspF and the promoter occupancy**: The schematic representation explains the possible oligomeric states of V-PspF. V-PspF could bind to the UAS as a hexamer and depending on the promoter occupancy V-PspF might be present in the cell as multiple of 6-mers.

Thus far, with the help of SMI studies (see Chapter 3 and 4), it has been established that the regulation of the Psp response originates at the nucleoid. Furthermore the PspF-PspA inhibitory complex is predominantly nucleoid bound under non-stress conditions. Under stress inducing conditions the inhibitory complex is resolved either at the membrane or nucleoid and the effector PspA binds the lateral membrane. However, there could be another form of regulation of the Psp response governing the switch from the repressed to non-repressed state of PspF, which is the change in the oligomeric state of PspF. So determining the functional stoichiometry of V-PspF and the changes in the oligomerisation is crucial. Moreover the evaluation of the oligomeric state of V-PspF could indirectly determine its promoter occupancy and characterise the extended *psp* regulon that consists of the *pspA* promoter (29.4 centisomes on *E. coli* map) and the distant *pspG* promoter (91.8 centisomes on *E. coli* map).

5.1 Introduction

The oligomeric states of protein molecules in a functional complex have been reported by *in vitro* protein studies such as gel filtration, structural methods such as cryoelectron microscopy, mass spectrometry, crystallography and by cross-linking techniques (Rappas *et al*., 2005; Joly *et al*., 2006; Bose *et al*., 2008 and Joly *et al*., 2010). These *in vitro* methods are limited by ensemble averaging and lack a complete native cellular environment. Therefore the need for understanding the functional stoichiometry of protein

complexes *in vivo* has rapidly grown. Technique such as step-wise photobleaching of the fluorescent fusion proteins has been employed to study stoichiometry of functional protein complexes (Lenn *et al*., 2010 and Chiu and Leake, 2011 and Methods 2.15.3.3). Step-wise photobleaching studies can be done in live cells, in its native physiological environments and can estimate the stoichiometry of functional protein complexes. Such a method has been used to determine the stoichiometry of PspA at the cell poles (polar complexes) (Lenn *et al*., 2010); DNA replication machinery (Reyes-Lamothe *et al*., 2010) and in studying viral capsid proteins (Shu *et al*., 2007). In the same way step-wise photobleaching will be used to determine the stoichiometry of V-PspF under non-stress and stress conditions (more details of Methods in Section 2.15.3.3).

The structure of the monomer of PspF has been resolved by crystallography (see 1.5.1 - Phage Shock Protein F), and the predicted structure of the hexameric ring has been generated to understand the intra-subunit interactions within the hexamer (see Figure 1.7) (Buck *et al*., 2000, Rappas *et al*., 2005; Bose *et al*., 2008 and Joly *et al*., 2010). The oligomeric states of PspF and PspA in the PspF-PspA inhibitory has also been reported using gel filtration to be 1:1 ratio, i.e. 6 molecules of PspF interact with 6 molecules of PspA (Joly *et al*., 2006). All the *in vitro* structural studies have been performed with the AAA+ domain of PspF – $PspF_{1-275}$. The active self-associated state of native full length PspF or indeed any other bEBP *in vivo* is unknown. The amounts of native PspF in the cells is around 20 hexamers (Jovanovic and Model, 1997) and the amounts of chromosomal V-PspF should be similar to native PspF. The stepwise bleaching analysis can be challenging for proteins expressed in very high amounts such as σ factors (Chiu and Leake, 2010 and Lenn and Leake, 2012). Therefore the smaller amounts and constant production of V-PspF under non-stress and stress conditions will make the comparison of the oligomeric states of V-PspF much more credible and help in understanding the role of oligomerisation in the activation of PspF. The detailed knowledge of stoichiometry of V-PspF will not only help in unravelling whether oligomerisation plays a role in driving the activation of the Psp response, but also help to define the promoter occupancy by V-PspF.

5.2 Photobleaching studies of PspF

Often a single V-PspF foci was observed in the cell, predominantly localised in the nucleoid under non-stress and stress conditions (Section 3.6). These foci also exhibited DNA binding protein like dynamics in the cells (Section 3.9.2 Cellular dynamics defined by Diffusion coefficient values). More than a single foci was seldom observed. All these findings thus far suggest that there may be only a single assembly of V-PspF which occupies in principle any of the three UAS at a given time. Alternatively, it is possible that the UAS are so close to each other that the foci cannot be physically resolved. Thus it was priority to determine the oligomeric state of V-PspF under non-stress and stress conditions and thereby answer many of these intriguing questions.

5.2.1 Photobleaching methodology

The stoichiometry of V-PspF was determined by photobleaching experiments where the fluorescent protein fusion is bleached until it disappears from the field of view. Each bleach step corresponds to a step-size in an intensity trace. In this way the stoichiometry of the protein can be determined by counting the bleach steps obtained for the fluorescent protein as shown in Figure 5.2. This method has some limitations such as the dark states of the fluorescent protein that cannot be accounted for which could underestimate the stoichiometry. The stepwise photobleaching traces of a fluorescent protein which rapidly bleaches may not be very clear (i.e. poor temporal resolution), which could make the downstream data analysis difficult. Furthermore, the estimation of stoichiometry of self assemblies *in vivo* is complicated and requires careful attention so rigorous data analysis is crucial for stoichiometric estimations. The slow maturation of the reporter protein can also confound estimation of stoichiometry (Lenn and Leake, 2012).

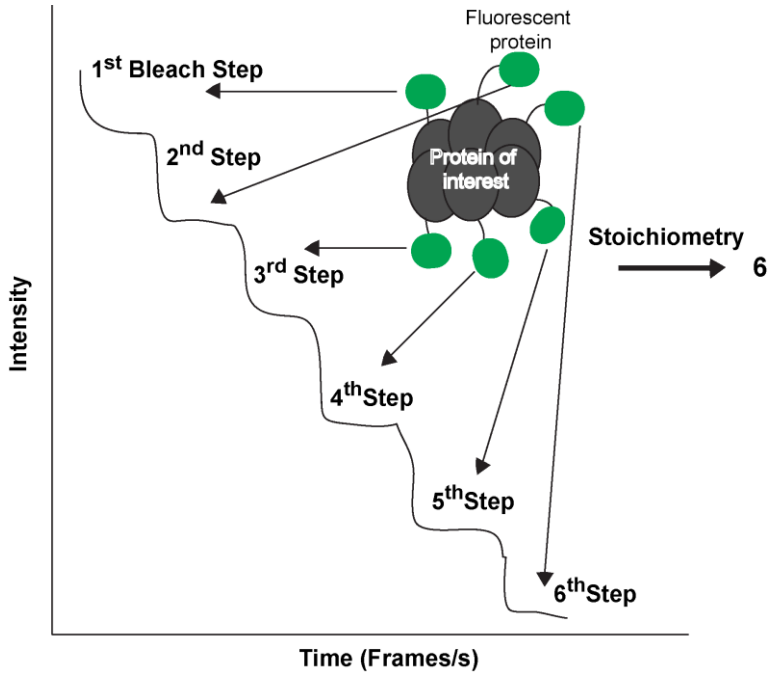

Figure 5.2 **The principle behind step-wise photobleaching experiment**: The figure illustrates the bleach steps of a fluorescent protein fusion which is bleached over a time period and the intensity trace is obtained. Ideally a monomer of fluorophore fused to a molecule of the protein will correspond to one step in the intensity trace as shown and thus the number of steps obtained will give the number of monomers of fluorescent protein fused to the protein. For example in this case 6 steps were obtained, i.e. the stoichiometry of the protein assembly is most likely to be six.

The details of the data collection and processing have been described in the Methods section 2.15-SMI and image analysis methods. In brief, an edge-preserving non-linear digital filter method based on the Chung-Kennedy algorithm (Chung and Kennedy, 1991 and Lenn *et al*., 2010 and Methods 2.15.3.3) was applied to the photobleach trace in order to effectively discard additive Gaussian-like noise. The output

of this filter is a smoother and clearer signal, with an improved signal to noise ratio. This signal is subsequently used to calculate the Pairwise Difference Distribution Function (PDDF) (Methods 2.15.3.3.1) and Power spectrum. Subsequently peaks in the power spectrum were detected and the number of steps present in the original photobleaching trace was determined using the sample size (I_s) and by dividing the difference between the initial intensity (I_i) and final intensity (I_f) with $I_s – I_i\text{-}I_f/I_s$ (see Equation 2.3). In this thesis the photobleaching trace data for V-PspF was analysed by two more methods besides the edge-preserving algorithm. The number of bleaching steps were counted manually (blinking of the Venus fluorescence was taken into account) and the distribution data were confirmed by calculating the average step size from the data to estimate stoichiometry (see Methods 2.15.3.3 Photobleaching studies).

5.2.2 *V-PspF binds a single promoter as a hexamer*

The photobleaching studies were carried out for fairly stationary nucleoid associated (central or lateral) V-PspF foci under non-stress and stress conditions. With the help of photobleaching analysis methods the following traces of V-PspF were obtained, as shown in Figure 5.3A and B.

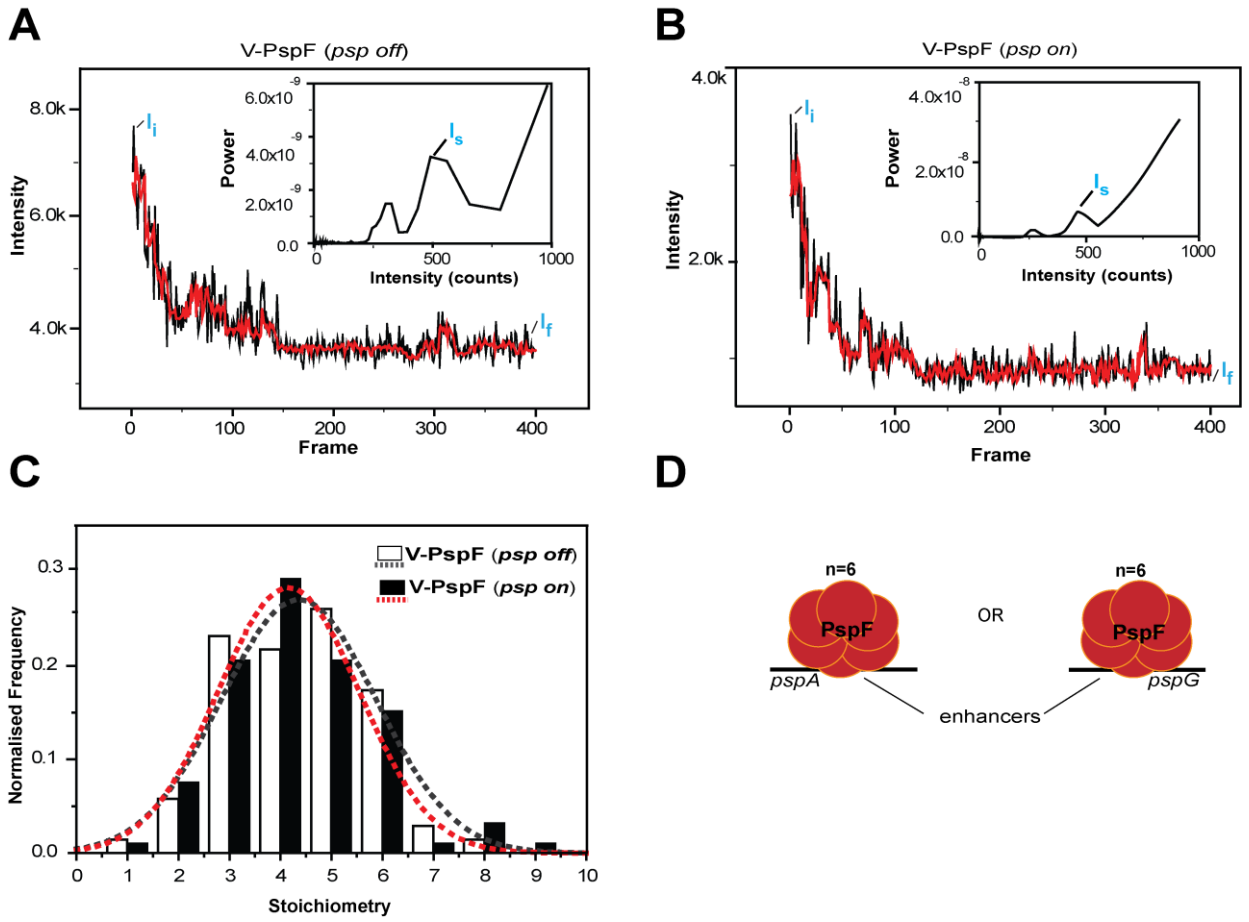

Figure 5.3 **Photobleaching trace of V-PspF**: A representative photobleaching trace of a nucleoid associated self-assembly of a PspF complex under (A) non-stress (*psp off*, n=69 foci studied) and (B) stress (*psp on*, n=92 studied) growth conditions and the corresponding filtered trace (in red) based on the Chung–Kennedy algorithm. The insets present the Fourier spectrum of the corresponding pairwise difference distribution curve giving the I_s (sample size); the stoichiometries are calculated using I_i-I_f/I_s (difference of the initial intensity - I_i and the final intensity - I_f from the raw data divided by the step size - I_s. (C) The distribution of stoichiometries and the corresponding Gaussian fit curves calculated from the data obtained for the V-PspF traces under non-stress (*psp off*) and stress (*psp on*) conditions. (D) A schematic illustration of V-PspF hexamer binding a single *psp* enhancer element at a time per cell.

The V-PspF traces with the raw as well as filtered data gave around 4-6 steps (as shown by representative traces (see Figure 5.3). The Figure 5.3C shows the distribution of stoichiometries determined for V-PspF under non-stress as well stress conditions. The peak of the distribution of the V-PspF assembly was around 4 to 5-mers with a sharp decrease beyond 6 in the number of bleach steps under both non-stress and stress conditions. Lower oligomeric states (< 2) of V-PspF were also measured (see Figure 5.3C) providing evidence for sub-assemblies, intermediate assemblies or slow maturing fluorescent fusion protein. The manual step counting or analysis of step using average step size also gave similar distribution (see Appendix-2). Thus a range of V-PspF assemblies from dimer up to hexamer but not often if ever beyond a hexamer were reported as DNA found PspF self-assemblies. Similar kinds of distribution patterns have been observed and reported in literature such as Shu *et al.*,

2007 who reported hexameric organisation of a particular packaging RNA in phi29 bacteriophage in the DNA-packaging motor. The peak of stoichiometric distribution for the packaging RNA deduced by photobleaching analysis was around 4 - 5mers and backing the distribution with statistical analysis and modelling it was shown independently by structural studies that the oligomeric state was indeed a hexamer. A similar kind of stoichiometric distribution and sharp decrease after the hexamer of single V-PspF foci (see Figure 5.3) consolidates with the *in vitro* data of $PspF_{1-275}$ that functions as a hexamer (Rappas *et al*., 2005; Bose *et al*., 2008 and Joly *et al*., 2009). If each UAS within the *psp* regulatory region binds one hexameric PspF complex, then three hexamers of V-PspF might be found (see Figure 5.1). The photobleaching studies of the single V-PspF foci suggests that the single foci of V-PspF observed in the cell is a hexamer and not any higher than a hexamer. This implies that three UAS's together in the *pspA* and *pspG* regulatory region set the affinity rather than the stoichiometry of the PspF self-assembly and that probably only one UAS sequence within the two *psp* promoters (either *pspA* promoter or the *pspG* promoter) is occupied by a V-PspF hexamer at any one time (see schematic in Figure 5.3D). The absence of any higher order oligomer above the hexamer of the single foci eliminates simultaneous occupancy of all or any two UAS at a time, as also rarely more than one foci is ever observed in the cells. The rare observation of more than a single V-PspF foci is more likely to be due to the replicating chromosome rather than simultaneous occupancy of UAS at P*pspA* and P*pspG* promoters Thus single hexamer corresponding to single V-PspF foci suggests that there is sequential binding and activation of either *pspA* or *pspG* promoters as explained in the Figure 5.3D schematic.

5.2.3 Correlation between the UASI and UASII in pspA promoter

It is physically very difficult and may be impossible to study the functional correlations between the UASI and UASII present within the *pspA* promoter without causing sequence damage to both UAS's and or changes in the expression levels of *pspF*. The deletion of either UAS can affect the production of PspF and PspA protein due to overlapping regulatory regions for *pspF* and *pspA* promoters. The presence of three UAS could help in more efficient binding, in promptly forming stable activation complex or it may be a general feature of the expanded *psp* regulon (Lloyd *et al*., 2004 and Huvet *et al*., 2010). However, some preliminary data was generated regarding the relationship between UASI and UASII. pEXT22 borne V-PspF were imaged in the WT cellular background and *ΔpspF* background strain (strains Table 2.3 and plasmids Table 2.4). The *ΔpspF* background strain lacked the specific UASII sites retaining the rest of *psp* operon (see Appendix-1). The plasmid borne production of V-PspF is comparatively higher than chromosomal production of V-PspF therefore more foci are observed for the plasmid borne V-PspF. In the *ΔpspF* background strain the plasmid borne V-PspF foci were much less than those observed in the WT cells. The UASII lacking *ΔpspF* cells showed not more than one to two foci. This observation indicates the importance of the presence of UASII for stable binding of V-PspF on the nucleoid as

compared to the WT cells in which more cluster-like V-PspF foci binding to nucleoid were observed. Thus the presence of three UAS sites within the *pspA* and *pspG* regulatory region is integral to the enhancer DNA binding ability of V-PspF.

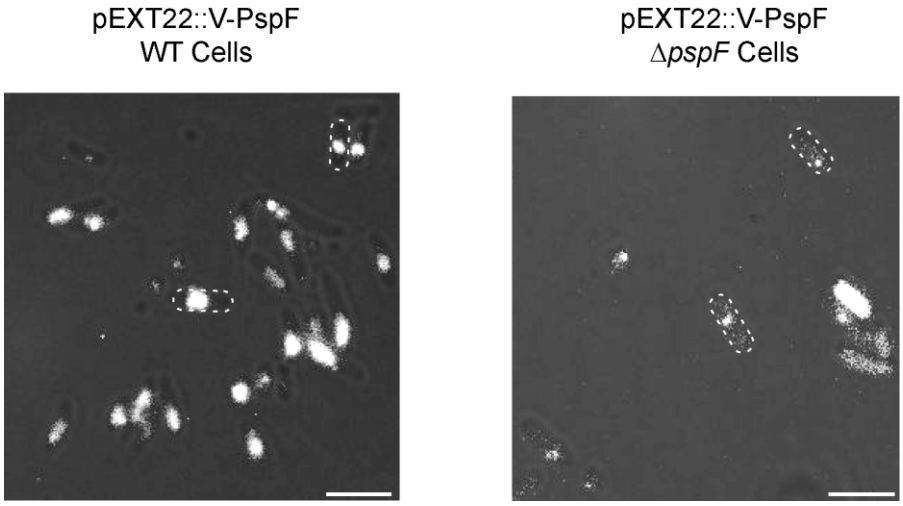

Figure 5.4 **Plasmid borne V-PspF and its interaction with UASI and UASII**: The merge of bright field and fluorescent images shows the important binding interaction of V-PspF with UAS I and UASII. *ΔpspF* cells lacking UASII showed lesser foci as compared to those observed in WT cellular background. Scale bar = 1 µm

5.3 The *pspA* and *pspG* promoters cross-talk

The potential movement of PspF between the P*pspA* and P*pspG* promoters is a key previously unknown feature of the system. V-PspF probably functions as a single hexamer regulating the expression from the *psp* promoters, possibly one at a time (see Figure. 5.5).

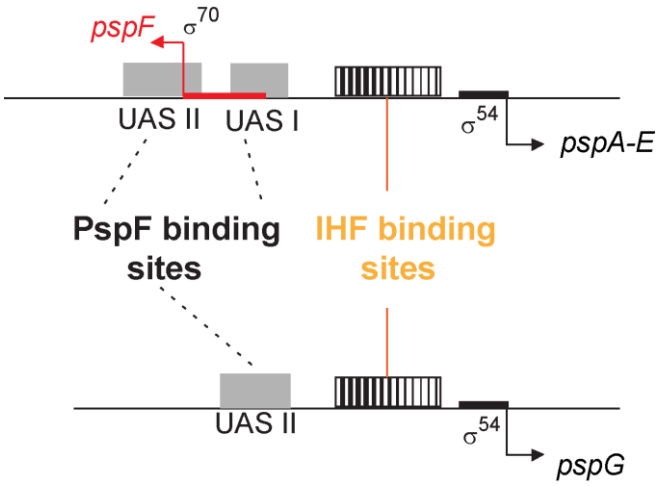

Figure. 5.5 **The promoter architecture of *pspA* and *pspG* promoters**: The *pspA-E* genes are part of the regulon under the *pspA* promoter while *pspG* promoter only controls the *pspG* gene. These promoters are physically separated on the physical map but the physical proximity on the nucleoid is not known.

The sequential activation of P*pspA* or P*pspG* promoters would then require physical movement of a V-PspF hexameric assembly from one promoter to the other, or *de novo* assembly of a hexameric species at the previously unoccupied UAS. The *psp* regulon may have interspersed organisation on the chromosome map but it may still be regulated by a single active PspF hexamer due to proximity on the nucleoid (Figure 5.5). This section will elucidate the extent of interaction between P*pspA* and P*pspG* promoters mediated by V-PspF.

5.3.1 Techniques used to study the promoter interactions

To investigate the interplay of V-PspF activating the *pspA* and *pspG* promoters, a strain was constructed lacking the P*pspG* promoter (ΔP*pspG*) and producing chromosomal V-PspF. The *pspG* gene was replaced with the kanamycin cassette using red recombineering method (see details in Method 2.2.1.2-Red-Recombineering Technique). The ΔP*pspG* was inserted in MG1655 cells producing V-PspF using P1 transduction (see details in Methods 2.2.1.1 - P1 Transduction). The dynamics of V-PspF between the P*pspA* and P*pspG* promoter was studied using single molecule tracking, where the *pspG* promoter was deleted. The strain with deletion of *pspG* promoter was also studied to measure expression from the P*pspA* promoter with a β-Gal assay under non-stress and stress conditions using chromosomal ϕ (*pspA-lacZ*) transcriptional fusion (see Method 2.8 - □-Galactosidase Assay).

The correlation between the P*pspA* (pSJ1) and P*pspG* (pLL1) promoters was studied by comparing the change in the number of V-PspF foci observed when plasmids carrying extra copies of P*pspA* and P*pspG* promoters were introduced in the cells producing V-PspF.

5.3.2 Limiting amounts of V-PspF governs specific binding to psp promoters

The production of PspF is unchanged by stress and there are up to 20 hexamers per cell, suggesting a pool of non UAS-bound PspF molecules (as hexamers or partial assemblies) (Jovanovic and Model, 1997 and Jovanovic *et al*., 1999). The limited amounts of a transcriptional factor are found to be important for the regulation and further add heterogeneity to the gene expression (Di Liberto and Cavalli; 2012; Dulin *et al*., 2012 and Loehlin and Werren, 2012). In order to study the relationship between the PspF and the available binding sites in the cell, extra copies of P*pspA* and P*pspG* promoter binding sites on the plasmid were introduced in the cells. Introduction of extra copies of plasmid-localised P*pspA* or P*pspG* promoters showed up to 2 foci moving faster than nucleoid-associated one(s) as shown in the images Figure 5.6.

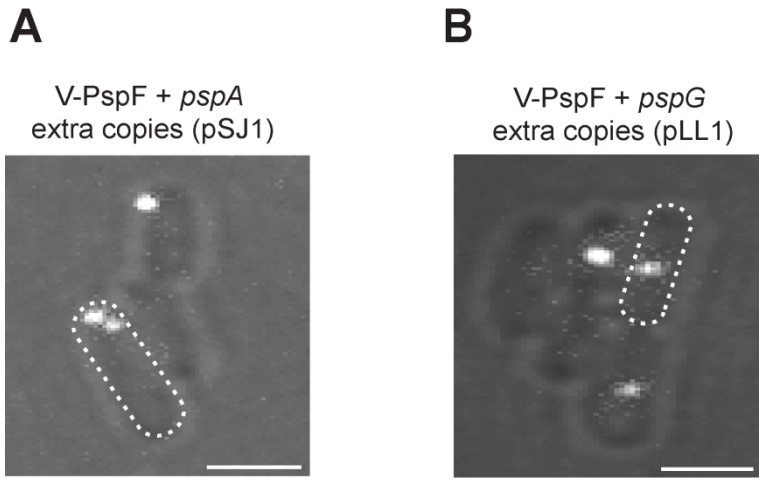

Figure 5.6 **Extra copies of *pspA* and pspG promoters to study change in number of V-PspF foci**: The MG1655 strain (*psp off*) producing V-PspF was transformed with the plasmids carrying extra copies of the (A) P*pspA* promoter (pSJ1; ~50 copies per cell) or (B) P*pspG* promoter (pLL1; ~5 copies per cell) to examine their effects on the localisations and/or total number of V-PspF foci observed; The addition of extra copies of P*pspA* promoter did not lead to an increase in the number of V-PspF foci but the foci were found to be more polar (extra-chromosomal) with up to two foci observed; the addition of P*pspG* promoter did not show an obvious change in the number or localisation of the V-PspF foci. The images A and B consists of scale bar=1μm.

The images of V-PspF with additional available P*pspA* promoter sites (UAS sites) showed two V-PspF foci in the cells as shown in the Figure 5.6A under non-stress conditions. The foci were observed at the extra-chromosomal locations in the cells besides the characteristic nucleoid localised spots. The cells with extra copies of P*pspG* promoters did not show extra foci in addition to the single nucleoid associated foci under non-stress conditions. These results and the number of V-PspF foci per cell (Section 3.5 Distribution of foci/cell) indicated that the total amount of available V-PspF complexes could be limited and can form one and not more than two DNA-bound foci supporting a model in which the P*pspA* and P*pspG* promoters/enhancers are rarely if ever occupied at the same time by PspF. It is proposed that the two *psp* promoters are not often, if ever, activated at the same precise time. Presumably, as with LacI and its operators (Elf *et al*., 2007), the V-PspF self-assemblies and their chromosomal DNA binding constants for specific UAS sites (two to three) and non-specific DNA sites (several million) reflects a thermodynamic requirement of 20 hexamers for stable UAS occupancy. Next it was important to characterise the interaction and dynamics between the two promoters with respect to V-PspF.

5.3.3 The dynamic movement of V-PspF between pspA and pspG promoters

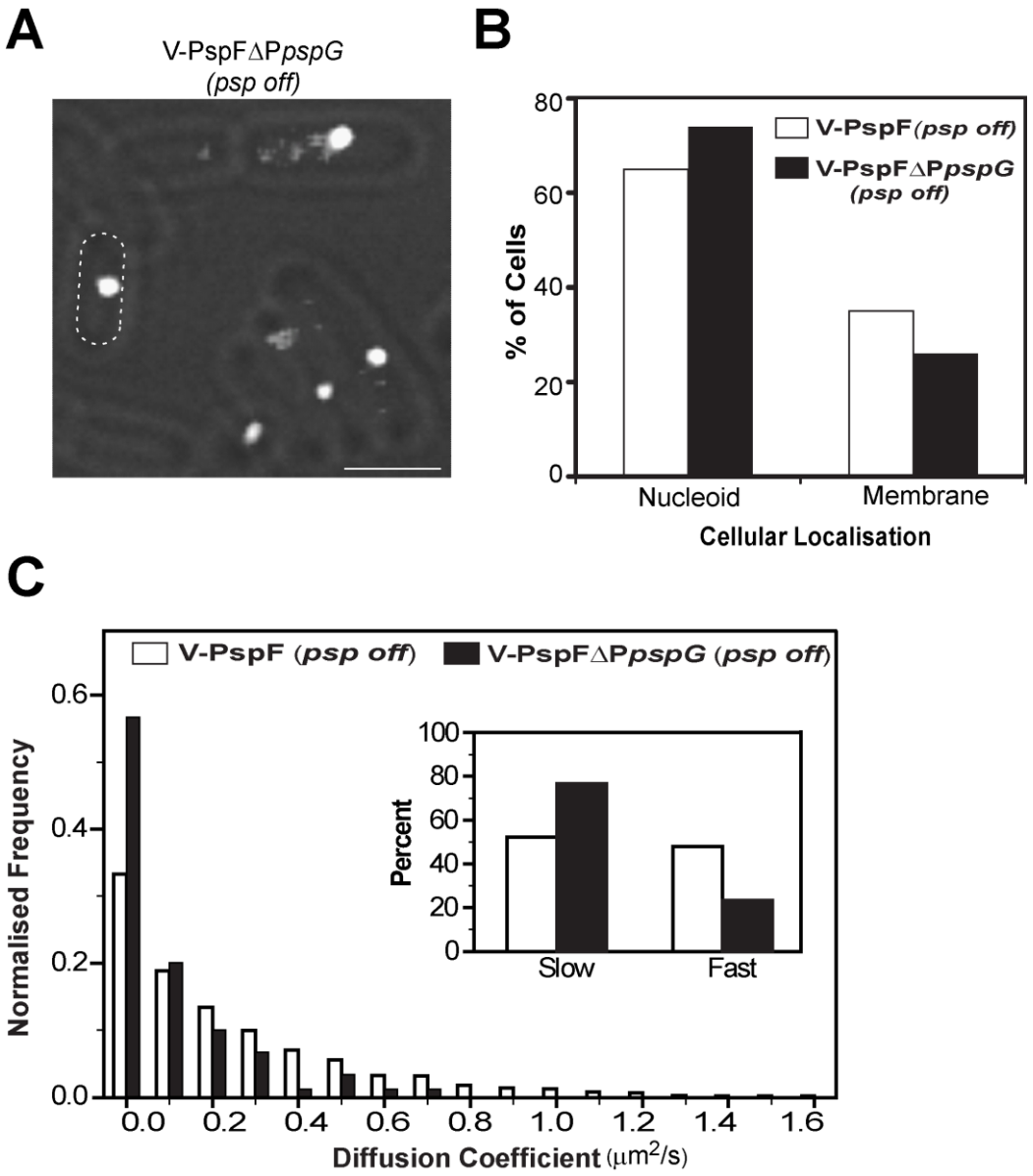

Figure 5.7 **The V-PspF localisation in the ΔP*pspG* mutant**: (A) The merge image of fluorescent image with bright field image shows the V-PspF foci in the ΔP*pspG* mutant under non-stress conditions (*psp off*); cell boundary has been defined by the dotted lines. The scale bar = 1 μm. (B) The spatial localisation of V-PspF foci were calculated and compared between the WT MG1655 and the cells with the ΔP*pspG* mutant as shown in the graph. (C) Normalised distribution of diffusion coefficients ($\mu m^2/s$) representing dynamics of V-PspF in either non-stress WT cells (white, n=1423 cells) or cells lacking the *pspG* promoter (ΔP*pspG*, grey, n=90). Inset: the percentage of foci with slow (0-0.15 $\mu m^2/s$) and fast (>0.15 $\mu m^2/s$). The apparent diffusion coefficient of V-PspF in *psp off* was 0.134 $\mu m^2/s$ while apparent diffusion coefficient of V-PspFΔP*pspG* was 0.03 $\mu m^2/s$.

Since the UAS occupancy is limited by PspF availability, non-simultaneous expression bursts are expected from the P*pspA* and P*pspG* promoters on a time scale that would reflect the dissociation and physical passage of PspF from one promoter and binding to the other. Thus the spatial and temporal

properties of V-PspF were studied in ΔP*pspG* promoter strains. In the absence of stress, the spatial organisation of V-PspF in ΔP*pspG* was similar to WT P*pspG,* as shown in the Figure 5.7. However >70% slow diffusing V-PspF foci were observed, with the apparent diffusion coefficient of 0.030 $\mu m^2 s^{-1}$ as compared to 0.134 $\mu m^2 s^{-1}$ for V-PspF WT under non-stress conditions (see Figure 5.7C) (see details Methods 2.15.3.2). The V-PspF diffusion coefficients were reduced in a ΔP*pspG* mutant possibly because the local movements of V-PspF are curtailed in the absence of the P*pspG* promoter. The reduction in dynamics shows that there exists a continuous interaction between distantly placed *psp* promoters on the nucleoid. The deletion of the P*pspG* promoter did not affect the spatial localisation showing that the inherent V-PspF interaction with the nucleoid and the membrane were intact. The intensity of the diffraction limited foci was observed to be same for V-PspF in WT cells and ΔP*pspG* mutant. The next important study related to V-PspF in the ΔP*pspG* mutant was to measure the effect on the expression from the *pspA* promoter.

5.3.4 Imbalance in expression from pspA promoter in ΔPpspG mutant

The basal level transcription from the *pspA* promoter increased >3-fold in the ΔP*pspG* strain in comparison to WT (see Figure 5.8) under non-stress conditions. No difference in the expression levels were found between WT and ΔP*pspG* under pIV induced stress conditions (see Methods Section 2.15.1.1) as shown in Figure 5.8.

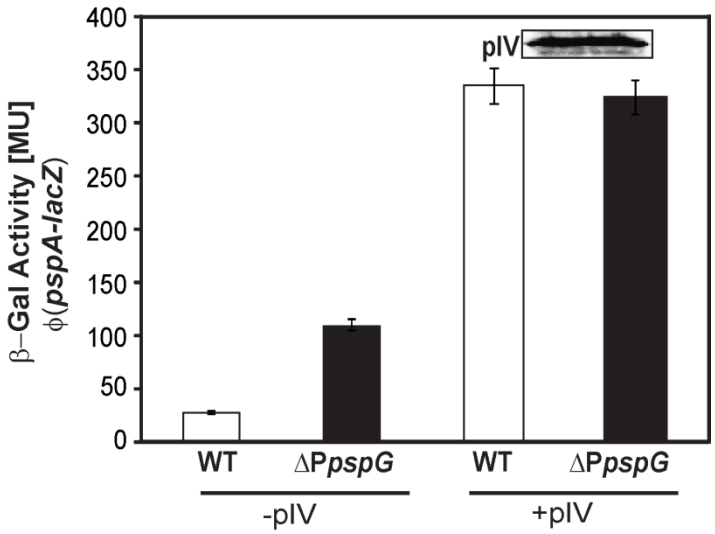

Figure 5.8 **The β-Galactosidase (β-Gal) activity of WT vs. ΔP*pspG***: β-Gal activity was measured using chromosomal transcription fusion ϕ(*pspA-lacZ*) in MG1655 wild type (WT, white) or MG1655 strain lacking *pspG* promoter region (ΔP*pspG*, black) under non-stress (-pIV- *psp off*) or pIV inducing stress (+pIV- *psp on*) conditions. The results showed the increased basal level expression of *pspA* in the absence of *pspG* promoter. The assay was performed in triplicate for two independent biological samples and data are the mean values with SD error bars.

Thus, removing the P*pspG* promoter led to an imbalanced control of the *pspA* promoter under non-stress conditions. It has already been shown that the production of PspA is not affected in the absence of *pspG* gene knock-out (with intact P*pspG* promoter) (Lloyd *et al*., 2004). Therefore functional communication and dynamics exists between the P*pspA* and P*pspG* promoters via PspF. This kind of intricate cross-talk between physically separated promoters regulated by the same transcriptional factor has been reported for the first time *in vivo*.

5.4 Conclusion

Our analysis of the stoichiometry of V-PspF indicates that a hexameric assembly of PspF forms a functional and active assembly (see Figure 5.3C-D). It is inferred that the hexameric assemblies are active for stimulating transcription. The stoichiometry of the repressed and the activating ATP hydrolysing states of PspF were the same implying no regulation by changes in the oligomeric state of this bEBP *in vivo*. Therefore changes in the oligomeric state of PspF from non-stress to stress conditions do not appear to be the mechanism of release of PspA inhibition for subsequent activation of *psp* promoters. Some sub-assemblies containing less than six subunits were also detected (see Figure 5.3A-D). Such smaller assemblies may be intermediates en route to forming mature hexamers and such sub-hexameric assemblies are likely to be inactive for the ATPase activity needed to stimulate RPo formation.

The stoichiometry data strongly suggested that PspF stably binds only one promoter at a time. For the proper and balanced expression from P*pspA* and P*pspG* promoters, V-PspF would need to bind either of the two target promoters (Figure 5.3D and Figure 5.7C). This promoter order strategy might be a general feature of regulons controlled by a limiting amount of a regulator and may be commonly observed when a regulon expands (Stern, 2000; and Di Liberto and Cavalli, 2012). Unless compensated by up-regulation of the transcription factor involved, single promoter occupancies may lead to increase in heterogeneity of gene expression between cells under stress. In the case of the P*pspA* and P*pspG* promoters, the absence of the P*pspG* promoter led to increased expression of *pspA* gene under non-stress conditions (see Figure 5.8). So far, results establish that the V-PspF foci in stressed cells were predominantly the less dynamic single hexameric foci centrally located in the nucleoid. The data suggests that the nucleoid-associated lateral foci seen in non-stressed cells may be related to the repressed V-PspF self-assemblies, likely to be V-PspF-PspA co-complexes and so implying these two PspF assemblies have different states of association with the DNA and the same oligomeric state. To complement V-PspF analyses, the localisation and dynamics of either PspA fused to Venus (V-PpsA) produced from the chromosome or plasmid borne fusion of eGFP-PspA under non-stress and stress conditions was studied.

CHAPTER 6

6 PspA as a dual function protein: a regulator and an effector

The imaging studies of eGFP-PspA with moderate level production from a plasmid mimicked the PspA levels found in pIV induced stress conditions (Engl *et al*., 2009). With the imaging it was shown that the eGFP-PspA polar static foci were hexamers, which were implicated in the PspA-PspBC regulatory complexes (Engl *et al*., 2009 and Lenn *et al*., 2010). The dynamic lateral complexes were correlated with IM repair and PMF maintenance (Engl *et al*., 2009) (see Figure 6.1). It was shown using co-immunoprecipitation in *Yersinia enterocolitica* that PspA switches its binding partners from PspF to PspBC upon induction (Yamaguchi *et al*., 2013). Yamaguchi *et al*., 2013 also showed that PspA-GFP in *Yersinia* were highly mobile, distributed along the cytoplasm under non-stress conditions and with stress conditions PspA-GFP became less mobile and formed organised structures at the membrane and colocalize with PspBC under stress inducing conditions (Yamaguchi and Darwin, 2012 and Yamaguchi *et al*., 2013). In this chapter the production, spatial and temporal localisation and stoichiometry of the chromosomally expressed Venus-PspA fusion under non-stress and stress (i.e. pIV inducing) conditions will be studied. As illustrated in the schematic Figure 6.1 the PspA localisation is expected to change with the specific function, central-nucleoid associated PspA with the PspF-PspA inhibitory complex, polar membrane associated as regulatory complexes and lateral membrane complexes as effectors of membrane “repair”. All these different PspA assemblies are predicted to have significantly different dynamics and oligomeric states while occupying such diverse cellular localisations.

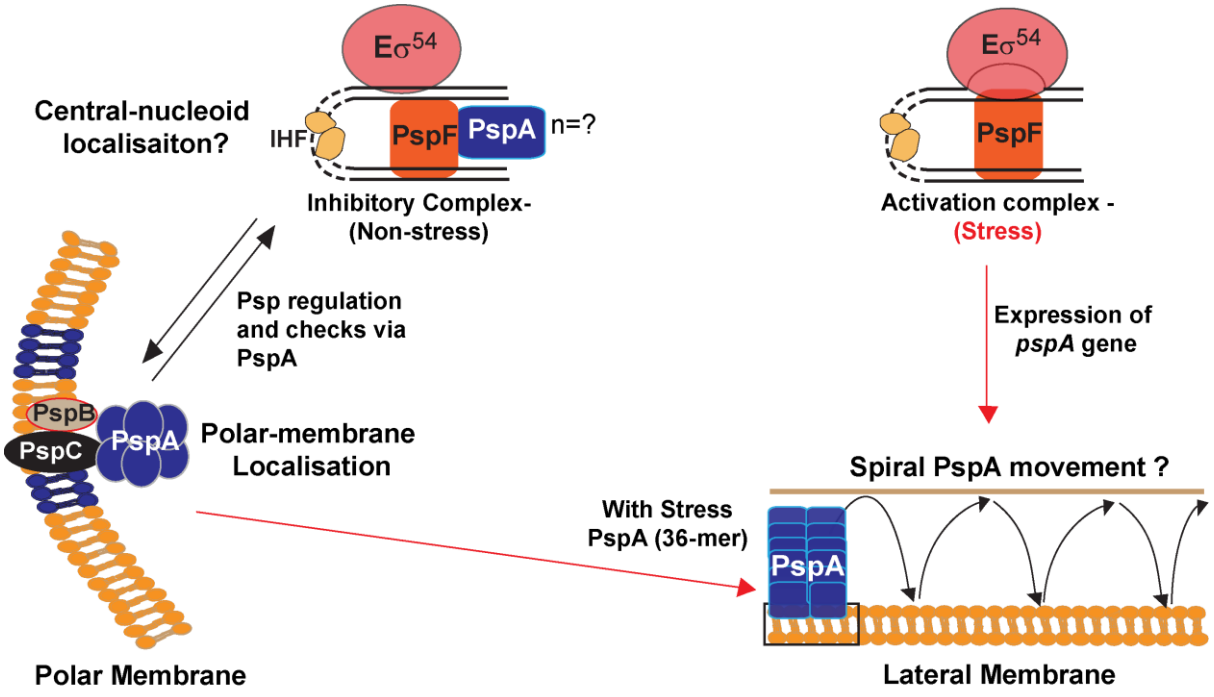

Figure 6.1 **The possible spatial and temporal localisations of different PspA assemblies**: PspA assemblies can localise at different subcellular locations in *E. coli.* PspA could be both central-nucleoid associated with PspF and polar under non-stress conditions and then change to more lateral membrane associated with stress. It is also possible that the different localisations in the cells under different conditions could help to resolve the mechanism of control and activation of the Psp response.

6.1 Introduction

The highly conserved bacterial peripheral membrane protein PspA, functions as a dual function protein (Section 1.5.2 - Phage Shock Protein A). It regulates the ATPase activity of PspF under non-stress conditions and with the onset of stress conditions it functions as a major effector of the membrane repair (Kleerebezem *et al*., 1996; Becker *et al*., 2005; Guilvout *et al*., 2006; Jovanovic *et al*., 2006; Kobayashi *et al*., 2007; and Joly *et al*., 2010). The Psp system in Gram-negative bacteria is induced by variety of membrane stress stimuli (see 1.6-Inducing Stimuli for the Psp Response). The Psp response in bacterial pathogens protects the cell envelope during infection and supports growth and biofilm formation (Joly *et al*., 2010; Dhamdhere and Zgurskaya, 2010 and Karlinsey *et al*., 2010). PspB and PspC function as signal sensors, shown to transduce the stress signal to PspA (Jovanovic *et al*., 2010, Yamaguchi and Darwin 2012 and Yamaguchi *et al*., 2013) that results in release of inhibition on PspF and activation of Psp response. SMI of PspF (Chapter3 and Chapter5) confirmed that the UAS associated repressed PspF is readily available once the PspA inhibition is relieved to associate with RPc, and to activate σ^{54}-dependent transcription of *psp* genes. However the stress perception by PspA and the subsequent changes that PspA undergoes proceeding to the switch to effector is fairly unknown (see Figure 6.1). A

drop in pmf may not be sufficient to induce the Psp response and multiple signals might be integrated somehow by PspBC to induce the Psp response in enterobacteria (Engl *et al*., 2011).

The SMI studies of a chromosomal Venus-PspA (V-PspA) fusion under control of the native *pspA* promoter will be used to ascertain changes in spatial localisation, cellular dynamics and stoichiometry under non-stress and stress conditions (Method section 2.15 - SMI and image analysis methods).

6.2 V-PspA studies

In this section the results of the spatial, temporal and stoichiometric studies of chromosomally expressed V-PspA have been reported.

6.2.1 V-PspA construction, production and stability in the WT cells

This section explains the successful recombination of the V-PspA fusion in the chromosome and its production and stability.

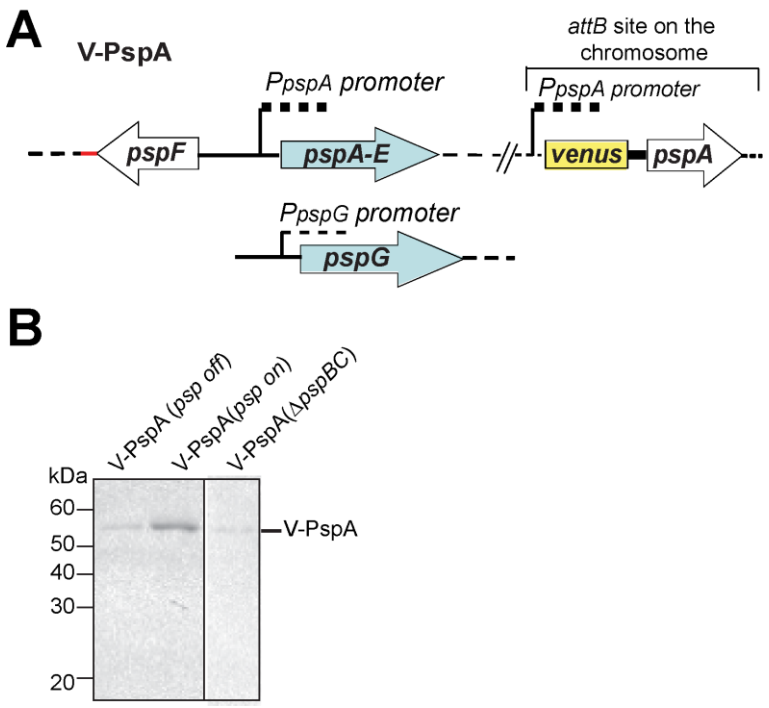

Figure 6.2 **The genetic organisation and production of V-PspA:** (A) A schematic sketch showing the organisation of the construct producing chromosomal Venus-PspA (V-PspA) under control of the *pspA* promoter (P_{pspA}) in cells with intact *psp* genes (MVA101- table of strains Table 2.3). (B-i) Western blot was performed with Venus antibodies (anti-GFP antibodies specific to Venus) to show the presence of stable V-PspA (~53 kDa molecular weight). The stability and production of V-PspA was compared in MVA101 cells under non-stress conditions (*psp off*); stress conditions (*psp on*) and in *ΔpspBC* cells under non-stress conditions.

A strain with chromosomal Venus-PspA (V-PspA) fusion protein under the control of *pspA* promoter (P_{pspA}-V-PspA) was engineered by lambda phage transduction (see Methods - 2.2.1.3). The P_{pspA}-V-PspA was integrated as a single copy into the *attB* site of the *E. coli* chromosome of a wild type strain expressing native PspA (see Figure 6.2A). The P_{pspA}-V-PspA was also introduced in the *ΔpspBC* strain by standard P1 transduction (details Methods - 2.2.1.1); in these no PspBC proteins were expressed. Using Western blotting, the production, stability and functionality of V-PspA fusion was tested (see Methods – 2.7.4). The Western blot in Figure 6.2B shows that V-PspA was stably expressed (53 kDa) in the WT cells and its production was regulated at the physiological level as WT PspA was also produced in these cells. The native PspA produced in the cells producing V-PspA efficiently regulated the production of V-PspA. However under stress conditions V-PspA production increased as represented by darker band corresponding to V-PspA due to the release of PspA dependent regulation of the production of WT PspA and V-PspA (Figure 6.2B). The increased amount of V-PspA was comparable with the native PspA amount in the WT cells with the onset of stress (Appendix-3-A). The V-PspA was also stably produced in the *ΔpspBC* strain under non-stress conditions and the production was similar in WT and *ΔpspBC* cells. The P_{pspA}-V-PspA was also introduced in a low copy plasmid (Table 2.4) and was stably produced (low copy number = 5-10) from this plasmid in WT cells under non-stress conditions (Appendix-3-A).

6.2.2 Subcellular localisation of V-PspA in WT cells

The functional chromosomally encoded V-PspA was produced and imaged by wide-field microscopy. V-PspA was produced at native levels because of the presence of WT PspA to efficiently negatively regulate the expression of V-PspA and for the first time imaging of physiological levels of V-PspA was reported. V-PspA was localised at the poles of cells and was also observed to localise at the central nucleoid locations in the cells under non-stress conditions (see images Figure 6.3A). The central localisation of V-PspA is consistent with central V-PspF localisation (Chapter 3) as part of the PspF-PspA inhibitory complex.

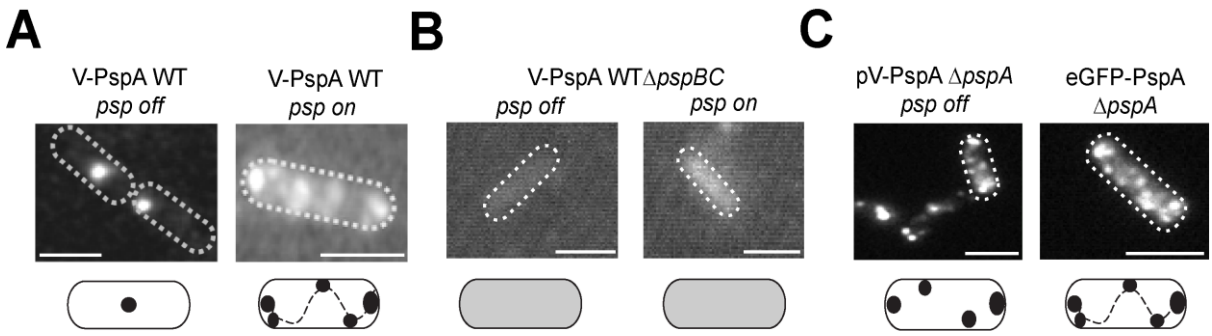

Figure 6.3 **The localisation of V-PspA foci in the WT live *E. coli* cells**: (A) The wide-field merge image of bright field and fluorescent image of V-PspA in non-stress conditions with central foci and polar foci observed for V-PspA foci. The images under stress conditions showed many more V-PspA foci, the localisation was more lateral membrane associated. (B) The images of V-PspA produced in the *ΔpspBC* background strains under non-stress and stress conditions where no V-PspA foci were observed. (C) The fluorescent image of low copy plasmid borne production of V-PspA. The V-PspA foci were observed at the poles and also in the cytoplasm as central or lateral nucleoid associated foci as part of the inhibitory complex. The V-PspA from low copy plasmid was very similar to the eGFP-PspA. The eGFP-PspA (pCE1) in *ΔpspA* showed foci at the poles, along the lateral membrane and some in the cytoplasm. The chromosomal V-PspA (image A) under *psp on* condition was similar to plasmid borne V-PspA or eGFP-PspA (image C). Scale bar = 1 µm

With the onset of pIV induced stress the V-PspA concentration increased significantly (similar amounts to native PspA). The increase in the amount of V-PspA was reflected in the imaging (see images Figure 6.3A). More V-PspA foci under stress conditions were observed associated with the lateral membrane than with non- stress conditions (Figure 6.3A). These images showed a very similar localisation to that observed with plasmid borne V-PspA or plasmid borne eGFP-PspA (Figure 6.3A, C).

6.2.2.1 PspBC defines the V-PspA localisation

PspBC are integral membrane proteins and function as sensors and signal transducers during the Psp response under stress conditions. The effects of the deletion of PspBC were studied in cells expressing chromosomal V-PspA. The images shown in the Figure 6.3B illustrate that all V-PspA foci were lost in the non-stress as well as stress conditions. This suggests that PspBC plays a very crucial role in defining the subcellular localisation of V-PspA at the poles and along the membrane in the presence of comparable amounts of V-PspA (Figure 6.2B).

Although we failed to construct a stable and functional PspB-eGFP/Venus fusion protein to directly localise the Psp sensor(s). The eGFP or Venus expressing plasmids were used to construct C-terminal fusions to PspB. However the construct was not stable in Western Blotting (Appendix-3-B). Indirect experiments have shown that PspBC recruits the V-PspF-PspA complex to the IM in the polar region (Results section 3.7.2). Furthermore, Yamaguchi *et al*., 2013 determined that under stress conditions PspA, B and C co-localise in the polar region of *Yersinia enterocolitica* cells.

6.2.2.2 Plasmid borne V-PspA

The images of V-PspA under non-stress conditions were compared with the V-PspA expressed from the plasmid in *ΔpspA* background cells under non-stress conditions. The image in Figure 6.3C shows plasmid borne V-PspA in the absence of native PspA, predominantly localised at the poles of the cells. Some foci were also observed in the central location of the cell but it was very difficult to clearly define the central foci. The localisation of V-PspA was comparable to eGFP-PspA foci. In both the cases the imaging was done in *ΔpspA* cells with reduced negative regulation. The eGFP-PspA localisation was very similar to that observed for V-PspA under stress conditions forming a spiral like localisation along the lateral membrane as seen in the Figure 6.3C.

The imaging with V-PspA in the WT cell background was very useful in establishing the central localisation of PspA. The central localised V-PspA has been observed for the first time and consolidates the nucleoid bound state of the PspF-PspA inhibitory complex. However, in order to obtain information regarding the dynamics of V-PspA and its stoichiometry it was important to ensure that no native PspA interferes with the SMI. Since it is possible that the native PspA assembles with the V-PspA and form a mixed population of PspA in the cells, it was important to study V-PspA in a cleaner background by deleting the native PspA.

6.2.3 V-PspA studies in the ΔpspA cell background

The chromosomal single copy P_{pspA}-V-PspA was transduced in the cells lacking native *pspA* gene (Methods section 2.2.1.3). In these cells V-PspA replaced native PspA to function as a regulator as well as an effector. Shown in the Figure 6.4A is the genomic organisation of P_{pspA}-V-PspA in *ΔpspA* cells. The production, stability and functionality of V-PspA were studied in *ΔpspA* cells using Western blot (Method 2.7.4) (Figure 6.4Bi). V-PspA was stably produced in the *ΔpspA* cells however its production was not regulated as efficiently as in the presence of native PspA (Figure 6.4B). However, with pIV induced stress the production of V-PspA increased 1.5-times (as shown in the graph Figure 6.4Bii) from already existent higher amounts of V-PspA.

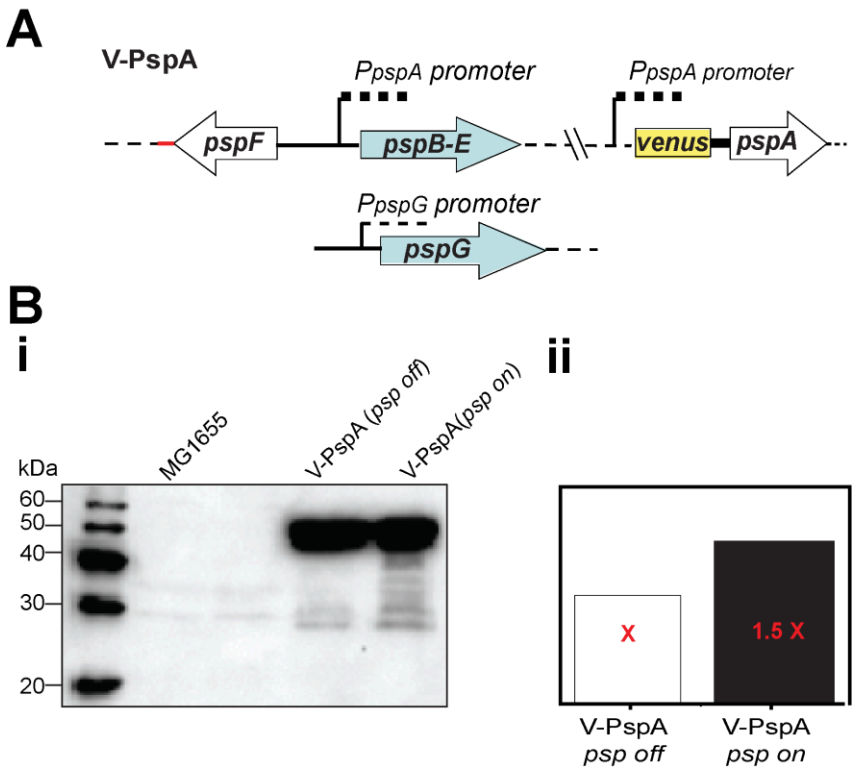

Figure 6.4 **The genetic organisation and production of V-PspA in *ΔpspA* cells:** (A) Schematic representation of the organisation of the *venus-pspA* gene under the native *pspA* promoter. The native *pspA* gene is deleted in this strain (MVA127, Table 2.3). (B-i) Western blot to show the production and stability of V-PspA (~ 53 kDa) under non-stress (*psp off*) and pIV (pGJ4) stress (*psp on*) conditions using anti-GFP antibodies (Venus specific). The WT MG1655 cells did not show any band around 53 kDa corresponding to the V-PspA fusion. The production of V-PspA increased by 1.5 times with the pIV induced stress conditions as shown in the graph. The band intensity in the Western blot for V-PspA under non-stress and stress conditions was measured using ImageJ and has been represented in arbitrary units.

The 1.5 times increase in production of V-PspA should be enough to study the specific V-PspA characteristics in the *ΔpspA* cells corresponding to the respective growth conditions. After establishing the stability and functionality of V-PspA in *ΔpspA* cells (MVA127, see Table 2.3), V-PspA was used for SMI studies to determine the specific changes in the spatial localisation, dynamics and stoichiometry under stress conditions.

6.2.4 Spatial localisation of V-PspA under non-stress and stress conditions

The details of microscopy, slide preparation and image analysis are described in Method section 2.15.

6.2.4.1 Non-stress conditions - *psp off*

The wide field illumination showed V-PspA foci were mainly localised at the IM polar regions (70 %) with a minority of V-PspA foci in the IM lateral (17%) and in nucleoid central regions (13%) as shown in images Figure 6.5A and C. The TIRF imaging confirmed that the polar foci were membrane associated

(Figure 6.5D). In the *ΔpspA* background, V-PspA is not a very efficient negative inhibitor of PspF and therefore the transcription of *psp* genes is comparatively higher (as seen in the Western blot Figure 6.4Bi) and therefore proteins such as PspBC are present in higher amounts than in the WT cells.

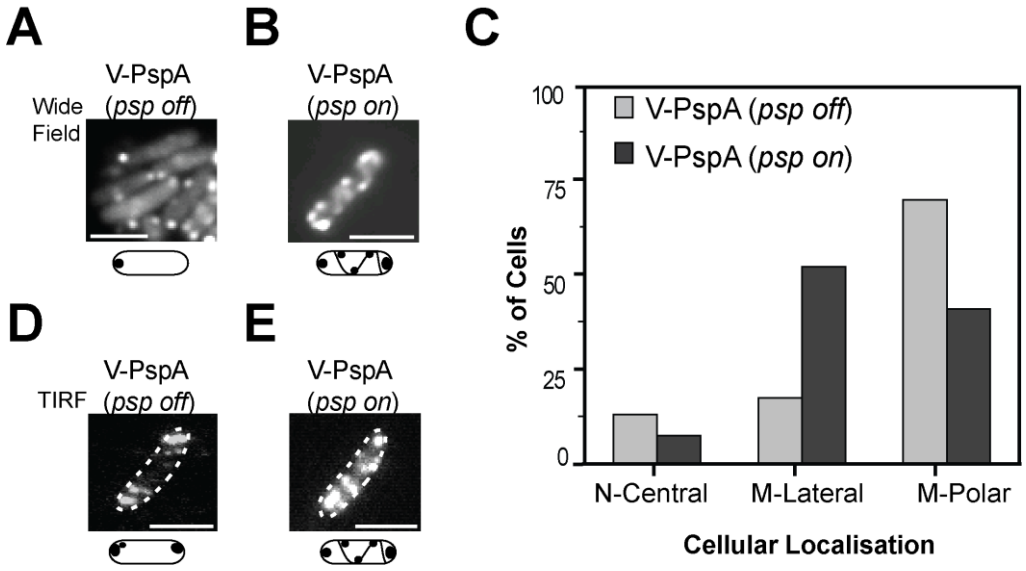

Figure 6.5 **Localisations of V-PspA under non-stress and stress conditions in *ΔpspA* cells:** Images of MG1655Δ*pspA* cells expressing chromosomal V-PspA under control of *pspA* promoter (A) fluorescent images of cells under non-stress (*psp off*) conditions displaying the V-PspA foci at predominantly polar localisations; with corresponding cell and foci illustration. (B) V - PspA foci localisations under pIV inducing stress conditions (*psp on*) shows increase in the number of foci, with polar and lateral foci; and cell illustration. These images were taken with widefield mode. (C) The profiles of V-PspA localisations under *psp off* (light grey, cells = 115) and *psp on* (dark grey, cells = 135) conditions; N-Central - nucleoid central, M -Lateral - membrane lateral, M-Polar – membrane polar. TIRF images of V-PspA expressed under (D) non-stress (*psp off*) and (E) stress (*psp on*) conditions in MG1655Δ*pspA* cells (with defined cell boundary); the V-PspA polar and lateral foci observed confirms the membrane (proximity) association. Images A, B, D and E (scale bar=1μm).

The increased concentration of PspBC facilitates the formation of PspBC-V-PspA assemblies and therefore more foci were observed in the polar regions. In WT cells it was easier to capture centrally located V-PspA foci, while in the *ΔpspA* background V-PspA production was much higher and therefore it was tricky to visualise centrally located V-PspA foci.

6.2.4.2 Stress conditions - *psp on*

Stress conditions were created by mislocalisation of pIV protein in the inner membrane from a plasmid (pGJ4) in the cells producing V-PspA with a *ΔpspA* background (see Section 2.15.3.1). With stress, V-PspA production increased by 1.5 times from a comparatively higher level of V-PspA under non-stress conditions than WT PspA. Around 51% of V-PspA was localised at the lateral membrane location in the stressed cells and the number of polar localised foci reduced by almost 40% as shown in the images Figure 6.5B and graph C. The lateral membrane associated foci exhibited a spiral configuration in the

cells (see cell illustration Figure 6.5B). This spiral path attributed to V-PspA may have some correlation with the bacterial cytoskeletal protein MreB (Engl *et al*., 2009). Very few (7%) centrally localised V-PspA foci were observed under the stress conditions (Figure 6.5C). The TIRF images of V-PspA under stress also showed the predominant lateral association along with polar foci (see Figure 6.5E). The change in the V-PspA localisation from more polar to lateral foci indicates that V-PspA assembles at the poles as a regulator in association with PspBC before becoming an effector.

6.2.4.3 V-PspA localisation studies with real time stress induction

The changing localisation of V-PspA was studied in detail with the real time induction stress by mislocalisation of pIV. The cells producing V-PspA in *ΔpspA* cells were transformed with an IPTG inducible pIV producing plasmid (pMJR129, see Table 2.4 and Methods section 2.15.1.1, Engl *et al*., 2009). The cells were imaged before induction, at induction and at 10 and 20 minutes intervals after induction of pIV with 0.1 mM IPTG (images in Appendix-4). With time and presence of IPTG the production of pIV will increase, which would result in its mislocalisation in the IM and activation of Psp response. Figure 6.6A shows the consequence of prolonged stress with the increase in the amounts PspA. At induction with IPTG (t=0 minutes) more lateral membrane foci started appearing (see Figure 6.6A). With the increase in stress intensity the number of V-PspA foci also increased reflected in the increase in total fluorescence intensity from t=0 to t=10 minutes and 20 minutes intervals (see Figure 6.6Aii). The intensity was analysed using the cell intensity analysis (see Methods 2.15.3.1, 131) and the total fluorescence intensity was calculated. At 20 minutes after induction 80% of observed foci were lateral membrane associated and showed highest total cell intensity (see Figure 6.6A). The real time studies of the effect of stress on the V-PspA localisation showed that the polar membrane not only contributes towards the regulatory centre for PspA-PspBC complex for signal perception and transduction, but also suggests that the poles could also be the collection centre for PspA to oligomerize to its effector form.

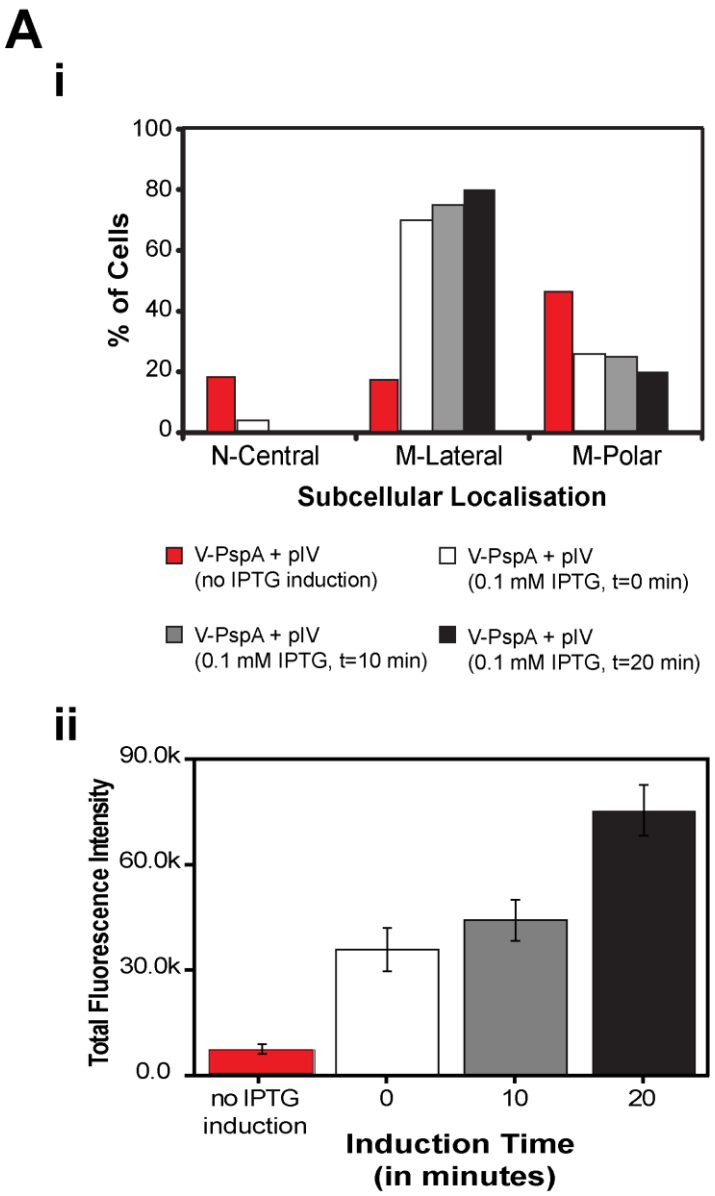

Figure 6.6 **V-PspA localisation and fluorescence intensity with real time stress induction using IPTG inducible pIV production**: (A-i) The cells with varying amounts of V-PspA depending on presence or absence of IPTG were used for the localisation studies to compare changes in the localisation of V-PspA with stress. The graph shows the total percentage of foci calculated and classified as nucleoid-central, membrane-lateral or membrane-polar n= 27 foci (+pIV, no IPTG), n= 57 foci (pIV, 0.1mM IPTG at t=0 min), n=73 foci (pIV, 0.1mM IPTG at t=10 min) and n=100 foci (pIV, 0.1mM IPTG at t=20 min). (A-ii) The graph shows the total cell intensity measured at no IPTG and at different IPTG induction time of pIV from the plasmid, the varying amounts of pIV in the cells will lead to different intensity of Psp response. The activation of Psp response is represented by the increase in the production of V-PspA in the cells with different amounts of pIV produced at different time points starting from no IPTG, at induction, 10 minutes after induction and 20 minutes after induction under the same imaging conditions and n=16 cells for this analysis.

So far with the localisation studies it is clear that V-PspA shows distinct changes in the subcellular localisation in line with the change in its function in *E. coli* cells as illustrated in Figure 6.7. PspA is mainly nucleoid associated with PspF under non-stress conditions with intermittent sampling of the

membrane at the poles via PspBC sensors. With stress it localises at the lateral membrane (see Figure 6.7).

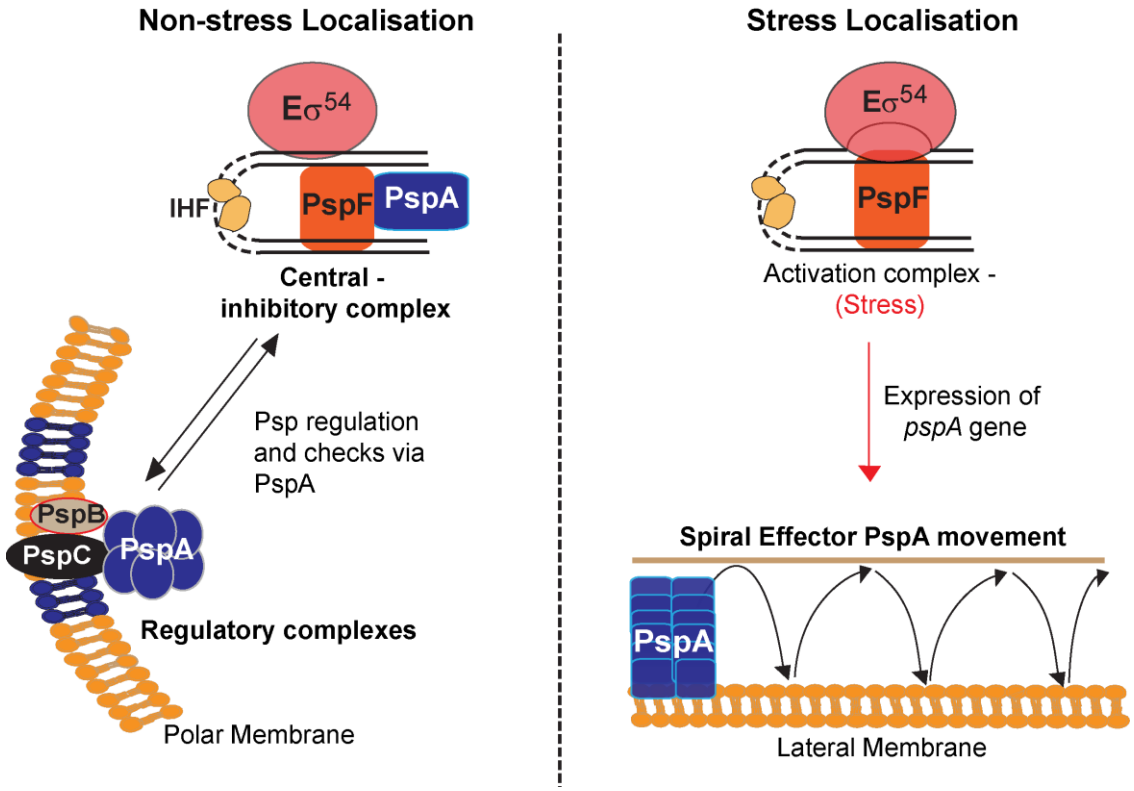

Figure 6.7 **Schematic showing localisation of V-PspA under non-stress and stress conditions**: The figure explains the different localisation of V-PspA corresponding to the specific function of PspA in the cell. Under non-stress conditions V-PspA as part of the PspF-PspA inhibitory complex localises at the central nucleoid position in the cell. V-PspA also occupies the polar region in the cell interacting with PspBC as part of the regulatory complex to check the membrane status. With the onset of stress V-PspA predominantly localises along the lateral membrane possibly moving in a spiral fashion as shown in the diagram and PspF activates the transcription.

As described in Section 3.9 - Temporal localisation of V-PspF, V-PspF exhibited different cellular dynamics under different growth conditions. The same dynamics studies were performed on V-PspA in order to define the changes in the V-PspA movement with the stress conditions.

6.2.5 Temporal localisation of V-PspA

The temporal localisation of V-PspA was also defined by the diffusion coefficient as explained in Section 3.8- Temporal localisation of V-PpsF. The custom Matlab scripts were used to track the V-PspA foci over 100 frames (3 s) (details Section 2.15.3.2) and the distribution of diffusion coefficients was obtained as shown in Figure 6.8.

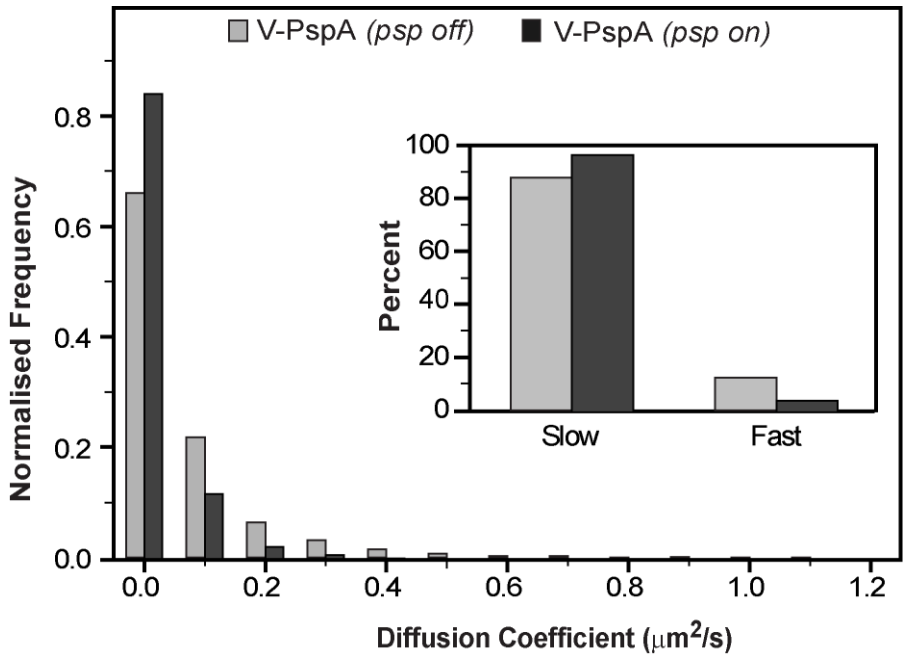

Figure 6.8 **Dynamics of V-PspA under different growth conditions:** The V-PspA were tracked under (non-stress-, *psp off*, n=7172 or pIV induced stress-, *psp on*, n=6485) and presented as normalised distribution of the diffusion coefficients (μm^2/s). Inset: the slow/fast foci are classified according to distribution of diffusion coefficients with cut off at 0-0.15 μm^2/s - slow and >0.15 μm^2/s - fast. The apparent diffusion coefficient of V-PspA in non-stress conditions was 0.03 μm^2/s while the apparent diffusion coefficient of V-PspA in stress conditions was 0.008 μm^2/s.

The apparent diffusion coefficient distribution for V-PspA under non-stress conditions gave ~90% slow and ~10% fast diffusing foci with an apparent diffusion coefficient of 0.030 μm^2/s (see graph Figure 6.8). Only two foci were observed to display diffusion coefficient of > 1 μm^2/s and the maximum diffusion coefficient reported was 1.18 μm^2/s. This result strongly suggests that the majority of V-PspA foci display membrane dependent slow dynamics in the cell. The very small population of more dynamic foci could be nucleoid associated, likely to be PspF-PspA inhibitory complexes. The onset of stress enforced lateral membrane association of PspA and further reduced the apparent diffusion coefficient to 0.008 μm^2/s, with >90% of foci slowly diffusing (see graph Figure 6.8). No foci were observed to have a diffusion coefficient of > 1 μm^2/s and the maximum diffusion coefficient was calculated to be 0.79 μm^2/s. Thus the diffusion studies of V-PspA showed that V-PspA moves along the cell mainly associated with the membrane and therefore displays much slower movement in the cell as compared to fairly dynamic nucleoid (cytoplasmic) associated V-PspF (apparent diffusion coefficient of 0.134 μm^2/s under non-stress conditions . V-PspF even under stress conditions displayed much faster dynamics (apparent diffusion coefficient of 0.018 μm^2/s) as compared to the membrane associated effector V-PspA under stress conditions (apparent diffusion coefficient of 0.008 μm^2/s) The rare species of V-PspA assemblies that formed the fast moving species under non-stress conditions could be the V-PspF-PspA inhibitory complex communicating between the nucleoid and the membrane (see graph Figure 6.8). However

majority of V-PspA assemblies predominantly showed very slow cellular dynamics and thus possibly indicating towards its membrane association in the cells under non-stress conditions With the onset of stress the membrane association of effector PspA becomes much stronger and prolonged, and thus PspA dynamics were further reduced by 3.75 times.

The cells under stress conditions switch to a more energy efficient lifestyle (Bury-Monè *et al*., 2009 and Joly *et al*., 2010), and therefore it is possible that the PspA moves along a devised path along the lateral membrane organised by the bacterial skeletal protein such as MreB (discussed later in Section 6.2.7). In this way the directed movement along the membrane of PspA facilitated by MreB could be more efficient in targeting the damaged membrane regions. Due to the directed movement of PspA along the membrane its cellular dynamics could be different from the dynamics of PspF. The extracytoplasmic stress leads to many changes in localisation and dynamic changes of V-PspF and V-PspA. These changes are the consequence of a switch in the protein functions, activation of more genes and many fold increase in concentration of different proteins to deal with the membrane damage in the cell. It is likely that Psp system behaves and changes upon stress in the following chronological order: the PspF-PspA inhibitory complex is released at the poles (mainly), PspF binds the RPc to activate the σ^{54}-dependent transcription of *psp* genes*,* the production of Psp protein increases, subsequently more PspA organises at the poles and is recruited on the lateral membrane as an effector. However there is another very important mechanistic switch that is speculated to occur during the Psp response, which is the change in oligomeric state of V-PspA. It has been demonstrated in this thesis that the oligomeric state of V-PspF is the same under repressed (non-stress conditions) or non-repressed (stress conditions) (Chapter 5). It is already known that *pspF* transcription under stress is unchanged while the transcription of *pspA* is elevated ~100-fold (Lloyd *et al*., 2004). However the comparison of images and number of V-PspA foci under non-stress and stress conditions does not reflect the scale of increment in the production of V-PspA (Figure 6.5) with stress. This indicates and is in agreement that PspA must increase its oligomeric state to form an effector. In the next section data from the photobleaching studies of V-PspA will be presented.

6.2.6 Stoichiometry of V-PspA under non-stress and stress conditions

Biochemical experiments so far indicate that the PspA-PspF complex contains six PspF and six PspA subunits (Joly *et al*., 2009). Kobayashi *et al*., 2007 provided evidence that the higher oligomeric form (36-mer) of purified PspA binds phosphatidylglycerol (PG) and can prevent proton leakage from membrane vesicles. The polar static eGFP-PspA complexes were photobleached for 1000 frames with 25 frames per second frame rates. The photobleaching traces were obtained and the Chung-Kennedy algorithm (explained in 2.15.3.3 - Stoichiometric analysis) was applied to remove the statistical noise and the filtered trace was obtained as shown in the Figure 6.9 (Lenn *et al*., 2011). The sample size was

determined by the power spectrum obtained from the PDDF values that enabled to calculate the stoichiometry by dividing the difference of intensity (I_i-I_f) by sample size (I_s) adapted from Lenn *et al*., 2011.

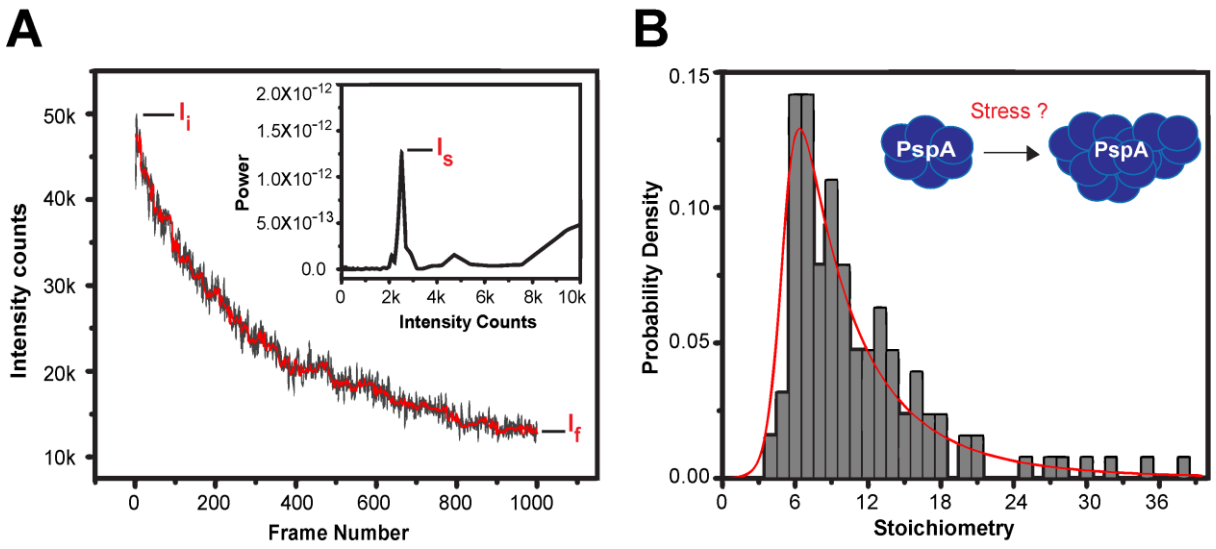

Figure 6.9 **Determination of polar eGFP-PspA stoichiometry *in vivo* in *E. coli* cells using single molecule fluorescence photobleaching analysis:** The stoichiometry of individual complexes is defined as (I_i - I_f)/I_s. (A) A representative photobleaching trace of a single PspA complex (black) and the corresponding filtered trace (red) based on the Chung–Kennedy algorithm. The inset shows Power spectrum of the PDDF of the filtered trace giving I_s. (B) Stoichiometry distribution of 127 PspA complexes. The fitted distribution peaks at 6.3 with a full width half maximum (FWHM) of 5.6, indicating PspA may exist as a hexamer at the cell membrane in association with PspBC regulatory complex. Adapted from Lenn *et al*., 2011

The graph shows the distribution of eGFP-PspA stoichiometry distribution with a peak around a 6-mer, but gave a wide distribution of stoichiometry until the 36-mer, as shown by the distribution in Figure 6.9B. The data strongly suggest that the PspA-regulator behaves as a hexamer but the transition from lower order oligomer to higher order oligomer is not clear from this analysis. It is important to evaluate this change in oligomerisation of PspA in context with stress inducing conditions. Therefore V-PspA will be used as a tool for the photobleaching studies under non-stress and stress conditions to compare the oligomeric states of PspA in these different states. In addition, V-PspA – central nucleoid foci will be studied by single molecule fluorescence photobleaching to see if their oligomeric state is also a hexamer coinciding with the V-PspF hexameric assembly at the nucleoid in the non-stress conditions. This will show for the first time that PspA-full length binds PspF as a hexamer *in vivo*.

The V-PspA foci were imaged for 1000 frames with 38 frame/s frame rate until all the foci were completely bleached under non-stress and stress conditions in the wide-field mode of illumination (explained Methods - 2.15.2). The single molecule photobleach traces were treated with the Chung-Kennedy algorithm to filter the statistical noise and the Figure 6.10A shows a representative curve.

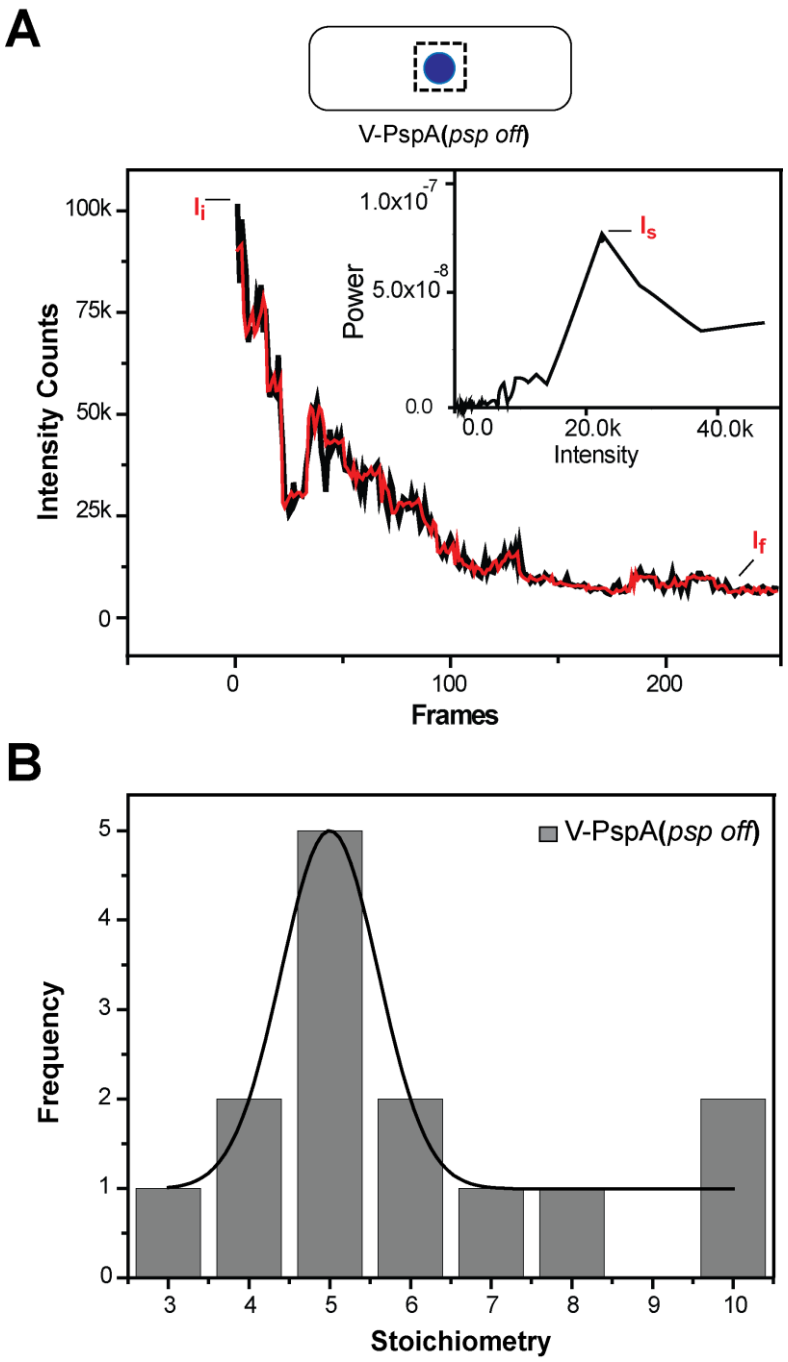

Figure 6.10 **Stoichiometry of nucleoid associated V-PspA under non-stress conditions**: The stoichiometry of individual complexes is defined as $(I_i - I_f)/I_s$. (A) A representative photobleaching trace of a nucleoid associated central V-PspA complex as shown in the cartoon of the cell. The graph shows the photobleaching trace (black) and the corresponding filtered trace (red) based on the Chung–Kennedy algorithm. The inset shows the Power spectrum of the PDDF of the filtered trace giving I_s. (B) Stoichiometry distribution of 11 V- PspA complexes was determined using the $(I_i - I_f)/I_s$. The peak of the stoichiometric distribution is 5.

The trace shows the raw data overlapping with the filtered red trace and was used to determine PDDF values. Firstly the V-PspA central nucleoid foci were used to obtain photobleaching traces to determine the stoichiometry of these foci. The data collection for the photobleaching was demanding since the

central foci were more mobile as compared to the relatively static polar V-PspA complexes. The data was collected for 11 V-PspA foci and the distrubution of stoichiometry is illustrated in the graph Figure 6.10B. The distrubution peak is centered around 5-mer, a distribution very similar to that of V-PspF suggesting that V-PspA in the nucleoid are most likely hexameric assemblies (Figure 6.12A). This suggests that regulator PspA might exist as a hexamer under non-stress conditions, and associating with the hexameric V-PspF at the *psp* promoters (Chapter 5).

Next the static polar foci were analysed under non-stress or stress conditions using photobleaching analysis. Figure 6.11A represents the photobleaching traces with its corresponding filter traces. The distribution comparing the stoichiometries of V-PspA polar foci under non-stress and stress conditions shows a clear shift in the distrubution towards higher order oligomers with stress (See graph Figure 6.11B). The distribution is centered near a 4-mer under non-stress conditions while more to a 10-mer under stress conditions (see Figure 6.11B).

During stress V-PspA in polar complexes is found as both low order and high order assemblies as illustrated in the diagrams Figure 6.12 . It is possible that under stress V-PspA assembles as low order complexes in the polar regions of the cell, some of which may be regulatory whereas others may be “en route” to forming higher order effector complexes (see Figure 6.12B). This data also imply that the poles of *E. coli* are not only the regulatory centers, but also the storage and collection center for PspA to assemble and then further redistribute within the cell. Photobleahcing analysis of Venus-PspF and Venus-PspA established that the PspF and PspA oligomeric states *in vivo* is a low-order oligomer/hexamer associated as PspF-PspA nucleoid-bound inhibitory complex under non-stress conditions (Mehta *et al*., 2013). Under stress, PspA switches its dominant partner from PspF to PspBC, where PspF is associated with transcription activation complex at the nucleoid (Yamaguchi and Darwin, 2012).

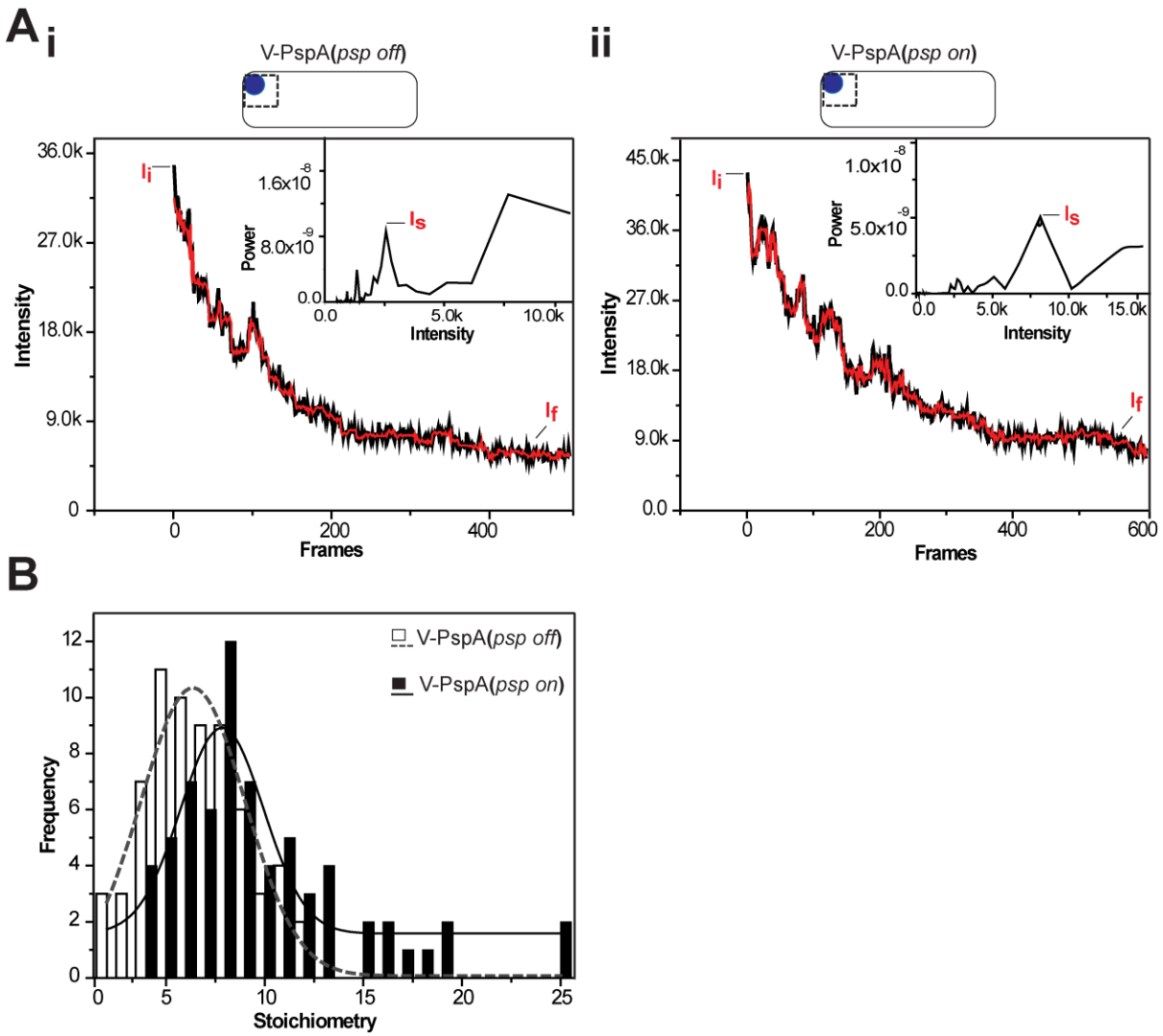

Figure 6.11 **Comparison of stoichiometry of V-PspA under non-stress and stress conditions:** (A-i) The cartoon of the *E. coli* cell defines the V-PspA polar localised foci observed under non-stress conditions (*psp off*), which were used for the analysis of photobleaching. And the graph represents the photobleaching traces obtained for the foci (black) with the corresponding filtered trace (red) determined by employing the Chung-Kennedy algorithm. The inset represents the power spectrum used to obtain sample size (I_s). (A-ii) The photobleaching trace and the corresponding filtered trace for V-PspA polar foci under stress conditions (*psp on*) and inset shows the Power spectrum. The I_s was calculated from the power spectrum. (B) The stoichiometry for the V-PspA foci under non-stress and stress conditions was calculated using the formulae- I_i-I_f / I_s and the graph shows the distribution of stoichiometries calculated for V-PspA in *psp off* (number of cells = 67) and *psp on* (number of cells = 67), which shows a shift in distribution to higher order oligomers in the stress conditions (black bars, black straight line).

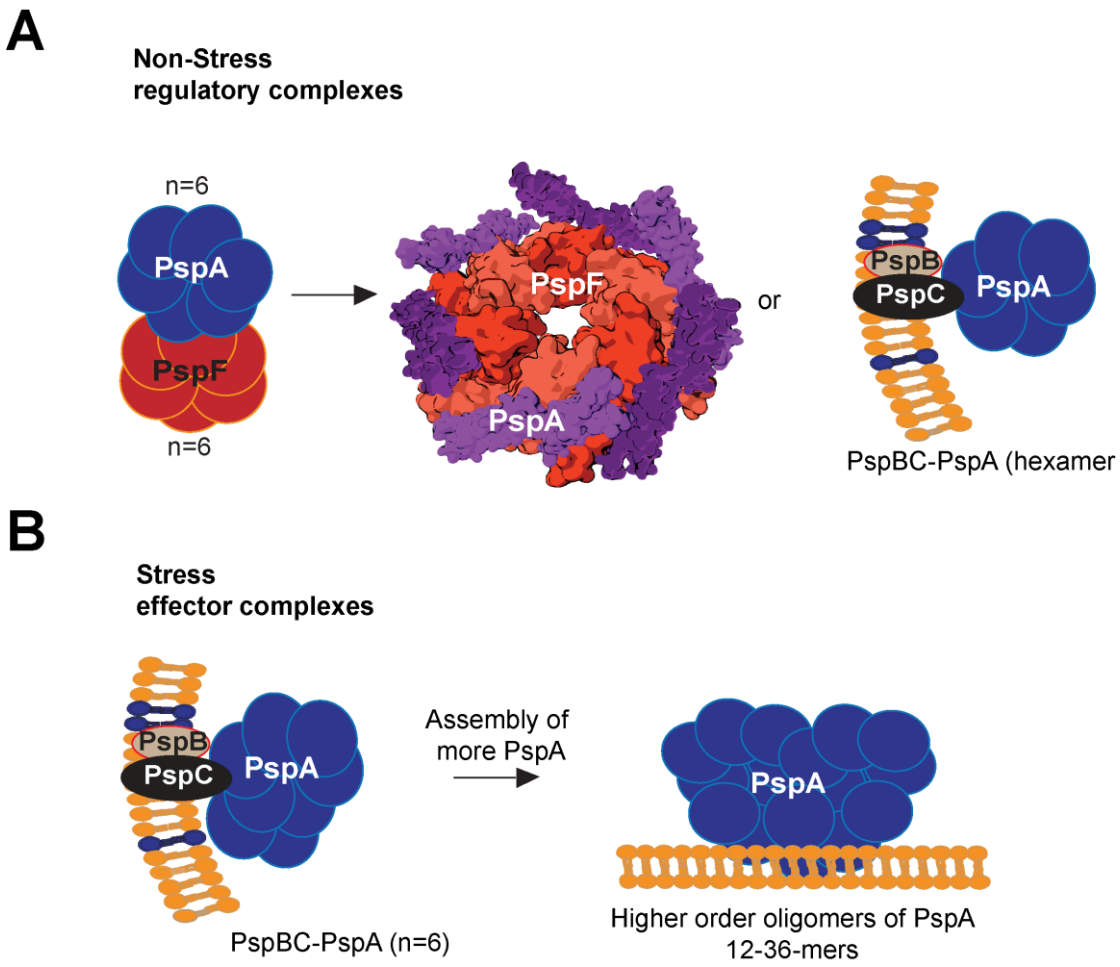

Figure 6.12 **Schematic to show the different oligomeric states of V-PspA in cells:** (A) The hexamer of PspA either associates with a hexamer of PspF as part of the inhibitory complex bound at the *psp* promoter, or six monomers of PspA could also associate with the hexameric PspF ring to form an inhibitory complex as shown by the 3D diagrams (courtesy Edward Lawton). The hexamer of PspA could also form regulatory complex with PspBC at the polar membrane regions under non-stress conditions. (B) Under Psp activating stress conditions PspA oligomerises into higher order oligomers starting from the polar membrane and then resorts to spiral dynamics along the lateral stressed membrane.

Yamaguchi *et al*., 2013 showed that PspA and PspBC colocalized at the poles under stress conditions. These polar complexes of PspA-PspBC are regulatory that help in signalling and mounting the Psp response under stress conditions (Engl *et al*., 2009 and Yamaguchi *et al*., 2013). PspA is a dual action protein in the cell resorting to many different oligomeric states and many different cellular localisation. Thus it is vital to characterise the membrane association of V-PspA and how it governs cellular functioning of PspA under non-stress and stress conditions.

6.2.7 *Membrane association of V-PspA*

The bacterial IM in Gram-negative cells consits of around 80% of non-charged phosphotidylethanolamine (PE) and 15% phosphotidylglycerol (PG) and around 5% cardiolipin (CL) (Romantsov *et al*., 2007 and Foss *et al*., 2011) both being charged anionic lipids. The respective subcellular localisation of these lipids has been characterised and has been reported in Foss *et al*., 2011, PG has been found to localise in lateral as well as polar regions of the cell while CL mainly localised at the poles Figure 6.13.

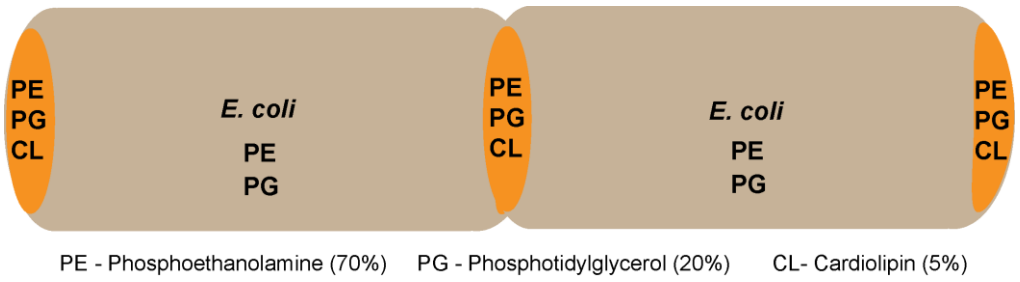

Figure 6.13 **Schematic presentation of the *E. coli* cell with respective anionic lipid localisations**: The polar and lateral membrane consists of – PE (phosphotidylethanolamine, total 70-75%) and PG (phosphotidylglycerol, total 15-25%) and CL (cardiolipin total ~5%) (Foss *et al*., 2011). The lateral membrane is constituted of PE and PG while CL is predominantly localised at the polar membrane along with PE and PG.

Along with lipids the bacterial membrane also encompasses a network of morphogenetic proteins, supports the so called bacterial rafts and also associates with the bacterial cytoskeletal proteins such as actin-like MreB (van den Ent *et al*., 2010). It also supports the peptidoglycan synthesis machinery proteins such as RodZ, MurG etc (White *et al*., 2010). The focus of this part of the chapter will be to determine if some of these determinants influence V-PspA organisation and functions during stress.

6.2.7.1 Phosphotidylglycerol influences PspA effector function

PspA was shown to directly bind PG *in vitro* (Kobayashi *et al*., 2007). In this thesis the effect of PG on the effector function of PspA was studied *in vivo.* A Δ*pgsA::kan* mutant strain lacking in both PG and CL was used, CL was absent as PG is the precursor for the formation of cardiolipin by cardiolipin synthase. These cells were still viable. The absence of PG (Δ*pgsA*) did not induce the Psp response (graphs in Figure 6.14A) under non-stress conditions. Furthermore, the induction of the Psp response was not hampered in Δ*pgsA* cells under stress conditions (Figure 6.14A).

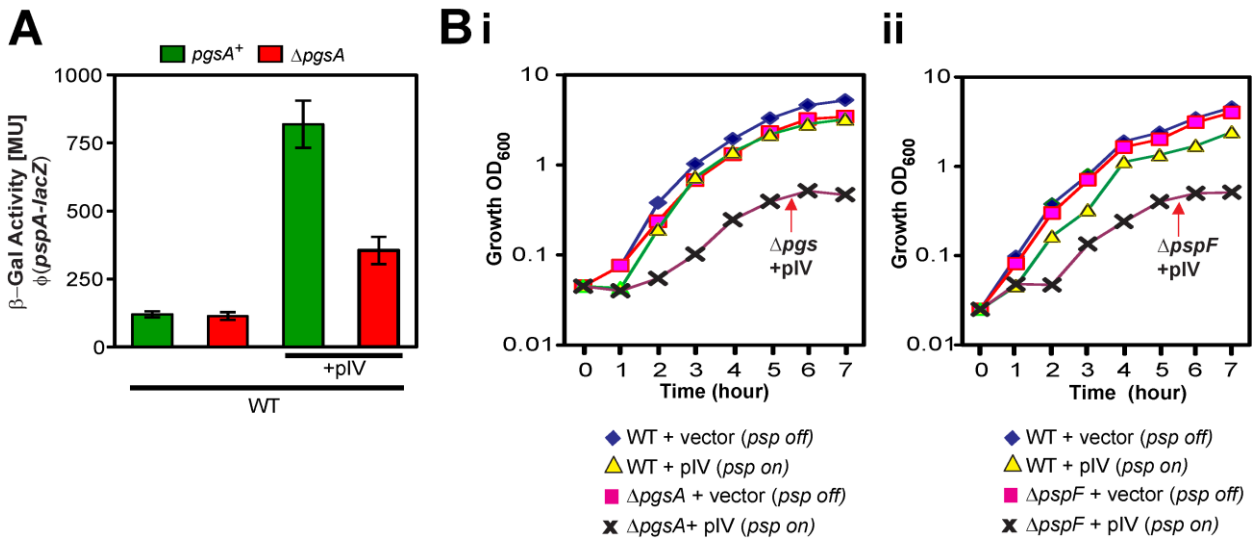

Figure 6.14 **Anionic lipids such as PG effect PspA functionality:** (A) β-Gal activity of the ϕ (*pspA-lacZ*) in WT and *ΔpgsA* cells under non-stress (empty vector pBR325D) or stress (+pIV, pGJ4) conditions. (B) Growth curve comparing growth of (i) WT and *Δpgs* and cells under non-stress and stress conditions and (ii) WT and *ΔpspF* cells under non-stress and stress conditions.

These results indicate that the change in the membrane anionic lipid composition is not an inducing signal for the Psp response. The overproduction of PgsA from a plasmid also did not induce the Psp response in WT cells under non-stress conditions (Appendix-3-C). The *ΔpgsA* cells exhibited impaired growth under stress conditions, comparable to a *ΔpspF* mutant under stress conditions as shown in Figure 6.14B. The absence of PG might have an effect on the effector function of the PspA *in vivo* in agreement with *in vitro* observations that PspA directly binds the PG to repair the membrane and conserve the pmf under stress (Kobayashi *et al*., 2007). The *ΔpgsA* deletion could not be successfully introduced into cells producing V-PspA using P1 transduction because the membrane was too damaged to sustain phage infection to form lysogens for transduction. The SMI of eGFP-PspA produced in the *ΔpgsA* cells could not be achieved anyway because the *ΔpgsA* cells were not viable in minimal media.

6.2.7.2 Cardiolipin affects the PspA polar localisation and *psp* induction

The anionic phospholipid cardiolipin (CL) has affinity for the membrane curvature is at the cell poles (Renner and Weibel, 2011) as shown in the Figure 6.13. PspA possibly forms polar complexes through direct interactions with the PspBC complex (Engl *et al*., 2009 and Yamaguchi *et al*., 2013).

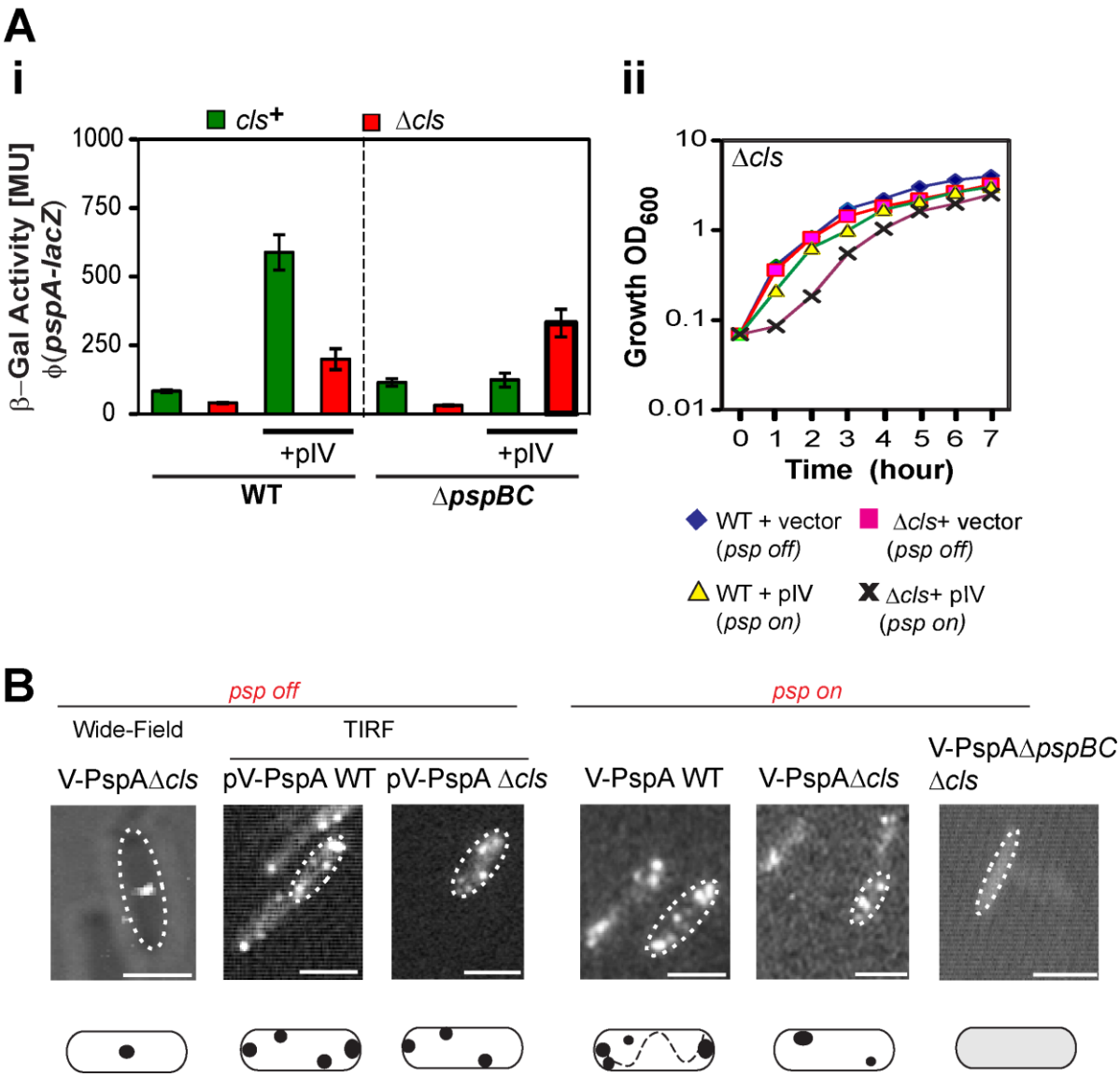

Figure 6.15 **Effects of *Δcls* on PspA functionality**: (A-i) β-Gal activity of the ϕ (*pspA-lacZ*) in WT, *Δcls*, *ΔpspBC Δcls* cells under non-stress (empty vector pBR325D) or stress (+pIV, pGJ4) conditions. (A-ii) Comparing growth rates of the MG1655 (WT) and *Δcls* under non stress (vector) or stress (+pIV) conditions. (B) Wide field and TIRF SMI of V-PspA in *Δcls* in non-stress conditions, the merge images mainly showed central foci. The TIRF image of V-PspA produced from plasmid is illustrated in the WT and *Δcls* strain showing the loss of polar foci. Under stress conditions V-PspA showed loss of spiral dynamics in *Δcls* and no foci were observed for *ΔpspBC Δcls* under stress. Each image has been represented with a corresponding cell cartoon showing the foci localisation with the black circular spot. The scale bar of the images is 1 μm.

The contribution of CL to PspA functionality and to cell growth in a *cls* mutant (lack of CL) was examined. V-PspA in *E. coli Δcls* background under non-stress or stress was imaged using wide field and TIRF modes. With the help of *in vivo* β-Gal assays and growth assays the effect of expression from *pspA* promoter was tested in the *Δcls* mutant as shown in Figure 6.15A. The lack of CL did not have an impact on the transcription of *psp* genes and the excess amounts of CL did not induce *psp* (Appendix-3-D) under non-stress conditions. However cells lacking CL showed reduced *psp* induction under stress and

notably the induction of the Psp response was somewhat independent of PspBC as shown in graph Figure 6.15A in *Δcls* cells as compared to WT cells. Under stress conditions the growth of the *cls* mutant was impaired in the logarithmic phase but overall final growth was not limited (See Figure 6.15Aii). After these *in vivo* assays the V-PspA in the *Δcls* cells was studied by SMI as illustrated in the images in Figure 6.15B. Under non-stress conditions *Δcls* cells displayed central V-PspA foci and very few polar foci, as observed in the WT cells (see V-PspA *Δcls* and the plasmid borne V-PspA in *Δcls* mutants in Figure 6.15B). Under stress the lateral membrane associated V-PspA foci exhibited changed dynamics (in lacking the helix-like circumferential dynamic of WT) in *Δcls* cells (see V-PspA (*psp on*) images in Figure 6.15B). The double mutant of CL and PspBC (*ΔpspBCΔcls*) showed no foci as seen with the absence of PspBC in WT cells. These results show that CL establishes the PspBC-dependent induction of Psp response and governs the polar PspA localisation. PspA as an effector does not directly bind CL *in vitro* (Kobayashi *et al*., 2007) and the position of the PspBC-dependent PspA regulatory complexes being close to poles (Engl *et al*., 2009; Lenn *et al*., 2011 and Yamaguchi *et al*., 2013) underlines the possibility that the CL/negative curvature might be involved in localisation and function of the PspBC sensors and/or PspA-BC complexes.

6.2.7.3 Lipid rafts might exist in bacterial membrane and regulate the PspA functionality

Anionic lipids such as PG and CL are enriched in specific domains in the cells as also shown in Figure 6.13 (Matsumoto *et al*., 2006 and Mileykovskaya and Dowhan, 2009). It has been shown that heterogeneous domains of lipids can drive localisation of many classes of proteins (Romantsov *et al*., 2007). CL has been shown to mediate the localisation of integral membrane proteins such as the ProP symporter (Romantsov *et al*., 2007) and membrane associated proteins such as MinD (Mileykovskaya *et al*., 2003) and the PspA effector interacts with PG *in vitro* (Kobayashi *et al*., 2007). The lipids may govern the compartmentalisation or sectoring of the membrane but the role of proteins in organising such domains is unknown (Bach and Bramkamp, 2013). One such abundant membrane protein is called flotilin in eukaryotic cells, which has been isolated from detergent resistant membrane domains and therefore has been speculated to be important for the organisation of lipid rafts or special membrane microdomains (Bach and Bramkamp, 2013). Recently, a potential flotilin 1 homologue in *E. coli* called YqiK has been identified that might act in scaffolding detergent-resistant micro-domains under specific stress conditions (Hinderhofer *et al*., 2009 and López and Kolter, 2010) in bacterial cells. The *Bacillus subtilis* flotilin equivalent called YuaG has been shown to actively interact with many membrane proteins involved in protein secretion, cell wall metabolism, transport and even membrane related signalling processes. Such YuaG mediated lipid raft proteins influence membrane fluidity and introduce heterogeneity in the membrane organisation (Bach and Bramkamp, 2013). It was also shown that membrane embedded protein machineries require a specialised lipid environment and even the

oligomerisation of proteins could be defined by the properties of phospholipids (Lee *et al*., 2003 and Bach and Bramkamp, 2013). Bach and Bramkamp (2013) also published an important result where they showed that the functioning of Sec machinery is highly dependent on the interfacial areas between highly ordered and disordered membrane domains. In the absence of flotilin such suitable areas become limited and that could affect the recruitment and organisation of the Sec pathway.

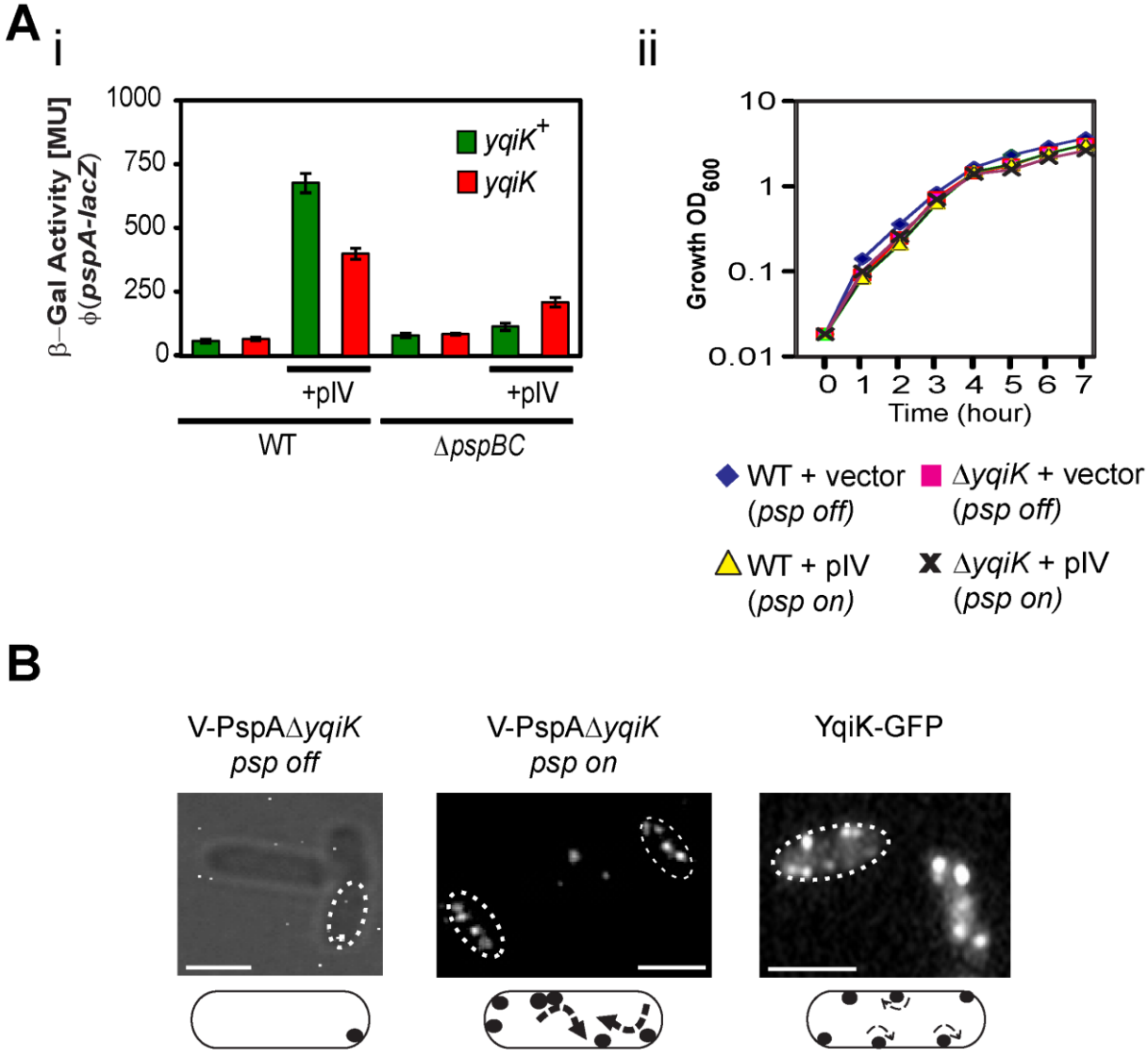

Figure 6.16 **The effect of lipid raft protein YqiK on the organisation and dynamics of V-PspA and the Psp response:** (A-i) β-Gal activity of the ϕ (*pspA-lacZ*) in WT, *ΔyqiK*, *ΔpspBC ΔyqiK* cells under non-stress (empty vector pBR325D) or stress (+pIV, pGJ4) conditions. (A-ii) Comparing the growth rates of strains MG1655 (WT) and *ΔyqiK* under non stress (vector) or stress (+pIV) conditions. (B) Wide field SMI of V-PspA in *ΔyqiK* in non-stress conditions showed very few foci, shown here as a single foci observed in the focal plane. Under stress conditions V-PspA showed more foci, foci localised at the lateral membrane showing local movement along the membrane not spiral dynamics (as shown by the arrows). YqiK-GFP was also imaged in WT cells to understand the precise localisation of YqiK in the cell. It formed patches interspersed along the membrane with local movement along the membrane. Scale bar = 1μm

E. coli YqiK, *Bacillus* YuaG and eukaryotic flotilin could all be vital for the recruitment of proteins to specific lipid domains and consequently governing their functional localisation in cells. To address the possible role of anionic lipid-rich domains in signal perception, IM-interactions and the effector function of PspA the contribution of YqiK was investigated (Hinderhofer *et al*., 2009 and López and Kolter, 2010). Firstly, the absence of YqiK was studied to evaluate its impact on the induction of the Psp response and examine how its loss affects the growth of the cells. The lack of YqiK (∆*yqiK*) did not induce the Psp response but resembled the Psp induction in the *Δcls* cells with reduced induction and was partially PspBC-independent as shown in the graph (see Figure 6.16Ai). The growth of the *ΔyqiK* cells under stress was very similar to WT cells (see growth curve graph Figure 6.16Aii). Like any of the PG or CL mutant cells, the *yqiK* mutation did not impact on unregulated transcription of *psp* genes in the *ΔpspA* mutant strain Appendix-3D). The overproduction of YqiK did not induce *psp* in the WT cells (Appendix-3D).

The localisation of V-PspA in ∆*yqiK* cells was slightly different from WT cells under stress conditions, with lateral V-PspA showing local movements rather than the spiral dynamics seen in WT cells (Figure 6.16B). Under non-stress conditions the V-PspA foci were not so easily imaged, a single central foci was observed as shown in the Figure 6.16B.

YqiK-GFP foci localised at the membrane and formed more static (with only local movement) complexes in polar and lateral membrane regions of the cell (see Figure 6.16B). It was shown that YqiK influences and probably occupies certain specific locations on the bacterial membrane suggesting lipid rafts occur within the bacterial membrane. These lipid rafts might govern the recruitment of specific membrane associated proteins such as PspA, especially when encountering membrane stress. The *in vivo* assays show that the phospholipids such as PG as well as specific lipid raft proteins such as YqiK could play a part in the PspA dependent signalling of the Psp response during stress conditions. Additionally, CL contributes to the polar membrane localisation of the Psp proteins affecting the regulatory aspect of the response.

6.2.7.4 Bacterial cytoskeletal involvement in the Psp response

Eukaryotic cells show a unique form of molecular clustering along the membrane facilitated by the treadmilling motion of actin filaments (Goswami *et al*., 2008) linked to lipid microdomains. In the same way bacterial cells could also have close relationship between the regulatable lipid microdomains and cytoskeletal protein. Such cytoskeletal potential targets in *E. coli* could be the actin-like MreB proteins and the proteins forming part of the phenolic glycolipids (PGL) synthesis machinery such as RodZ, MurG etc. This part of the chapter elaborates on the potential role of cytoskeletal protein like MreB and peptidoglycan synthesis machinery proteins like RodZ on the regulatory and effector role of PspA.

6.2.7.4.1 MreB – cytoskeletal protein in bacteria

The key protein of the cytoskeletal system in *E. coli* is MreB (an actin-homologue) which assembles along the long-axis in a spiral – like configuration and maintains cell shape (Bendezú *et al*., 2009 and White *et al*., 2010). MreB plays an important role in maintaining cell shape as a key cytoskeletal protein by not only organising the newly synthesised peptidoglycan along the helical MreB path and also by recruiting murein synthases (van den Ent *et al*., 2010 and White *et al*., 2010).

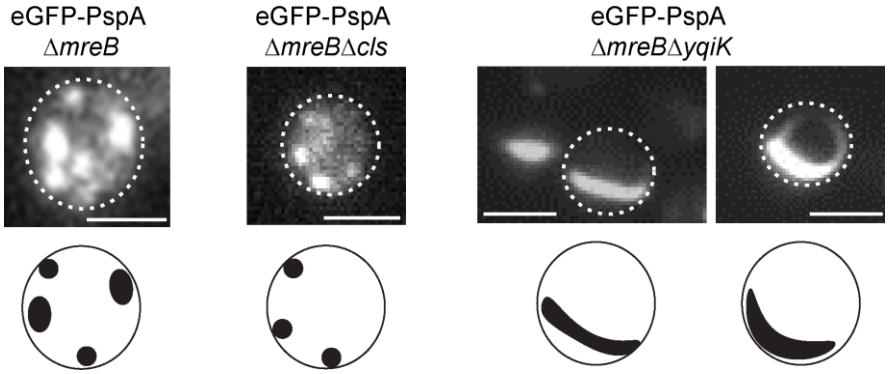

Figure 6.17 **The connection between cytoskeleton and membrane determinants and their influence on PspA**: The Figure illustrates the wide-field images of eGFP-PspA in *ΔmreB* cells and in the double mutants *ΔmreBΔcls* and *ΔmreBΔyqiK*. The changes in the localisation of PspA are highlighted in the corresponding schematic diagrams of the spherical cells. The MreB organises the lateral PspA foci and in the absence of MreB the helical dynamics of eGFP-PspA were abolished. CL does not affect the eGFP-PspA localisation in the absence of MreB. While in the absence of YqiK and MreB, eGFP-PspA localisation changed from defined localised multiple foci to a single disc like macro feature. Scale bar = 1µm

The effect of MreB on the organisation of effector PspA was studied using eGFP-PspA because the MreB deletion was not successfully introduced in cells with chromosomal V-PspA. The plasmid borne eGFP-PspA (pCE1- Table 2.4) with leaky expression under non-stress conditions mimicked the V-PspA amounts in pIV induced stress conditions (Engl *et al*., 2009 and see images on Figure 6.4). *E. coli* cells lost the rod shaped morphology in *ΔmreB* cells and were spherical in their morphology (see Figure 6.17). Thus the spherical cells lost their defined poles as compared to the poles of the rods. The eGFP-PspA fusion (having similar behaviour to V-PspA under stress) localised as specific membrane patches that displayed more locally restricted movements (as also published in Engl *et al*., 2009 and Figure 6.17). These localised foci at the membrane could be the delegated regulatory complexes usually associated with the poles of the rod shaped bacterial. The lateral spiral dynamic eGFP-PspA foci were not observed in the spherical *ΔmreB* cells as shown in the cell cartoons (Figure 6.17). MreB could form the highway recruiting PspA onto the spiral path along the lateral membrane. However PspA contact with the membrane could be mediated by many other membrane proteins and components such as anionic lipids, lipid rafts and PGL proteins such as RodZ. Therefore the studies were complemented by studying double mutants of MreB and CL, MreB and YqiK, and MreB and RodZ.

The double mutant of MreB and CL showed similar eGFP-PspA localisation in terms of the foci along the membrane with restricted movement in the cell (as shown in Figure 6.17). Thus the absence of CL did not aggravate the effect of MreB. As established in Section 6.2.7.2- where CL was associated with the polar regulatory complexes under non-stress conditions, PspA localisation under stress conditions did not depend on the CL. The MreB-dependent lateral dynamics of PspA (shown by eGFP-PspA in WT cells) is not obviously regulated in a CL-dependent manner.

Next the effect of lipid raft protein YqiK was examined on MreB-dependent PspA localisation. YqiK has been shown to play a role in defining the interaction of PspA to the lateral membrane, possibly via interaction with PG. Thus YqiK governs the localisation of effector PspA under stress conditions. Thus, it was possible that YqiK could form a link between MreB and the lateral membrane regions. The eGFP-PspA localisation was totally disrupted in the Δ*mreB* Δ*yqiK* mutant (see Figure 6.17). In the absence of MreB and YqiK, eGFP-PspA foci localised as a membrane static "disc-shaped" macro-feature. This showed the existence of a very important link between MreB and lipid microdomains which could be mediated by lipid raft protein YqiK. Thus MreB and YqiK could work coherently to establish the membrane association of PspA, functioning as an effector of the stress response.

6.2.7.4.2 Role of RodZ in PspA effector function

Cell morphogenetic such as RodZ colocalize with MreB spiral patches and anchor its connection with the IM (MreB can also bind membrane without the aid of RodZ) (Alyahya *et al*, 2009 and van den Ent *et al*., 2010). RodZ plays a crucial role in functionally connecting MreB with the periplasm. It is an inner-membrane associated protein with its C-terminal extending into the periplasm. It facilitates the production and localisation of phenolic glycolipids (PGL) which form an important connection between the inner membrane and the cell wall core in the periplasm (van den Ent *et al*., 2010 and White *et al*., 2010).

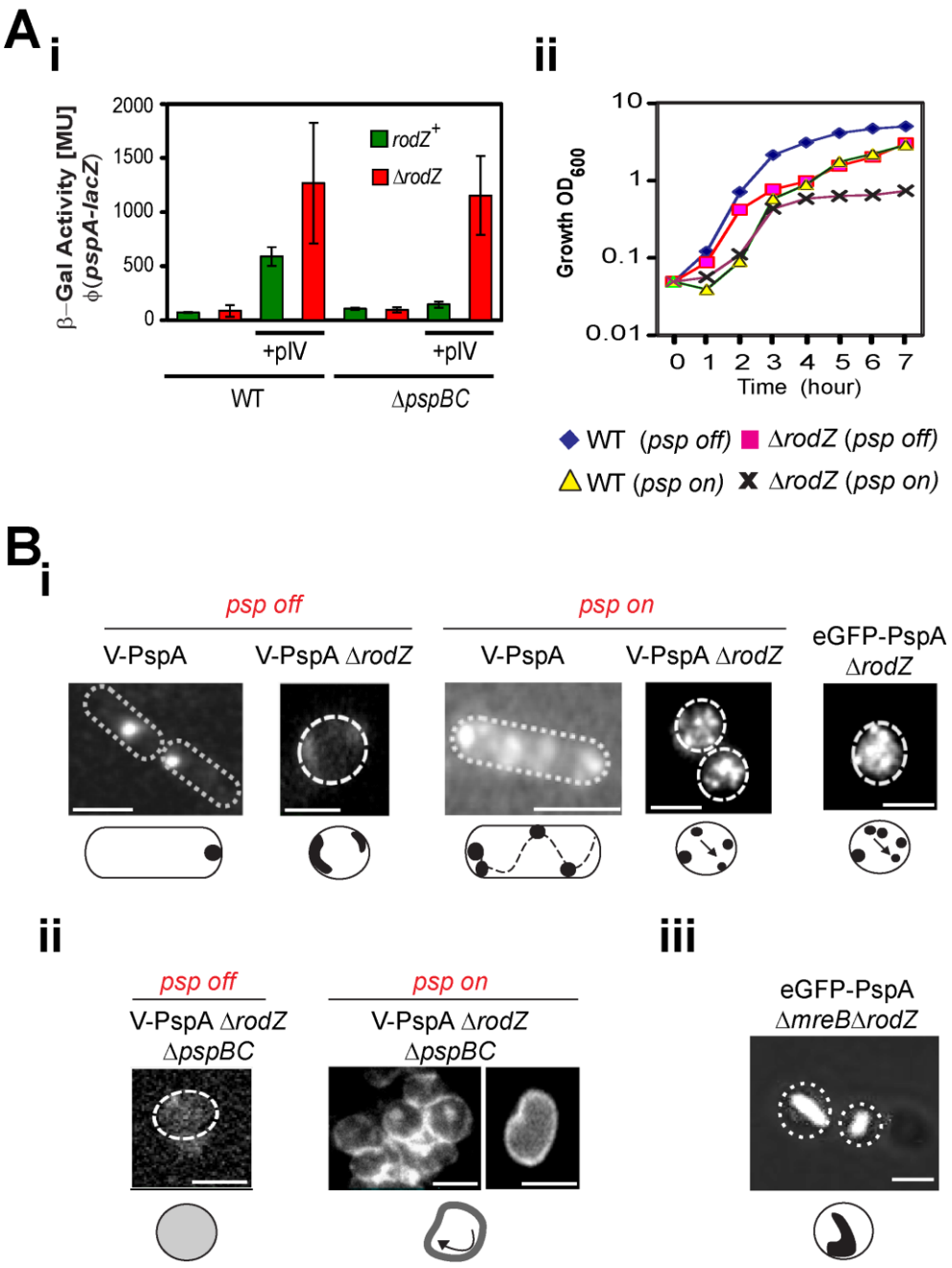

Figure 6.18 **The importance of RodZ in effector function of PspA**. (A-i) β-Gal activity of the ϕ (*pspA-lacZ*) under non-stress (empty vector- *psp off*) or stress (+pIV plasmid- *psp on*) conditions measured in WT (MG1655), *ΔrodZ, ΔpspBC*, and *ΔpspBC ΔrodZ* cells. (A-ii) Growth of the WT and *ΔrodZ* mutant under non stress (vector) and stress (+pIV) conditions. (B-i) V-PspA in *ΔrodZ* cells under non-stress and stress conditions. The wide-field images show that the cells lose their rod shaped morphology and therefore no poles can be distinguished. V-PspA foci lose diffraction limited bright fluorescent spots in *ΔrodZ* cells under non-stress conditions. Under stress conditions V-PspA is present in higher amounts and localises along the membrane and in patches along the cell membrane with local movement. The localisation and dynamics of eGFP-PspA in *ΔrodZ* cells resembles V-PspA +pIV in *ΔrodZ* cells. (B-ii) Images of V-PspA in *ΔpspBC ΔrodZ* cells in non-stress conditions do not show any foci. The images in the stress conditions show decoration of the membrane. The V-PspA foci move along the membrane as illustrated in the cellular cartoon. (B-iii) The image shows the localisation of eGFP-PspA in the *ΔmreB ΔrodZ* double mutant displaying complete disruption of V-PspA localisation forming a single static macro-feature. Scale bar in images is 1 μm.

In this way RodZ couples the movements of the PGL synthesis machinery and MreB filaments along the membrane (van den Ent *et al*., 2010 and White *et al*., 2010). It is important to probe the contribution of RodZ to PspA localisation and how PspA could interact with RodZ in response to membrane stress. The membrane regions associated with RodZ (PGL synthesis machinery) could be the target for the MreB-driven lateral membrane PspA effectors. The lateral membrane associated PspA might support the elongation of the lateral cell wall upon membrane stress. It is also important to study how RodZ and MreB work in concert with respect to the Psp response. In order to address this potential link between the PspA and RodZ, *rodZ* mutants were used to perform *in vivo* assays. The absence of RodZ did not influence the expression from the ϕ (*pspA-lacZ*) in the β-Gal assay (see graph Figure 6.18Ai). The overproduction of RodZ did not induce the Psp response in WT cells under non-stress conditions (Appendix-3-C). The absence of RodZ did not induce *psp* but caused PspBC-independent induction of *psp* genes upon stress (see graph Figure 6.18Ai). The *psp* induction under stress was more pronounced in Δ*rodZ* as compared to WT cells (see graph Figure 6.18Ai). The growth of the *ΔrodZ* mutant was impaired in comparison to WT cells and the growth defects were similar to *ΔpspF* cells (See graph Figure 6.18Aii). RodZ was shown to be important for the induction of the Psp response during stress conditions. The effect of RodZ was independent of PspBC sensors under pIV inducing stress conditions. This indicated that the absence of RodZ aggravates the Psp response. Next the changes in localisation changes of PspA in *ΔrodZ* cells were examined.

The Δ*rodZ* cells displayed defective cell morphology; the cells appeared as short oblong spheres (see images in Figure 6.18B). The SMI studies in *ΔrodZ* were carried out with the chromosomal V-PspA under non-stress and stress conditions and using plasmid borne eGFP-PspA. As in the spherical MreB mutant cells, the short-oblong *ΔrodZ* cells also did not have defined poles. As shown in the Figure 6.18Bi, V-PspA under non-stress conditions did not show any defined foci. The V-PspA foci under stress conditions localised in patches along the membrane with some local movements (see Figure 6.18Bi- *psp on* images). The same observation was made with plasmid borne eGFP-PspA. In Δ*rodZ* cells the usual distinct polar membrane foci were not distinguishable because of the oblong shaped cells (see Figure 6.18Bi). The deletion of PspBC in *ΔpspBC*Δ*rodZ* double mutant cells did not show any discernible foci under non-stress conditions (see Figure 6.18Bii) and V-PspA under stress conditions in *ΔpspBC*Δ*rodZ* cells decorated the entire IM and exhibited movement along the membrane (see Figure 6.18Bii). As shown in Figure 6.18Biii, the eGFP-PspA in the double Δ*mreB*Δ*rodZ* mutant localised as a static elongated single macro-feature that resembled the structure seen in Δ*mreB*Δ*yqiK* cells. This shows that RodZ assists in an interaction of MreB with the specific IM regions. Therefore, RodZ is a vital membrane determinant assisting MreB in recruiting PspA along the damaged membrane regions during the stress

response. Such specific membrane domains could be rich in PG and associate with the so-called bacterial lipid rafts in the membrane.

6.3 Conclusion

REGULATOR PspA – *psp off*	EFFECTOR *PspA – psp on*
Localise at poles and nucleoid	Localise at poles or lateral membrane following a helical path
Membrane associated dynamics, slower compared to V-PspF	Much slower membrane associated movement
Predominantly lower order oligomer- around hexamer	More high order oligomers – 10-mer or more
PspBC dependent localisation of PspA	
MEMBRANE DETERMINANTS IN *psp off*	MEMBRANE DETERMINANTS IN *psp on*
Deletion of PG does not induce Psp	Deletion of PG impairs growth
CL governs the polar PspA localisation	CL deletion induces Psp independent of PspBC in the presence of pIV Lateral membrane association does not show spiral configuration
Absence of RodZ disrupts PspA localisation	Absence of RodZ aggravated the Psp response in the presence of pIV. Induction was PspBC independent Localisation of PspA was disrupted Absence of RodZ and MreB totally disrupted PspA localisation
MreB ,YqiK and RodZ disrupted the lateral dynamics of PspA	

Table 6.1 The table sums up the results discussed in this chapter highlighting the changes in PspA localisation, dynamics and oligomeric state associated with the switch to stress conditions. It also highlights the major membrane determinants of PspA effector function.

In this chapter the intracellular mechanisms that lead to the switch of regulated Psp response to the activating state have been evaluated. The major facilitator of the switch is the dual function protein PspA showing multiple cellular interactions with proteins, lipids and membrane proteins as listed in Table 6.1.

Under non stress conditions the hexameric PspA binds a PspF hexamer to form the inhibitory complex (Figure 6.12A) that resides in the nucleoid bound to target *psp* promoters. This inhibitory complex PspF-PspA often communicates with membrane integrated PspBC sensors to check the status of the membrane at the poles of the cells. If the membrane stress is perceived at the poles via PspBC, the PspF-PspA inhibitory complex could either resolve at the membrane or at the nucleoid. With stress induction, PspF stably binds the *psp* promoters activating their transcription. The chromosomally produced V-PspA (Section 6.2.2) foci were observed at the central or polar locations in the cells while in the stress conditions V-PspA localised at the polar and lateral membrane exhibiting a spiral configuration. The onset of stress also reduced the dynamics of V-PspA by 3.75 times suggesting a more pronounced membrane association (Section 6.2.5). The oligomeric state of PspA changed from hexamer to higher order oligomer (> 10-mer).

Besides the changes in the properties of PspA, the interaction with other accessory proteins is also very critical in establishing the response. Various anionic phospholipids, membrane associated proteins and bacterial cytoskeletal proteins assisted PspA in its effector role (see Table 6.1). Anionic lipids such as CL localised at the poles governed the organisation of the PspBC-PspA regulatory complex and helped in stress perception and signal transduction. PG rich regions may form lipid rafts that form a link between the PspA oligomers and the membrane association. The difference in anionic lipids, such as PG composition does not induce *psp* but changes in the chemical/physical (e.g. charge, curvature, fluidity) properties of the membrane are likely to contribute in generating the signal. It is hypothesized that the protonation of CL dominates micro-domains in the polar region (White *et al*., 2010) and so might be used as a cellular proton sink to further advance the stress signal.

The more general cytoplasmic membrane stress is linked with the disturbance in H^+ gradient and change in the membrane potential (e.g. reduction of polar CL and lateral membrane PG). PspBC may sense the change in IM charge/membrane potential via CL leading to switch in the PspC topology. PspBC controls the oscillations of Psp induction by either integrating or simply transducing the signal. Therefore, PspBC function as the signal transducers but also modulate the signal depending on its intensity. The pIV-dependent induction of *psp* in ∆*pspBC* cells is not effective (Model *et al*., 1997; Darwin, 2005; Joly *et al*., 2010) while extreme stress inducers such as 10% ethanol treatment or extreme temperatures lead to a PspBC independent Psp induction (Model *et al*., 1997 and Joly *et al*., 2010). It is proposed that under continual medium level membrane stress (e.g. with pIV) the PspBC are membrane status checkpoints and gates through which PspA under physiological level enters to bind the IM/PG and self- assembles (Jovanovic *et al*., 2010).

The purpose of PspA effector complexes could be firstly to target the damaged protein translocons in the polar regions and secondly to target the anionic lipid domains where RodZ (cell wall synthesis machinery) is localised. RodZ employs MreB to organise PspA into lateral dynamic complexes. As a result, laterally dynamic PspA complexes follow the route of MreB spirals and move circumferentially along the membrane. Membrane determinants such as RodZ, MreB and YqiK all affect the PspA effector complexes. It is possible that lipid rafts may exist in *E. coli* and the lipid raft protein YqiK may play a vital role in mounting the Psp response in the stress conditions. YqiK could also be essential in devising the vital link between MreB and the lipid microdomains and RodZ. The absence of RodZ leads to impaired growth of the cells under pIV inducing stress and also activated the Psp response independent of PspBC. Genomic analyses showed that RodZ function is conserved and unique to bacteria and that *rodZ* and *pgsA* genes are often adjacent, suggesting they are functionally linked (Alyahya *et al*., 2009). It is formally possible that PspA has a role in recruiting the membrane repair machinery. So far we have understood how intracellular protein interactions influence the functionality of PspA. However, there are aspects of intramolecular interactions between the different domains of PspA that can drive the different functions of PspA. The next chapter will describe some of the major structural domains within PspA and their specific roles contributing to dual function of PspA.

CHAPTER 7

7 The structural determinants of PspA govern its regulatory and effector roles

PspA is at the heart of the adaptive Psp response, where it streamlines and links membrane stress with the σ^{54} transcription machinery. PspA is a dual function protein which not only regulates the Psp response at the transcription level, but also manages the response by way of "repairing" the membrane. In this chapter the understanding of the spatial and temporal localisation of PspA (Chapter 6) will be extended further to examine the structural properties and domains of PspA. Clearly, there are structural determinants of PspA which are vital in order for PspA to exist in many different oligomeric states and interact with many different types of proteins. Figure 7.1 summarises in brief the role of helix domain 1 (HD1) which contains two putative N-terminal amphipathic helices (as suggested by secondary structure prediction software). Genetic and biochemical tools complemented with the SMI of plasmid borne fluorescent fusions of PspA mutants will be used to determine the outcomes of mutating, retaining or deleting different HDs and amphipathic helices. PspA has been shown to play a crucial role in membrane maintenance in all the three domains of life (DeLisa *et al*., 2004 and Joly *et al*., 2010). Hence an understanding of the structure-function organisation of PspA could help to understand many different PspA homologues present in different organisms such as Vipp1 in plants and cyanobacteria.

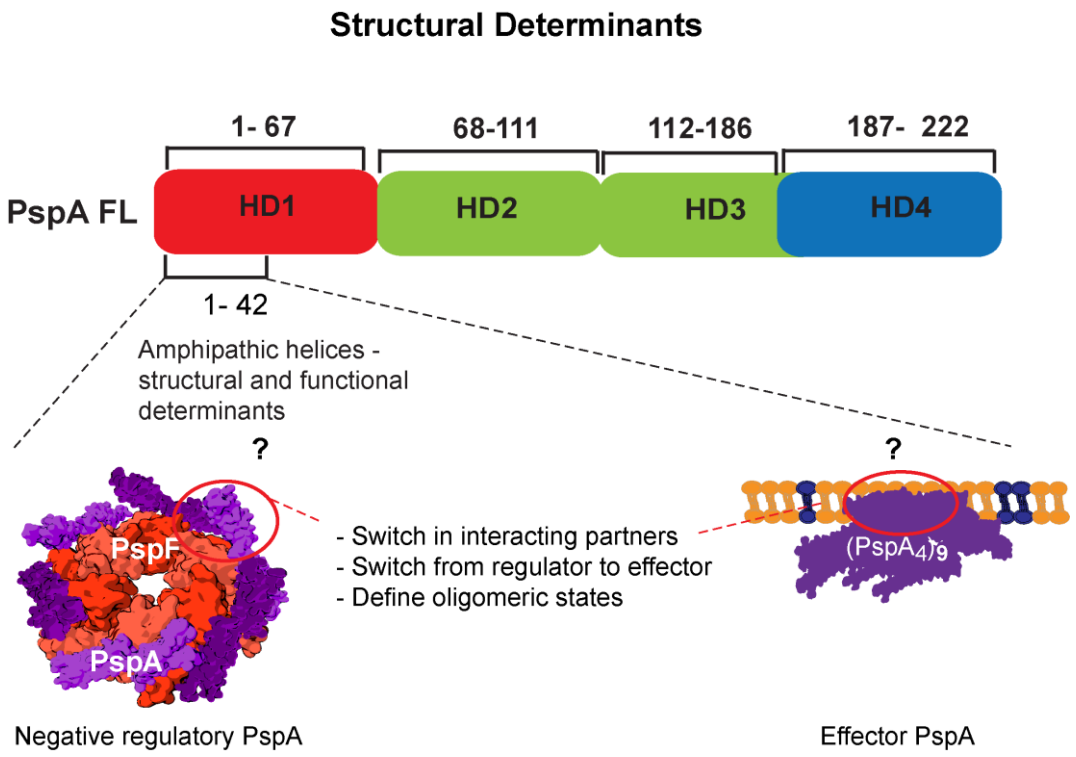

Figure 7.1 **Helical domains of PspA with emphasis on the HD1**: PspA consists of 4 helix domains. HD1 out of the 4 domains is the target of studies described in this chapter. The predicted structure of HD1 consists of structurally important putative amphipathic helices. As described in the illustration amino acids 1-42 could potentially form amphipathic helices. This diagram also indicates which features dictate binding to PspF, to IM and PspBC sensors and which govern PspA self-assembly.

7.1 Introduction

PspA exhibits multitude of protein-protein interactions and form many different functional complexes (Elderkin *et al*., 2005; Joly *et al*., 2009 and Joly *et al*., 2010). The many different aspects of PspA functionality are probably characterised by the different oligomeric states; such diverse oligomerisation can only be achieved by dynamic interactions between different PspA subunits (Joly *et al*., 2009).

In silico protein structure analysis predicted that PspA forms a helical coiled coil structure comprising of four helical domains (HD1-HD4) (Elderkin *et al*., 2005; Joly *et al*.,2009 and Joly *et al*., 2010) (see Figure 7.1). Typically coiled coil structures in prokaryotes are associated with membrane-bound proteins, signal transducers and also some membrane spanning transporters and secretion proteins (Liu and Rost, 2001 and Joly *et al*., 2010). Low resolution structural studies of PspA showed that it can form a high order oligomer (36-mer ring) or combine in a 1:1 ratio with hexameric ring of $PspF_{1-275}$ (Kobayashi *et al*., 2007 and Joly *et al*., 2009). Hankamer *et al*., 2004 reported 3-D reconstruction of gel filtered PspA visualized by electron microscopy and single particle analysis. They showed that the PspA self-assembly of a 36-mer displays a 9-fold symmetry with tetramers of PspA making up each of the 9 domains.

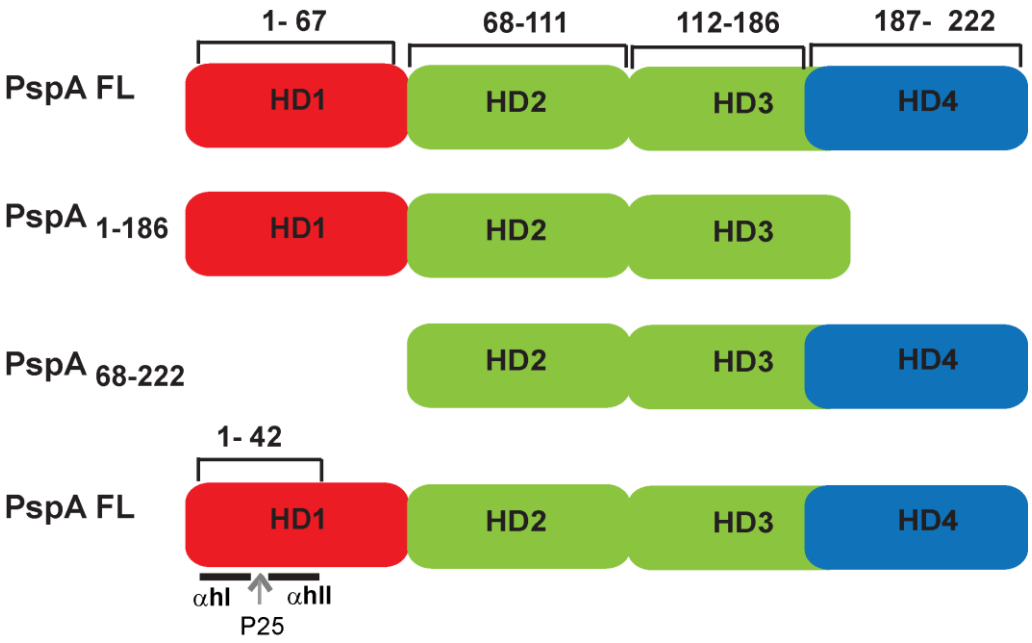

Figure 7.2 **Domain architecture of PspA helices:** The predicted domain architecture of the four helical domains of PspA highlighting the different organisation of the domains. The diagram explains the different mutant forms of PspA studied with the characteristic HD deletions. (Adapted from Joly *et al*., 2009).

A protein fragmentation approach, along with *in vitro* studies showed that each of the putative domains of PspA (see Figure 7.2) plays a certain role in the oligomerisation of PspA (Joly *et al*., 2009). Joly *et al*., 2009 reported that $PspA_{1-67}$ (HD1) or $PspA_{68-110}$ (HD2) on its own did not interact with $PspF_{1-275}$ and so did not inhibit PspF ATPase activity. However $PspA_{68-222}$ (HD2-HD3-HD4) showed weak interaction with $PspF_{1-275}$ and also inhibited ATPase activity when present in much higher concentrations than that needed by WT PspA. $PspA_{68-222}$ formed a heterodimeric complex with $PspF_{1-275}$. $PspA_{1-186}$ (HD1-3) self-assembled into monomer/dimer instead of 36-mer and still retained the ability to negatively control $PspF_{1-275}$ (Joly *et al*., 2009). $PspA_{68-186}$ (HD2-HD3) in the absence of HD1 and HD4 formed an apparent hexamer. This showed that HD4 counteracts the influence of HD1 interactions within PspA to form higher order oligomers. $PspA_{68-186}$ only weakly interacted with $PspF_{1-275}$ and had no inhibitory action on $PspF_{1-275}$. The 36-mer PspA does not have regulatory function and does not inhibit PspF ATPase activity since PspF was not found to associate with these large PspA assemblies (Joly *et al*., 2009). The deletion of either of the domains causes severe effects on the organisation of PspA oligomer (Joly *et al*., 2009 and Joly *et al*., 2010). HD1 is crucial in establishing the regulatory hetero-dodecameric complex between PspF and PspA (Joly *et al*., 2009) and also in modulating the oligomerisation of HD2-HD3. HD1 may have a central organising function.

HD1 has potential N-terminal amphipathic helices predicted by helical wheel projections using Java Applet called I-TASSER (discussed later in section 7.3.2). These amphipathic helices possibly facilitate the membrane anchoring and organisation of PspA. In line with this proposition is RNaseII in *E. coli*

which functions as an exoribonuclease and degrades mRNA, and even tRNA and stable RNAs in the absence of other cellular exoribonucleases (Lu and Taghbalout, 2013). The RNaseII self-assembly associates with the membrane forming a coiled structure along the cell periphery very similar to that of PspA observed in imaging studies (Lu and Taghbalout, 2013). Importantly it was shown that the membrane association and oligomerisation was dependent on the N-terminal amphipathic helices. The deletion or amino acid changes within the amphipathic helices impaired RNaseII membrane association, oligomerisation and functions. In the same way, it is possible that the N-terminal HD1 could also play a similar role in PspA, governing its membrane association, spiral organisation on the membrane and switch in oligomerisation from regulator to effector.

In this chapter the N-terminal HD1 will be studied in detail and some of its functional mutants will be tested for PspA regulatory and effector functions *in vivo* and *in vitro*.

7.2 Approaches to study helical domains

The protein fragmentation approach used previously (Joly *et al*., 2009) will be employed to study in detail the cross-talk and inter-dependency between different domains. Site-directed mutagenesis was performed to obtain different HD1 mutants of PspA, and *in vivo* and *in vitro* assays were performed (Methods section – 2.5.3.3).The regulatory role of PspA and the various mutant were studied by testing the regulation of expression from *pspA-lacZ* promoter fusion using β-Gal assays (Methods 2.8). The PspA effector role was studied by testing cell motility (Method 2.10). Over-production of PspA decreased bacterial motility independent of other Psp proteins; the cell motility assays were consistently used to empirically determine the motility effector function of PspA (Lloyd *et al*., 2004; Jovanovic *et al*., 2006 and Engl *et al*., 2009) (Methods 2.10). The interaction between PspF, PspC and PspA HD1 mutants was studied using bacterial two hybrid system (BACTH) (Methods 2.9). The SMI of plasmid borne eGFP fusions of the PspA HD1 mutants was done (Methods 2.15) using wide-field as well as TIRF microscopy.

Along with *in vivo* assays the specific His-tagged PspA HD1 mutants were purified and characterised *in vitro* to define their oligomeric states using gel filtration (Methods 2.11 and 2.12). The interaction of PspA mutants with PspF was studied using native gel assays (Methods 2.7.2). The inhibition of the PspF ATPase activity by the PspA HD1 mutants was reported (Methods 2.13).

7.3 Results

This section reports the results from the *in vitro* and *in vivo* imaging of the different structural and functional mutants of PspA. The strains and plasmids used in the experiments described in this thesis are listed Table 2.3 and Table 2.4.

7.3.1 PspA domains contribute to specific PspA functions but also work in coalition

As explained above and reported in Joly et al., (2009) the protein fragmentation approach for PspA proved to be very informative. Using the same approach, more detailed study into the roles of HD1 and HD4 domains of PspA is reported. It was hypothesized that HD1 and HD4 not only exhibit specific roles in establishing PspA functions but also have strong interactions. Figure 7.3 shows the results comparing *in vivo* assays between PspA FL, $PspA_{1-186}$ (HD4 absent) and $PspA_{68-222}$ (HD1 absent). Figure 7.3A shows the result of the β-Gal assay of $PspA_{1-186}$ (HD4 absent) produced in a *ΔpspA* strain (MVA27; Table 2.3) under non-stress and pIV inducing stress conditions (Methods 2.8). It showed that $PspA_{1-186}$, like PspA FL negatively regulated the expression from the *pspA* promoter *in vivo*. With the pIV induction of stress, the negative regulation of PspF by $PspA_{1-186}$ was abolished. $PspA_{68-222}$ (HD1 absent) did not negatively regulate the expression from *pspA* promoter in the non-stress activating conditions (in *ΔpspA* cells) (see Figure 7.**3**A). This result suggests that PspA HD1 is required for the negative regulation of PspF *in vivo*.

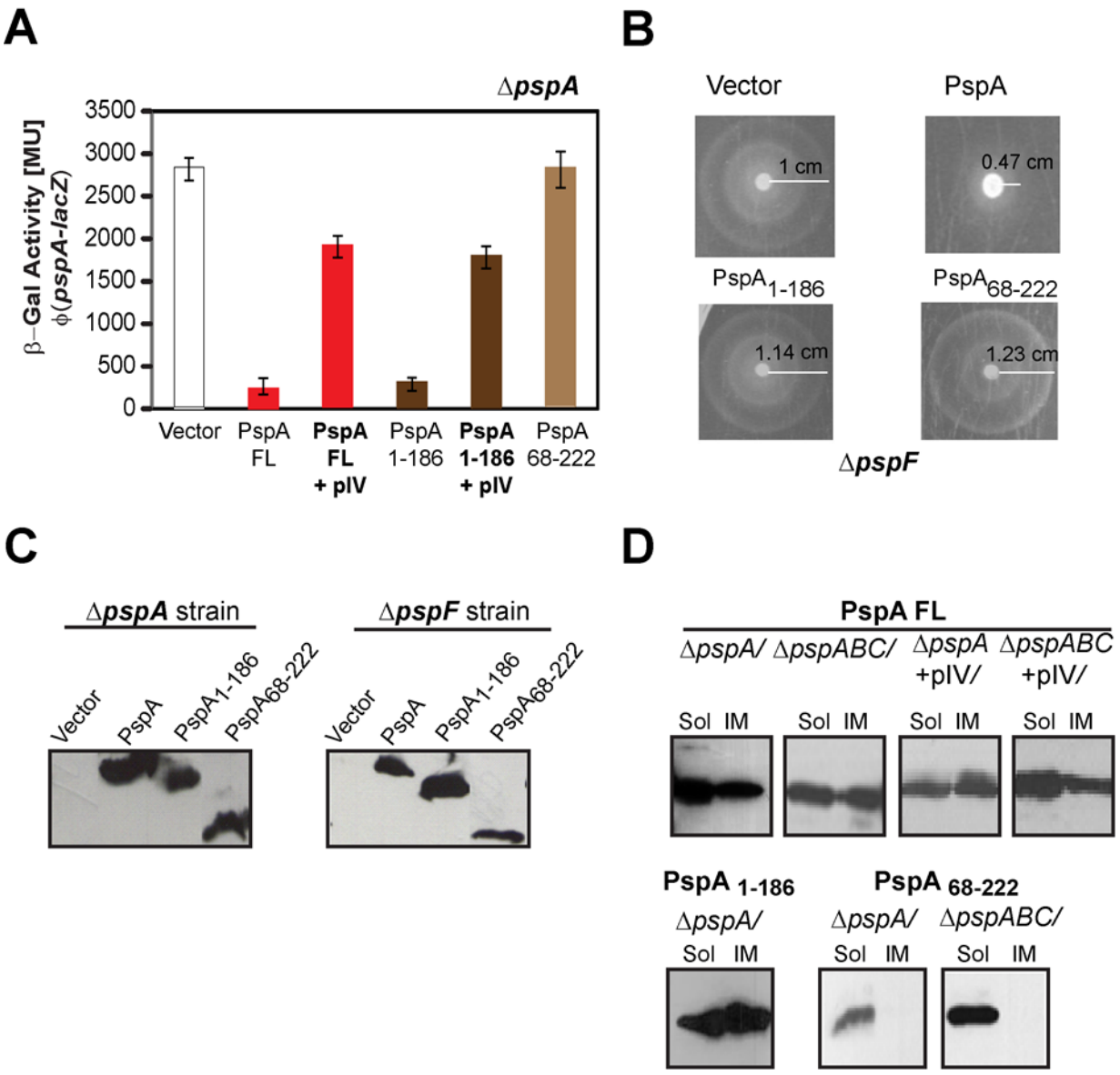

Figure 7.3 **In vivo analysis of PspA HD1 and HD4 variants**: (A) Activation of the chromosomal transcriptional fusion [ϕ (*pspA-lacZ*)] was measured through β-Gal activity in *ΔpspA* strain (MVA27). The strain is complemented with the plasmid borne wild type PspA FL (pPB10), $PspA_{1-186}$ (pPB13; lack HD4) or $PspA_{68-222}$ (pPB15; lack HD1). The expression from the plasmids was induced by 0.02% arabinose (Ara). The loss of negative control by PspA is obtained after stress (+pIV expressed from pGJ4 plasmid Table 2.4). Vector control is pBAD18. (B) The image illustrates the motility of *ΔpspF* cells (MG1655*ΔpspF*) on Soft Agar (SA) plates at 30°C producing PspA and its HD1 and HD4 variants, induced by 0.1% (w/v) Ara. The motility is indicated in the figure in cm. In the control cell with empty vector (mimic WT cells types) the motility was measured to be 1 cm. In the presence of overproduced PspA FL the motility reduced to 0.47 cm. The HD1 and HD4 variants showed increased motility radii. (C) Western blot using α-PspA was performed to show similar levels of PspA proteins in the cells used for β-Gal activity (*ΔpspA* cells) and motility assay (*ΔpspF* cells). (D) Western blot to show the cell fractionation assay for PspA FL, $PspA_{1-186}$ and $PspA_{68-222}$. The PspA localisation in the cells is classified into either soluble or inner membrane (IM). The fractionation was carried out in the *ΔpspA* and *ΔpspABC* cell backgrounds in the absence and presence of pIV.

7.3.1.1 Motility effector function is governed by HD1 and HD4

The effector function of PspA can be evaluated by either its membrane binding property in stressed cells or by studying the cell motility. Overproduced PspA reduced the cell motility, possibly by causing a reduction in the energy consumption of the cells under pIV induced stress conditions (Lloyd *et al*., 2004 and Joly *et al*., 2010). As shown in the Figure 7.3B the reduced motility was observed in cells producing PspA FL. The cells producing $PspA_{1-186}$ and $PspA_{68-222}$ did not have reduced motility and this was similar to the cells with empty vector. Western blotting was used to confirm the amounts of PspA FL, $PspA_{1-186}$ and $PspA_{68-222}$ in the *ΔpspF* background (see Figure 7.3C). The effector function of PspA is dependent on HD1 and HD4. In the absence of either of the domains the motility effector function was lost. HD4 is vital for the formation of higher order oligomers and thus is implicated in the effector role of PspA.

7.3.1.2 HD1 contains the membrane binding determinants

The membrane binding of PspA is determined using a Triton-100 X based cell fractionation (details in Methods 2.6). The fractionated samples are analysed with Western blotting using anti-PspA antibodies. The PspA fractionation sample was divided into the soluble fraction and IM (inner membrane) fraction. As shown in the Figure 7.3D comparable amounts of PspA FL were detected in soluble and IM fractions in *ΔpspA* and *ΔpspABC* strains + or - pIV. $PspA_{1-186}$ protein was present in the soluble as well as the IM fraction of the cell (see Figure 7.3D). This indicates that HD4 does not play a dominant role in defining the membrane association of PspA. However the $PspA_{68-222}$ variant fractionated predominantly in the soluble fraction of the cell and little or no $PspA_{68-222}$ was detected in the IM in the presence or absence of PspBC (see Figure 7.3D). The HD1 of PspA could be the principle factor facilitating the IM binding. WT PspA FL effectively binds the IM in PspBC-independent manner when over-produced (see Figure 7.3D).

Clearly, PspA HD1 is required for negative regulation of PspF, the effector function, IM-binding and high order oligomer formation. In the next section the HD1 domain will be studied in greater detail and the specific deterministic N-terminal amphipathic helices will be characterised for their specific contribution to the PspA functioning in HD1.

7.3.2 HD1 consists of important sub-domains important for PspA functions

I-TASSER is an online platform for protein structure and function predictions. It was used to predict the secondary structure of PspA, PspA consists of coiled-coil (C) and α-helices (H) (see Figure 7.4).

A

MGIFSRFADIVNANINALLEKAEDPQKLVRLMIQEMEDTLVEVRSTSAR
ALAEKKQLTRRIEQASAREVEWQEKAELALLKEREDLARAALIEKQKLT
DLIKSLEHEVTLVDDTLARMKKEIGELENKLSETRARQQALMLRHQAAN
SSRDVRRQLDSGKLDEAMARFESFERRIDQMEAEAESHSFGKQKSLDDQ
FAELKADDAISEQLAQLKAKMKQDNQ

Amino acid sequence

CCHHHHHHHHHHHHHHHHHHCCCHHHHHHHHHHHHHHHHHHHHHHHHH
HHHHHHHHHHHHHHHHHHHHHHHHHHHHHHHHHCCCHHHHHHHHHHHHH
HHHHHHHHHHHHHHHHHHHHHHHHHHHHHHHHHHHHHHHHHHHHHHHHH
HHHHHHHHHH CCCCCCHHHHHHHHHHHHHHHHHHHHHHHHCCCCHHHH
CCCHHHHHHHHHHHCCCCCC

Coiled coil and Helix

B

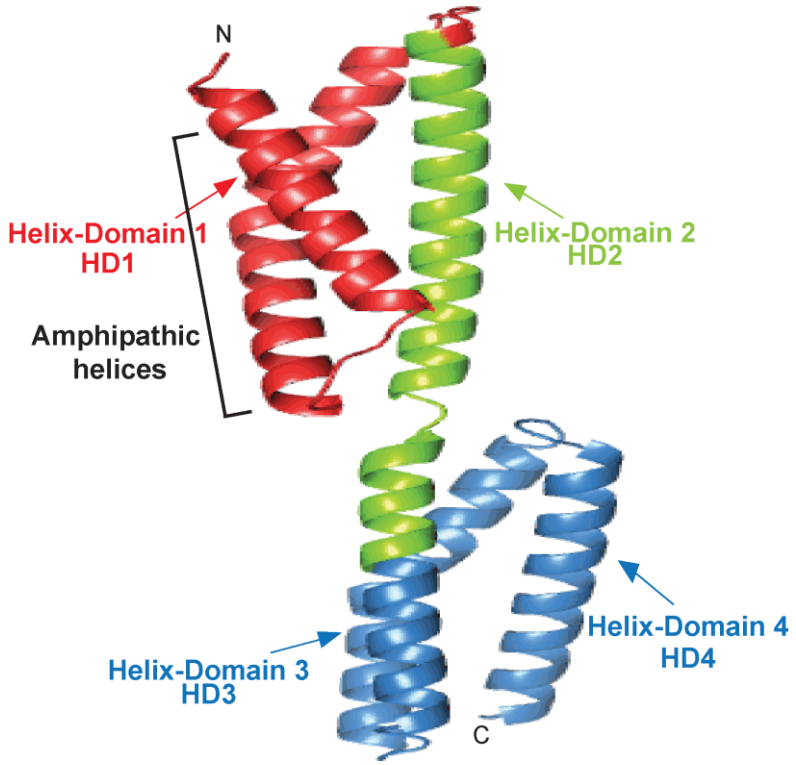

Figure 7.4 **Predicted secondary structure of PspA**: (A) I-TASSER prediction software was used to generate the secondary structure of PspA. It was predicted that the N-terminal forms amphipathic helices along with some coiled coil structures. (B) The corresponding secondary structure of PspA was generated with high confidence score showing the different helical domains of PspA and the predicted coiled coil structures and how each of the domains closely interact with a coiled coil link.

Figure 7.4 also illustrates the predicted secondary structure of PspA with the defined helical domains. The HD1 consists of two N-terminal amphipathic helices (ahs) – ahI and ahII.

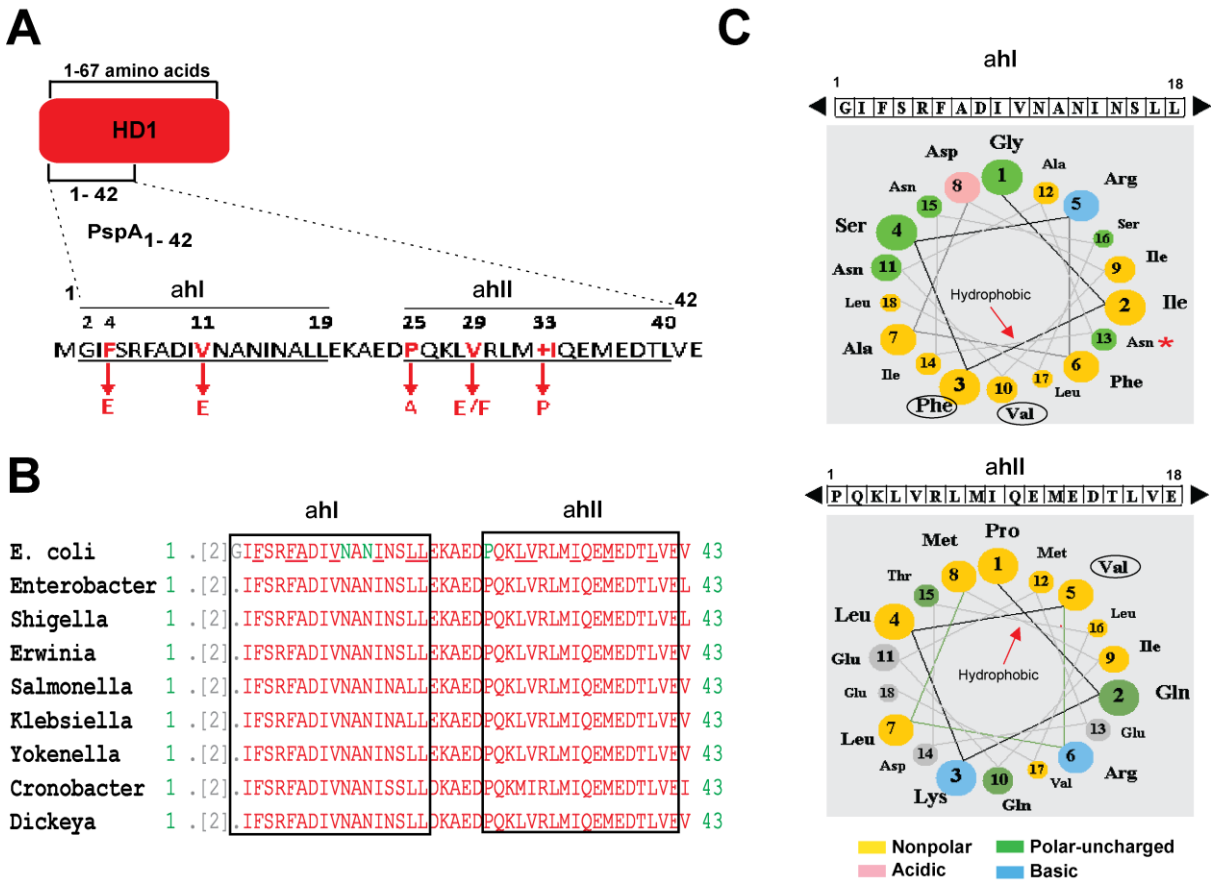

Figure 7.5 **PspA HD1 wheel diagrams and homologies with other enterobacterial PspA**: (A) The N-terminal (1-42) amino acid residues within the HD1 domain. These residues were proposed to form two amphipathic helices, ahI and ahII. (B) Amino acids 1-43 were compared for homology with some other enterobacterial PspA. Alignment (BLASTP aligning software) of the PspA residues (1-43) showed highly conserved residues forming ahI and ahII as highlighted by the black boxes. (C) Shows the wheel diagram projections of ahI and ahII (numbers in brackets correspond to amino acids position in the protein). The wheel diagrams helped to identify the regions associated with amphipathic helices that will be the targets for mutation studies of PspA HD1. The red arrows show the hydrophobic moments of the ahI and ahII and some of the amino acids mutated in this chapter are highlighted with a black circle (Phe and Val). Red asterisk shows the substitution mutation of N14D that abolished PspA IM-binding (Yamaguchi *et al*., 2010).

A wheel diagram of HD1 predicted the N-terminal amphipathic helices and the potential residues of interest for further characterisation and study (Generated by Goran Jovanovic). Figure 7.5A and C illustrates that the PspA HD1 sequence includes two putative amphipathic helices, ahI (residues 2-19) and ahII (residues 25-42) with proline (Pro, P) at position 25. The sequence and organisation of the amphipathic helices is highly conserved (Figure 7.5B) across many bacteria. The ahs can recognise membrane curvature, which could facilitate membrane association (as seen for the RNaseE and degradosome, FtsA-FtsZ binding to membrane) (Löwe *et al*., 2004 and Taghbalout and Rothfield, 2007). Taking into account the hydrophobic moment for ahI and ahII (Figure 7.5C) the potential critical residues within the hydrophobic stretches were substituted with the polar or non-polar amino acids as listed in Table 7.1.

MUTATIONS WITHIN ahI	MUTATIONS WITHIN ahII
In frame Deletion of ahI (2-19) – $PspA_{\Delta 2\text{-}19}$	In frame Deletion of ahII (25-40)- $PspA_{\Delta 25\text{-}40}$
4^{th} Phe with Glu (acid) – $PspA^{F4E}$	29^{th} Val with Glu (acid) – $PspA^{V29E}$
11^{th} V with Glu (acid) – $PspA^{V11E}$	29^{th} Val with Phe – $PspA^{V29F}$
	Addition of Pro – $PspA^{+P33}$

Table 7.1 The table lists the substitution mutations with the corresponding amino acids.

Firstly PspA ahI mutants will be studied in detail and will be used in *in vivo* and *in vitro* assays to resolve their contribution as explained in the Table 7.2.

PspA FUNCTION STUDIED	EXPERIMENTAL ASSAY
Negative regulation	β-Galactosidase assay with ϕ*(pspA-lacZ)* promoter and ATPase assay
Effector Function	Bacterial motility
Interaction with PspF, PspC	Bacterial two hybrid assay
Membrane association	Cell fractionation and SMI
Self-organisation and oligomeric state	*In vitro* protein gel filtration
Subcellular localisation and membrane organisation	SMI using eGFP fusions of the PspA variants as the eGFP-PspA full length was available in the lab (Engl *et al*., 2009)

Table 7.2 The table highlights the functions for which the PspA HD1 variants will be tested. It also shows the corresponding assays employed to study the particular function.

7.3.2.1 Detailed study of the role of ahI in PspA HD1

The following mutants of ahI were constructed: (i) $PspA_{\Delta 2\text{-}19}$; (ii) $PspA^{F4E}$; (iii) $PspA^{V11E}$ (Table 7.1 and Figure 7.5C) and used to perform the experimental procedures listed in Table 7.2. The different experiments were carried out in different cellular backgrounds with the respective PspA mutant carrying plasmid (details are provided in the Table 2.4 for the different plasmid backbones and mutagenesis).

7.3.2.1.1 PspA ahI does not influence negative regulation of PspF

The graph in Figure 7.6A compares the β-Gal results for the ϕ(*pspA-lacZ*) promoter activity in the cells producing PspA FL, PspA ahI mutants and $PspA_{68-222}$ under non-stress as well as stress conditions.

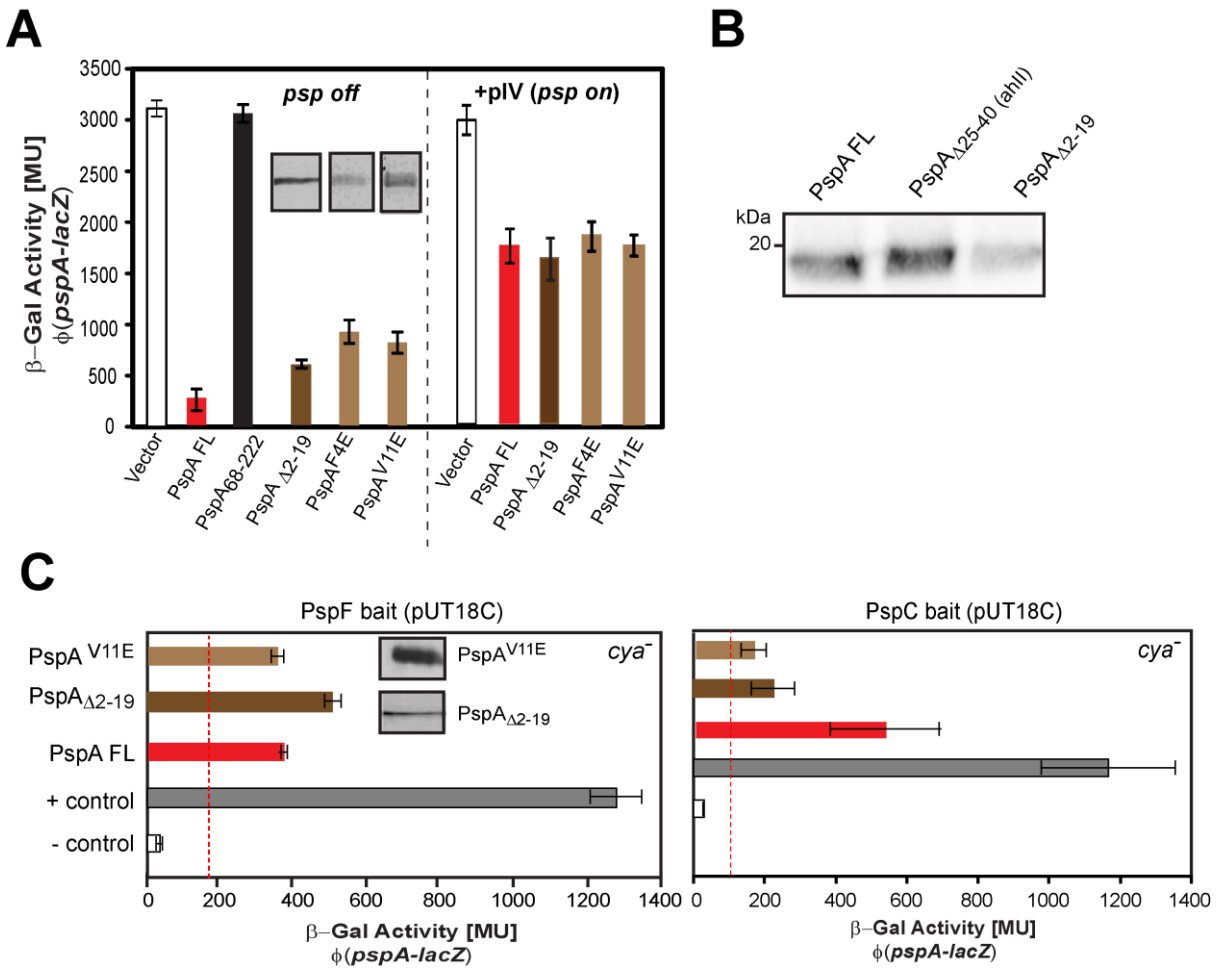

Figure 7.6 **Negative control of PspF by PspA ahI mutant**: Activities (β-Gal activity) of the chromosomal fusion promoter [Δ (*pspA-lacZ*)] in *ΔpspA* strain (MVA27) were measured under non-stress and stress conditions (+pIV, pGJ4). The cells were complemented with the plasmid borne wild type PspA FL (pPB10), ahI mutants $PspA_{\Delta 2-19}$ (pPGJ67), $PspA^{F4E}$ (pGJ68) and Psp^{AV11E} (pGJ69) induced by 0.02% (w/v) arabinose. Loss of negative control was compared to PspA lacking entire HD1, $PspA_{68-222}$ (pPB15). Vector control, pBAD18-cam was the negative control. Western blot using PspA antibodies (α-PspA) was performed to show the production levels of PspA and mutants used in the β-Gal assay as shown by the bands in the graph. (B) Western blot to show the negative regulatory function of $PspA_{\Delta 2-19}$ like PspA WT, by detecting the amounts of PspC (C) BACTH assay was used to determine the pair-wise interactions between pKT25 borne PspA FL or PspA ahI mutants with (i) the interaction between pUT18C PspF bait and (ii) the pUT18C PspC bait. The PspF or PspC plasmids with pKT25 were co-transformed in the BTH101 (cya-) strain. The values 3-times above the negative control (pKT25 and pUT18C vectors alone; red dashed line) are considered as interaction. Positive control is shown by the interaction between pKT25zip and pUT18Czip. Western blot using α-PspA showed the levels of PspA fusion proteins.

PspA ahI mutants retained the negative regulatory function unlike the PspA HD1 mutant. The PspA ahI mutants with the pIV stress conditions induced the expression from *pspA* promoter like FL PspA. PspA

ahI mutants $PspA_{\Delta 2\text{-}19}$ and $PspA^{V11E}$ clearly interacted with PspF, this interaction was detected by the production of cAMP that activated the β-Gal activity of *lacZ* promoter (see Figure 7.6C – PspF bait graph). Positive interaction was detected between PspC and $PspA_{\Delta 2\text{-}19}$ and $PspA^{V11E}$ (see Figure 7.C-PspC bait graph). Besides the positive interaction between PspA ahI mutants and PspF and PspC. It was also shown that the production of PspC was also highly regulated in the ahI mutants even more so than in PspA FL producing cells. This was shown by Western blotting using anti-PspC antibodies (Figure 7.6B). Preliminary *in vitro* ATPase assay with purified $PspA_{\Delta 2\text{-}19}$ showed that the PspF ATPase activity was not totally shut down and some residual activity was present (Appendix-6C).

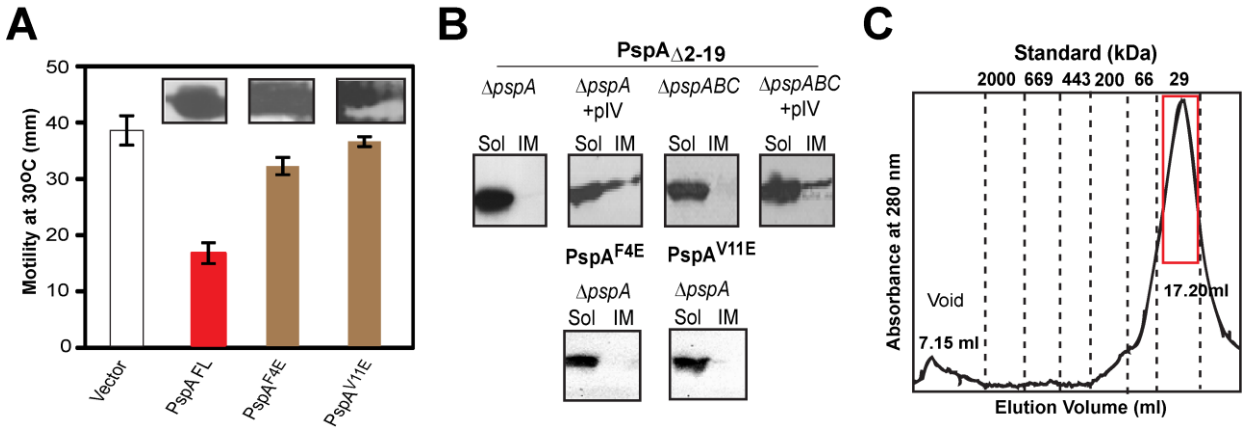

Figure 7.7 **PspA ahI is important for effector function, membrane localisation and oligomeric states**: (A) Motility of Δ*pspF* bacteria (MG1655Δ*pspF*) was measured for $PspA^{F4E}$ and $PspA^{V11E}$. $PspA_{\Delta 2\text{-}19}$ was detrimental for the cell growth. The motility of the cells was not reduced in the cells producing $PspA^{F4E}$ and $PspA^{V11E}$. The corresponding Western blot shows the levels of PspA proteins with anti-PspA antibodies of the corresponding proteins included in the graph. (B) The Western blots using PspA antibodies (α-PspA) was performed using the soluble (Sol) and the inner membrane (IM) fractions. PspA was not detected in the IM fractions. (C) The representative gel filtration profile of the purified His-tagged $PspA_{\Delta 2\text{-}19}$. It shows that $PspA_{\Delta 2\text{-}19}$ was an apparent monomer. The corresponding molecular weight of the standards has been defined by the dotted line

7.3.2.1.2 PspA ahI governs motility effector function

The motility effector function assay showed that PspA ahI mutants were incompetent in reducing the bacterial motility to the extent observed with the PspA FL (see Figure 7.7A). The stable production of $PspA^{F4E}$ and $PspA^{V11E}$ was confirmed using the Western blot. The $PspA_{\Delta 2\text{-}19}$ was not tested for the bacterial motility because its overproduction caused two-fold decrease in growth that could have detrimental effect on the motility measurements (as shown by see Figure 7.7A).

7.3.2.1.3 PspA ahI is implicated in membrane association

The data so far suggests that the ahI mutant retains negative regulation while lacking effector function. Next the membrane association of ahI mutants using Triton-X100 cell fractionation was examined. Cell fractionation showed that the $PspA_{\Delta 2\text{-}19}$ mutant was only detected in the soluble fraction and that little or

none of the $PspA_{\Delta 2\text{-}19}$ protein was found in the IM fraction in both the *ΔpspA* and *ΔpspABC* (see Figure 7.7B). However, the interaction with the membrane is augmented under the stress conditions because some of $PspA_{\Delta 2\text{-}19}$ was detected in the IM fraction for the cells under stress conditions (See Figure 7.7B). The membrane association of PspA is enhanced due its overproduction under stress and its IM binding is largely independent of PspBC. $PspA^{F4E}$ and $PspA^{V11E}$ were also not detected in the IM fraction in the *ΔpspA* cells (see Figure 7.7B). This showed that ahI is implicated in maintaining the membrane association of PspA under non-stress and stress conditions.

7.3.2.1.4 ahI is important for high order oligomer formation

The purified $PspA_{\Delta 2\text{-}19}$ resolved as apparent monomer in the protein gel filtration analysis (as shown in the profile Figure 7.7C). The ahI PspA mutant did not form higher order oligomers characteristic of the WT PspA effectors. Notably, it was found that the PspA with mutated ahI resolves as a monomer/dimer and retained negative regulatory function. The complete deletion of HD1 ($PspA_{68\text{-}222}$) formed an apparent hexamer in gel filtration (Joly *et al*., 2009). This suggests that PspA ahI communicates with HD4 to from high order oligomers. The purified His-tagged $PspA_{\Delta 2\text{-}19}$ interacted with purified $PspF_{1\text{-}275}$ on the native gel mobility shift assay Appendix-5-A).

The subcellular localisation of the PspA ahI mutants was also studied in live *E. coli* cells. SMI of the PspA variants was achieved by constructing plasmid borne eGFP fusions of $PspA_{\Delta 2\text{-}19}$. This mutant of ahI was chosen because it showed the most pronounced effect on the PspA effector role and membrane association and because it was important to compare the membrane associated localisation of $PspA_{\Delta 2\text{-}19}$ in comparison with PspA FL.

7.3.2.1.5 SMI of eGFP-$PspA_{\Delta 2\text{-}19}$

SMI of eGFP-$PspA_{\Delta 2\text{-}19}$ in Δ*pspA* cells was done using 488nm wavelength compatible with GFP excitation spectra (Methods 2.15). The eGFP fusion were used as the plasmid expressing eGFP-PspA full length was already studied by Engl *et al*., 2009 and was fully characterised to introduce HD1 mutations in this plasmid. Δ*pspA* cells were used instead of WT cells because in the presence of native PspA the eGFP fusions of PspA FL or mutants were not readily visualised (Engl *et al*., 2009). eGFP-$PspA_{\Delta 2\text{-}19}$ fusion was stably produced (53 kDa) with no lower background molecular weight bands (as shown in blot Figure 7.8A. After establishing its stability the cells with eGFP-$PspA_{\Delta 2\text{-}19}$ were grown in N^-C^- minimal media and immobilised on 0.1% (w/v) agarose pads to be visualised under the microscope. The polar membrane regulatory complexes (likely PspA-PspBC) were observed in the majority of cells similar to PspA FL (see Figure 7.8B). Some cells showed central probably nucleoid associated foci in complex with PspF (as shown in images in Figure 7.8B) and these centrally localised eGFP-$PspA_{\Delta 2\text{-}19}$

foci were not evident in TIRF confirming these foci are nucleoid associated far from the evanescent field (~ 100 nm above the surface) of a TIRF set-up (Figure 7.8C).

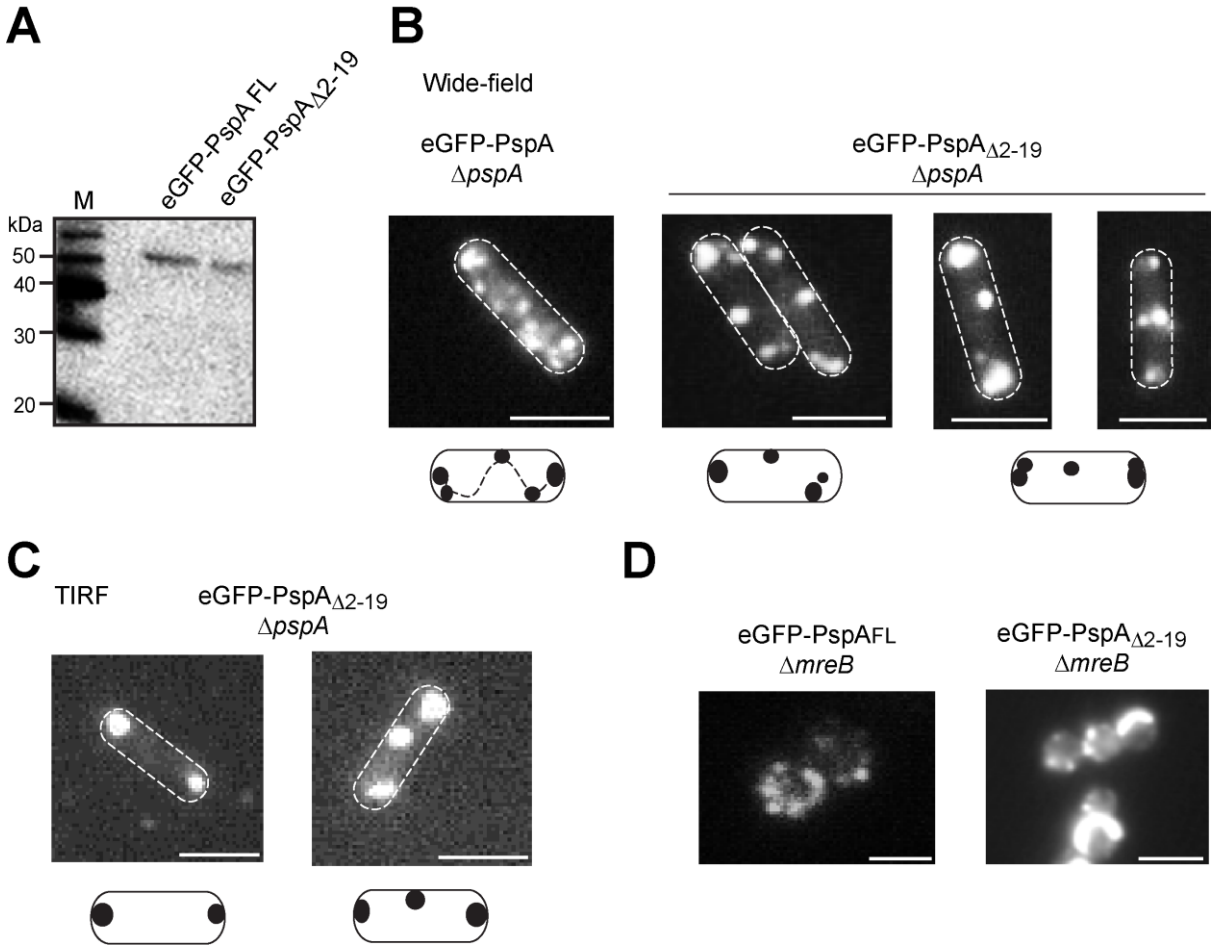

Figure 7.8 **SMI of stable eGFP-PspA$_{\Delta 2\text{-}19}$ in Δ*pspA* cells**: (A) The stability of eGFP-PspA$_{\Delta 2\text{-}19}$ was confirmed by Western blotting using anti-GFP antibodies. The eGFP-PspA$_{\Delta 2\text{-}19}$ fusion was around 53 kDa (~25 kDa PspA with 28 kDa GFP) with minimum lower molecular bands corresponding to either PspA or GFP. (B) Wide-field merge of fluorescent and bright-light image of eGFP-PspA FL with the defined boundary is shown. The illustration explaining the possible localisations of the PspA foci has been explained below the image with lateral foci showing dynamic spiral movement. The three merge images of the fluorescent and bright light illustrate the examples of different possible localisations of eGFP-PspA$_{\Delta 2\text{-}19}$ with the corresponding cell illustrations of the different localised foci. (C) The TIRF images of eGFP-PspA$_{\Delta 2\text{-}19}$ with mainly polar localised foci. (D) The images comparing the eGFP-PspA FL and eGFP-PspA$_{\Delta 2\text{-}19}$ in *ΔmreB* cells, deletion of MreB renders cells spherical with no defined poles. Scale bar = 1 µm

The lateral membrane associated foci (Engl *et al*., 2009) seen with eGFP-PspA FL were not evident in the PspA$_{\Delta 2\text{-}19}$ (see Figure 7.8B). Clearly the lateral membrane association of PspA$_{\Delta 2\text{-}19}$ (no motility effector function) is abolished (7.3.2.1.1 and 7.3.2.1.2). Therefore the subcellular localisation of eGFP-PspA$_{\Delta 2\text{-}19}$ is different from eGFP-PspA FL. With TIRF microscopy predominantly polar localised eGFP-PspA$_{\Delta 2\text{-}19}$ foci were observed with few cells with lateral foci (see Figure 7.8C). The behaviour of eGFP-PspA$_{\Delta 2\text{-}19}$ was assessed in absence of MreB and compared with eGFP-PspA FL. Figure 7.8D of eGFP-

$PspA_{\Delta 2\text{-}19}$ in *ΔmreB* cells showed that most foci were static and localised as bright patches along the spherical cell. This showed that MreB did not influence the formation of polar complexes and usually defined the lateral membrane associated dynamics of PspA. Next, SMI was done on eGFP-$PspA_{\Delta 2\text{-}19}$ produced in Δ*pspABC* cells. It was established in the Western blot that eGFP-PspA FL and eGFP-$PspA_{\Delta 2\text{-}19}$ fusion was unstable in the absence of PspBC (see Figure 7.9). In line with the Western blot data, the SMI images gave no distinct discernible foci for either WT or eGFP-$PspA_{\Delta 2\text{-}19}$ in Δ*pspABC* cells (Figure 7.9). This showed that PspBC plays a significant role in localisation of PspA at the membrane. The interactions between ahI and PspBC might stabilise the production of the fusion proteins and also facilitate spatial organisation of eGFP-$PspA_{\Delta 2\text{-}19}$ in *ΔpspA* cells (Engl *et al*., 2009; Yamaguchi *et al*., 2010 and Yamaguchi *et al*., 2013).

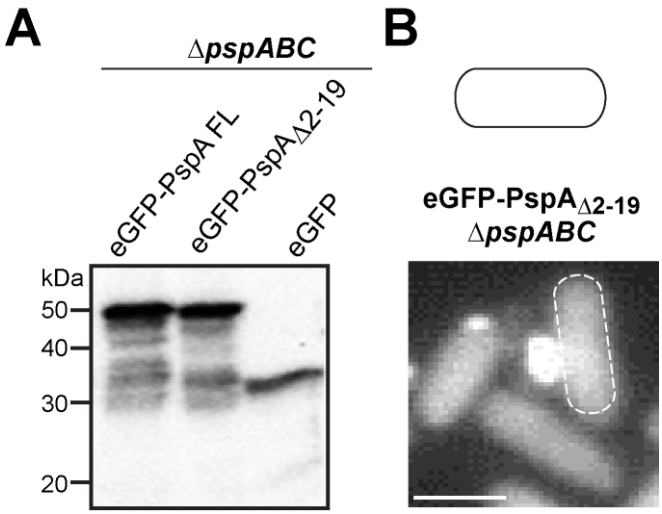

Figure 7.9 **eGFP-$PspA_{\Delta 2\text{-}19}$ is stable in the presence of PspBC and lost defined localisation**: (A) The Western blot compares the instability of PspA FL and $PspA_{\Delta 2\text{-}19}$ in the absence of PspBC. A number of lower molecular weight bands either corresponding to eGFP or unstable fusions were observed. (B) The imaging of $PspA_{\Delta 2\text{-}19}$, as shown in the representative images, they exhibit no discernible localised foci in the cell. A higher fluorescence background was observed in the cells. Scale bar = 1 µm

Yamaguchi *et al*., 2010 had published that the substitution mutation in the ahI of PspA - N14D abolished PspA-IM binding. This supports our inference that ahI is a major PspA IM-binding and effector determinant. PspA, like RNaseE via its ahI, promotes membrane binding and thus this IM interaction allows for its effector function (Lu and Taghbalout, 2013). N-terminal amphipathic helices can bind to membrane in a reversible and regulated fashion that is influenced by lipid composition, physical properties of the membrane and pmf (Strahl and Hamoen, 2010). Therefore, $PspA_{\Delta 2\text{-}19}$ ahI mutant can associate with the membrane under stress conditions in a PspBC independent manner, which shows that the amphipathic helix and membrane status both govern PspA membrane association. Overall, results establish that the ahI is implicated in IM-binding, high order oligomer formation and the effector

function of PspA that directly correlates with the presence of dynamic lateral membrane complexes. Next the PspA ahII mutants were evaluated for their functionality and cell localisation.

7.3.2.2 Detailed study of the role of ahII in PspA HD1

The following mutants of ahII (see Table 7.1): (i) $PspA_{\Delta 25\text{-}40}$; (ii) $PspA^{V29E}$- substitution of non-polar valine with acidic glutamic acid; (iii) $PspA^{V29F}$- substitution of non-polar valine with larger non-polar phenylalanine and $PspA_{+P33}$ - addition of non-polar proline after residue 32. These PspA ahII mutants were tested using the *in vivo* and *in vitro* experiments listed in Table 7.2 on page 10 (Methods 2.6 to 2.15).

7.3.2.2.1 ahII in negative regulation of PspF

As shown in the graph Figure 7.10A of promoter activity, the negative regulatory function of ahII deletion mutant $PspA_{\Delta 25\text{-}40}$ and $PspA_{+P33}$ was abolished completely *in vivo* and the expression from the *pspA-lacZ* promoter did not change with the stress conditions. The single amino acid substitution mutant, $PspA^{V29E}$, to an extent lost negative regulation and interaction with PspF. However, the mutant $PspA^{V29F}$ recovered the negative regulation in the same way as PspA FL and also responded to the stress conditions like PspA FL. In line with absence of negative regulatory function in $PspA_{\Delta 25\text{-}40}$ and $PspA_{+P33}$, the corresponding interactions with PspF were also reduced as shown by BACTH assay in Figure 7.10B-i. However $PspA_{+P33}$ and $PspA^{V29E}$ interacted with PspC in a similar way as PspA FL (see Figure 7.10B-ii). The recovery mutant $PspA^{V29F}$ showed positive interaction with PspF and PspC (see Figure 7.10B). As shown in the Appendix-6-C, the PspF ATPase activity was not inhibited by $PspA_{\Delta 25\text{-}40}$ *in vitro.*

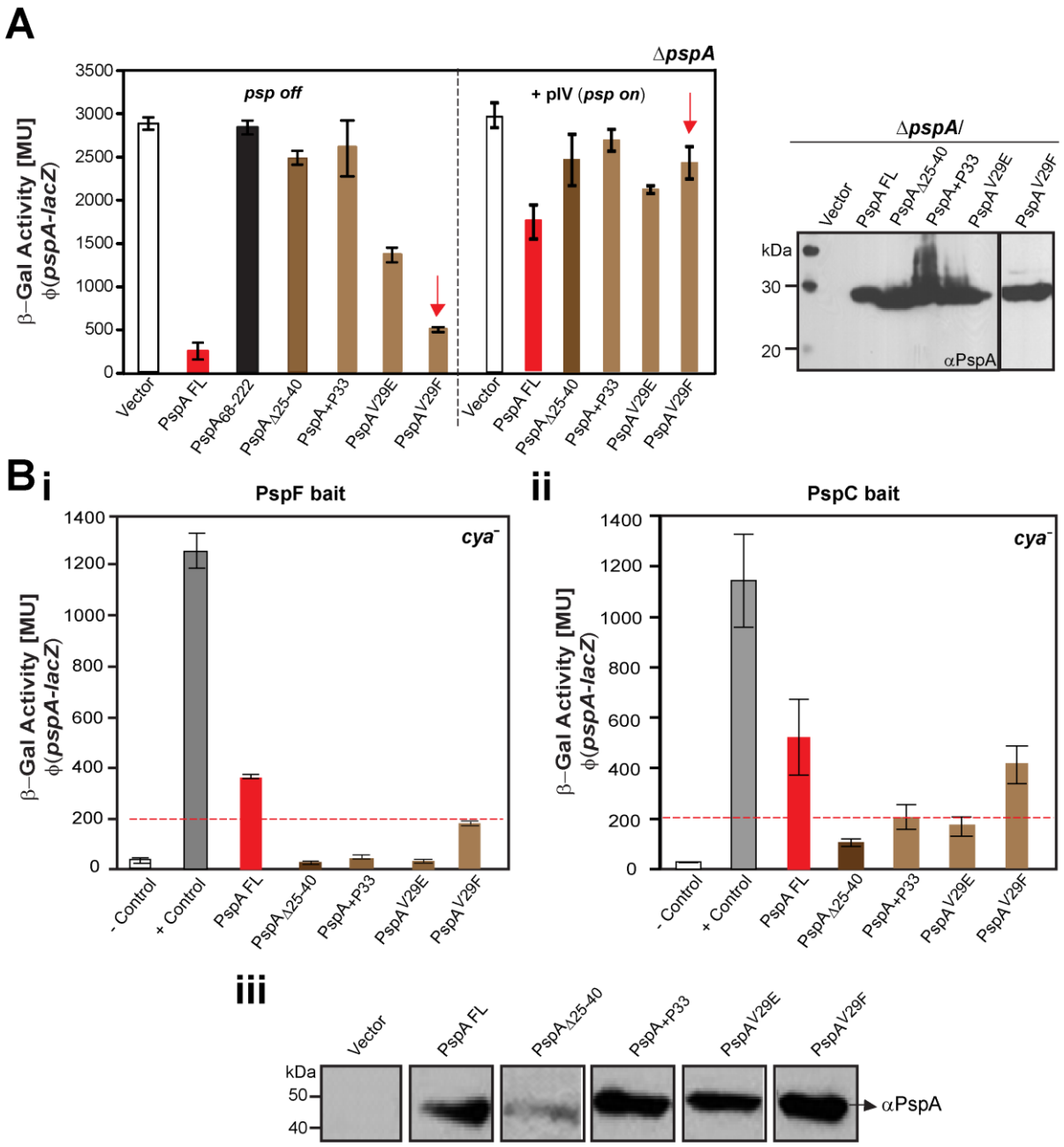

Figure 7.10 **PspA ahII mutants abolished the negative regulation of PspF**: (A) The graph shows the β-Gal activity of the chromosomal ϕ(*pspA-lacZ*) in *ΔpspA* strain (MVA27) complemented with the plasmid borne wild type PspA FL (pPB10), ahII mutants $PspA_{\Delta 25\text{-}40}$ (pPGJ62), $PspA^{+P33}$ (pGJ63), $PspA^{V29E}$ (pGJ64) and $PspA^{V29F}$ (pGJ65) under non-stress and stress conditions. Loss of negative control was compared to PspA lacking entire HD1, $PspA_{68\text{-}222}$ (pPB15). Western blot using PspA antibodies (α-PspA) was performed to show the levels of PspA and mutants used in the β-Gal assay. (B) BACTH assay was used to determine the pair-wise interactions between pKT25 borne PspA FL or PspA ahII mutants with (i) the pUT18C PspF bait (ii) pUT18C PspC bait. The interaction was determined by the β-Gal activity and the values 3-times above the negative control were considered as a positive interaction. Positive control is shown by the interaction between pKT25zip and pUT18Czip. (iii) Western blot using α-PspA shows the levels of PspA fusion proteins.

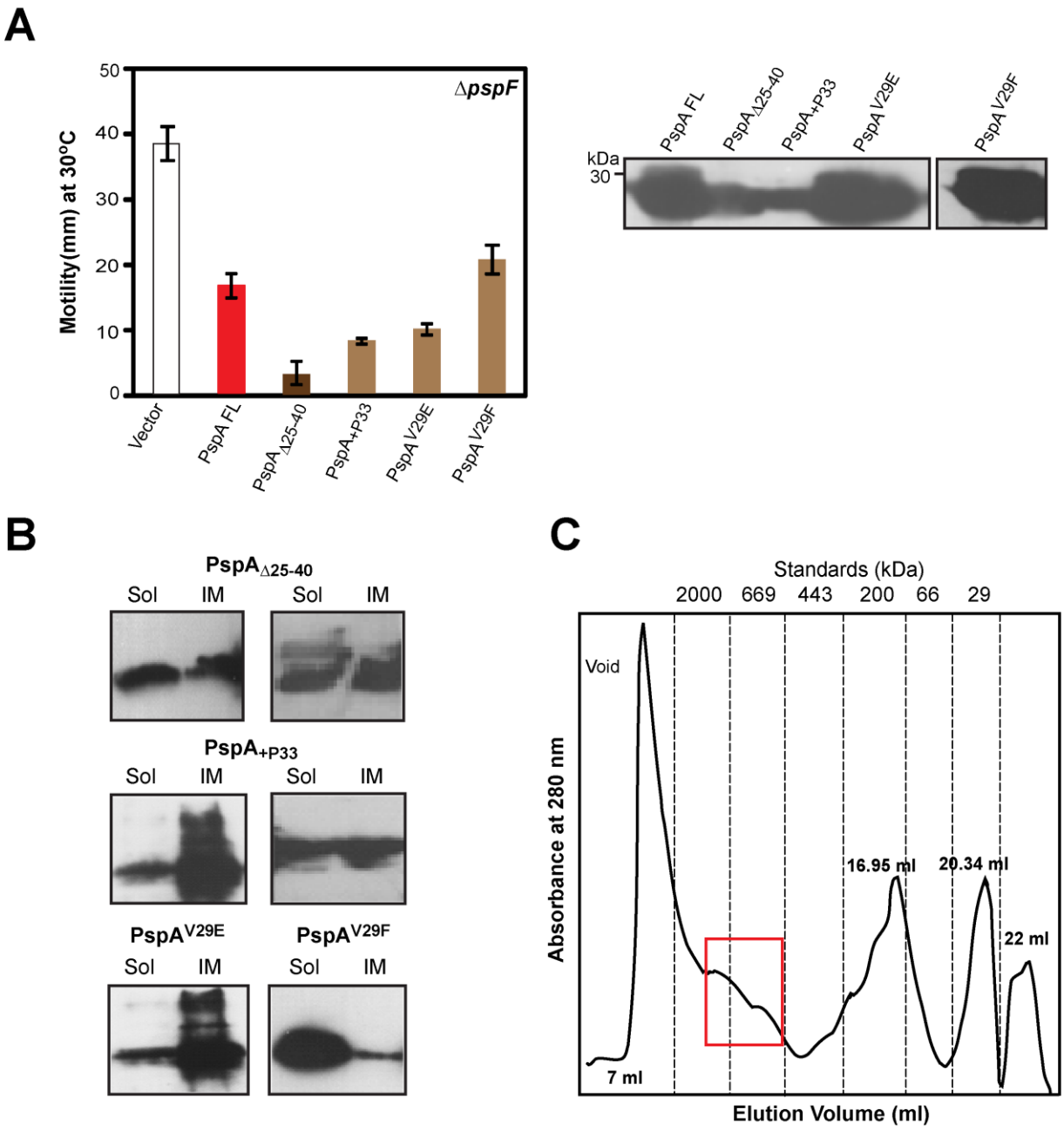

Figure 7.11 **The motility effector function and higher order oligomerisation retained in PspA ahII mutant**: (A) The motility of bacteria was studied as explained in methods (Section 2.10). The motility of bacteria is presented in mm; negative control is the empty vector pBAD18-cam. The $PspA_{\Delta 25\text{-}40}$, $PspA^{+P33}$ and $PspA^{V29E}$ showed reduced motility like PspA WT. The corresponding Western blot shows the amounts of PspA proteins with anti-PspA antibodies. (B) Western blot using anti-PspA antibodies was used to detect PspA in Sol and IM fractions. The IM association was retained in these mutants. (C) Gel filtration profiles of the purified His-tagged $PspA_{\Delta 25\text{-}40}$ (Methods 2.12). The red box highlights the potential higher order oligomers of His-tagged $PspA_{\Delta 25\text{-}40}$ not easily resolved in gel filtration. The solubilisation of His-tagged $PspA_{\Delta 25\text{-}40}$ protein purification was challenging during purification.

7.3.2.2.2 ahII did not influence the motility effector function and IM association

As shown in the Figure 7.11A, the reduction in the bacterial motility effector function was highly pronounced in $PspA_{\Delta 25\text{-}40}$, $PspA_{+P33}$ and $PspA^{V29E}$ when compared to PspA FL activity, with very small

motility radii. The result suggested that absence of ahII did not greatly decrease the negative motility effector function of PspA unlike ahI mutants (Figure 7.7A).The cell fractionation assay was performed to show the role of ahII and its components in forming and stabilising the IM association of PspA. It was clearly shown by Western blotting that deletion of ahII or substitution mutations did not affect the binding of PspA to the IM (see Figure 7.11B).

7.3.2.2.3 Oligomeric states of ahII mutants

The protein purification of His tagged $PspA_{\Delta 25\text{-}40}$ was challenging because of its very strong membrane association and therefore the solubilisation of $PspA_{\Delta 25\text{-}40}$ was difficult using CHAPS detergent. The yield of the $PspA_{\Delta 25\text{-}40}$ was not as high for the PspA FL, as determined by Folin Lowry protein assay (Lowry *et al*., 1951) (. Figure 7.11C shows a representative gel filtration profile of $PspA_{\Delta 25\text{-}40}$ revealing a mixture of higher order oligomers. The unresolved peaks highlighted in Figure 7.11C with a red box could be the higher order oligomers of PspA (like 36-mer). Thus ahII of HD1 is not involved in the formation of high order oligomers in conjunction with HD4.

7.3.2.2.4 SMI of $PspA_{\Delta 25\text{-}40}$

A stably produced eGFP-$PspA_{\Delta 25\text{-}40}$ was used for SMI studies in *ΔpspA* cells (see Figure 7.12A). The images were very different from the PspA FL and $PspA_{\Delta 2\text{-}19}$ presumably reflecting major contribution of $PspA_{\Delta 25\text{-}40}$ to the PspA regulatory functions. No nucleoid associated foci were observed in these cells and even the polar localised complexes were very limited in number (See Figure 7.12). On the other hand, the images were characterised by a predominant lateral membrane associated foci (Figure 7.12B, C-i). These foci decorated the membrane along the cell and exhibited non-helical circumferential dynamics (See Figure 7.12B). This phenotype of decorating the membrane has never been reported for PspA.

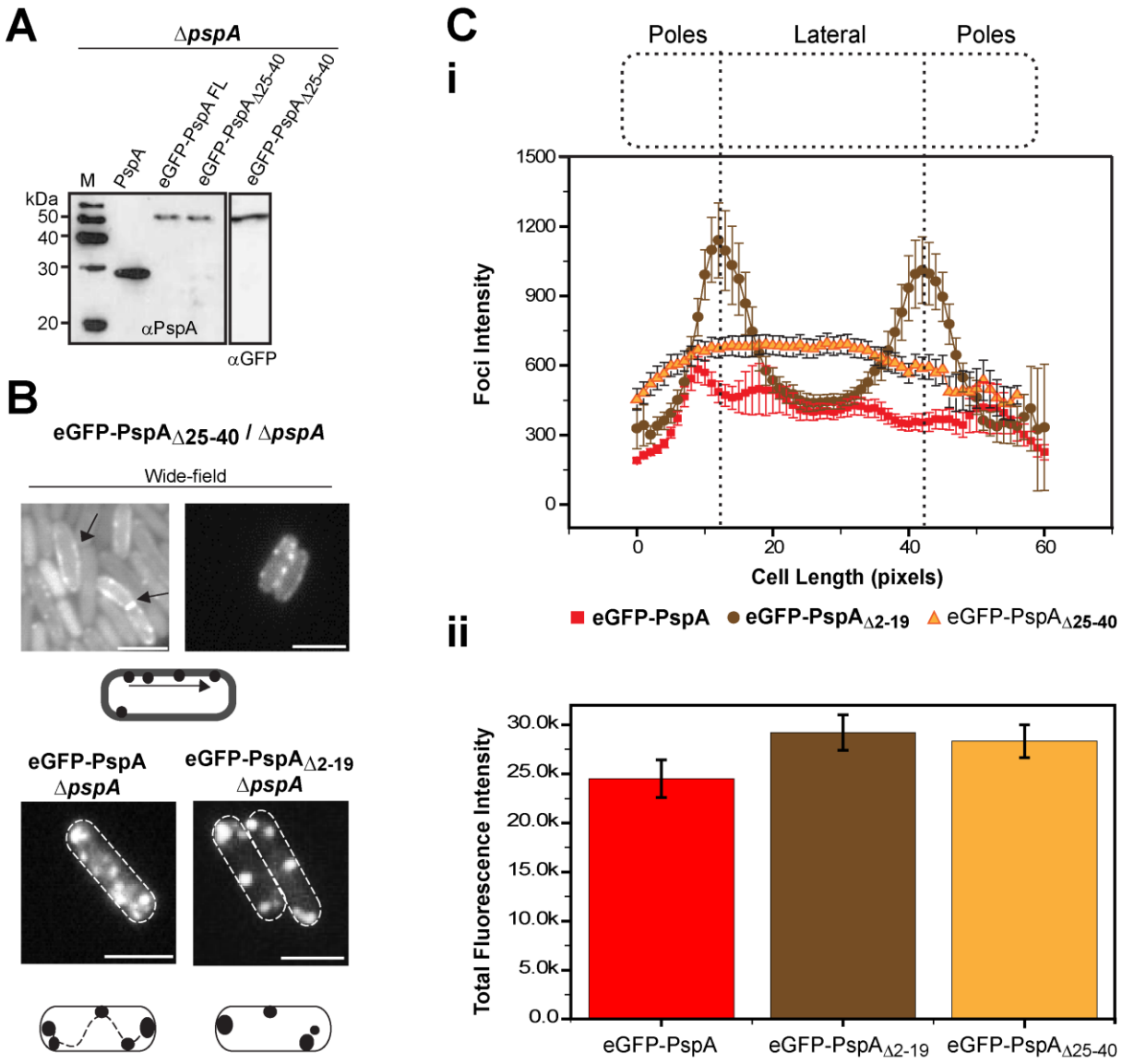

Figure 7.12 **SMI of stable eGFP-PspA$_{\Delta 25\text{-}40}$ in *ΔpspA* and *ΔpspABC* cells**: (A) The stability of eGFP- PspA$_{\Delta 25\text{-}40}$ was confirmed by Western blotting using anti-PspA and anti-GFP antibodies. The eGFP-PspA$_{\Delta 25\text{-}40}$ fusion was around 53 kDa (~<25 kDa PspA with 28 kDa GFP) with minimum lower molecular bands corresponding to either PspA or GFP. (B) The wide-field merge of fluorescent and bright-light image of eGFP-PspA$_{\Delta 25\text{-}40}$ comparing with the eGFP-PspA FL and eGFP-PspA$_{\Delta 2\text{-}19}$. The illustration explains the localisation of eGFP-PspA$_{\Delta 25\text{-}40}$ decorating the membrane with few lateral localised foci that do not show helical membrane associated dynamics. (C-i) The scatter plot shows the intensity on y-axis corresponding to the cellular location on x-axis giving the length of cells in pixels. About 60 pixels is the length of the cell, with the 0 pixel corresponding to the start of the measurement from the left pole of the cell ending with the right most pole (Methods 2.15.3.1). Each pixel should correspond to approximately 20 nm. The graph compares the intensity of eGFP-PspA FL, eGFP-PspA$_{\Delta 2\text{-}19}$ and eGFP-PspA$_{\Delta 25\text{-}40}$. And the graph clearly shows predominant polar localisation of eGFP-PspA$_{\Delta 2\text{-}19}$ foci , to largely lateral membrane associated for eGFP-PspA$_{\Delta 25\text{-}40}$ and more widespread localised foci in eGFP-PspA FL. (C-ii) The graph compares the total fluorescence intensity of the cells producing eGFP-PspA FL, eGFP-PspA$_{\Delta 2\text{-}19}$ and eGFP-PspA$_{\Delta 25\text{-}40}$. Scale bar = 1 µm-

The image analysis of the fluorescence intensity at the poles and along the lateral membrane for eGFP-PspA FL, eGFP-PspA$_{\Delta 2\text{-}19}$ and eGFP-PspA$_{\Delta 25\text{-}40}$ studied in this chapter showed a clear difference in the

intensities for the different mutants. eGFP-PspA$_{\Delta 2\text{-}19}$ showed two major intensity peaks at the poles of the cells, while the lateral membrane was not occupied by these foci; therefore, no intensity was measured. eGFP-PspA$_{\Delta 25\text{-}40}$, as shown in the images, was associated mainly with the lateral membrane which is reflected in its quite even scatter plot along the lateral membrane. Conversely, PspA FL was imaged localised at the poles as well as the lateral membrane, as seen by the multiple peaks in the scatter plot (Figure 7.12C-i). However, the total fluorescence intensity of the cells with eGFP-PspA$_{\Delta 2\text{-}19}$ and eGFP-PspA$_{\Delta 25\text{-}40}$ was a little higher than PspA FL (Figure 7.12C-ii). In the TIRF illumination amongst 20 cells observed in a focal plane, a maximum of 2 cells showed polar foci, but the specific phenotype of membrane decoration eGFP-PspA$_{\Delta 25\text{-}40}$ was also not evident (see TIRF image in Appendix-5-D).

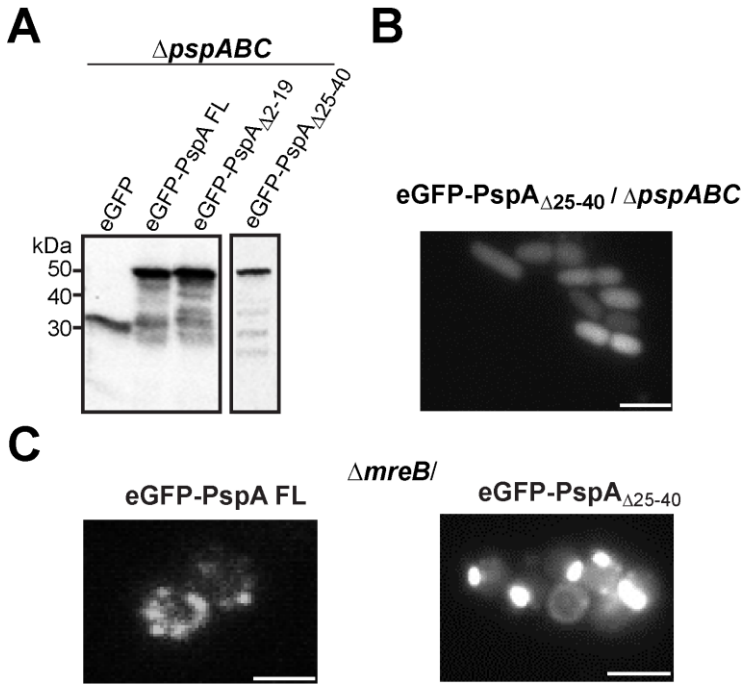

Figure 7.13 **eGFP-PspA$_{\Delta 25\text{-}40}$ in the *ΔpspABC* and *ΔmreB* cells**: (A) eGFP-PspA$_{\Delta 25\text{-}40}$ was not stable in *ΔpspABC* cells as shown by the Western blot with anti-GFP antibodies and (B) no discernible foci were observed in the SMI image. (C) The images comparing the eGFP-PspA FL and eGFP-PspA$_{\Delta 25\text{-}40}$ in *ΔmreB* cells. The deletion of MreB rendered cells spherical and there were no defined poles in these cells. The eGFP-PspA$_{\Delta 25\text{-}40}$ appeared as bright spots in patches along the spherical cell that were completely static unlike the eGFP-PspA FL foci.

Like eGFP-PspA and eGFP-PspA$_{\Delta 2\text{-}19}$, no discernible foci were observed in the *ΔpspABC* cells (see Figure 7.13A, B). The eGFP-PspA$_{\Delta 25\text{-}40}$ membrane association was MreB dependent because in *ΔmreB* cells the foci were completely static and localised as a bright single patch in the spherical cell (see Figure 7.13C). This showed that the membrane associated localisation and dynamics of eGFP-PspA$_{\Delta 25\text{-}40}$ was still facilitated by MreB, therefore, its absence abolished the dynamics of eGFP-PspA$_{\Delta 25\text{-}40}$.

So far, comparing the roles of ahI and ahII in PspA functioning shows that ahI is implicated in its membrane association and subsequent high order effector function under stress conditions. While ahII controls the negative regulatory function of PspA associating with PspF as a lower order oligomer under non-stress conditions. In addition, it was also studied that the absence of either of the PspA domains led to the see-saw effect of its functions. In the “see-saw” effect, absence of either of the ah domains led to predominance of the other, such as in $PspA_{\Delta 2\text{-}19}$ in which deletion of ahI lead to increased negative regulatory function. While in $PspA_{\Delta 25\text{-}40}$ deletion of ahII meant that the effector function and membrane association took precedent. Such an act of balancing between the two specific functions of PspA is mediated by the two amphipathic helices in the HD1. In addition to the sequence alignment and structure predictions, a conserved proline at residue 25 was identified that could link these two important AH (ahI and ahII).

7.3.3 Conserved P25 could be an important structural link between ahI and ahII

The Pro 25 could be structurally significant as in the structural prediction analysis it forms an important structural kink possibly connecting the ahI and ahII in the HD1 (Figure 7.5). To address whether the conserved Pro 25 (P25) impacts on the function of ahI and/or ahII, $PspA^{P25A}$ (Figure 7.5) was constructed, and the same *in vivo, in vitro* and SMI analyses were performed (Table 7.2). The negative regulation of PspF by $PspA^{P25A}$ was reduced, along with the interaction with PspF (Figure 7.14A, B). However, the interaction with PspC was retained (see Figure 7.B). The induction of the *pspA* promoter by pIV was moderately above the WT level (Figure 7.14A). Strikingly, the motility effector function was absent in $PspA^{P25A}$ (see Figure 7.14C).The IM binding was maintained by over-produced $PspA^{P25A}$ mutant (Appendix-6). The gel filtration studies with His-tagged $PspA^{P25A}$ were particularly challenging because it was difficult to solubilize the pelleted insoluble $PspA^{P25A}$ using CHAPS detergent. Thus the purification yield was very poor.

The localisations and dynamics of eGFP-$PspA^{P25A}$ foci were very similar to the eGFP-PspA FL (Figure 7.14D) indicating that the substitution mutation did not affect the overall binding interaction of PspA with the membrane. The mutation of P25 led to some defects on PspA negative regulatory function and its effector function. So it can be inferred that P25 allows ahI and ahII to function normally.

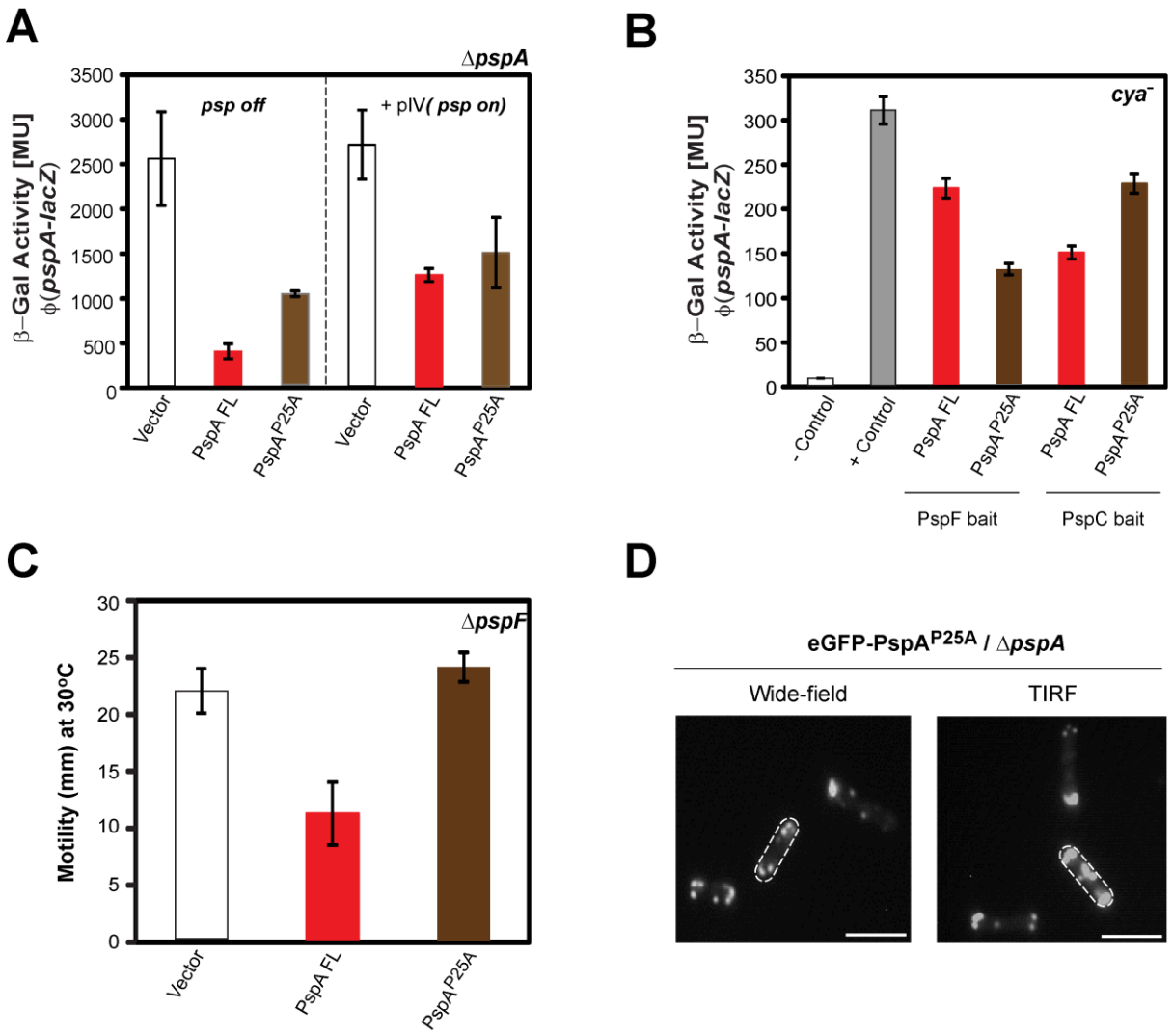

Figure 7.14 **Function and spatial localisation of the PspA^{P25A} mutant**: (A) The β-Gal activity of the chromosomal ϕ (*pspA-lacZ*) was measured in Δ*pspA* strain (MVA27) complemented either with the plasmid borne wild type PspA FL (pPB10) or PspA^{P25A} (pGJ89).The test was done under non-stress or pIV stress inducing conditions. (B) BACTH assay to determine the pairwise interactions between pKT25 borne PspA FL or PspA^{P25A} and pUT18C based PspF or PspC bait. The activation of the chromosomal *lacZ* was determined by measuring the β-Gal activity. The values 3-times above the negative control (pKT25 and pUT18C vectors alone; red dashed line) were considered as interaction. Positive control, pKT25 zip +pUT18C zip. (C) Motility of Δ*pspF* bacterial cells (MG1655Δ*pspF*) producing PspA FL (pPB10) or PspA^{P25A} (pGJ89) was measured. The motility of bacteria is presented in mm. (D) Wide-field and TIRF fluorescent image of eGFP-PspA^{P25A} foci resembling eGFP-PspA FL. The representative cells are defined with the white boundary in the images. Western blots showing stable levels of the proteins used in the assays and also of eGFP fusions are presented in Appendix-6. Scale bar = 1 μm

7.4 Conclusions

Peripheral IM-binding proteins such as PspA and RNase E are important examples establishing a crucial correlation between their localisations and functionalities. In addition the subcellular functions are further characterised by their intramolecular interactions within the self-assembly or with the membrane and

other proteins. This chapter proposes a mechanistic model of the PspA intra- and inter-molecular signalling and communication.

PspA PROTEIN	NEGATIVE REGULATION	pIV INDUCTION	MOTILITY EFFECTOR FUNCTION	IM ASSOCIATION	OLIGOMERIC STATES
PspA FL	+	+	+	+	36-mer
$PspA_{1-186}$ (HD1-3)	+	+	-	+	Apparent dimer
$PspA_{68-222}$	-	**NA**	-	-	Apparent hexamer
$PspA_{\Delta 2-19}$	+	+	ND	-	Apparent monomer/dimer
$PspA^{F4E}$	+	+	-	-	Apparent monomer/dimer
$PspA^{V11E}$	+	+	-	-	Apparent monomer/dimer
$PspA_{\Delta 25-40}$	-	-	+	+	Apparent higher order oligomer (36-mer)
$PspA_{+P33}$	-	-	+	+	Not obtained
$PspA^{V29E}$	-	-	+	+	Not obtained
$PspA^{V29F}$	+	+	+	+	Not obtained
$PspA^{P25A}$	+	+	-	+	Not obtained

Table 7.3 Summarizes the negative regulatory, pIV induction, motility effector function, membrane binding and oligomeric states of the PspA HD mutants.

Furthermore, the interactions between amphipathic helices in PspA HD1 (ahI and ahII) have varying impact on the effector and regulatory roles, respectively (see Table 7.3). It is also important to note how in a dual function protein like PspA different structural subunits counterbalance Psp regulation and membrane stress management.

The ahII of PspA HD1 is required for the negative regulation of PspF under non-stress conditions. The ahII of HD1 also forms regulatory complexes with PspBC at the poles of the cells. Moreover, it is formally possible that the engagement of ahII with PspF has a negative effect on the N-terminal ahI of HD1, which prevents higher order oligomerisation of PspA. It seems that the ahI of HD1 mediates the membrane association of PspA and its oligomerisation under membrane stress conditions. The stress conditions might activate PspBC which could further titrate and relieve PspF-PspA (ahII) inhibitory complex at the poles and lead to induction of *psp* genes (Jovanovic *et al*., 2010 and Yamaguchi *et al*., 2012). The localisation of ah mutants at the membrane was also influenced by MreB (Chapter 6) like PspA FL. This showed that the cellular factors such as membrane lipid composition, membrane curvature and cytoskeletal proteins engage PspA structural domains in signal perception and Psp response management. It establishes crucial crosstalk between protein architecture and cellular components, and suggests how they influence each other.

CHAPTER 8

8 Achievement of Aims and Perspectives

The main aim of the thesis was to evaluate spatial and temporal localisation of key components of a particular stress response system in *E. coli*. The extracytoplasmic stress response studied is the Phage Shock Protein (Psp) response found in enterobacteria, which manages membrane integrity (Darwin, 2005 and Joly *et al*., 2010). The Psp system is found to be implicated in multi-drug resistance in persister cells and during pathogenesis in *Yersinia* and *Salmonella* (Darwin, 2005; Karlinsey *et al*., 2010 and Vega *et al*., 2012). The expression of *psp* genes is σ^{54}-dependent and is regulated by two key interacting partners: a stress independent low level bEBP, PspF, and its cognate negative regulator PspA, which associates with the IM and PspBC sensors (Darwin, 2005 and Joly *et al*., 2010). SMI was chosen as the major technique to unravel the cellular landscape of the Psp response in the live *E. coli* cells taking into account the effects of cellular membrane, stress levels and diverse protein interactions as a complete system as compared to *in vitro* studies in which not all components of the stress response can be studied simultaneously. Until now, models describing Psp response have been incomplete and mainly based on the ensemble biochemical properties of isolated regulatory components. The detailed knowledge of the localisations of PspF and PspA and their states of self-association is vital in establishing how the system is controlled and functions *in vivo.* This chapter is aimed at highlighting the key findings reported in this thesis and how they have helped in developing a model of the Psp response.

8.1 PspF is a nucleoid associated hexameric bEBP

The SMI studies of chromosomal V-PspF offered new mechanistic insights into the genetic control of *psp* expression. With the help of quantification of images the difference in real subcellular localisation of PspF in the repressed state, as a PspF-PspA complex or non-repressed was established (see Figure 8.1). The cellular dynamics of the different PspF states along with its corresponding functional stoichiometries is briefly illustrated in Figure 8.1 which presents the cellular landscape of PspF and PspA in the *E. coli* cell. A stable repressive PspF-PspA complex was located in the nucleoid, transiently communicating with the IM via PspA (see Figure 8.1). The nucleoid association was abolished in the non-DNA binding mutant of PspF (V-PspF$_{1\text{-}275}$) and consequently no discernible foci were observed in this mutant. The UAS (nucleoid) associated PspF forms the first part of regulation driven by inhibition of PspF ATPase activity by PspA binding around the W56 region of PspF. The mutant of PspF, V-PspF^{W56A} exhibited localisation and dynamics different from V-PspF which were dependent on the interaction with PspA under non-stress conditions. In line with this the V-PspF$_{1\text{-}275}$ was weakly titrated at the membrane

by overproduction of PspA and PspBC from the plasmid. This indirectly showed that PspBC sensors localised in the polar regions of the cell which play a significant role in stabilising the contact of PspF-PspA (via PspA) with the membrane, thus influencing the signal perception

The nucleoid-bound PspF was classified into two different dynamic classes, a more dynamic PspA-dependent PspF and a more static form as part of the active transcription complex (Figure 8.1). The dynamic studies of PspF revealed that its cellular dynamics were similar to other DNA binding protein like LacI such as sliding on the DNA and Brownian diffusion across cytoplasm (Elf *et al*., 2007). Unlike PspA, PspF dynamics are independent of MreB. The repressed and non-repressed (active) PspF assembled as a single hexamer at the nucleoid (UAS) in non-stress as well as stress conditions. This ascertained that the switch in functional states of PspF is not characterised by a change in oligomeric state and also that it stably binds only one of the two *psp* promoters at a time. In addition, the interactions of PspF with the basal transcription complex greatly influenced the localisation and dynamics of the PspF hexamer-DNA complex (Figure 8.1). In the absence of the remodelling target of PspF, i.e. RPc, the PspF dynamics were reduced by 16- fold compared to WT cells.

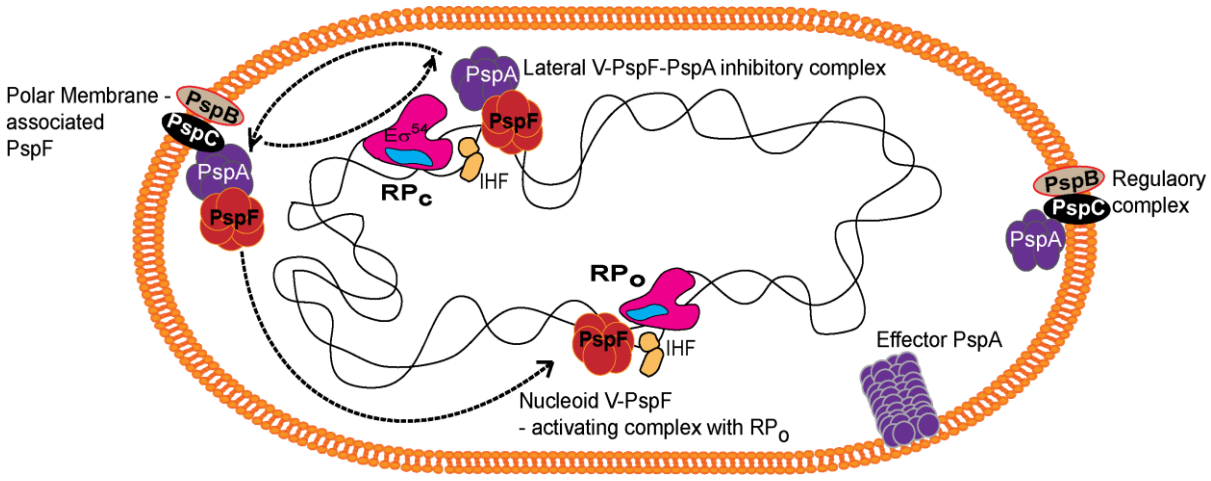

Figure 8.1 **Working model to show the key spatial, temporal and stoichiometric characteristics of different functional states of PspF in *E. coli*.** The nucleoid associated PspF-PspA complex is more dynamic and communicates with the polar membrane regions (shown by dotted arrows). With stress PspF associates with the active transcription complex and PspA switches to an effector.

The diagram in the Figure 8.1 illustrates the sequence of events resulting in the regulated activation of the Psp response. The stressed membrane triggers changes in the PspBC topology and interactions with the IM which alters the PspF-PspA complex, releasing PspF to be part of active transcription complex and PspA to be an effector upon stress conditions. In this way the control of Psp response and the switch of the Psp response from the repressed to activating state mediated by PspF and PspA was unravelled.

8.2 PspA and its dual functionality

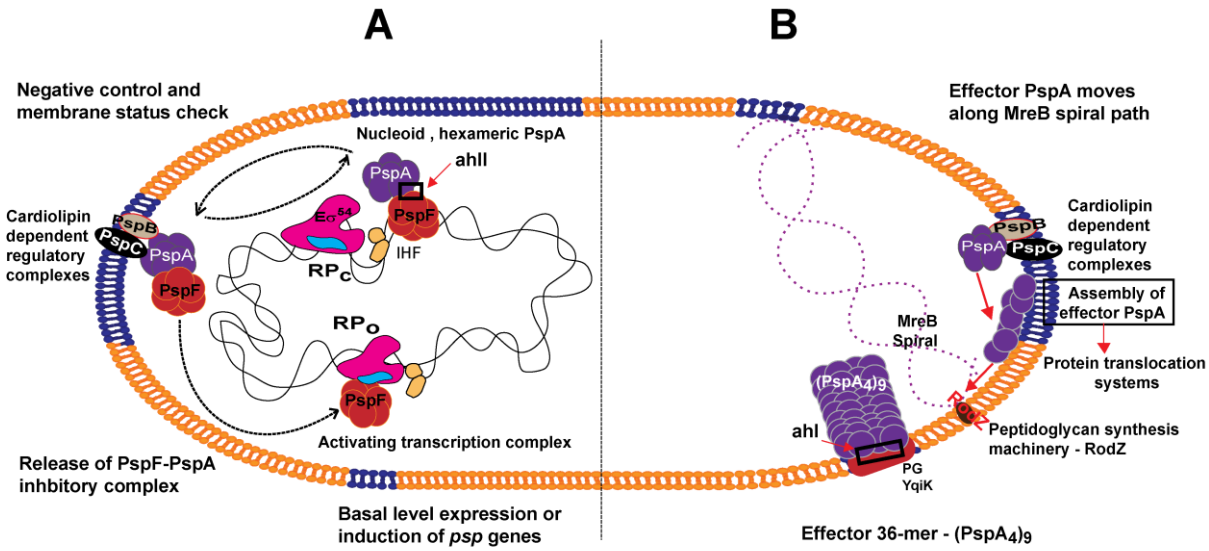

Figure 8.2 **The model showing regulatory and functional aspects of PspA**: (A) The regulatory PspA inhibits the ATPase activity of PspF. The inhibitory complex resides at the nucleoid and hexameric PspA binds the hexamer of PspF. The ahII of PspA HD1 is shown to play a vital role in the interaction with PspF and maintaining the hexameric oligomeric states. This PspF-PspA inhibitory complex patrols the membrane (B) Higher order effector PspA binds the lateral membrane. MreB and RodZ might play an important role in organising the lateral helical confirmation of effector PspA. CL (cardiolipin) also plays a vital role in Psp induction by defining the cellular poles with PspBC and translocation systems. The ahI of HD1 stabilises the membrane association and maintain higher order oligomers.

The SMI enabled to determine the localisations, dynamics and functional stoichiometry of the chromosomal V-PspA to be determined. SMI along with biochemical assays were employed to pin point the specific membrane determinants involved in organising PspA in the cells. The structural domain organisation within PspA was studied in detail and the role of N-terminal amphipathic helices was evaluated. The localisation of PspA changed from nucleoid/polar membrane to more lateral membrane associated with stress inducing conditions (see Figure 8.2). The PspA cellular dynamics were much slower under stress conditions compared to non-stress conditions. The slow membrane facilitated dynamics were further strengthened under the stress conditions. PspA stoichiometry as a regulator bound to PspF was found to be hexameric (lower order oligomer). The oligomeric state of PspA switched to higher order oligomer (up to 36-mer) as an effector with the activation of stress response (Figure 8.2). The membrane determinants were also shown to play a significant role in PspA organisation in the cells. Anionic phospholipid such as CL, predominantly localised at the poles was shown to be important for the PspBC mediated PspA-(-PspF) regulatory complexes at the poles. This strongly suggested that the stress signal was perceived at the poles and was transduced to PspA. A possible role of the potential lipid raft protein YqiK cannot be discounted for during the membrane repair mechanism of PspA effectors

during stress conditions. The localisation, dynamics and function of stabilising membrane integrity of the effector PspA is dependent on both MreB and RodZ during stress.

The data also proposes a mechanistic model of the intra-molecular signalling and communication between PspA α-helical domains (HDs) linking control and management of Psp response. The HD1 of PspA is vital for balancing both functions of PspA. The two N-terminal amphipathic helices in the HD1 are implicated in separate PspA functions and subsequent interactions between these helices maintained the balance between the regulatory and effector PspA functions. The ahI was involved in maintaining the membrane association of PspA and ahII was important for the negative regulation of PspF. The proline residue 25 probably provides an important link between ahI and ahII in order to keep a check on the stable interaction between these amphipathic helices.

The precise function of PspA as an effector during the membrane stress is unknown. Two possible mechanisms of action of effector PspA in maintaining the IM integrity and pmf are reported below. The PspA effector complexes could directly target the PG rich membrane regions where RodZ - cell wall synthesis machinery proteins are localised (see Figure 8.2). Or, as an effector PspA could associate with the damaged protein translocons associated with CL (and PG) in the cells polar regions (see Figure 8.2). It is already known that a PspA high order oligomer directly binds PG and repairs the membrane damage *in vitro* (Kobayashi *et al*., 2007). As illustrated in the Figure 8.2B the assembly of the polar IM PspA effectors possibly use MreB to organise its lateral dynamic complexes which then follow the route of IM-associated MreB patches along the membrane. Such lateral effector complexes could bind to the PG-rich domains marked by RodZ and their formation might be supported by MreB and YqiK. Such MreB filaments form membrane-associated patches coupled with RodZ and PGL/cell wall synthesis machinery and showed circumferential dynamics in *E. coli* (van den Ent *et al*., 2010; White *et al*., 2010; Teeffelen *et al*., 2011; Foss *et al*., 2011 and Salje *et al*., 2011). The data from this thesis formally shows that rather than physically plugging the potential “holes” made by mislocalised secretin(s) in the IM (Horstman and Darwin, 2012), PspA effectors may be are recruiting the membrane repair pathways with the help of MreB, RodZ and possibly lipid rafts.

Second function of PspA as an effector could be to maintain the protein translocation systems. It has been proposed (DeLisa *et al*., 2004) that the major conserved function of PspA and its homologues is to maintain protein translocations. Clade PspA (CL0235) has two members, PspA/IM30 and Snf7 (Huvet *et al*., 2010). Snf7 is a family of proteins involved in protein sorting and transport from the endosome to the vacuole/lysosome in eukaryotic cells that plays an important role in the degradation of both lipids and cellular proteins (Peck *et al*., 2004). The localisation of Tat, Sec and YidC translocons is polar and CL-dependent (Arias-Cartin *et al*., 2012) and their depletion induced production of PspA (Joly *et al*., 2010). The very strong PspA-Tat PspBC-dependent interaction (Mehner *et al*., 2012) suggests that the PspA effector function could involve a direct repair of the CL-associated translocon system(s). PspA functions

in repairing Tat pathway defects and this can be substituted by Vipp1 in *E. coli* while PspA substitutes for the same defect in the absence of Vipp1 (DeLisa *et al*., 2004) in cyanobacteria. Also, PspA stimulates protein export in *E. coli* (Arias-Cartin *et al*., 2012). CL associates with SecA (Gold *et al*., 2010), SecY and pmf, which are necessary to activate the SecA translocon ATPase (Dalal and Duong, 2011). SecY is important in reconstituting the defective Sec transcription and SecY protein is up-regulated when PspA amounts increased (Jovanovic *et al*., 2006). Therefore, one major role of PspA and PspA-like effectors may be in supporting protein translocation and export.

The research in thesis has shown the importance of studying native systems under physiological conditions in order to evaluate the protein-protein interactions eluded by biochemical ensemble-based assays. As indicated later in future work and prospects (see Chapter 9) there are unknowns in the Psp response including the specific signal(s) that triggers *psp* induction and the localisation and dynamics of the *psp* promoters. Another important unknown of the response is the mode of action of the PspA effectors in order to maintain IM integrity during stress conditions.

CHAPTER 9

9 Conclusions and Future Work

9.1 Concluding remarks

This thesis aimed at characterising and defining some of the fundamental molecular transactions and properties of the Phage Shock Protein (Psp) response *in vivo*. With the help of SMI *in vivo* PspF was shown to display predominant nucleoid dependent dynamics and was present in limiting amounts with only a single hexamer available at a time to activate either the *pspA* or *pspG* promoters. PspA as a dual function protein displayed a very diverse and dynamic spatial and temporal localisation with variable oligomeric states depending on the growth conditions. PspA facilitated the crucial interaction between the DNA bound PspF and enabled communication of this inhibitory complex with the membrane. The effector PspA is organised at the anionic lipid rich regions, interacting with the cell wall synthesis machinery via MreB and RodZ along the lateral membrane. Still much is unknown about the exact mechanism of action of PspA as an agent of membrane repair upon extracytoplasmic stress. Unfolding the widely conserved Psp response has clear implications for such systems in other organisms and in addition suggests the possible antimicrobial targets in enterobacteria, including the multi-drug resistant persister cells where *psp* is up regulated (Joly *et al*., 2010 and Vega *et al*., 2012).

9.2 Future Work

9.2.1 Elaborate on single molecule imaging studies of V-PspF and V-PspA

The Venus fusions of PspF and PspA can now be used as tools to answer many different questions regarding the molecular biology of enhancer dependent regulatory systems. As already mentioned in this thesis (Section 1 - Introduction) SMI methods can be successfully employed to report on stochasticity between cells in a population or even stochasticity between transcription and translation within a cell (Li and Xie, 2011 and Friedman and Gelles, 2012). In line with this, single cell single molecule methods can be used to study quantitatively whether or not this model enhancer dependent system displays bursts in gene expression, as seen in the Lac system (Golding *et al*., 2005; Yu *et al*. 2006 and Li and Xie, 2011). The bursts in gene expression lead to fluctuations in mRNA and protein content in the cells with transcription and translational cycles. It would be interesting to determine the bursts in gene expression in the enhancer dependent systems and the mathematical distribution of the expression bursts (Golding *et al*., 2005, Le *et al*., 2005, Yu *et al*., 2006 and Li and Xie, 2011). This can be achieved using Psp system by tracking the expression of fluorescent genes chromosomally fused to the *pspA* and *pspG* promoters respectively and observing their amounts of expression under PspA dependent regulation and

stress induced activation. Current views suggest that transcriptional outputs governed by a simple association-dissociation of transcription factors give a geometric distribution of expression bursts (Golding et al., 2005; Le et al., 2005; Yu et al., 2006, Li and Xie, 2011 and Friedman and Gelles, 2012).

Whether the outputs from the enhancer dependent system will follow geometric distribution is unclear because of the requirement for a transcriptional activator. This transcriptional activator protein is an ATPase that couples its nucleotide dependent functional states to create altered states of the RNA polymerase needed for transcription. Besides the expression bursts, the localisation of the *pspA* and *pspG* promoters in the cells with respect to each other will be determined under different growth conditions. The interactions between these sites will be studied in greater detail. Another interesting point of investigation would be to ascertain whether the activation of these promoters is governed by their proximity to the membrane at a particular time during the induction of response. It will also be interesting to study chromosomal expression of fluorescent proteins fused to PspG and correlate its spatial and temporal localisation with PspA to understand more about the mechanism of Psp response.

9.2.2 Understanding the membrane integrity during Psp stress response

Many different membrane determinants that play an important role during the Psp response have been reported in this thesis. Most of the membrane determinants were shown to play a role in organisation of PspA effectors. Some of the components studied in this thesis are the anionic phospholipids such as PG and CL and membrane determinant proteins, such as RodZ, MreB and YqiK, all help in the organisation of PspA. In preliminary proof of principle studies (Appendix-7), it was shown that a particular napthylstyryl-pyridinium dye called – (1-[2-Hydroxy-3-(N,N-di-methyl-N-hydroxyethyl) ammonio-propyl]-4-[β-[2-(di-n-butylamino)-6-napthyl] vinyl] pyridinium dibromide) (di-4-ANEPPDHQ), which has recently been used in eukaryotic cells to distinguish between the ordered membrane phase from the unordered phase (Obaid *et al*., 2003; Dinic *et al*., 2011 and Owen *et al*., 2011), dye can also be used in live *E. coli* cells . The identification of the different phases could be important because of the association of ordered phase with lipid rafts formation (Obaid *et al*., 2003; Dinic *et al*., 2011 and Owen *et al*., 2011). The same dye was used to stain the *E. coli* cell membrane under non-stress and stress conditions in order to study whether the different states of ordered or unordered membrane are present in prokaryotic cells. The different binding intensity of the dye may suggest the presence of different states of the membrane and indirectly show the occurrence of lipid rafts maintaining the ordered phase of the membrane. The MG1655 (WT), *ΔpspF* and *Δcls* cells were grown under non-stress and pIV induced stress conditions in minimal media. The cells with OD_{600} of 0.3 were stained with the 2 μM di-4-ANEPPDHQ and incubated for 20 minutes and then imaged using TIRF microscopy. The images of the cells stained with the dye

were used to measure the intensity distribution across the cell length (Appendix-7A). This analysis showed an increase in the total fluorescence intensity of the cells under stress by two-fold.

The intensity with respect to the location showed that the dye bound much more strongly at the poles under non-stress conditions; while under stress conditions the dye was predominantly associated with the lateral membrane (Appendix-7B) in much higher amounts. However this change in the amount and location of binding of the dye was independent of the presence of PspF and CL in the cells (Appendix-7Bii). In addition higher amounts of PspA did not increase the binding of the dye to the membrane under non-stress conditions (Appendix-7). Moreover this dye did not show any non-specific interaction with PspA in fluorescence anisotropy. The quantification of the preliminary data from the staining with di-4-ANEPPDHQ showed that the membrane resorts to ordered phase at the poles under non-stress conditions and the specific *psp*-inducing membrane stress conditions imposes the formation of ordered phase at the lateral membrane. Consequently the ordered phase at the lateral membrane can support the association of lipid raft proteins and thereby many different membrane repair mechanisms including Psp along the lateral membrane. Thus this dye could be potentially used to characterise the nature of the membrane architecture in its different states and how these different phases mobilise different signalling pathways.

So for the future work it would be interesting to test the binding and behaviour of this dye using lipid vesicles with different lipid composition *in vitro*. To evaluate the extent of di-4-ANEPPDHQ binding to anionic phospholipids PG and CL, and measure the binding constants in the presence or absence of purified PspA. This could suggest a possible mechanism of action of effector PspA, mediating the formation of ordered membranes by organising anionic lipids into specific lipid rafts and their subsequent stabilisation by lipid rafts proteins such as YqiK. Finally, understanding the stress dependent changes in the IM, which PspBC-PspA senses, remains a challenge and this method might shed some light on the possible signal(s) that induce Psp response.

REFERENCES

1. Adams, H., Teertstra, W., Demmers, J., Boesten, R., et al. (2003) Interactions between Phage-Shock Proteins in Escherichia coli. *Journal of Bacteriology*. 185 (4), 1174-1180.

2. Alley, M.R., Maddock, J.R. & Shapiro, L. (1992) Polar localization of a bacterial chemoreceptor. *Genes & Development*. 6 (5), 825-836.

3. Alteri, C.J., Lindner, J.R., Reiss, D.J., Smith, S.N., et al. (2011). The broadly conserved regulator PhoP links pathogen virulence and membrane potential in *Escherichia coli*. *Molecular Microbiology*. 82 (1), 145-163

4. Alyahya, S.A., Alexander, R., Costa, T., Henriques, A.O., et al. (2009) RodZ, a component of the bacterial core morphogenic apparatus. *Proceedings of the National Academy of Sciences*. 106 (4), 1239-1244.

5. Amit, R., Garcia, H., Phillips, R. & Fraser, S. (2011) Building Enhancers from the Ground Up: A Synthetic Biology Approach. *Cell*. 146 (1), 105-118.

6. Arous, S., Buchrieser, C., Folio, P., Glaser, A.N., et al. (2004). Global analysis of gene expression in an rpoN mutant of *Listeria monocytogenes*. *Microbiology*. 150, 1581-1599.

7. Arias-Cartin, R., Grimaldi, S., Arnoux, P., Guigliarelli, B., et al. (2012) Cardiolipin binding in bacterial respiratory complexes: Structural and functional implications. *Biochimica et Biophysica Acta*. 1817 (10), 1937-1949.

8. Ausmees, N., Kuhn, J. & Jacobs-Wagner, C. (2003) The Bacterial Cytoskeleton: An Intermediate Filament-Like Function in Cell Shape. *Cell*. 115, 705-713.

9. Baba, T., Ara, T., Hasegawa, M., Takai, Y., et al. (2006). Construction of Escherichia coli K-12 in-frame, single-gene knockout mutants: the Keio collection. *Molecular Systems Biology*. 2: 2006. doi:10.1038/msb4100050

10. Bach, J.N. & Bramkamp, M. (2013) Flotillins functionally organize the bacterial membrane. *Molecular Microbiology*. 88 (6), 1205-1217.

11. Badrinarayanan, A., Reyes-Lamothe, R., Uphoff, S., Leake, M.C., et al. (2012) In Vivo Architecture and Action of Bacterial Structural Maintenance of Chromosome Proteins. *Science*. 338 (6106), 528-531.

12. Baranova, N. & Nikaido, H. (2002) The BaeSR Two-Component Regulatory System Activates Transcription of the yegMNOB (mdtABCD) Transporter Gene Cluster in Escherichia coli and Increases Its Resistance to Novobiocin and Deoxycholate. *Journal of Bacteriology*. 184 (15), 4168-4176.

13. Barrios, H., Grande, R., Olvera, L. & E, M. (1998) In vivo genomic footprinting analysis reveals that the complex Bradyrhizobium japonicum fixRnifA promoter region is differently occupied by two distinct RNA polymerase holoenzymes. *Proceedings of the National Academy of Sciences*. 95, 1014-1019.

14. Barry, R.M. & Gitai, Z. (2011) Self-assembling enzymes and the origins of the cytoskeleton. *Current Opinion in Microbiology*. 14 (6), 704-711.

15. Basharov, M. (2003) Protein folding. *Journal of cellular and molecular medicine*. 7(3), 223-237.

16. Basler, M., Pilhofer, M., Henderson, G.P., Jensen, G.J., et al. (2012) Type VI secretion requires a dynamic contractile phage tail-like structure. *Nature*. 483 (7388), 182-186.

17. Batchelor, J.D., Lee, P.S., Wang, A.C., Doucleff, M., et al. (2013) Structural Mechanism of GAF-Regulated σ^{54} Activators from Aquifex aeolicus. *Journal of Molecular Biology*. 425 (1), 156-170.

18. Bates, D. & Kleckner, N. (2005) Chromosome and Replisome Dynamics in E. coli: Loss of Sister Cohesion Triggers Global Chromosome Movement and Mediates Chromosome Segregation. *Cell*. 121 (6), 899-911.

19. Becker, L.A., Bang, I., Crouch, M. & Fang, F.C. (2005) Compensatory role of PspA, a member of the phage shock protein operon, in rpoE mutant Salmonella enterica serovar Typhimurium. *Molecular Microbiology*. 56 (4), 1004-1016.

20. Beloin, C., Valle, J., Latour-Lambert, P., Faure, P., et al. (2004) Global impact of mature biofilm lifestyle on *Escherichia coli* K-12 gene expression. *Molecular Microbiology*. 51 (3), 659-674.

21. Bendezu, F., Hale, C., Bernhardt, T. & Boer, P. (2008) RodZ (YfgA) is required for proper assembly of the MreB actin cytoskeleton and cell shape in E. coli. *The EMBO Journal*. 28193-204.

22. Bergler, H., Abraham, D., Aschauer, H. & Turnowsky, F. (1994) Inhibition of lipid biosynthesis induces the expression of the pspA gene. *Microbiology*. 140, 1937-1944.

23. Bernardo, L.M., Johansson, L.U., Solera, D., Skarfstad, E., et al. (2006) The guanosine tetraphosphate (ppGpp) alarmone, DksA and promoter affinity for RNA polymerase in regulation of σ^{54}-dependent transcription. *Molecular Microbiology*. 60 (3), 749-764.

24. Bi, E. & Lutkenhaus, J. (1991) FtsZ ring structure associated with division in Escherichia coli. *Letters to Nature*. 354, 161-164.

25. Bidle, K.A., Kirkland, P.A., Nannen, J.L. & Maupin-Furlow, J.A. (2008). Proteomic analysis of *Haloferax volcanii* reveals salinity-mediated regulation of the stress response protein PspA. *Microbiology.*153 (Pt 5), 1436 - 43.

26. Biebricher, A., Wende, W., Escudé, C., Pingoud, A., et al. (2009) Tracking of Single Quantum Dot Labeled EcoRV Sliding along DNA Manipulated by Double Optical Tweezers. *Biophysical Journal*. 96 (8), 50-52.

27. Biteen, J.S. (2012) Extending the tools of single-molecule fluorescence imaging to problems in microbiology. *Molecular Microbiology*. 85 (1), 1-4.

28. Biteen, J.S., Shapiro, L. & Moerner, W.E. (2011) Exploring Protein Superstructures and Dynamics in Live Bacterial Cells Using Single-Molecule and Superresolution Imaging. *Methods Mol Biol.* 783, 139-158.

29. Biteen, J.S., Thompson, M.A., Tselentis, N.K., Bowman, G.R., et al. (2008) Super-resolution imaging in live *Caulobacter crescentus* cells using photoswitchable EYFP. *Nature Methods*. 5 (11), 947-949.

30. Bogdanov, M. & Dowhan, W. (2012) Lipid-dependent Generation of Dual Topology for a Membrane Protein. *Journal of Biological Chemistry*. 287 (45), 37939-37948.

31. Bordes, P., Wigneshweraraj, S.R., Schumacher, J., Zhang, X., et al. (2003) The ATP hydrolyzing transcription activator phage shock protein F of Escherichia coli: Identifying a surface that binds σ^{54}. *Proceedings of the National Academy of Sciences*. 100 (5), 2278-2283.

32. Bose, D., Pape, T., Burrows, P.C., Rappas, M., et al. (2008) Organization of an Activator-Bound RNA Polymerase Holoenzyme. *Molecular Cell*. 32 (3), 337-346.

33. Brissette, J.L., & Russel, M. (1990) Secretion and Membrane integration of a filamentous phage-encoded morphogenetic protein. *Journal of Molecular Biology*. 211, 565-580.

34. Brissette, J.L., Russel, M., Weiner, L. & Model, P. (1990) Phage shock protein, a stress protein of Escherichia coli. *Proceedings of the National Academy of Sciences*. 87, 862-866.

35. Browning, D.F. & Busby, S.J. (2004) The regulation of bacterial transcription initiation. *Nature Reviews Microbiology*. 2 (1), 57-65.

36. Buck, M., Bose, D., Burrows, P., Joly, N., et al. (2006) A second paradigm for gene activation in bacteria. *Biochemical Society Transactions*. 34 (44), 33717-33726.

37. Buddelmeijer, N., Krehenbrink, M., Pecorari, F. & Pugsley, A.P. (2008) Type II Secretion System Secretin PulD Localizes in Clusters in the *Escherichia coli* Outer Membrane. *Journal of Bacteriology*. 191 (1), 161-168.

38. Burrows, P., Wigneshweraraj, S., Bose, D., Joly, N., *et al*. (2008) Visualizing the organization and reorganization of transcription complexes for gene expression. *Biochemical Society Transactions*. 36(4), 776 - 779.

39. Burrows, P.C., Joly, N., Cannon, W.V., Cámara, B.P., et al. (2009) Coupling σ Factor Conformation to RNA Polymerase Reorganisation for DNA Melting. *Journal of Molecular Biology*. 387 (2), 306-319.

40. Bury-Moné, S., Nomane, Y., Reymond, N., Barbet, R., et al. (2009) Global Analysis of Extracytoplasmic Stress Signaling in *Escherichia coli*. *PLoS Genetics*. 5 (9), e1000651, 1-17.

41. Bush, M. & Dixon, R. (2012) The Role of Bacterial Enhancer Binding Proteins as Specialized Activators of σ^{54}-Dependent Transcription. *Microbiology and Molecular Biology Reviews*. 76 (3), 497-529.

42. Bustamante, C., Cheng, W. & Mejia, Y.X. (2011) Revisiting the Central Dogma One Molecule at a Time. *Cell*. 144 (4), 480-497.

43. Cannon, W., Gallegos, M. & Buck, M. (2000) Isomerization of a binary σ–promoter DNA complex by transcription activators. *Nature Structural Biology*. 7 (7), 594-601.

44. Cavalli, V. (2012) Ready, STAT, go: transcription factors on the move. *The EMBO Journal*. 31 (6), 1331-1333.

45. Chakraborty, A., Wang, D., Ebright, Y.W., Korlann, Y., et al. (2012) Opening and Closing of the Bacterial RNA Polymerase Clamp. *Science*. 337 (6094), 591-595.

46. Chen, B., Doucleff, M., Wemmer, D.E., de Carlo, S., et al. (2007) ATP ground- and transition states of bacterial enhancer binding AAA+ ATPases support complex formation with their target protein, σ^{54}. *Structure*. 15 (4), 429-440.

47. Chen, B., Sysoeva, T.A., Chowdhury, S., Guo, L., et al. (2010) Engagement of Arginine Finger to ATP Triggers Large Conformational Changes in NtrC1 AAA+ ATPase for Remodeling Bacterial RNA Polymerase. *Structure*. 18 (11), 1420-1430.

48. Chen, X. & Cremer, P.S. (2006) The Stochastic Nature of Gene Expression Revealed at the Single-Molecule Level. *ACS Chemical Biology*. 1 (3), 129-131.

49. Cherepanov PP, Wackernagel W (1995) Gene disruption in *Escherichia coli*: TcR and KmR cassettes with the option of Flp-catalyzed excision of the antibiotic-resistance determinant. *Gene*. 158: 9-14.

50. Chiu, S. & Leake, M.C. (2011) Functioning Nanomachines Seen in Real-Time in Living Bacteria

Using Single-Molecule and Super-Resolution Fluorescence Imaging. *International Journal of Molecular Sciences*. 12,122518-2542.

51. Chung SH, Kennedy RA (1991) Forward-backward non-linear filtering technique for extracting small biological signals from noise. *Journal of Neuroscience Methods.* 40, 71-86.

52. Cooper, S. (2006) Regulation of DNA synthesis in bacteria: analysis of the Bates/Kleckner licensing/initiation-mass model for cell cycle control. *Molecular Microbiology*. 62 (2), 303-307.

53. Crocker JC, Grier DG (1996) Methods of digital video microscopy for colloidal studies. *Journal of Colloid and Interface Science* .179, 298-310.

54. Cronan, J.E. (2003) Bacterial Membrane Lipids: Where Do We Stand? *Annual Review of Microbiology*. 57 (1), 203-224.

55. Dalal, K. & Duong, F. (2011) The SecY complex: conducting the orchestra of protein translocation. *Trends in Cell Biology*. 21 (9), 506-514.

56. Danese, P.N. & Silhavy, T.J. (1997) The σ^E and the Cpx signal transduction systems control the synthesis of periplasmic protein-folding enzymes in Escherichia coli. *Genes & Development*. 11 (9), 1183-1193.

57. Danese, P.N., Snyder, W.B., Cosma, C.L., Davis, L.J., et al. (1995) The Cpx two-component signal transduction pathway of Escherichia coli regulates transcription of the gene specifying the stress-inducible periplasmic protease, DegP. *Genes & Development*. 9 (4), 387-398.

58. Darst, S.A. (2004) New inhibitors targeting bacterial RNA polymerase. *Trends in Biochemical Sciences*. 29(4), 160-162.

59. Dartigalongue, C., Missiakas, D. & Raina, S. (2001) Characterization of the Escherichia coli σ^E Regulon. *Journal of Biological Chemistry*. 276 (24), 20866-20875.

60. Darwin, A. & Miller, V. (1999) Identification of *Yersinia enterocolitica* genes affecting survival in an animal host using signature-tagged transposon mutagenesis. *Molecular Microbiology*. 32 (1), 51-62.

61. Darwin, A.J. (2005) The phage-shock-protein response. *Molecular Microbiology*. 57 (3), 621-628.

62. Darwin, A.J. (2013) Stress Relief during Host Infection: The Phage Shock Protein Response Supports Bacterial Virulence in Various Ways. *PLoS Pathogens*. 9 (7), e1003388.

63. Darzacq, X., Yao, J., Larson, D.R., Causse, S.Z., et al. (2009) Imaging Transcription in Living Cells. *Annual Review of Biophysics*. 38 (1), 173-196.

64. Datsenko KA, Wanner BL (2000) One-step inactivation of chromosomal genes in Escherichia coli K-12 using PCR products. *Proceedings of the National Academy of Sciences*. 97, 6640-6645.

65. de Carlo, S., Chen, B., Hoover, T.R., Kondrashkina, E., et al. (2006) The structural basis for regulated assembly and function of the transcriptional activator NtrC. *Genes & Development*. 201485-1495.

66. deHaseth, P.L., Zupancic, M.L. & Record, M.T., Jr. (1998) RNA Polymerase-Promoter Interactions: the Comings and Goings Of RNA Polymerase. *Journal of Bacteriology*. 180 (12), 3019-3025.

67. DeLisa, M.P., Lee, P., Palmer, T. & Georgiou, G. (2003) Phage Shock Protein PspA of Escherichia coli Relieves Saturation of Protein Export via the Tat Pathway. *Journal of Bacteriology*. 186 (2), 366-373.

68. Dhamdhere, G. & Zgurskaya, H.I. (2010) Metabolic shutdown in Escherichia coli cells lacking the outer membrane channel TolC. *Molecular Microbiology*. 77 (3), 743-754.

69. Dinic, J., Biverståhl, H., Mäler, L. & Parmryd, I. (2011) Laurdan and di-4-ANEPPDHQ do not respond to membrane-inserted peptides and are good probes for lipid packing. *Biochimica et Biophysica Acta*. 1808 (1), 298-306.

70. Doherty, G.P., Fogg, M.J., Wilkinson, A.J. & Lewis, P.J. (2010) Small subunits of RNA polymerase: localization, levels and implications for core enzyme composition. *Microbiology*. 156 (12), 3532-3543.

71. Doucleff, M., Pelton, J.G., Lee, P.S., Nixon, B.T., et al. (2007) Structural Basis of DNA Recognition by the Alternative σ-factor, σ^{54}. *Journal of Molecular Biology*. 369 (4), 1070-1078.

72. Dove, S., Huang, F. & Hothschild, A. (2000) Mechanism for a transcriptional activator that works at the isomerization step. *Proceedings of the National Academy of Sciences*. 97 (24), 13215-13220.

73. Driessen, A.J.M. & Nouwen, N. (2008) Protein Translocation across the Bacterial Cytoplasmic Membrane. *Annual Review of Biochemistry*. 77 (1), 643-667.

74. Dulin, D., Lipfert, J., Moolman, M.C. & Dekker, N.H. (2012) Studying genomic processes at the single-molecule level: introducing the tools and applications. *Nature Reviews Genetics*. 14 (1), 9-22.

75. Dworkin, J., Jovanovic, G. & Model, P. (1997) Role of Upstream Activation Sequences and Integration Host Factor in Transcriptional Activation by the Constitutively Active Prokaryotic Enhancer-Binding Protein PspF. *Journal of Molecular Biology*. 273, 377-378.

76. Dworkin, J., Jovanovic, G. & Model, P. (2000) The PspA Protein of *Escherichia coli* is a Negative Regulator of σ^{54}-Dependent Transcription. *Journal of Bacteriology*. 182 (2), 311-319.

77. Dykxhoorn, D.M., St. Pierre, R., and Linn, T. (1996) A set of compatible tac promoter expression vectors. *Gene*. 177, 133-136.

78. Elderkin, S., Bordes, P., Jones, S., Rappas, M., et al. (2005) Molecular Determinants for PspA-Mediated Repression of the AAA Transcriptional Activator PspF. *Journal of Bacteriology*. 187 (9), 3238-3248.

79. Elderkin, S., Jones, S., Schumacher, J., Studholme, D., et al. (2002) Mechanism of Action of the Escherichia coli Phage Shock Protein PspA in Repression of the AAA Family Transcription Factor PspF. *Journal of Molecular Biology*. 320 (1), 23-37.

80. Elf, J., Li, G.-. & Xie, X.S. (2007) Probing Transcription Factor Dynamics at the Single-Molecule Level in a Living Cell. *Science*. 316 (5828), 1191-1194.

81. Elowitz, M., Surette, M., Wolf, P., Stock, J., et al. (1999) Protein Mobility in the Cytoplasm of *Escherichia coli*. *Journal of Bacteriology*. 181 (1), 197-203.

82. Engl, C., Beek, A.T., Bekker, M., Mattos, J.T., et al. (2011) Dissipation of Proton Motive Force is not Sufficient to Induce the Phage Shock Protein Response in *Escherichia coli*. *Current Microbiology*.62 (5), 1374-1385.

83. Engl, C., Jovanovic, G., Lloyd, L., Murray, H., et al. (2009) *In vivo* localizations of membrane stress controllers PspA and PspG in *Escherichia coli*. *Molecular Microbiology*. 73 (3), 382-396.

84. Erickson, J.W. & Gross, C.A. (1989) Identification of the σ^E subunit of Escherichia coli RNA polymerase: a second alternate σ factor involved in high-temperature gene expression. *Genes & Development*. 3 (9), 1462-1471.

85. Feng, J., Model, P. & Russel, M. (1999) A trans-envelope protein complex needed for filamentous phage assembly and export. *Molecular Microbiology*. 34 (4), 745-755.

86. Fenton, M. & Gralla, J. (2001) Function of the bacterial TATAAT− 10 element as single-stranded DNA during RNA polymerase isomerization. *Proceedings of the National Academy of Sciences*. 98 (16), 9020-9025.

87. Filloux, A., Hachani, A. & Bleves, S. (2008) The bacterial type VI secretion machine: yet another player for protein transport across membranes. *Microbiology*. 154 (6), 1570-1583.

88. Flores-Kim, J. & Darwin, A.J. (2012) Phage shock protein C (PspC) of Yersinia enterocolitica is a polytopic membrane protein with implications for regulation of the Psp stress response. *Journal of Bacteriology*. 194 (23), 6548-6559.

89. Foss, M.H., Eun, Y-J., and Weibel, D.B. (2011) Chemical-biological studies of subcellular organization in bacteria. *Biochemistry.* 50, 7719-7734.

90. Freundlich, M., Ramani, N., Mathew, E., Sirko, A., et al. (1992) The role of integration host factor in gene expression in Escherichia coli. *Molecular Microbiology*. 6 (18), 2557-2563.

91. Friedman, L., Mumm, J. & Gelles, J. (2013) RNA polymerase approaches its promoter without

long-range sliding along DNA. *Proceedings of the National Academy of Sciences*. 110(24), 9740-9745.

92. Friedman, L. & Gelles, J. (2012) Mechanism of Transcription Initiation at an Activator-Dependent Promoter Defined by Single-Molecule Observation. *Cell*. 148 (4), 679-689.

93. Garcia, H., Sanchez, A., Boedicker, J.Q., Osborne, M., et al. (2012) Operator Sequence Alters Gene Expression Independently of Transcription Factor Occupancy in Bacteria. *Cell Reports*. 2 (1), 150-161.

94. Gelles, J., Schnapp, B.J. and Sheetz, M.P. (1988). Tracking kinesin-driven movements with nanometer-scale precision. *Nature*. 331, 450-53

95. Ghosh, T., Bose, D. and Zhang, X. (2010) Mechanisms for activating bacterial RNA polymerase. *FEMS Microbiology Reviews*. 34(5), 611-627.

96. Gitai, Z. (2009). New fluorescence microscopy methods for microbiology: sharper, faster, and quantitative. *Current Opinion in Microbiology*. 12 (3), 341-346.

97. Gitai, Z., Dye, N.A., Reisenauer, A., Wachi, M., et al. (2005) MreB Actin-Mediated Segregation of a Specific Region of a Bacterial Chromosome. *Cell*. 120 (3), 329-341.

98. Gold, V.A., Robson, A., Bao, H., Romantsov, T., et al. (2010) The action of cardiolipin on the bacterial translocon. *Proceedings of the National Academy of Sciences*. 107 (22) 10044-10049.

99. Golding, I., Paulsson, J., Zawilski, S.M. & Cox, E.C. (2005) Real-Time Kinetics of Gene Activity in Individual Bacteria. *Cell*. 123 (6), 1025-1036.

100. Golding, I. & Cox, E. (2006) Physical Nature of Bacterial Cytoplasm. *Physical Review Letters*. 96 (9), 098102.

101. Goswami, D., Gowrishankar, K., Bilgrami, S., Ghosh, S., et al. (2008) Nanoclusters of GPI-Anchored Proteins Are Formed by Cortical Actin-Driven Activity. *Cell*. 135 (6), 1085-1097.

102. Grainger, D.C., Hurd, D., Goldberg, M.D. & Busby, S.J. (2006) Association of nucleoid proteins with coding and non-coding segments of the *Escherichia coli* genome. *Nucleic Acids Research*. 34 (16), 4642-4652.

103. Green, R.C. & Darwin, A.J. (2004) PspG, a New Member of the *Yersinia enterocolitica* Phage Shock Protein Regulon. *Journal of Bacteriology*. 186 (15), 4910-4920.

104. Gueguen, E., Flores-Kim, J. & Darwin, A.J. (2011) The *Yersinia enterocolitica* phage-shock-proteins B and C can form homodimers and heterodimers in vivo with the possibility of close association between multiple domains. *Journal of Bacteriology*. 193 (20), 5747-5758.

105. Guilvout, I., Chami, M., Engel, A., Pugsley, A., et al. (2006) Bacterial outer membrane secretin PulD assembles and inserts into the inner membrane in the absence of its pilotin. *The EMBO Journal*. 25 (22), 5241-5249.

106. Hammar, P., Leroy, P., Mahmutovic, A., Marklund, E.G., et al. (2012) The lac Repressor Displays Facilitated Diffusion in Living Cells. *Science*. 336 (6088), 1595-1598.

107. Haneburger, I., Fritz, G., Jurkschat, N., Tetsch, L., et al. (2012) Deactivation of the E. coli pH Stress Sensor CadC by Cadaverine. *Journal of Molecular Biology*. 424 (1-2), 15-27.

108. Hankamer, B.D., Elderkin, S.L., Buck, M. & Nield, J. (2004) Organization of the AAA+ Adaptor Protein PspA Is an Oligomeric Ring. *Journal of Biological Chemistry*. 279 (10), 8862-8866.

109. Hardie, K., Lory, S. & Pugsley, A. (1996) Insertion of an outer membrane protein in Escherichia coli requires a chaperone-like protein. *The EMBO Journal*. 15 (5), 978-988.

110. Hassani, A.S., Amirmozafari, N. & Ghaemi, A. (2009) Virulence Increasing of Salmonella typhimurium in Balb/c Mice After Heat-Stress Induction of Phage Shock Protein A. *Current Microbiology*. 59 (4), 446-450.

111. Henning, U., Rehn, K., Volkmar, B. & Höhn, B. (1972) Cell envelope and shape of Escherichia coli K12. *European Journal of Biochemistry*. 26, 570-586.

112. Hinderhofer, M., Walker, C.A., Friemel, A., Sturmer, C.A., et al. (2009) Evolution of prokaryotic SPFH proteins. *BMC Evolutionary Biology*. 9:10. 1-18

113. Hirakawa, H., Inazumi, Y., Masaki, T., Hirata, T., et al. (2005) Indole induces the expression of multidrug exporter genes in Escherichia coli. *Molecular Microbiology*. 55 (4), 1113-1126.

114. Hong, E., Doucleff, M. & Wemmer, D.E. (2009) Structure of the RNA polymerase core-binding domain of σ^{54} reveals a likely conformational fracture point. *Journal of Molecular biology*. 390, 70-

115. Hopper, S. & Böck, A. (1995) Effector-mediated stimulation of ATPase activity by the σ^{54}-dependent transcriptional activator FHLA from Escherichia coli. *Journal of Bacteriology*. 177 (10), 2798-2803.

116. Horstman, N.K. & Darwin, A.J. (2012) Phage shock proteins B and C prevent lethal cytoplasmic membrane permeability in Yersinia enterocolitica. *Molecular Microbiology*. 85 (3), 445-460.

117. Huang, Y., Ferrières, L. & Clarke, D.J. (2006) The role of the Rcs phosphorelay in Enterobacteriaceae. *Research in Microbiology*. 157 (3), 206-212.

118. Hunke, S., Keller, R. & Müller, V.S. (2012) Signal integration by the Cpx-envelope stress system. *FEMS Microbiology Letters*. 326 (1), 12-22.

119. Huo, Y., Zhang, Y., Xiao, Y., Zhang, X., et al. (2009) IHF-binding sites inhibit DNA loop formation and transcription initiation. *Nucleic Acids Research*. 37 (12), 3878-3886.

120. Huvet, M., Toni, T., Sheng, X., Thorne, T., et al. (2011) The Evolution of the Phage Shock Protein Response System: Interplay between Protein Function, Genomic Organization, and System Function. *Molecular Biology and Evolution*. 28 (3), 1141-1155.

121. Huvet, M., Toni, T., Tan, H., Jovanovic, G., et al. (2009) Model-based evolutionary analysis: the natural history of phage-shock stress response. *Biochemical Society Transactions*. 37 (4), 762 - 767

122. Ishihama, A. (2000) Functional modulation of Escherichia coli RNA polymerase. *Annual Reviews in Microbiology*. 54, 499-518.

123. Iyer, L.M., Leipe, D.D., Koonin, E.V. & Aravind, L. (2004) Evolutionary history and higher order classification of AAA+ ATPases. *Journal of Structural Biology*. 146 (1-2), 11-31.

124. Joly, N., Burrows, P.C., Engl, C., Jovanovic, G., et al. (2009) A Lower-Order Oligomer Form of Phage Shock Protein A (PspA) Stably Associates with the Hexameric AAA+ Transcription Activator Protein PspF for Negative Regulation. *Journal of Molecular Biology*. 394 (4), 764-775.

125. Joly, N., Engl, C., Jovanovic, G., Huvet, M., et al. (2010) Managing membrane stress: the phage shock protein (Psp) response, from molecular mechanisms to physiology. *FEMS Microbiology Reviews*. 34, 797-827.

126. Jones, S.E., Lloyd, L.J., Tan, K.K. & Buck, M. (2003) Secretion Defects That Activate the Phage Shock Response of *Escherichia coli*. *Journal of Bacteriology*. 185 (22), 6707-6711.

127. Jordan, S., Junker, A., Helmann, J.D. & Mascher, T. (2006) Regulation of LiaRS-Dependent Gene Expression in Bacillus subtilis: Identification of Inhibitor Proteins, Regulator Binding Sites, and Target Genes of a Conserved Cell Envelope Stress-Sensing Two-Component System. *Journal of Bacteriology*. 188 (14), 5153-5166.

128. Jovanovic, G. & Model, P. (1997) PspF and IHF bind co-operatively in the psp promoter-

regulatory region of Escherichia coli. *Molecular Microbiology*. 25 (3), 473-481

129. Jovanovic, G., Dworkin, J. & Model, P. (1997) Autogenous Control of PspF, a Constitutively Active Enhancer-Binding Protein of *Escherichia coli*. *Journal of Bacteriology*. 179 (16), 5232-5237.

130. Jovanovic, G., Engl, C. & Buck, M. (2009) Physical, functional and conditional interactions between ArcAB and phage shock proteins upon secretin-induced stress in Escherichia coli. *Molecular Microbiology*. 74 (1), 16-28.

131. Jovanovic, G., Engl, C., Mayhew, A.J., Burrows, P.C., et al. (2010) Properties of the phage-shock-protein (Psp) regulatory complex that govern signal transduction and induction of the Psp response in Escherichia coli. *Microbiology*. 156 (10), 2920-2932.

132. Jovanovic, G., Lloyd, L.J., Stumpf, M.P., Mayhew, A.J., et al. (2006) Induction and Function of the Phage Shock Protein Extracytoplasmic Stress Response in Escherichia coli. *Journal of Biological Chemistry*. 281 (30), 21147-21161.

133. Jovanovic, G., Rakonjac, J. & Model, P. (1999) In Vivo and in Vitro Activities of the Escherichia coli σ^{54} Transcription Activator, PspF, and its DNA-binding Mutant, PspFΔHTH. *Journal of Molecular Biology*. 285, 469-483.

134. Jovanovic, G., Weiner, L. & Model, P. (1996) Identification, Nucleotide Sequence, and Characterization of PspF, the Transcriptional Activator of the *Escherichia coli* Stress-Induced psp Operon. *Journal of Bacteriology*. 178 (7), 1936-1945.

135. Jovanovic, M., James, E.H., Burrows, P.C., et al. (2011).Regulation of the co-evolved HrpR and HrpS AAA+ proteins required for Pseudomonas syringae pathogenicity. *Nature Communications*. 2:177, DOI: 10.1038/ncomms1177, 1-9.

136. Juarez, J.R. & Margolin, W. (2012) A bacterial actin unites to divide bacterial cells. *The EMBO Journal*. 31 (10), 2235-2236.

137. Kang, H.Y., Srinivasan, J. & Curtiss, R., III (2002) Immune Responses to Recombinant Pneumococcal PspA Antigen Delivered by Live Attenuated *Salmonella enterica* Serovar Typhimurium Vaccine. *Infection and Immunity*. 70 (4), 1739-1749.

138. Kao-huang, Y., Revzin, A., Butler, A.P., O'Conner, P., et al. (1977) Nonspecific DNA binding of genome-regulating proteins as a biological control mechanism: Measurement of DNA-bound *Escherichia coli* lac repressor *in vivo*. *Proceedings of the National Academy of Sciences*. 74 (10), 4228-4232.

139. Kaplan, T. & Friedman, N. (2012) Gene expression: Running to stand still. *Nature*. 484, 171-172.

140. Karimova, G., Pidoux, J., Ullmann, A., and Ladant, D. (1998) A bacterial two-hybrid system based on a reconstituted signal transduction pathway. *Proceedings of the National Academy of Sciences*. 95, 5752-5756.

141. Karlinsey, J.E., Maguire, M.E., Becker, L.A., Crouch, M.V., et al. (2010) The Phage Shock Protein PspA Facilitates Divalent Metal Transport and is required for Virulence of *Salmonella enterica sv. Typhimurium*. *Molecular Microbiology*. 78 (3), 669-685.

142. Kashyap, des, D.R., Kashyap, des, R., Wang, M., Liu, L., et al. (2011) Peptidoglycan recognition proteins kill bacteria by activating protein-sensing two-component systems. *Nature Medicine*. 17 (6), 676-683.

143. Kazmierczak, B., Mielke, D.L., Russel, M. and Model, P. (1994). pIV, a filamentous Phage protein that mediates Phage export across the bacterial cell envelope, forms a multimer. *Journal of Mol. Biol.* 238, 187-198.

144. Keren, I., Shah, D., Spoering, A., Kaldalu, N., et al. (2004) Specialized Persister Cells and the Mechanism of Multidrug Tolerance in *Escherichia coli*. *Journal of Bacteriology*. 186 (24), 8172-8180.

145. Kern, D., Volkman, B., Luginbühl, P., Nohaile, M., et al. (1999) Structure of a transiently phosphorylated switch in bacterial signal transduction. *Nature*. 402, 894-898.

146. Kim, S.Y., Gitai, Z., Kinkhabwala, A., Shapiro, L., et al. (2006) Single molecules of the bacterial actin MreB undergo directed treadmilling motion in *Caulobacter Crescentus*. *Proceedings of the National Academy of Sciences*. 103 (29), 10929-10934.

147. Kint, C.I., Verstraeten, N., Fauvart, M. & Michiels, J. (2012) New-found fundamentals of bacterial persistence. *Trends in Microbiology*. 20 (12), 577-585.

148. Kleerebezem, M., Crielaard, W. & Tommassen, J. (1996) Involvement of stress protein PspA (phage shock protein A) of *Escherichia coli* in maintenance of the proton motive force under stress conditions. *The EMBO Journal*. 15(1), 162-171.

149. Kitagawa, M., Ara, T., Arifuzzaman, M., Ioka-Nakamichi, T., Inamoto, E., Toyonaga, H., et al. (2005) Complete set of ORF clones of Escherichia coli ASKA library (A Complete Set of E. coli K-12 ORF Archive): Unique Resources for Biological Research. *DNA Research*. 12, 291-299.

150. Kobayashi, R., Suzuki, T. & Yoshida, M. (2007) *Escherichia coli* phage-shock protein A (PspA) binds to membrane phospholipids and repairs proton leakage of the damaged membranes. *Molecular Microbiology*. 66 (1), 100-109.

151. Kobayashi, H., Yamamoto, M. & Aono, R. (1998) Appearance of a stress-response protein, phage-shock protein A, in Escherichia coli exposed to hydrophobic organic solvents.

Microbiology. 144353-359.

152. Kubitschek, H. & Friske, J. (1986) Determination of bacterial cell volume with the coulter counter. *Journal of Bacteriology*. 168 (3), 1466-1467.

153. Kuhlman T E, Cox EC (2010) Site-specific chromosomal integration of large synthetic constructs. *Nucleid Acid Research*. 38: e92, Doi:10.1093/nar/gkp1193

154. Kuo SC, Gelles J, Steuer E, Sheetz MP (1991) A model for kinesin movement from nanometer level movements of kinesin and cytoplasmic dynein and force measurements. *Journal of Cell Science*. 14, 135-138.

155. Kustu, S., Santero, E., Keener, J., Popham, D., et al. (1989) Expression of σ^{54} (*ntrA*)-dependent genes is probably united by a common mechanism. *Microbiological and Molecular Biology Reviews*. 53 (3), 367-376.

156. Lafont, F., Abrami, L. & van der Goot, F.G. (2004) Bacterial subversion of lipid rafts. *Current Opinion in Microbiology*. 7 (1), 4-10.

157. Landgraf, D., Okumus, B., Chien, P., Baker, T.A., et al. (2012) Segregation of molecules at cell division reveals native protein localization. *Nature Methods*. 9 (5), 480-482.

158. Le T., Harlepp, S., Guet, C.C., Dittmar, K., et al. (2005) Real-time RNA profiling within a single bacterium. *Proceedings of the National Academy of Sciences*. 102 (26), 9160-9164.

159. Leake, M.C. (2013) The physics of life: one molecule at a time. *Philosophical transitions of the royal society*. 368, 20120248.

160. Leake, MC., Chandler JH., Wadhams, GH., Bai, F ., Berry RM., Armitage, JA., (2006) Stoichiometry and turnover in single, functioning membrane protein complexes. *Nature.* 443, 355-358.

161. Lee, D.J., Minchin, S.D. & Busby, S.J.W. (2012) Activating Transcription in Bacteria. *Annual Review of Microbiology*. 66 (1), 125-152.

162. Lee, S., La Torre, de, A., Yan, D., Kustu, S., et al (2003) Regulation of the transcriptional activator NtrC1: structural studies of the regulatory and AAA+ ATPase domains. *Genes & Development*. 17 (20), 2552-2563.

163. Lee, S., Shin, J.Y., Lee, A. & Bustamante, C (2012) Counting single photoactivatable fluorescent molecules by photoactivated localization microscopy (PALM). *Proceedings of the National Academy of Sciences*. 109 (43), 17436-17441.

164. Lenn, T. & Leake, M.C. (2012) Experimental approaches for addressing fundamental biological questions in living, functioning cells with single molecule precision. *Open Biology*. 2 (6), 120090-120090.

165. Lenn, T., Gkekas, C.N., Bernard, L., Engl, C., et al. (2010) Measuring the stoichiometry of functional PspA complexes in living bacterial cells by single molecule photobleaching. *Chemical Communications*. 47 (1), 400-2.

166. Lenn T, Leake MC, Mullineaux CW (2008) Clustering and dynamics of cytochrome bd-I complexes in the *Escherichia coli* plasma membrane *in vivo*. *Molecular Microbiology* 70, 1397-1407.

167. Lennen, R.M., Kruziki, M.A., Kumar, K., Zinkel, R.A., et al. (2011) Membrane Stresses Induced by Overproduction of Free Fatty Acids in *Escherichia coli*. *Applied and Environmental Microbiology*. 77 (22), 8114-8128.

168. Li, G. & Xie, X.S. (2011) Central dogma at the single-molecule level in living cells. *Nature*. 475 (7356), 308-315.

169. Libby, E.A., Ekici, S. & Goulian, M. (2010) Imaging OmpR Binding to Native Chromosomal Loci in Escherichia coli. *Journal of Bacteriology*. 192 (15), 4045-4053.

170. Linderoth, N., Simon, M.A. and Russel, M. (1997). The Filamentous Phage pIV multimer visualized by scanning transmission electron microscopy. *Science*. 278, 1635 – 1637.

171. Lima, S., Guo, M.S., Chaba, R., Gross, C.A., et al. (2013) Dual Molecular Signals Mediate the Bacterial Response to Outer-Membrane Stress. *Science*. 340 (6134), 837-841.

172. Lipinska, B., King, J., Ang, D. & Georgopoulos, C. (1988) Sequence analysis and transcriptional regulation of the *Escherichia coli grpE* gene, encoding a heat shock protein. *Nucleic Acids Research*. 16 (15), 7545-7562.

173. Liu, J. & Rost, B. (2001) Comparing function and structure between entire proteomes. *Protein Science*. 10, 1970-1979.

174. Llopis, P.M., Jackson, A.F., Sliusarenko, O., Surovtsev, I., et al. (2010) Spatial organization of the flow of genetic information in bacteria. *Nature*. 466 (7302), 77-81.

175. Lloyd, L.J., Jones, S.E., Jovanovic, G., Gyaneshwar, P., et al. (2004) Identification of a New Member of the Phage Shock Protein Response in *Escherichia coli*, the Phage Shock Protein G (PspG). *Journal of Biological Chemistry*. 279 (53), 55707-55714.

176. Locke, J.C., Young, J.W., Fontes, M., Jimenez, M.J., et al. (2011) Stochastic Pulse Regulation in

Bacterial Stress Response. *Science*. 334 (6054), 366-369.

177. Loehlin, D.W. & Werren, J.H. (2012) Evolution of Shape by Multiple Regulatory Changes to a growth gene. *Science*. 335 (6071), 943-947.

178. Lopez, D. & Kolter, R. (2010) Functional microdomains in bacterial membranes. *Genes & Development*. 24 (17), 1893-1902.

179. Lord, S.J., Lee, H.D. & Moerner, W.E. (2010) Single-Molecule Spectroscopy and Imaging of Biomolecules in Living Cells. *Analytical Chemistry*. 82 (6), 2192-2203.

180. Löwe, J., van den Ent, F. & Amos, L.A. (2004) Molecules of the Bacterial Cytoskeleton. *Annual Review of Biophysics and Biomolecular Structure*. 33 (1), 177-198.

181. Lowry, O.H., Rosebrough, N.J., Farr, A.L. & Randall, R.J. (1951) Protein measurement with the Folin phenol reagent. *J. Biol. Chem.* 193, 265-275.

182. Lu, F. & Taghbalout, A. (2013) Membrane Association via an Amino-terminal Amphipathic Helix Is Required for the Cellular Organization and Function of RNase II. *Journal of Biological Chemistry*. 288 (10), 7241-7251.

183. Lu, Y., Guan, Z., Zhao, J. & Raetz, C.R. (2011) Three Phosphatidylglycerol-phosphate Phosphatases in the Inner Membrane of *Escherichia coli*. *Journal of Biological Chemistry*. 286 (7), 5506-5518.

184. Lyubetsky, V.A., Zverkov, O.A., Rubanov, L.I. & Seliverstov, A.V. (2011) Modeling RNA polymerase competition: the effect of σ-subunit knockout and heat shock on gene transcription level. *Biology Direct*. 6 (1), 3.

185. Magdziarz, M., Weron, A., Burnecki, K. & Klafter, J. (2009) Fractional Brownian Motion Versus the Continuous-Time Random Walk: A Simple Test for Sub diffusive Dynamics. *Physical Review Letters*. 103 (18), 180602 (4).

186. Mao, X.J., Huo, Y.X., Buck, M., Kolb, A., et al. (2007) Interplay between CRP-cAMP and PII-Ntr systems forms novel regulatory network between carbon metabolism and nitrogen assimilation in Escherichia coli. *Nucleic Acids Research*. 35 (5), 1432-1440.

187. Margolin, W. (2012) The Price of Tags in Protein Localization Studies. *Journal of Bacteriology*. 194 (23), 6369-6371.

188. Matlack, K.E., Mothes, W. & Rapoport, T.A. (1998) Protein Translocation: Tunnel Vision. *Cell*. 92, 381-390.

189. Matsumoto, K., Kusaka, J., Nishibori, A. & Hara, H. (2006) Lipid domains in bacterial membranes. *Molecular Microbiology*. 61 (5), 1110-1117.

190. Maxson, M. & Darwin, A. (2006) Multiple promoters control expression of the *Yersinia enterocolitica* phage-shock-protein A (pspA) operon. *Microbiology*. 152 (4), 1001-1010.

191. Maxson, M.E. & Darwin, A.J. (2004) Identification of Inducers of the *Yersinia enterocolitica Phage Shock Protein System and Comparison to the Regulation of the RpoE and Cpx Extracytoplasmic* Stress Responses. *Journal of Bacteriology*. 186 (13), 4199-4208.

192. Mehner, D., Osadnik, H., Lunsdorf, H. & Bruser, T. (2012) The Tat System for Membrane Translocation of Folded Proteins Recruits the Membrane-stabilizing Psp Machinery in *Escherichia coli*. *Journal of Biological Chemistry*. 287 (33), 27834-27842.

193. Mehta, P., Jovanovic, G., Lenn, T., Bruckbauer, A., et al. (2013) Dynamics and stoichiometry of a regulated enhancer-binding protein in live Escherichia coli cells. *Nature Communications*. 4:1997, DOI : 10.1038/ncomms2997, 1-9.

194. Mika, J.T. & Poolman, B. (2011) Macromolecule diffusion and confinement in prokaryotic cells. *Current Opinion in Biotechnology*. 22 (1), 117-126.

195. Mileykovskaya, E. & Dowhan, W. (2000) Visualization Of Phospholipid Domains in *Escherichia coli* by Using the Cardiolipin-Specific Fluorescent Dye 10-N-Nonyl Acridine Orange. *Journal of Bacteriology*. 182 (4), 1172-1175.

196. Mileykovskaya, E. & Dowhan, W. (2009) Cardiolipin membrane domains in prokaryotes and eukaryotes. *Biochimica et Biophysica Acta*. 1788 (10), 2084-2091.

197. Mileykovskaya, E., Fishov, I., Fu, X., Corbin, B.D., et al. (2003) Effects of Phospholipid Composition on MinD-Membrane Interactions in Vitro and *in vivo*. *Journal of Biological Chemistry*.278 (25), 22193-22198.

198. Miller, J. H. (1992). A short course in Bacterial Genetics: A laboratory manual and handbook for Escherichia coli and related bacteria. Cold Spring Harbor Laboratory Press, Cold Spring Harbor, N.Y.

199. Model, P., Jovanovic, G. & Dworkin, J. (1997) The *Escherichia coli* phage-shock-protein (psp) operon. *Molecular Microbiology*. 24 (2), 255-261.

200. Moerner, W.E. (2007) New directions in single-molecule imaging and analysis. *Proceedings of the National Academy of Sciences*. 104 (31), 12596-12602.

201. Moerner, W.E. (2012) Microscopy beyond the diffraction limit using actively controlled single molecules. *Journal of Microscopy*. 246 (3), 213-220.

202. Mogensen, J.E. & Otzen, D.E. (2005) Interactions between folding factors and bacterial outer membrane proteins. *Molecular Microbiology*. 57 (2), 326-346.

203. Morett, E. & Buck, M. (1989) In Vivo Studies on the Interaction of RNA Polymerase-σ^{54} with the *Klebsiella pneumoniae* and Rhizobium meliloti nifH Promoters. *Journal of Molecular Biology*. 210, 65-77.

204. Morett, E. & Segovia, L. (1993) The σ^{54} Bacterial Enhancer-Binding Protein Family: Mechanism of Action and Phylogenetic Relationship of Their Functional Domains. *Journal of Bacteriology*. 175 (19), 6067-6074.

205. Muhlradt, P.F. & Golecki, J.R. (1975) Asymmetrical distribution and artefactual reorientation of Lipopolysaccharide in the Outer Membrane Bilayer of *Salmonella typhimurium*. *European Journal of Biochemistry*. 51, 343-352.

206. Munsky, B., Neuert, G. & van Oudenaarden, A. (2012) Using Gene expression noise to understand gene regulation. *Science*. 336 (6078), 183-187.

207. Nagai T, Ibata K, Park ES, Kubota M, Mikoshiba K, Miyawaki A (2002) A variant of yellow fluorescent protein with fast and efficient maturation for cell-biological applications. *Nature Biotechnology*. 20, 87-91.

208. Nair, G. & Raj, A. (2011) Time-Lapse Transcription. *Science*. 332 (6028), 431-432.

209. Nenninger, A., Mastroianni, G. & Mullineaux, C.W. (2010) Size Dependence of Protein Diffusion in the Cytoplasm of *Escherichia coli*. *Journal of Bacteriology*. 192 (18), 4535-4540.

210. Ng, L.C., O'Neill, E. & Shingler, V. (1996) Genetic Evidence for Interdomain Regulation of the Phenol-responsive σ^{54}-dependent Activator DmpR. *Journal of Biological Chemistry*. 271 (29), 17281-17286.

211. Niba, E.T., Li, G., Aoki, K. & Kitakawa, M. (2010) Characterization of *rodZ* mutants: RodZ is not absolutely required for the cell shape and motility. *FEMS Microbiology Letters*. 30, 935-42.

212. Nichols, R.J., Sen, Saunak, Choo, Y.J., Beltrao, P., et al. (2011) Phenotypic Landscape of a Bacterial Cell. *Cell*. 144 (1), 143-156.

213. Nickelsen, J., Rengstl, B., Stengel, A., Schottkowski, M., et al. (2011) Biogenesis of the cyanobacterial thylakoid membrane system - an update. *FEMS Microbiology Letters*. 315 (1), 1-5.

214. Nilsen, T., Yan, A.W., Gale, G. & Goldberg, M.B. (2005) Presence of Multiple Sites Containing

Polar Material in Spherical *Escherichia coli* Cells That Lack MreB. *Journal of Bacteriology*. 187 (17), 6187-6196.

215. Nørby, J. (1988). Coupled assay of Na+, K+-ATPase activity. *Methods in Enzymology*. 156, 116-119.

216. Northrup, D. & Zhao, K. (2011) Application of ChIP-Seq and related techniques to the study of immune function. *Immunity*. 34 (6), 830-842.

217. Obaid, A.L., Loew, L.M., Wuskell, J.P. & Salzberg, B.M. (2004) Novel naphthylstyryl-pyridinium potentiometric dyes offer advantages for neural network analysis. *Journal of Neuroscience Methods*. 134 (2), 179-190.

218. Ogura, T. & Wilkinson, A. (2001) AAA+ superfamily ATPases: common structure–diverse function. *Genes to Cells*. 6, 575-597.

219. Osterberg, S., Skarfstad, E. & Shingler, V. (2010) The σ-factor FliA, ppGpp and DksA coordinate transcriptional control of the *aer2* gene of *Pseudomonas putida*. *Environmental Microbiology*. 12 (6), 1439-1451.

220. Owen, D.M., Rentero, C., Magenau, A., Abu-Siniyeh, A., et al. (2011) Quantitative imaging of membrane lipid order in cells and organisms. *Nature Protocols*. 7 (1), 24-35.

221. Paget, M. & Helmann, J. (2003) The σ^{70} family of σ factors. *Genome Biol.* 4:203. 1-6

222. Palmer, T. & Ben Berks, B.C. (2012) The twin-arginine translocation (Tat) protein export pathway. *Nature Reviews Microbiology*. 10, 483-496.

223. Park, S., Zhang, H., Jones, A.D. & Nixon, B.T. (2002) Biochemical Evidence for Multiple Dimeric States of the DctD Receiver Domain. *Biochemistry*. 41 (36), 10934-10941.

224. Patel, S. & Latterich, M. (1998) The AAA team: related ATPases with diverse functions. *Trends in Cell Biology*. 8, 65-71.

225. Peck, J.W., Bowden, E.T. & Burbelo, P.D. (2004) Structure and function of human Vps20 and Snf7 proteins. *Biochemical Journal*. 377 (3), 693-700.

226. Pelczar, M.J., Chan, E.C.S., Krieg, N.R. Microbiology. 5th edition, 2003. Tata McGraw-Hill, New Delhi.

227. Pohl, T., Uhlmann, M., Kaufenstein, M., Friedrich, T. (2007) Lambda Red-mediated mutagenesis and efficient large scale affinity purification of the *Escherichia coli* NADH:ubiquinone oxidoreductase (complex I). *Biochemistry*. 46, 10694-10702.

228. Qian, H., M. P. Sheetz, and E. L. Elson. (1991) Single-particle tracking: analysis of diffusion and flow in two-dimensional systems. *Biophys. J*. 60, 910 –921

229. Raivio, T. & Silhavy, T. (1997) Transduction of Envelope Stress in *Escherichia coli* by the Cpx Two-Component System. *Journal of Bacteriology*. 179 (24), 7724-7733.

230. Ramamurthi, K.S. & Losick, R. (2009) Negative membrane curvature as a cue for subcellular localization of a bacterial protein. *Proceedings of the National Academy of Sciences*. 106 (32), 13541-13545.

231. Rappas, M., Bose, D. & Zhang, X. (2007) Bacterial enhancer-binding proteins: unlocking σ^{54}-dependent gene transcription. *Current Opinion in Structural Biology*. 17 (1), 110-116.

232. Rappas, M., Schumacher, J., Beuron, F., Niwa, H., et al. (2005) Structural Insights into the Activity of Enhancer-Binding Proteins. *Science*. 307 (5717), 1972-1975.

233. Rappas, M., Schumacher, J., Niwa, H., Buck, M., et al. (2006) Structural Basis of the Nucleotide Driven Conformational Changes in the AAA+ Domain of Transcription Activator PspF. *Journal of Molecular Biology*. 357 (2), 481-492.

234. Reitzer, L. & Schneider, B.L. (2001) Metabolic Context and Possible Physiological Themes of σ^{54}-Dependent Genes in *Escherichia coli*. *Microbiology and Molecular Biology Reviews*. 65 (3), 422-444.

235. Rekas, A., Alattia, J., Nagai, T., Miyawaki, A., et al. (2002) Crystal Structure of Venus, a Yellow Fluorescent Protein with Improved Maturation and Reduced Environmental Sensitivity. *Journal of Biological Chemistry*. 277 (52), 50573-50578.

236. Renner, L.D. & Weibel, D.B. (2012) MinD and MinE Interact with Anionic Phospholipids and Regulate Division Plane Formation in *Escherichia coli. Journal of Biological Chemistry*. 287 (46), 38835-38844.

237. Reyes-Lamothe, R., Sherratt, D.J. & Leake, M.C. (2010) Stoichiometry and Architecture of Active DNA Replication Machinery in *Escherichia coli*. *Science*. 328 (5977), 498-501.

238. Rice, P.A., Yang, S., Mizuuchi, K. & Nash, H.A. (1996) Crystal structure of an IHF-DNA complex: a protein induced DNA U-turn. *Cell*. 87, 1295-1306.

239. Ried, JL, Collmer A (1987) An *nptI-sacB-sacR* cartridge for constructing directed, unmarked mutations in gram-negative bacteria by marker exchange-eviction mutagenesis. *Gene*. 57, 239-246.

240. Ritchie, K., Lill, Y., Sood, C., Lee, H. *et al*. (2013) Single molecule imaging in live bacteria cells. *Phil. Trans. R. Soc. Biological Sciences*. 368, 2012:0355

241. Ritchie, K., Shan, X.Y., Kondo, J., *et al*. (2005) Detection of non-Brownian diffusion in the cell membrane in single molecule tracking. *Biophys. J.* 88, 2266-2277.

242. Robson, A., Burrage, K. & Leake, M.C. (2013) Inferring diffusion in single live cells at the single molecule level. *Philosophical transactions of the royal society biological sciences*. 368, 1-14.

243. Romantsov, T., Helbig, S., Culham, D.E., Gill, C., et al. (2007) Cardiolipin promotes polar localization of osmosensory transporter ProP in *Escherichia coli*. *Molecular Microbiology*. 64 (6), 1455-1465.

244. Rowley, G., Spector, M., Kormanec, J. & Roberts, M. (2006) Pushing the envelope: extracytoplasmic stress responses in bacterial pathogens. *Nature Reviews Microbiology*. 4 (5), 383-394.

245. Ruiz, N. & Silhavy, T.J. (2005) Sensing external stress: watchdogs of the *Escherichia coli* cell envelope. *Current Opinion in Microbiology*. 8 (2), 122-126.

246. Russel, M. & Kaźmierczak, B. (1993) Analysis of the Structure and Subcellular Location of Filamentous Phage pIV. *Journal of Bacteriology*. 175 (13), 3998-4007.

247. Salje, J., van den Ent, F., de Boer, P. & Löwe, J. (2011) Direct Membrane Binding by Bacterial Actin MreB. *Molecular Cell*. 43 (3), 478-487.

248. Sallai, L. & Tucker, P.A. (2005) Crystal structure of the central and C-terminal domain of the σ^{54}-activator ZraR. *Journal of Structural Biology*.151 (2), 160-170.

249. Sambrook, J., Fritsch, E.F. and Maniatis, T., Molecular Cloning: A Laboratory Manual. 1989, New York: Cold Spring Harbor.

250. Sánchez-Romero M-A., Lee, D.J., Sánchez-Morán E., Busby, J.W. (2012) Location and dynamics of an active promoter in *Escherichia coli* K-12. *Biochemical Journal*. 441, 481-485.

251. Sauer, M. (2013). Localization microscopy coming of age: from concepts to biological impact. *Journal of Cell Sciences.* 126*,* 3505-3513.

252. Saxton, M.J. (2008) Single particle tracking: connecting the dots. *Nature Methods*.5 (8), 671-72.

253. Schindelin, J., Arganda-Carreras, I., Frise, E., Kaynig,V., Longair, M., *et al* (2012). Fiji: an open-source platform for biological-image analysis. *Nature Methods.*9(7), 676-682

254. Schumacher, J., Joly, N., Rappas, M., Zhang, X., et al. (2006) Structures and organisation of

AAA+ enhancer binding proteins in transcriptional activation. *Journal of Structural Biology*. 156 (1), 190-199.

255. Seo, J., Brencic, A. & Darwin, A.J. (2009) Analysis of Secretin-Induced Stress in *Pseudomonas aeruginosa* suggests Prevention Rather than Response and Identifies a Novel Protein Involved in Secretin Function. *Journal of Bacteriology*. 191 (3), 898-908.

256. Shaner, N.C., Steinbach, P.A. & Tsien, R.Y. (2005) A guide to choosing fluorescent proteins. Nature Methods. 2(12), 905-909.

257. Shepherd, N., Dennis, P. & Bremer, H. (2001) Cytoplasmic RNA polymerase in *Escherichia coli*. *Journal of Bacteriology*. 183(8), 2527 - 34.

258. Shiba, Y., Yokoyama, Y., Aono, Y., Kiuchi, T., Kusaka, J., Matsumoto, K., and Hara, H. (2004) Activation of the Rcs signal transduction system is responsible for the thermosensitive growth defect of an *Escherichia coli* mutant lacking phosphatidylglycerol and cardiolipin. *Journal of Bacteriolgy*. 186, 6526-6535.

259. Shingler, V. (2011) Signal sensory systems that impact σ^{54}-dependent transcription. *FEMS Microbiology Reviews*. 35 (3), 425-440.

260. Shu, D., Zhang, H., Jiashum, J. & Guo., P. (2007). Counting of size pRNAs of phi-29 DNA-packaging motor with customized single-molecule dual-view system. *The EMBO Journal*. 26, 527-537.

261. Simons R W, Houman F Kleckner N (1987) Improved single and multicopy *lac*-based cloning vectors for protein and operon fusions. *Gene*. 53, 85-96.

262. Singh, S. & Darwin, A.J. (2011) FtsH-Dependent Degradation of Phage Shock Protein C in Yersinia enterocolitica and *Escherichia coli*. *Journal of Bacteriology*. 193 (23), 6436-6442.

263. Stern, D. (2000) Perspective: evolutionary developmental biology and the problem of variation. *Evolution*. 54 (4), 1079-1091.

264. Strahl, H. & Hamoen, L.W. (2010) Membrane potential is important for bacterial cell division. *Proceedings of the National Academy of Sciences*. 107 (27), 12281-12286.

265. Studholme, D.J. & Dixon, R. (2003) Domain Architectures of σ^{54}-Dependent Transcriptional Activators. *Journal of Bacteriology*. 185 (6), 1757-1767.

266. Swulius, M.T. & Jensen, G.J. (2012) The Helical MreB Cytoskeleton in *Escherichia coli* MC1000/pLE7 Is an Artifact of the N-Terminal Yellow Fluorescent Protein Tag. *Journal of Bacteriology*. 194 (23), 6382-6386.

267. Sze, C. & Shingler, V. (1999) The alarmone (p) ppGpp mediates physiological-responsive control at the σ^{54}-dependent Po promoter. *Molecular Microbiology*. 31 (4), 1217-1228.

268. Szwedziak, P., Wang, Q., Freund, S.M., Löwe, J., et al. (2012) FtsA forms actin-like protofilaments. *The EMBO Journal*. 31 (10), 2249-2260.

269. Taghbalout, A. & Rothfield, L. (2007) RNaseE and the other constituents of the RNA degradosome are components of the bacterial cytoskeleton. *Proceedings of the National Academy of Sciences*. 104 (5), 1667-1672.

270. Taniguchi, Y., Choi, P.J., Li, G.-., Chen, H., et al. (2010) Quantifying *E. coli* Proteome and Transcriptome with Single-Molecule Sensitivity in Single Cells. *Science*. 329 (5991), 533-538.

271. Thibault, G., Shui, G., Kim, W., McAlister, G., et al. (2012) The Membrane Stress Response Buffers Lethal Effects of Lipid *Disequilibrium* by Reprogramming the Protein Homeostasis Network. *Molecular Cell*. 48 (1), 16-27.

272. Thompson, M.A., Biteen, J.S., Lord, S.J., Conley, N.R., et al. (2010) Molecules and Methods for Super-Resolution Imaging. *Methods Enzymology.* 475, 27-59.

273. Toni, T., Jovanovic, G., Huvet, M., Buck, M., et al. (2011) From qualitative data to quantitative models: analysis of the phage shock protein stress response in *Escherichia coli*. *BMC Systems Biology*.5 : 69, 1-16.

274. Torella, J., Holden, S., Santoso, Y., Hohlbein, J., et al. (2011) Identifying Molecular Dynamics in Single-Molecule FRET Experiments with Burst Variance Analysis. *Biophysical Journal*. 100 (6), 1568-1577.

275. Treanor B, Depoil D, Gonzalez-Granja A, Barral P, Weber M, Dushek O, Bruckbauer A, Batista FD (2009) The membrane skeleton controls diffusion dynamics and signaling through the B cell receptor. *Immunity*. 32, 187-199.

276. Trevors, J. (2012) A Perspective on the Mobilization, Localization and Delivery of Molecules in the Crowded Bacterial Cytoplasm. *Current Issues in Molecular Biology*. 14 (2), 39-46.

277. Trotochaud, A.E. & Wassarman, K.M. (2006) 6S RNA Regulation of *pspF* Transcription Leads to Altered Cell Survival at High pH. *Journal of Bacteriology*. 188 (11), 3936-3943.

278. Tucker, N.P., Ghosh, T., Bush, M., Zhang, X., et al. (2010) Essential roles of three enhancer sites in σ^{54}-dependent transcription by the nitric oxide sensing regulatory protein NorR. *Nucleic Acids Research*. 38 (4), 1182-1194.

279. Umbarger, M., Toro, E., Wright, M., Porreca, G., et al. (2011). The Three-Dimensional

Architecture of a Bacterial Genome and Its Alteration by Genetic Perturbation. *Molecular Cell*. 44 (2), 252-264.

280. Unoson, C. & Wagner, E.G. (2008) A small SOS-induced toxin is targeted against the inner membrane in *Escherichia coli*. *Molecular Microbiology*. 70 (1), 258-270.

281. van den Ent, F., Johnson, C.M., Persons, L., de Boer, P., et al. (2010) Bacterial actin MreB assembles in complex with cell shape protein RodZ. *The EMBO Journal*. 29 (6), 1081-1090.

282. van Teeffelen, S., Wang, S., Furchtgott, L., Huang, K.C., et al. (2011) The bacterial actin MreB rotates, and rotation depends on cell-wall assembly. *Proceedings of the National Academy of Sciences*.108 (38), 15822-15827.

283. Vega, N.M., Allison, K.R., Khalil, A.S. & Collins, J.J. (2012) Signaling-Mediated Bacterial Persister Formation. *Nature Chemical Biology*. 8 (5), 431-433.

284. Vothknecht, U.C., Otters, S., Hennig, R. & Schneider, D. (2012) Vipp1: a very important protein in plastids?! *Journal of Experimental Botany*. 63 (4), 1699-1712.

285. Vrancken, K., de Keersmaeker, S., Geukens, N., Lammertyn, E., et al. (2006) *pspA* overexpression in *Streptomyces lividans* improves both Sec- and Tat-dependent protein secretion. *Applied Microbiology and Biotechnology*. 73 (5), 1150-1157.

286. Vrancken, K., van Mellaert, L. & Anne, J. (2008) Characterization of the *Streptomyces lividans* PspA Response. *Journal of Bacteriology*. 190 (10), 3475-3481.

287. Wang, Q., Frye, J., McClelland, M. & Harshey, R.M. (2004) Gene expression patterns during swarming in Salmonella typhimurium: genes specific to surface growth and putative new motility and pathogenicity genes. *Molecular Microbiology*. 52 (1), 169-187.

288. Wang, W., Li, G.-., Chen, C., Xie, X.S., et al. (2011) Chromosome Organization by a Nucleoid-Associated Protein in Live Bacteria. *Science*. 333 (6048), 1445-1449.

289. Weber, H., Polen, T., Heuveling, J., Wendisch, F.V., et al. (2005) Genome-Wide Analysis of the General Stress Response Network in *Escherichia coli*: σ^S-Dependent Genes, Promoters, and σ Factor Selectivity. *Journal of Bacteriology*. 187 (5), 1591-1603.

290. Weiner, L. & Model, P. (1994) Role of an *Escherichia coli* stress-response operon in stationary-phase survival. *Proceedings of the National Academy of Sciences*. 91, 2191-2195.

291. Weiss, D.S., Chen, J.C., Ghigo, J.M., Boyd, D., and Beckwith, J. (1999) Localization of FtsI (PBP3) to the septal ring requires its membrane anchor, the Z ring, FtsA, FtsQ, and FtsL. *Journal of Bacteriolgy*.181, 508–520.

292. Westphal, S., Heins, L., Soll, J. & Vothknecht, U.C. (2001). Vipp1 deletion mutant of *Synechocystis*: A connection between bacterial phage shock and thylakoid biogenesis? *Proceedings of the National Academy of Sciences*. 98(7), 4243-4248.

293. White, C.L., Kitich, A. & Gober, J.W. (2010). Positioning cell wall synthetic complexes by the bacterial morphogenetic proteins MreB and MreD. *Molecular Microbiology*. 76 (3), 616-633.

294. Whitman, W.B. (2009). The Modern Concept of the procaryote. *Journal of Bacteriology*. 191 (7), 2000-2005.

295. Wigneshweraraj, S., Bose, D., Burrows, P.C., Joly, N., et al. (2008). Modus operandi of the bacterial RNA polymerase containing the σ^{54} promoter-specificity factor. *Molecular Microbiology*. 68 (3), 538-546.

296. Wigneshweraraj, S., Chaney, M.C., Ishihama, A. & Buck, M. (2001) Regulatory sequences in sigma 54 localise near the start of the DNA melting. *Journal of Molecular biology*. 306, 681-701.

297. Wortham, C., Grinberg, L., Kaslow, D.C., Briles, D.E., et al. (1998). Enhanced Protective Antibody Responses to PspA after Intranasal or Subcutaneous Injections Of PspA Genetically Fused to Granulocyte-Macrophage Colony-Stimulating Factor or Interleukin-2. *Infection and Immunity*. 66 (4), 1513-1520.

298. Xiao, J., Elf, J., Li, Gene-Wei., Yu, J. & Xie, S. In: Selvin, P.R & Ha, T's Single Molecule Techniques: A laboratory manual. (2008). Cold Spring Harbor Press, Cold Spring harbor, N.Y.149-169.

299. Xie, X., Yu, J. & Yang, W. (2006). Living cells as Test Tubes. *Science*. 312, 228-230.

300. Xie, X.S., Choi, P.J., Li, G., Lee, N.K., et al. (2008). Single-Molecule Approach to Molecular Biology in Living Bacterial Cells. *Annual Review of Biophysics*. 37 (1), 417-444.

301. Xu, H. & Hoover, T. (2001). Transcriptional regulation at a distance in bacteria. *Current Opinion in Microbiology*. 4,138-144.

302. Yamaguchi, S. & Darwin, A.J. (2012). Recent findings about the *Yersinia enterocolitica* Phage Shock Protein Response. *The Journal of Microbiology*. 50 (1), 1-7.

303. Yamaguchi, S., Gueguen, E., Horstman, N.K. & Darwin, A.J. (2010). Membrane association of PspA depends on activation of the phage-shock-protein response in *Yersinia enterocolitica*. *Molecular Microbiology*. 78 (2), 429-443.

304. Yamaguchi, S., Reid, D.A., Rothenberg, E. & Darwin, A.J. (2013). Changes in Psp protein

binding partners, localization and behaviour upon activation of the *Yersinia enterocolitica* phage shock protein response. *Molecular Microbiology*. 87 (3), 656-671.

305. Yu D, Court D L (1998) A new system to place single copies of genes, sites and *lacZ* fusions on the *Escherichia coli* chromosome. *Gene*. 223, 77-81.

306. Yu, J., Xiao, J., Ren, X., Lao, K., et al. (2006). Probing Gene Expression in Live Cells, One Protein Molecule at a Time. *Science*. 311 (5767), 1600-1603.

307. Zakrzewska, K. & Lavery, R. (2012). Towards a molecular view of transcriptional control. *Current Opinion in Structural Biology*. 22 (2), 160-167.

308. Zhang, L., Kato, Y., Otters, S., Vothknecht, U.C., et al. (2012). Essential Role of VIPP1 in Chloroplast Envelope Maintenance in Arabidopsis. *The Plant Cell*. 24 (9), 3695-3707.

309. Zhang, N., Joly, N & Buck, M. (2012) A common feature from different subunits of a homomeric AAA+ protein contacts three spatially distinct transcription elements. *Nucleic Acids Research*. 40(18), 9139-9152

310. Zingaro, K.A. & Papoutsakis, E.T. (2012) Toward a Semisynthetic Stress Response System to Engineer Microbial Solvent Tolerance. *mBio*. 3 (5), e00308-12-e00308-12.

Web links:

http://www.ucmp.berkeley.edu/bacteria/bacteriamm.html - Bacterial morphology diagram

http://www.uniprot.org/uniprot/P0AFM6 - *E. coli* gene database

APPENDICES

Appendix-1

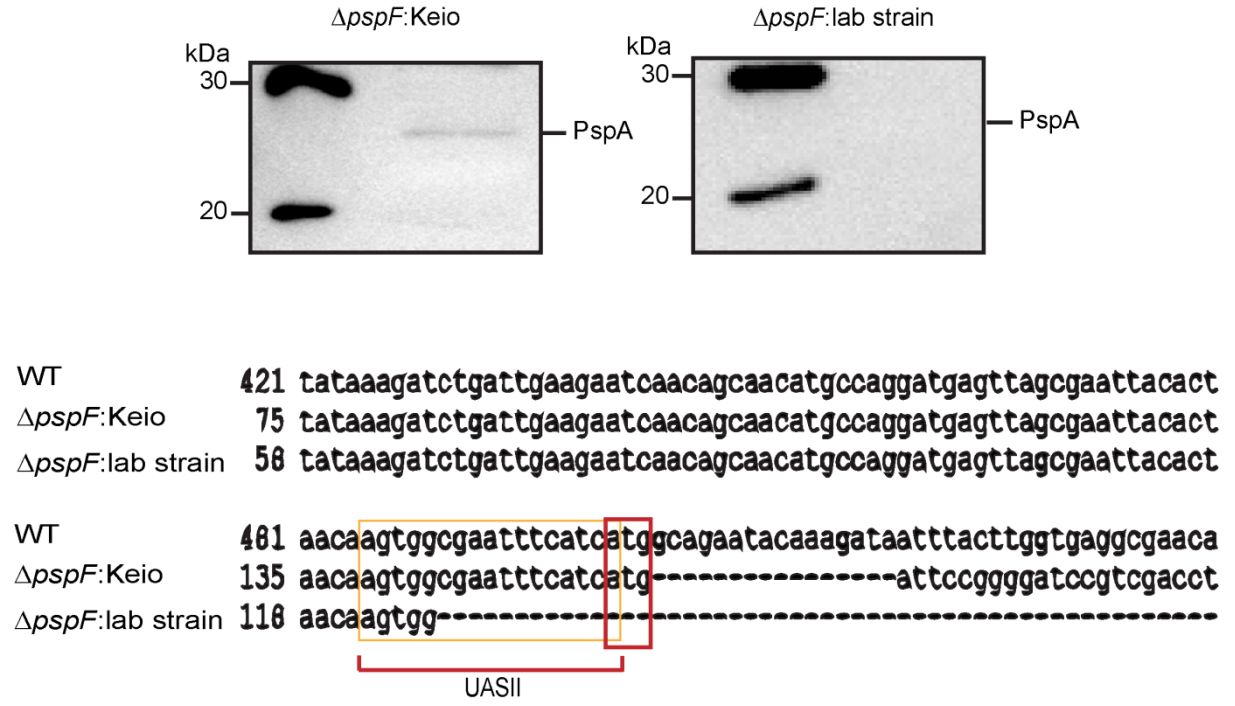

Figure 1 **The comparisons in the functionality of *ΔpspF* strain from Keio collection and the one generated in the lab***:* The Western blot to show the residual expression of PspA using anti-PspA antibodies in the *ΔpspF* from the Keio collection. The *ΔpspF* generated in the lab was much cleaner for the PspA expression. The sequence comparisons between the WT, *ΔpspF*: Keio and *ΔpspF:* lab strain showed that the *ΔpspF:* lab strain lacked the major part of the UASII. This could be crucial in the proper expression of the *psp* genes. This strain was used in particular for the imaging of V-PspF plasmids in order to exploit the absence of UAS II in order understand the importance of the UASI and UASII within the P*pspA* promoter and the importance of the presence of two PspF binding sites within the P*pspA* promoter. The imaging data has been presented in Chapter 5.

Appendix-2

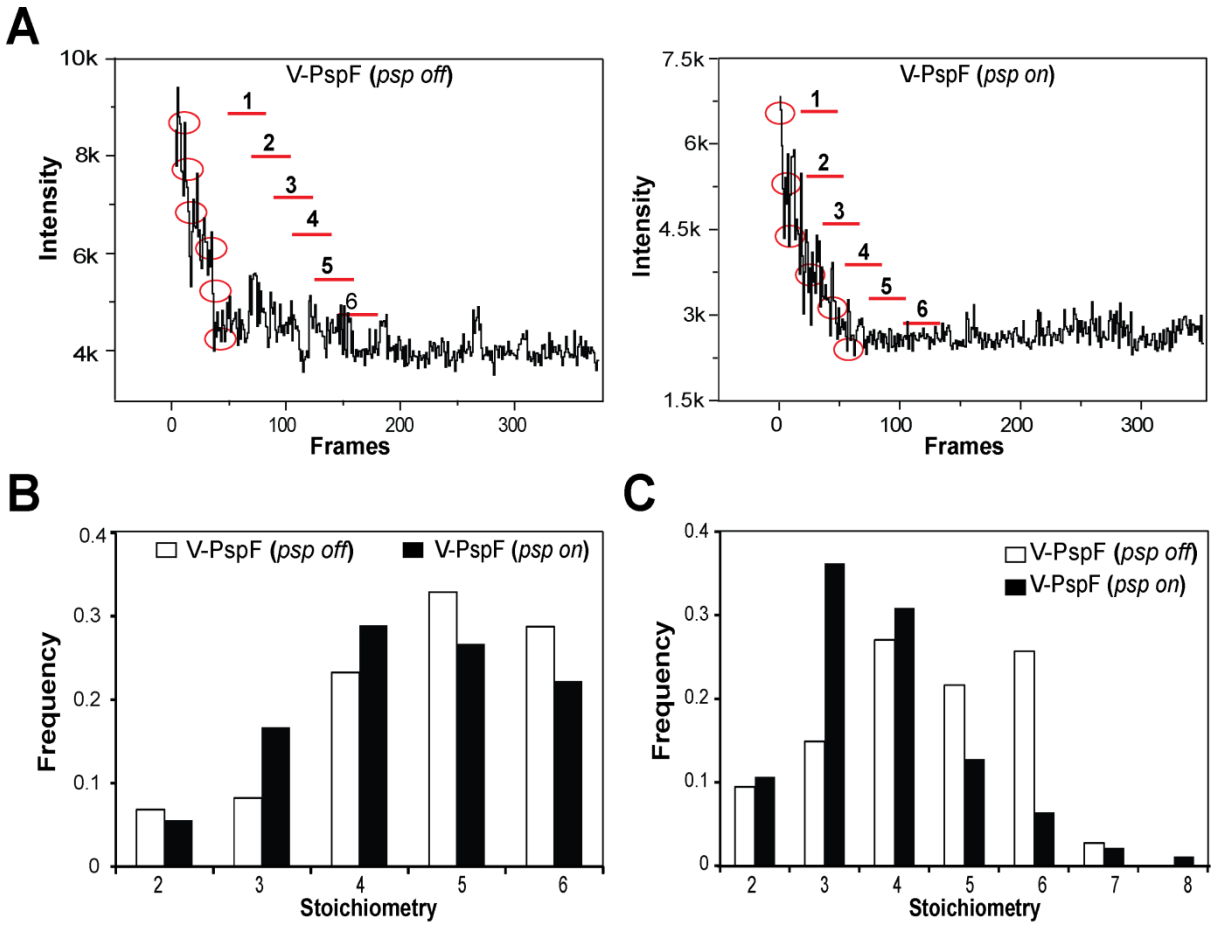

Figure 2 **Manual stoichiometry estimation**: (A) Curves represent the bleaching steps of V-PspF under non-stress (*psp off*) and stress (*psp on*) growth conditions. Their manual analysis consolidates that of the edge preserving approach (Chapter 5). Inspection of the bleaching steps reveals a single step corresponding to a monomer of V-PspF. (B) The distribution of stoichiometries calculated by manual counting of the bleaching and/or blinking steps for V-PspF foci [white, under non-stress (n=73) and black, under stress conditions (n=90)]. (C) The distribution of stoichiometries determined for each bleaching trace by dividing the estimated average step size with difference between the initial intensity and final intensity [white, under non-stress (n=75) and black, under stress conditions (n=94)].

Appendix-3

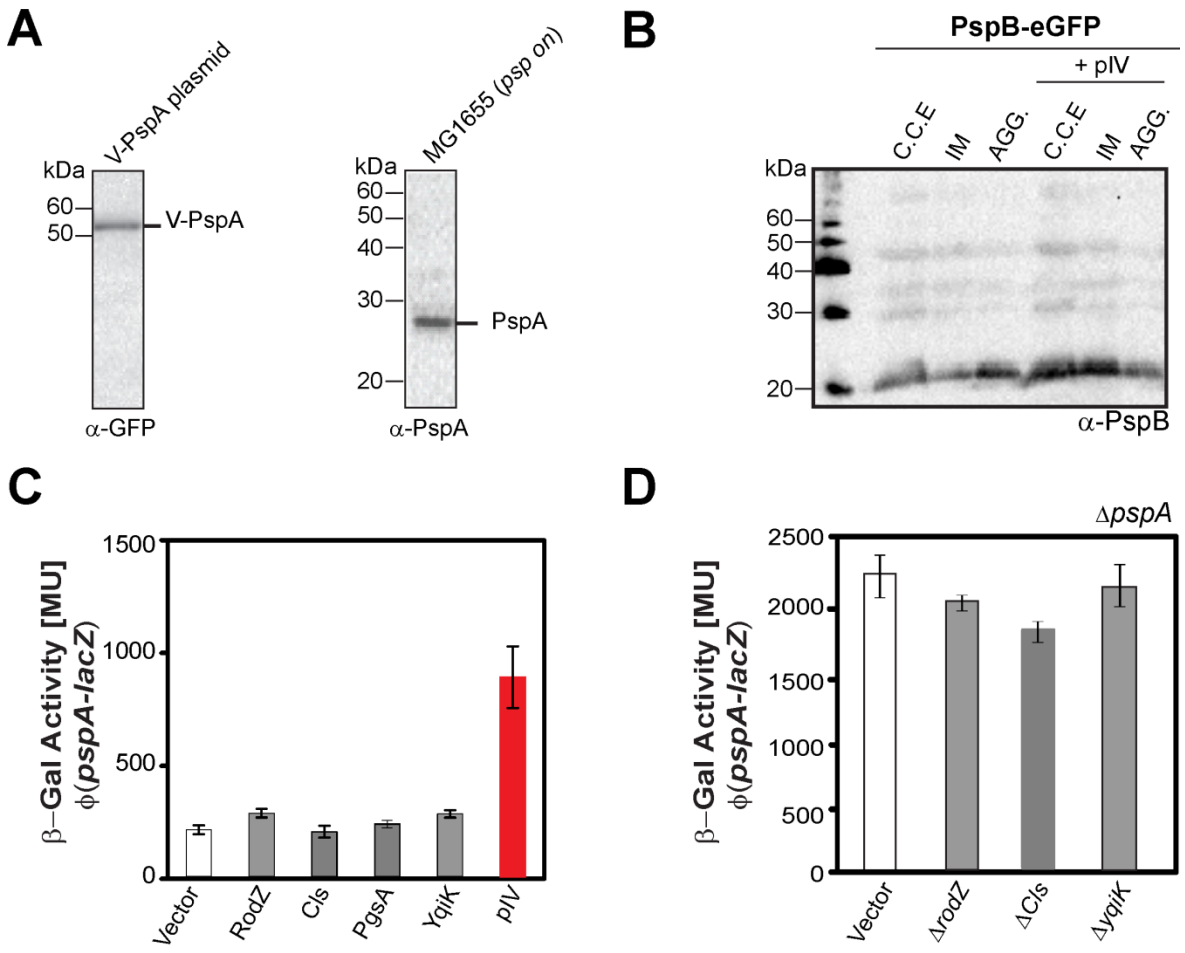

Figure 3 **Additional control experiments to support the production of V-PspA fusion and some β-Gal assay using membrane determinants**: (A)) Western blot to show stable production of V-PspA from a low copy plasmid. The second western to show the production of WT FL PspA under pIV induced stress conditions. (B) Western blot to show the cell fractionation of PspB-eGFP [~35 kDa – PspB (7 kDa) + eGFP (28 kDa)]. The graph shows that no prominent band for the PspB-eGFP fusion was obtained which was around 35 kDa under non-stress as well as stress conditions. (C) β-Gal assay to show that overproduction of the membrane determinants did not induce the *psp* [ϕ (*pspA-lacZ*)] in the WT MG1655 cells, MVA44- empty vector, RodZ, Cls, PgsA and YqiK. (D) Control experiments showing that additional mutations of the membrane determinants did not affect the σ^{54} transcription from the ϕ (*pspA-lacZ*) in the absence of PspA (Δ*pspA*). Strains: Δ*pspA* (MVA27, white bar), Δ*pspA* Δ*rodZ* (MVA27 Δ*rodZ*), Δ*pspA* Δ*cls* [MVA27 Δ*cls*, Δ*pspA* Δ*yqiK* (MVA27 Δ*yqiK*). The error bars are standard deviation of the means.

Appendix-4

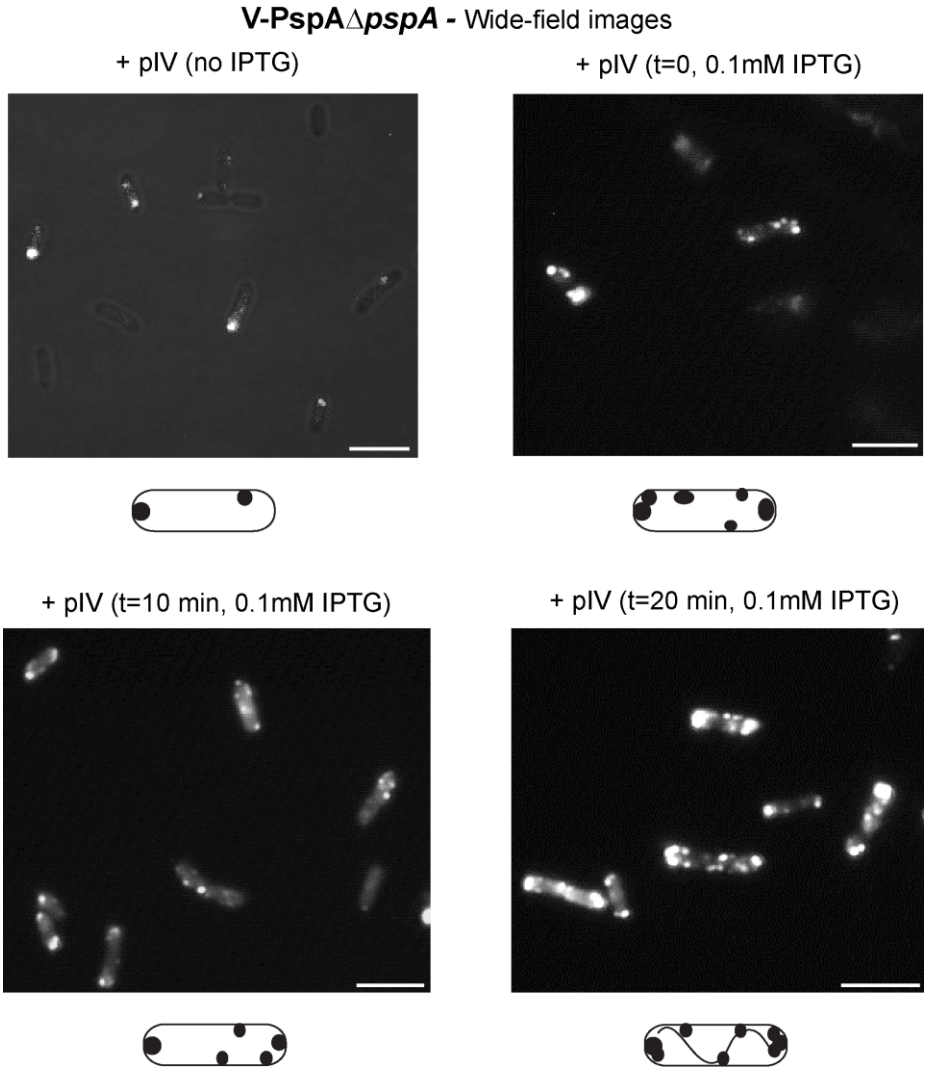

Figure 4 **The wide-field images of chromosomal V-PspA in *ΔpspA* cells studied with real time induction of stress with pIV:** The images were taken at induction, 10 minutes after induction and 20 minute after induction. The pIV production was induced with 0.1 mM IPTG and the stress was induced with the mislocalisation of pIV in the IM. Along with the images the cell illustrations have been given to show the changing localisation of PspA with the increase in the intensity of the stress. The longer incubation in IPTG would lead to higher amounts of pIV and thus more mislocalisation. This will lead to changes in the production and localisation of PspA. Scale bar in the images = 1 μm

Appendix-5

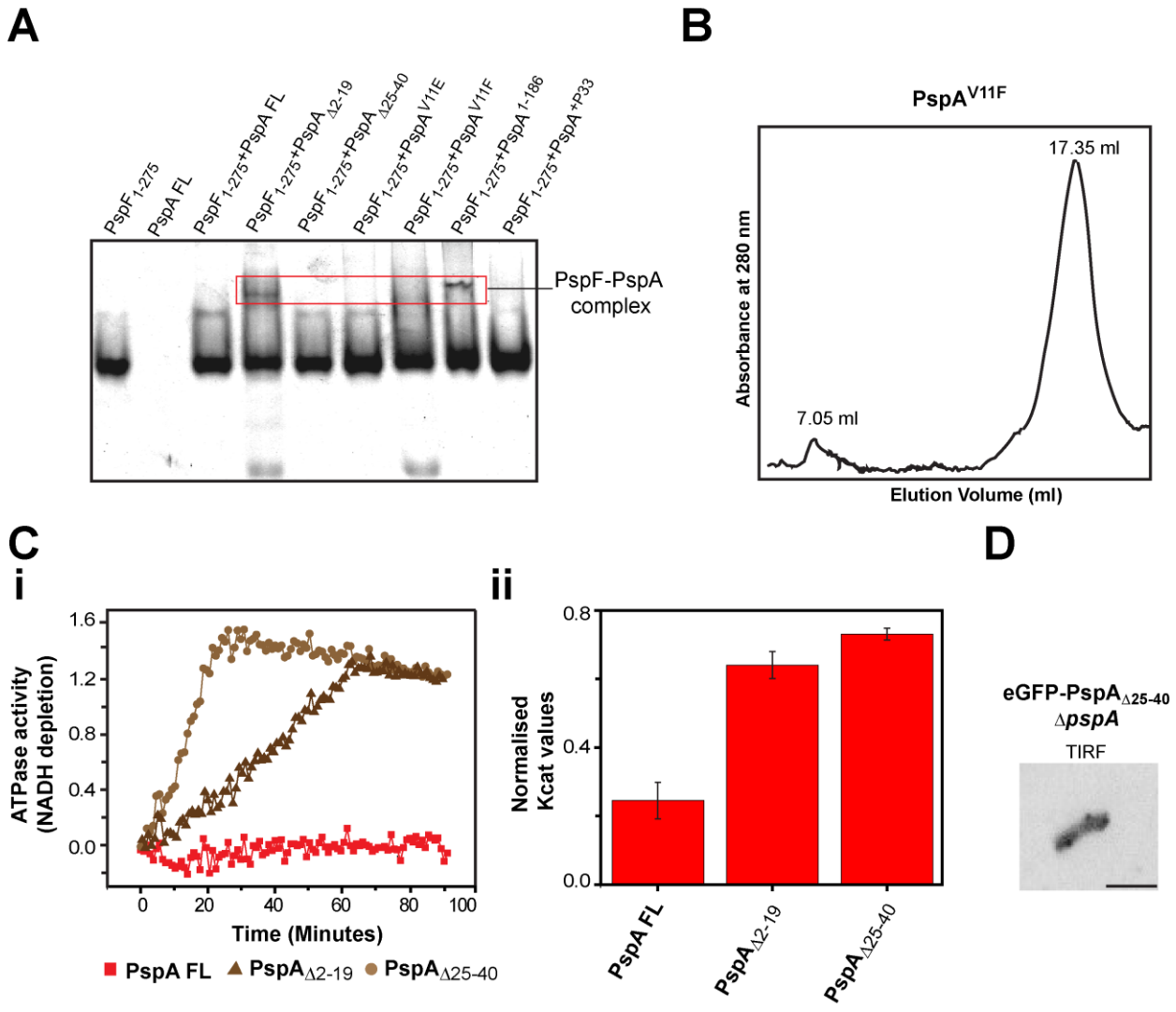

Figure 5 **Images to show *in vitro* and *in vivo* assays of PspA structural domain mutants**: (A) The native gel to show the interactions between $PspF_{1-275}$ and PspA FL, $PspA_{1-186}$, $PspA_{\Delta 2-19}$, $PspA_{\Delta 25-40}$, $PspA^{V11E}$, $PspA^{V11F}$ and $PspA^{+P33}$. The interaction between PspF and PspA WT was difficult to detect because possibly the concentration of PspA FL was not high enough to form a stable complex with PspF that could be resolved in the native gel. However $PspA_{1-186}$ (HD1-3) formed a complex with $PspF_{1-275}$. $PspA_{\Delta 2-19}$, the ahI mutant only formed a complex with $PspF_{1-275}$ as shown by other experimental evidence in Chapter 6. (B) The Gel filtration profile of the single amino acid substitution mutant in the ahI of PspA – $PspA^{V11F}$ showed that like $PspA_{\Delta 2-19}$ it also formed an apparent dimer or monomer. (C-i) The graph shows the depletion in NADH concentration with the ATPase activity of PspF in a plate reader based ATPase assay. PspA FL effectively inhibits the ATPase activity of PspF therefore the ATPase activity is shut down and the NADH concentration does not reduce. While the $PspA_{\Delta 25-40}$ with limited negative regulatory function was not able to inhibit the PspF ATPase activity so effectively like PspA FL. And even the $PspA_{\Delta 2-19}$ did not show such an effective inhibition of ATPase assay. (C-ii) The graph compares the Kcat values of the PspF-ATPase and that indirectly reflects on the extent of PspA dependent inhibition of PspF. PspA FL gave the least Kcat value while the $PspA_{\Delta 25-40}$ and $PspA_{\Delta 2-19}$ gave high values that showed that the PspF ATPase was active. The error bars represent the standard errors of the normalised values.(D) The TIRF inverted image of eGFP-$PspA_{\Delta 25-40}$ (black foci) to show that no polar foci were observed and only lateral membrane associated foci were observed. Scale bar = 1µm

Appendix-6

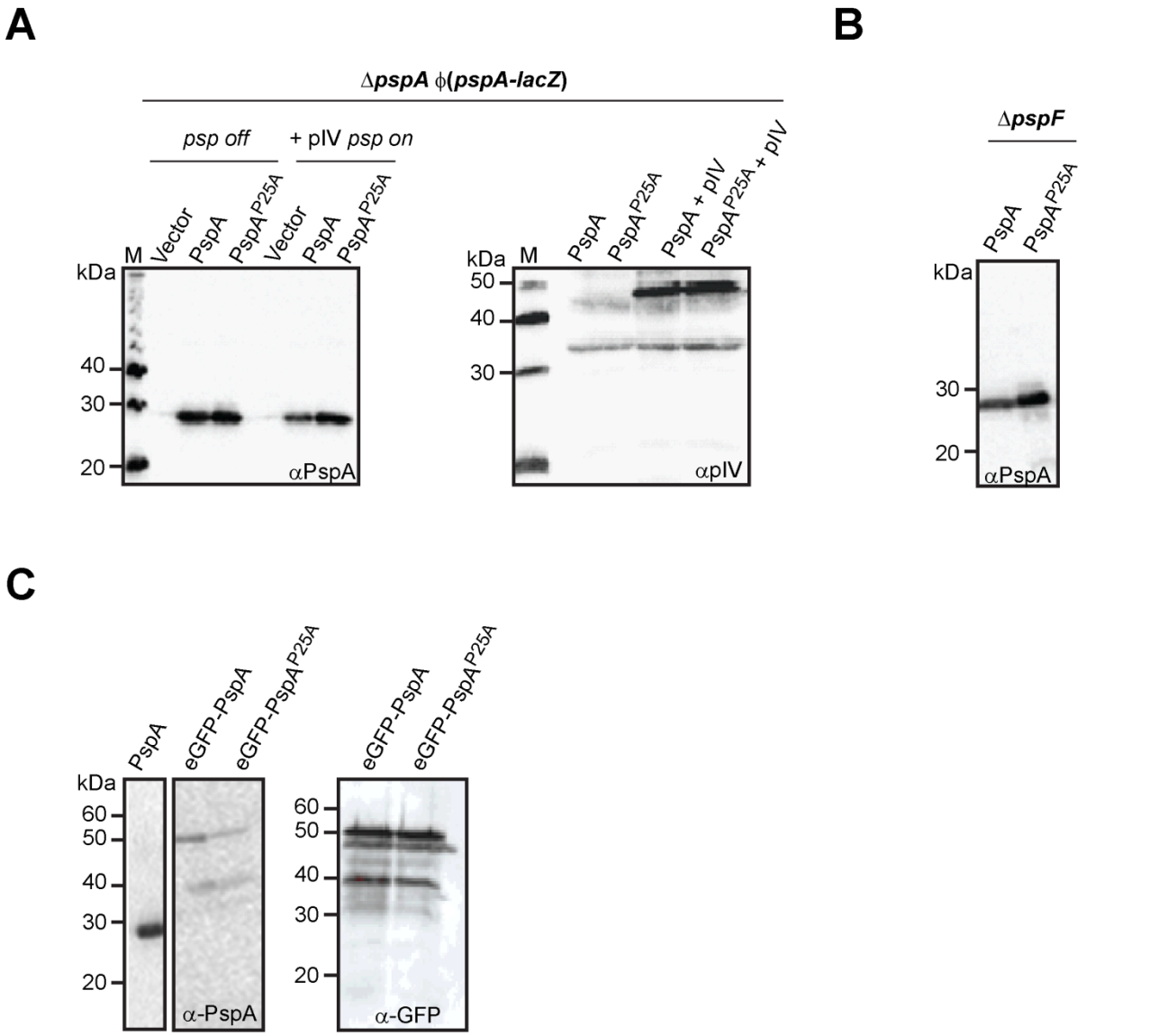

Figure 6 **Western blots of PspA^{P25A} mutant**: (A) Western blots were performed to show the production levels of PspA and PspA^{P25A} proteins used in β-Gal assay to compare the regulation of Psp response by Psp^{P25A}with PspA full length. The pIV antibodies were used to assess the production of pIV (~46 kDa) in the stress cells. M is molecular weight marker. (B) Western blots to show the comparable production of PspA FL and PspA^{P25A} in the *ΔpspF* strain used in the motility assay. (C) Western blots were conducted using α-PspA or GFP antibodies (α-GFP) to show the levels of leaky production and stability of plasmid borne eGFP-PspA^{P25A} (~53 kDa) fusion protein (pGJ90) in Δ*pspA* (MG1655Δ*pspA*). Control is eGFP-PspA FL (pEC1).

Appendix-7

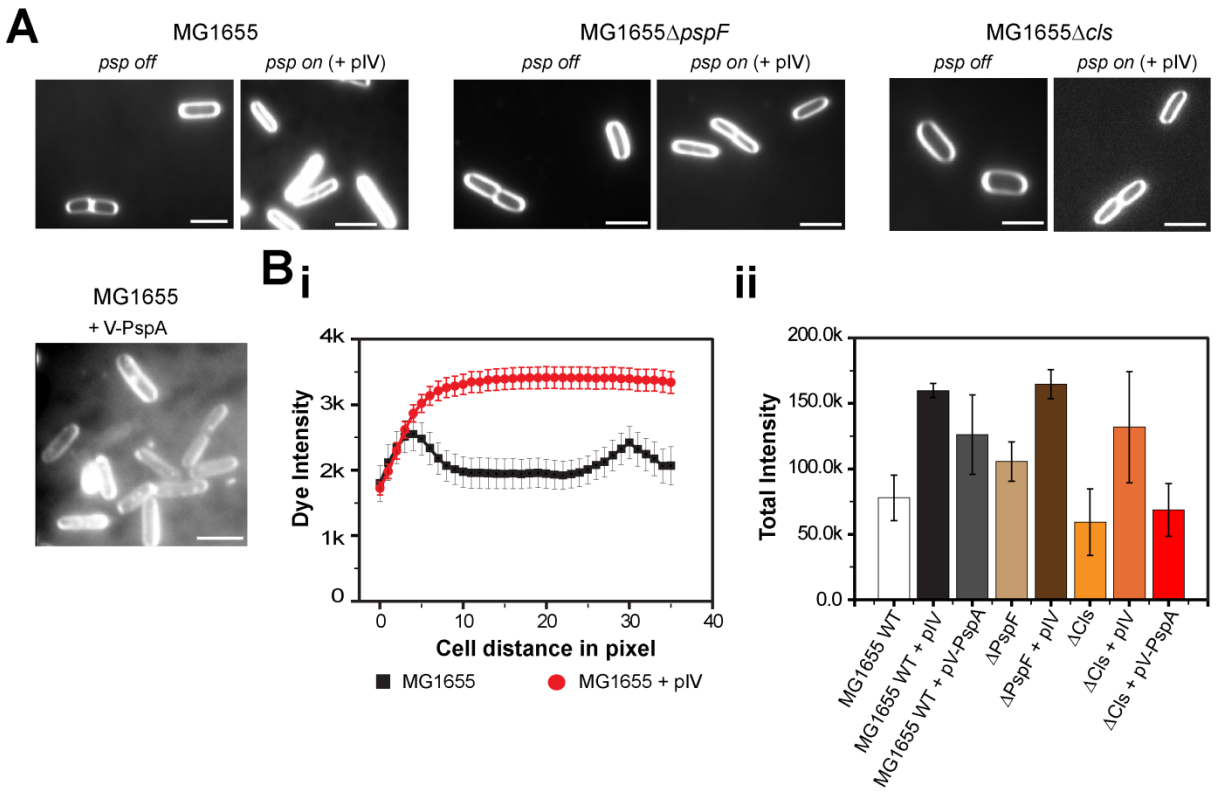

Figure 7 **SMI of the di-4-ANEPPDHQ**: (A) The SMI images showing the staining of *E. coli* cells with the dye as described in the Methods 2.15.4. The dye stained the cells much more efficiently under the pIV induced stress conditions in the WT cells, in *ΔpspF* and *Δcls* cells. The addition of V-PspA produced from the plasmid did not change the staining with this dye. (B-i) The graph shows the fluorescence intensity of the dye along the cell length (see Methods 2.15.3.1, 131). Under non-stress conditions in the WT cells the dye stained the poles much more efficiently, but with the stress inducing conditions the cell across the whole length was stained. The error bars represent standard error of the intensity. (B-ii) The graph represents the total intensity of the stained cell. The bars show that the total cell intensity was higher for the cell under pIV induced stress conditions. The increase in the intensity was irrespective of PspF and CL. Even overproduction of PspA did not increase the staining of the cells with the dye. This staining with the dye shows the different states of the *E. coli* membrane in the growth conditions. It appears that in the stress conditions membrane changes to a more ordered phase which results in more efficient staining of these cells with the dye. While in the non-stress conditions only the poles of the membrane display an ordered phase which is why it was stained much more strongly than the rest of the lateral membrane. The error bars are the standard error of the normalised mean values calculated for 10-15 cells. The scale bar = 1µm

Appendix 8

For individual trajectories of N points (x_i, y_i) measured at time intervals Δt, the mean square displacement *MSD* for a time lag $n\Delta t$ was calculated using a running average along the trajectory (Ritchie *et al.*, 2005).

$$MSD(n\Delta t) = \frac{1}{N-n-1}\sum_{i=1}^{N-n-1}(x_{i+n}-x_i)^2 + (y_{i+n}-y_i)^2$$

In the case of Brownian diffusion the MSD increases linearly with time lag. The diffusion coefficient can be obtained from the slope of the MSD vs. time-lag curve, for diffusion in two dimensions the relation is: $MSD = 4\,D\,n\Delta t$, while for 3D diffusion it is $MSD = 6\,D\,n\Delta t$. Diffusion coefficients for individual trajectories were determined from the first three data points of the *MSD* curves of the individual trajectories. The restriction to just three points was used because the error in *MSD* increases with time lag as the number of independent measurements decreases (Qian *et al.*, 1991).